Urs Lübbert

Target Position Estimation with a Continuous Wave Radar Network

Cuvillier Verlag Göttingen

Target Position Estimation with a Continuous Wave Radar Network

Vom Promotionsausschuss der
Technischen Universität Hamburg-Harburg
zur Erlangung des akademischen Grades
Doktor-Ingenieur
genehmigte Dissertation

von

Urs Lübbert

aus

Hannover

2005

Bibliografische Information Der Deutschen Bibliothek
Die Deutsche Bibliothek verzeichnet diese Publikation in der Deutschen Nationalbibliografie; detaillierte bibliografische Daten sind im Internet über http://dnb.ddb.de abrufbar.
1. Aufl. - Göttingen : Cuvillier, 2005
Zugl.: Hamburg-Harburg, Univ., Diss., 2005
ISBN 3-86537-546-4

1. Gutachter: Prof. Dr. Hermann Rohling
2. Gutachter: Prof. Dr. Friedrich Mayer-Lindenberg

Tag der mündlichen Prüfung: 06. Juni 2005

© CUVILLIER VERLAG, Göttingen 2005
Nonnenstieg 8, 37075 Göttingen
Telefon: 0551-54724-0
Telefax: 0551-54724-21
www.cuvillier.de

Alle Rechte vorbehalten. Ohne ausdrückliche Genehmigung des Verlages ist es nicht gestattet, das Buch oder Teile daraus auf fotomechanischem Weg (Fotokopie, Mikrokopie) zu vervielfältigen.
1. Auflage, 2005
Gedruckt auf säurefreiem Papier

ISBN 3-86537-546-4

Danksagung

Die vorliegende Arbeit entstand während meiner Tätigkeit als wissenschaftlicher Mitarbeiter im Arbeitsbereich Nachrichtentechnik der Technischen Universität Hamburg Harburg.

Ganz besonders danke ich meinem Doktorvater Herrn Prof. Dr. Hermann Rohling für die grossartige Unterstützung, Inspiration und die Ermöglichung vieler Freiräume.

Vielen Dank an Herrn Prof. Dr. Friedrich Mayer-Lindenberg für die Übernahme des Zweitgutachtens und an Herrn Prof. Dr. Jan Luiken ter Haseborg für die Übernahme des Prüfungsvorsitzes.

Allen ehemaligen Kolleginnen und Kollegen im Arbeitsbereich Nachrichtentechnik, besonders meinem Projektkollegen Dr. Mark Schiementz, danke ich für die stets sehr angenehme und freundschaftliche Zusammenarbeit.

Zusammenfasung

Diese Arbeit untersucht Verfahren zur Zieldetektion und Positionsbestimmung in einem Radarnetzwerk. Ausgehend von bekannten Verfahren der Signalverarbeitung werden neue Methoden zur Erhöhung der Leistungsfähigkeit erarbeitet. Ein experimentelles Radarnetzwerk für den Einsatz an einem Automobil wird vorgestellt.

Ein Radarnetzwerk besteht aus einem Verbund von mehreren am Fahrzeug angebrachten Einzelsensoren. Die Sensoren vermessen getrennt voneinander die Umgebung und melden die gemessenen Entfernungen an einen Zentralrechner. Der Rechner vergleicht die gemessenen Entfernungen der Einzelsensoren miteinander und bestimmt im Trilaterationsverfahren den Zielwinkel. Der Einzelsensor kommt ohne Winkelmessung aus und ist deshalb einfacher aufgebaut als ein winkelmessender Sensor.

Die Umfeldwahrnehmung durch Radarsysteme ermöglicht viele Komfort- und Sicherheitsanwendungen für ein Automobil. Muss ein weiter Beobachtungsbereich um das Automobil abgedeckt werden, ist ein Radarnetzwerk mit einfachen Einzelsensoren besonders günstig.

Im Rahmen dieser Arbeit wurde die Signalverarbeitung für linear frequenzmodulierte (LFM) Dauerstrichradare im 77GHz Bereich und für ein Radarnetwerk entwickelt. Erstmals wurde ein Radarnetzwerk aufgebaut, welches mit 77GHz LFM Sensoren arbeitet.

Die vorliegende Arbeit beschreibt zunächst die klassischen LFM- und Radarnetzwerktechniken. Sie zeigt anschließend, worin die besonderen Anforderungen an die LFM Sensoren im Radarnetzwerk liegen. Für das Trilaterationsverfahren werden hohe Messgenauigkeit und Detektions-Wahrscheinlichkeit benötigt. Insbesondere müssen die Sensoren in Mehrzielsituationen mit einer relativ hohen Anzahl von Zielen funktionieren.

Beim Aufbau des 77GHz LFM-Radarnetzwerkes hat sich herausgestellt, dass die etablierten LFM-Signalverarbeitungs-Verfahren für ein Radarnetzwerk verbessert werden müssen. Bisherige LFM-Verfahren trennen zwischen Signal-Vorverarbeitung und Zielverfolgung. Diese Arbeit stellt für den Einzelsensor einen Tracker vor, der in die LFM-Vorverarbeitung integriert ist. Es ergibt sich ein großer Gewinn an Messgenauigkeit und Trackstabilität.

Auf der Seite der Netzwerkverarbeitung wurden bisher erste Erfahrungen gemacht, Trilateration und Tracking in einem nichtlinearen Tracker zusammenzuführen. Dies wurde auch in dem vorgestellten Netzwerk untersucht. Zusätzlich wird ein neues Verfahren vorgestellt, in dem auch die LFM-Signalverarbeitung der Einzelsensoren in die Netzwerkverarbeitung integriert ist.

Abschließend wird das Experimental-System vorgestellt, und Messergebnisse präsentiert. Insgesamt zeigt sich, dass die Integration von Verarbeitungsschritten in LFM-Sensoren, im Radarnetzwerk sowie im Gesamtsystem eine wesentlich effizientere Verwertung der Messdaten zulässt.

Contents

1 Introduction **11**
- 1.1 Short History of Radar . . . 11
- 1.2 Automotive Applications . . . 12
  - 1.2.1 Adaptive Cruise Control (ACC) . . . 12
  - 1.2.2 Blind Spot Surveillance . . . 13
  - 1.2.3 Pre-Crash Recognition . . . 13
  - 1.2.4 Collision Avoidance . . . 14

2 A Radar Network with Four 77 GHz Sensors **15**
- 2.1 System Requirements . . . 17
- 2.2 Requirements for Networked Single Sensors . . . 19

3 Radar Waveforms **21**
- 3.1 Observable Target Parameters . . . 22
  - 3.1.1 Target Range . . . 23
  - 3.1.2 Target Radial Velocity . . . 23
- 3.2 Pulse Radar . . . 24
  - 3.2.1 Range Measurement . . . 24
  - 3.2.2 Range Resolution . . . 24
  - 3.2.3 Range Ambiguity . . . 25
  - 3.2.4 Estimation Accuracy . . . 26
  - 3.2.5 Pulse Doppler Radar . . . 26
- 3.3 Continuous Wave Radar without Range Resolution . . . 26
  - 3.3.1 Mono-frequency CW Radar . . . 27
  - 3.3.2 FSK CW Radar . . . 27
- 3.4 Linear Frequency Modulation . . . 28
  - 3.4.1 Measurement of Range and Velocity for a Single Target . . . 31
  - 3.4.2 Multiple Target Situations . . . 31
  - 3.4.3 Ghost Target Reduction by Using Multiple Chirps . . . 32

3.4.4 Additional Considerations 34

4 Single Sensor Processing **37**
4.1 LFMCW Processing Overview 37
4.2 Windowing and FFT 38
4.3 Detection 40
4.3.1 Determination of the False Alarm Rate 43
4.3.2 Determination of the Detection Rate 43
4.3.3 Detection Rate for Fluctuating Targets 43
4.4 CFAR Techniques 44
4.4.1 CA-CFAR 45
4.4.2 OS-CFAR 46
4.5 Frequency Estimation 46
4.6 Range of Observable Frequency Values 48
4.7 Frequency to Range-Velocity Processing 49
4.7.1 Precalculation of the Frequency Equations 49
4.7.2 Range-Velocity Processing for a Single Target 50
4.7.3 Range-Velocity Processing in a Multiple Target Environment 51
4.7.4 Considerations on Quality of Target Detection 54

5 Improved LFMCW Processing **55**
5.1 Center of Gravity Algorithm with Compensation 56
5.1.1 Model of the Estimation Error 58
5.1.2 Determination of the Correction Factor 59
5.1.3 COG Correction for a Noisy Signal 60
5.1.4 COG Simulation Results 60
5.2 Compensation of Target Movement 62
5.3 Simulation of a Multiple Target Scenario 67
5.4 Single Sensor Target Tracking 76
5.4.1 Standard Tracker 76
5.4.2 Range-Velocity Measurement to Track Update 77
5.4.3 Direct Frequency Measurement to Track Update . . . 79
5.4.4 Implementation of the Single Sensor Tracking 80

6 Measurement of the Target Position **83**
6.1 Classical Measurement of Target Azimuth 83
6.1.1 Definition of Azimuth and Elevation 83
6.1.2 Azimuthal Scanning Technique 84
6.1.3 Monopulse Technique 86
6.1.4 Sequential Lobing Technique 88
6.2 Advantages of Position Estimation with a Radar Network . . 88

6.3 Trilateration 89
6.4 Gauss-Newton Algorithm 93
6.5 The Kalman Filter 95
6.5.1 The Linear Kalman Filter 95
6.5.2 The Extended Kalman Filter 98
6.6 Multilateration with Synchronized Networks 99
6.6.1 Multistatic Radar Network 99
6.6.2 Multilateration Algorithm 100
6.7 Requirements on the Single Sensors 102

7 Classical Radar Network Signal Processing 105
7.1 Data Assignment 106
7.2 Lateration Processing 109
7.3 Target Tracking 110
7.3.1 Association of Measurements and Tracks 111
7.3.2 Weighted Distance Metric and Adaptive Gate Size . . 114
7.3.3 Track Validation and Deletion 115
7.3.4 Additional Track Validation and Deletion Criteria . . 116
7.3.5 Target Model of Motion 116
7.3.6 Update Rate of the Tracked Target List 117
7.4 Synchronization between Sensors 118
7.4.1 Implemented Radar Network Synchronization 118
7.5 Performance Considerations 121

8 Improved Radar Network Processing Strategies 123
8.1 Track Update by Range to Track Association Strategy 124
8.1.1 Adaptation of the Kalman Filter 125
8.1.2 Adaptation of the Assignment Stage 126
8.2 Track Update by Frequency to Track Association Strategy . . 128

9 Experimental System 131
9.1 Single Sensor Hardware 131
9.2 Network Hardware 133
9.3 Sensor Positioning 133
9.4 Network coordinates 133

10 Single Sensor Experimental Results 137
10.1 Single Point Target Range Measurement 138
10.2 Single Extended Target Range Measurement 139
10.2.1 Deviation of Frequency Measurements 140
10.2.2 Investigation of Proposed Tracking Algorithm 140
10.3 Measurement of a Road Traffic Scenario 144

10.4 Discussion of Results 145

11 Radar Network Experimental Results 151
11.1 Single Point Target Detection and Position Measurement . . 152
11.2 Measurement of an Extended Target 157
11.3 Arbitrarily Oriented Extended Targets 161
11.4 Stop and Go Traffic Scenario 166

12 Conclusions 171

A Derivation of the LFMCW Base Band Receive Signal 173
A.1 Continuously Rising LFM Chirp 173
A.2 Stepped LFM Chirp 176

B Detection Theory 179
B.1 Maximum Likelihood Detector 179
B.2 Maximum a Posteriori Detector 180
B.3 Neyman-Pearson Detector 181
B.3.1 Proof of the Neyman-Pearson Lemma 182

C A Radar Simulation Tool (RASI) 185
C.1 Simulating a Radar Scenario 186
C.2 Developing a Radar Signal Processing System 186
C.3 Overview of RASI 187
C.4 Structure of the Simulation 188
C.5 Real Time Capability and Support of Hardware 190
C.6 RASI Used as an Environment for Prototypes 191
C.7 Results 192

List of Figures 193

Bibliography 197

Chapter 1

Introduction

1.1 Short History of Radar

The word RADAR is an acronym that stands for RAdio Detection And Ranging. The history of radar started at the beginning of the 20th century with an invention of the engineer Christian Hülsmeyer. Driven by the tragedy of a ship collision on the river Weser, the German engineer invented and built the first Radar in 1904 [Huelsmeyer 1904]. He called his invention the Telemobiloskop and the intended use was to detect approaching ships under foggy weather conditions, in other words an all weather collision avoidance system for ships. Although his presentations of the Telemobiloskop were internationally recognized, the engineer did not find financial support for his invention and finally dropped his work on radar.

Nevertheless, this was the beginning of what today is an independent field of electrical engineering. The first practical applications of radar were military. Radar techniques were developed to detect approaching ships and aircraft as early as possible. Today many of those techniques can be found within civil navigation for air and sea traffic control.

Also, the natural environment has increasingly become a favored object to be observed with radar systems. Weather radars are used in meteorology to detect areas with rain fall. Geology and geography examine the earth surface by using airborne synthetic aperture radars (SAR) or satellite SAR systems.

All these applications of radar have one thing in common: The radar device is the prominent center of a system which delivers data and services to a huge number of users. This way, despite the great cost of the radar itself, the construction and operation of these systems can be a profitable

business. The arrival of modern microwave technology has expanded the range of possible applications by making small and low cost radar sensors viable.

Today small radar sensors can be developed for basic detection and ranging tasks such as the measurement of the liquid level in a tank. More advanced systems that can resolve multiple targets and estimate the targets angular position are under development, some such systems are already available. Radar systems which enable the robust interpretation of a target scenario like a road traffic scene are currently under research. A radar with this performance allows many comfort and safety applications for road vehicles.

After a century of radar research, fields like automotive radar follow the inspiration of Christian Hülsmeyer and keep alive the idea to use radar for a safer journey and to protect human lives.

A detailed overview of the history of Radar can be found in [Willis 1991].

1.2 Automotive Applications

Automotive applications provide an interesting field of research in advanced radar systems today. Small automotive radar sensors are already available for adaptive cruise control (ACC) systems. However, new safety applications have higher demands on the sensor specifications. These new applications and appropriate sensors are still under research. Examples for safety applications are blind spot surveillance, pre-crash recognition, and collision avoidance.

1.2.1 Adaptive Cruise Control (ACC)

A standard cruise control system keeps the vehicle at a constant, preselected speed. An ACC system has an increased functionality. It keeps the vehicle speed constant until another car with a lower speed appears in the path of the controlled car. The ACC will then adapt the driving speed to the speed of the car ahead. When the car that is followed changes lane or accelerates, the ACC increases the speed until the preselected speed is reached.

The ACC system is a comfort system, although some systems also alert the driver when there is a potential danger of colliding with a preceding car. At present ACC radars solely detect moving objects as this is a situation readily managed by todays technology. The systems work well when the vehicle is on a highway and both the vehicle and the surrounding traffic is moving. An additional "stop and go" functionality increases the range of use to situations where the traffic ahead comes to a full stop.

It is crucial for an ACC system to correctly determine whether a preceding car is in the driving lane of the host vehicle or not. Practical systems equipped with a far distance sensor show that this is basically possible for moving objects. Moving objects can be separated well from other objects, especially from the many stationary objects in a typical traffic scene. Their target angle can be measured very precisely when integrating over multiple measurements. The actual difficulty lies within the prediction of the host vehicle's drive path.

The development of a "stop and go" functionality is aiming at the use of the ACC in dense traffic scenarios on motorways, in traffic jams, and in city traffic situations. In these situations, distances to other road users are smaller. To have sufficient time to react to a changing of lanes and in cut-in situations, a wide angular coverage of the near distance area around the front of the car is desired. The "stop and go" functionality also raises the question how to handle stationary objects that enter the observation area. Since it is not clear yet how the angular position estimation and the determination of the drive path can be made sufficiently accurate, the fallback solution is to react to stationary objects only if they were previously recognized as moving objects that have since decelerated to a full stop.

1.2.2 Blind Spot Surveillance

When turning or changing lane, other road users approaching on the neighboring lane can be overlooked. A blind spot surveillance system alarms the driver during a turn or lane change if another road user is getting dangerously close.

1.2.3 Pre-Crash Recognition

Safety systems for road vehicles like airbags and seat-belt tensioners have proven to be effective life-savers. These systems require some time to reach their maximum effectiveness. Especially for side-impact airbags that protect passengers from impacts in the area of the vehicle doors, the deployment time is still a very crucial point. Pre-crash recognition systems are under research to detect impacts earlier than conventional mechanical systems do, in order to gain a few milliseconds of time for the deployment of airbags and belt tensioners. Also, the type and severeness of the crash can be reported to adaptively adjust the restraint systems.

1.2.4 Collision Avoidance

The next level of complexity for radar aided safety applications is represented by collision avoidance systems. For these systems, a likely collision has to be detected early enough to have time for automatically initiated countermeasures. These can be applying the brakes or performing evasive maneuvers. The goal is either to completely avoid the crash or to at least reduce the energy of the impact.

While blind spot surveillance and pre-crash recognition applications are aiming at very specific situations, a collision avoidance system needs a detailed interpretation of the traffic scene including a prediction of the vehicles drive path. A collision avoidance application can be regarded as the extention of an ACC stop and go system that also reacts to stationary targets. To perform evasive maneuvers, the observation area has to be greater and oncoming traffic has to be detected. Additionally, this application requires a high target detection rate and a very low false alarm rate under all circumstances. This requirement is a real challenge in the system design.

Chapter 2

A Radar Network with Four 77 GHz Sensors

The basis of this work was given by the European research project "multi-functional automotive radar network" (RadarNet). One of the goals of this research project was to provide a common sensor network for a wide range of applications. Since all applications use the same data generated by all the available sensors, a great reduction in system complexity and cost can be achieved.

As shown in Figure 2.1, four distributed sensors are mounted along the front side behind the bumper of the vehicle. The individual sensor does not provide any measurement of the target angle. Instead, a network processor combines the range measurements of each individual sensor and does a target position estimation by means of lateration techniques. This strategy reduces complexity in the production of the individual sensors. The concept of trilateration is shown in Figure 2.2. Additionally, a long distance sensor is provided for ACC functionality.

Each sensor transmits a continuous wave (CW) signal in the 77 GHz domain. The CW signal is modulated by a linear frequency modulation (LFM) technique. This waveform allows the simultaneous measurement of target range and radial velocity. Also the relatively low complexity of the high frequency front-end for a CW sensor reduces the overall system cost.

Within this work, the signal processing software for the LFMCW processing in the individual sensor (single sensor processing) and the radar network processing are both investigated. For the first time 77 GHz LFMCW sensors were designed as near distance sensors to be used in a radar network. At first, classical LFMCW processing techniques were implemented

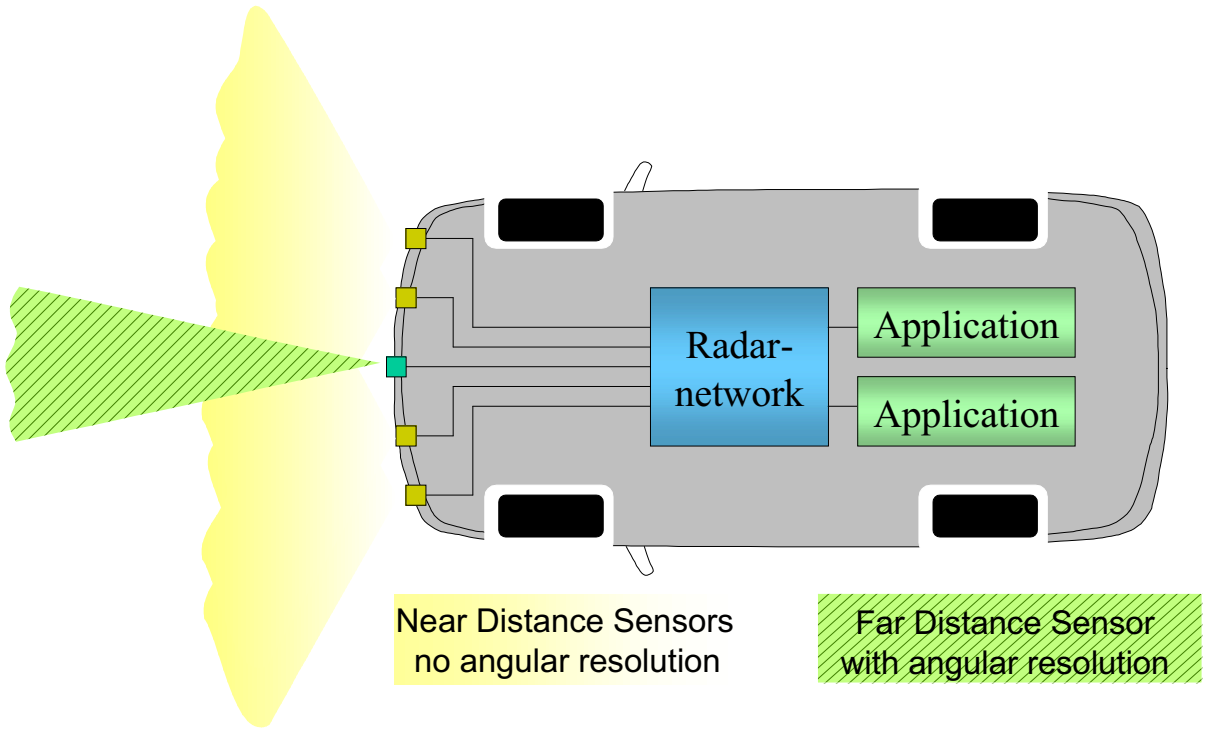

Figure 2.1: Radar network overview

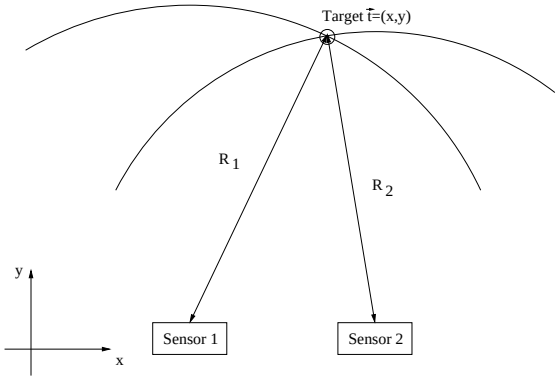

Figure 2.2: Concept of trilateration

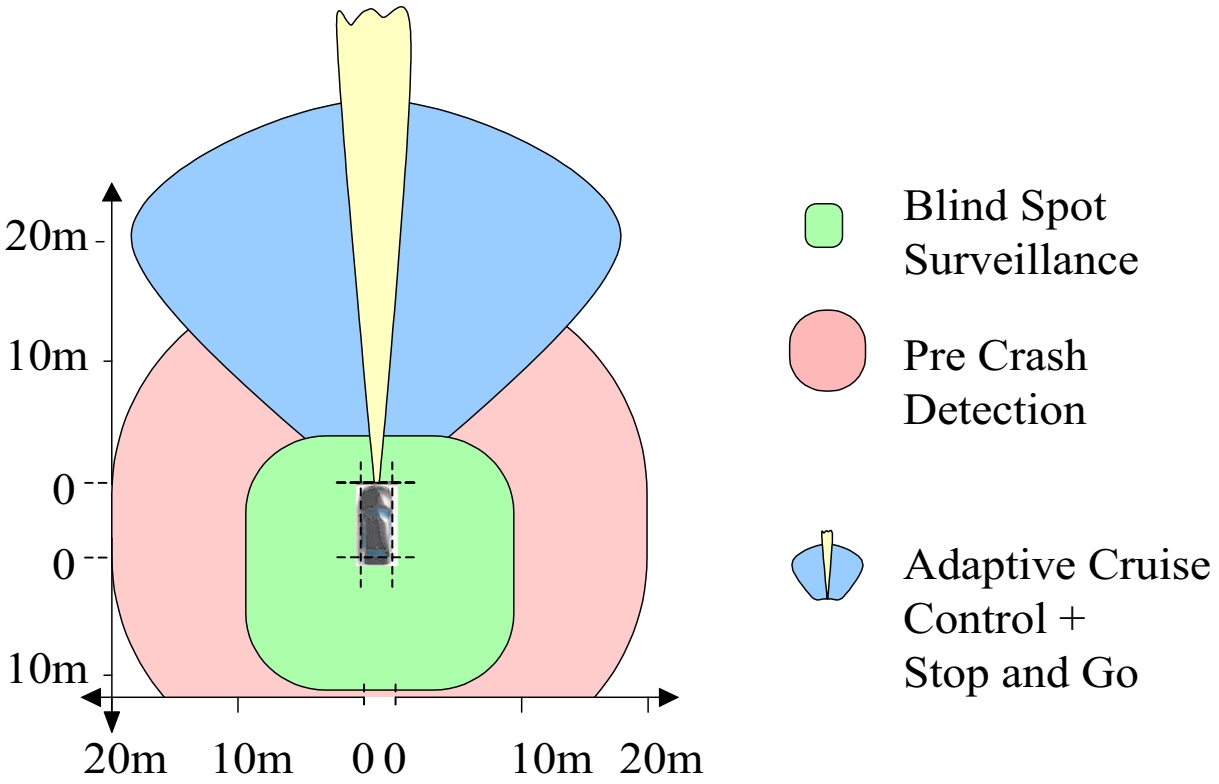

Figure 2.3: Observation areas for some applications

and it was recognized that these techniques had to be enhanced to achieve good results.

Also the classical radar network processing can be adapted to the characteristics of LFMCW sensors to improve performance.

2.1 System Requirements

The above-mentioned applications have different requirements on the radar system. Most obvious is the difference in the required observation area. As shown in Figure 2.3, the adaptive cruise control (ACC) application needs targets to be detected at a far distance but only within the drive path in front of the car. It therefore requires only a small azimuth coverage area. For the collision avoidance system, a wide area around the car needs to be observed to also detect traffic from the side. The blind spot surveillance has to observe the sides of the car. The pre-crash sensing application should be able to detect impacts in all areas of the car where deployment of passenger restraint systems is useful.

Collision avoidance and pre-crash sensing are safety applications that should quickly react on potentially colliding objects with high relative velocities. Therefore, these applications have a particularly high demand for fast object detection and a high update rate of the target reports to the application.

The ability of the radar system to resolve targets with different ranges and velocities is a requirement of nearly all applications that have to interpret road traffic scenes.

The following table shows possible specifications of the radar network requirements for different applications. These values are commonly agreed to be a useful basis on which to do research for the described automotive applications.

Parameter		ACC	Pre-crash	Collision avoidance
Target acquisition time	/ s	0.3	0.03	0.03
Update rate	/ Hz	50	100	100
Max. range	/ m	170	25	30
Range accuracy	/ m	0.1	0.1	0.1
Range resolution	/ m	>2	1	0.1
Angular accuracy	/ deg	<1°	1°	0.5°
Angular resolution	/ deg	-	5°	2°
Max. rel. velocity	/ $\frac{m}{s}$	50	-5	100
Min. rel. velocity	/ $\frac{m}{s}$	-110	-250	-160
Velocity accuracy		$0.5\frac{m}{s}$	5%	2%
Velocity resolution	/ $\frac{m}{s}$	2	3	3

Table 2.1: Radar system specifications for researched applications

The target acquisition time is the maximum time the radar system has available to report a new target that has entered the observation area. For most applications, the actually critical parameter is the time available to react to a detected target. This time depends on the maximum expected object speed, the range of the observation area and the target acquisition time.

For safety applications the range- and angular resolution needs to be good enough to resolve all objects of interest. To react to moving targets, the ability to resolve targets by their velocity can replace the need for a high range or azimuth resolution.

2.2 Requirements for Networked Single Sensors

The radar network approach is to process the ranges measured by the individual sensors within a central radar network to obtain the target azimuth angle. Instead of measuring the angle by monopulse or sequential lobing techniques, the range measurements from spatially distributed sensors are trilaterated. In the previous section, Figure 2.2 shows the principal of the trilateration technique.

From this measurement principle it follows that the single sensor range accuracy needs to be very high to achieve good angular measurement results [Klotz 2002]. In numbers, the single sensor range accuracy needs to be in the range of 3 cm. It has been shown that this is technically accomplishable. Section 6.7 goes into the connection between sensor range accuracy and network position estimation accuracy in more detail.

LFMCW processing has proven to be practically useful for many applications. A major benefit of the used waveform is that it meets an important requirement of many applications. It is possible to measure target range and radial velocity simultaneously even in multitarget situations. Knowing this, it is of interest under which circumstances and for which applications the described radar network based on the 77 GHz LFMCW sensors is useful.

Chapter 3

Radar Waveforms

Every radar system utilizes the same physical effect of electromagnetic wave propagation. The radar transmits a high frequency signal and listens to backscattered echoes. The modulation used on the transmitted signal is called "waveform". The two basic types of waveforms used for radar systems are the pulse waveform and the continuous waveform (CW). The radar waveform used for the single sensors is an important question in the design of a radar network.

A pulse radar transmits a short pulse and afterwards listens for a certain time for backscattered signals arriving at the receiver. If multiple targets with different distances are within the observation area, the radar will receive multiple echoes at different times.

The CW radar on the other hand transmits and receives continuously, so it needs a more sophisticated way of resolving the superposed echo signals from multiple targets. As far as the design of the high frequency part of the sensor is concerned, the CW radar is less complex than the pulse radar.

The waveform of a pulse radar is usually visualized with a signal power versus time graph while the instantaneous frequency is shown for a CW waveform, this can be seen in Figure 3.1.

The CW-Radar, due to its nature, needs additional frequency modulation to resolve or at least measure target range at all. Two common types of frequency modulation suitable for a CW radar are:

- Linear frequency modulation,
- frequency shift keying.

Pulse and CW modulation techniques are not mutually exclusive, as a combination of both techniques shows [Mende 1999].

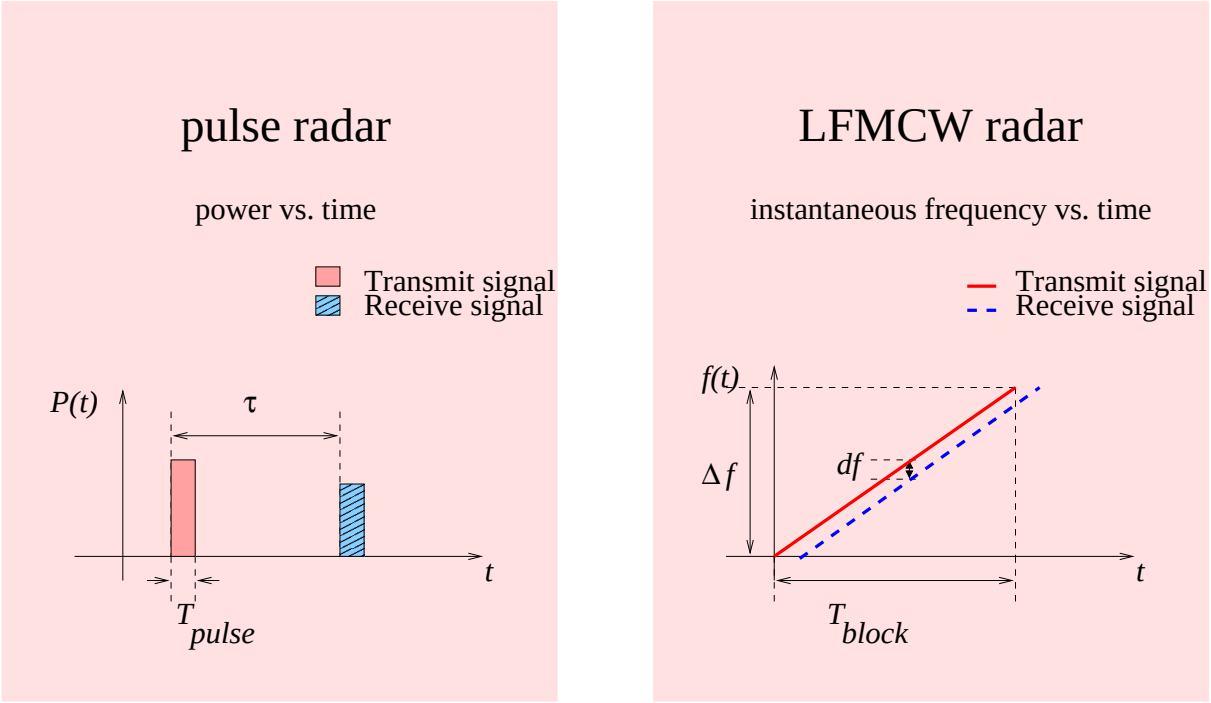

Figure 3.1: Pulse- and linear frequency modulated waveform

3.1 Observable Target Parameters

The radar is used to detect objects in the observation area and to retrieve information about these objects. The waveform plays an important role in the ability of the radar to detect objects and measure their parameters. For detection and measurement the radar transmits the waveform and interprets the objects backscattered echo signals. Most commonly, the following object parameters are estimated by the radar:

target parameter	physical equivalent
range R	signal propagation delay τ
radial velocity v_r	Doppler frequency shift f_D
azimuth/elevation	direction of wave / antenna directivity (not waveform relevant, discussed in Sec.6.1)

Table 3.1: Object parameters measured by the radar

The waveform predominantly determines how the target parameters range R and radial velocity v_r are measured within the radar. For automotive safety applications range and radial velocity need to be measured simultaneously.

3.1.1 Target Range

The target range parameter R refers to the distance between the radar antenna and the target. The target range is proportional to the time τ it takes the signal to travel from the radar transmitter to the reflecting target and back to the radar receiver:

$$R = \frac{c \cdot \tau}{2}$$

Where c is the speed of light.

3.1.2 Target Radial Velocity

The relative radial velocity v_r between target and radar is determined by the Doppler effect. Christian Doppler discovered around the year 1840 that the frequency of a received sound wave is changed depending on the relative velocity between transmitter and receiver. The same effect occurs when a radar receives a reflection from a target that has a radial velocity relative to the radar. The Doppler effect is caused by the continuous change of distance between the radar and the target that squeezes or expands the receive signal in time. Assuming a target at initial range R_0 with constant radial velocity v_r, the receive signal $r(t)$ is delayed by the time dependent signal propagation delay $\tau(t) \approx \frac{2(R_0+v_r t)}{c}$. In the case of a transmit signal $s(t)$ being a harmonic oscillation with frequency f_C, the Doppler shift of the received oscillation can be determined as follows:

$$s(t) = sin\left(2\pi f_C t\right)$$

$$r(t) \approx s\left(t - \frac{2(R_0 + v_r t)}{c}\right)$$

$$r(t) \approx sin\left(2\pi f_C \left(t - \frac{2(R_0 + v_r t)}{c}\right)\right)$$

$$r(t) \approx sin\left(2\pi f_C t - 2\pi f_C \frac{2v_r}{c} t - \varphi_R\right)$$

The middle term of the sine function argument contains the Doppler frequency shift:

$$f_D \approx -\frac{2 f_C v_r}{c} = -\frac{2v_r}{\lambda}$$

Where λ is the signal's wavelength $\lambda = \frac{c}{f_C}$. Only the radial component of the relative target velocity has an impact on the Doppler frequency. The tangential component has no impact on the deviation of the target range and so does not add to the Doppler frequency shift.

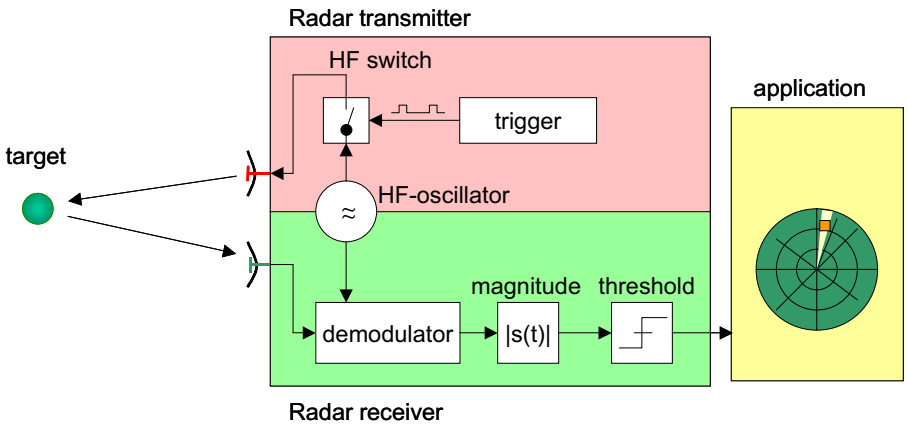

Figure 3.2: Simple pulse radar

3.2 Pulse Radar

Figure 3.2 shows a simple pulse radar with a transmitter and receiver circuit. The transmitter, generating the transmit signal, and the receiver, down converting the echo signal, use the same oscillator. Therefore the radar receives the echo signal coherently. The example shows a quadrature demodulator that produces a complex low pass signal.

The transmitter issues short pulses of duration T_P. It repeatedly transmits these pulses with the Pulse Repetition Frequency $PRF = 1/T_{PI}$. In the time between the transmissions, the receiver listens to backscattered echoes and down-converts the incoming receive signal into base band. In this very simple example, the phase of the received echo signal is discarded and the magnitude is compared with a threshold.

3.2.1 Range Measurement

Let us assume a target at a distance of R_1. The radar transmits the first pulse at $t = t_0$. The pulse will propagate as an electromagnetic wave at the speed of light $c \approx 3 \cdot 10^8 \frac{m}{s}$. At the target, a fraction of the wave is reflected back to the radar. The complete delay of the wave is $\tau_1 = \frac{2R_1}{c}$. Since the transmit pulse was issued at t_0, the reflected wave is received at time $t = t_0 + \tau_1$. Via the relation $R = \frac{\tau c}{2}$, the target distance is obtained.

3.2.2 Range Resolution

Figure 3.3 shows the signal power of the transmit and receive signal over time for a scenario with 2 targets at ranges R_1 and R_2. In this example, the two targets are well separated from each other. If the distance between

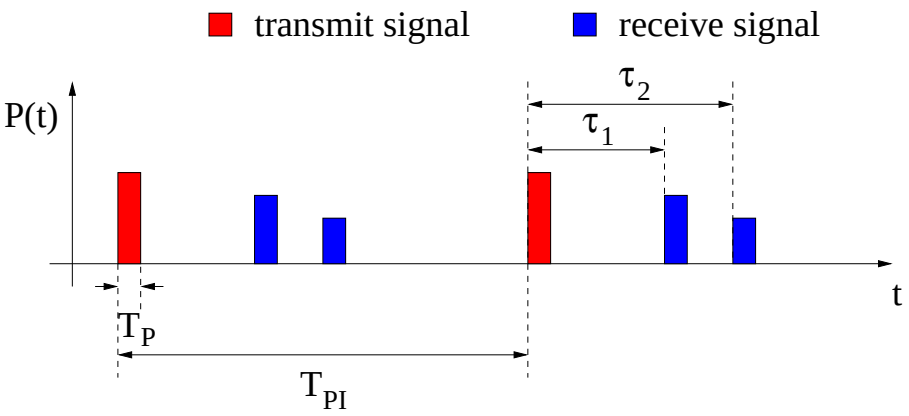

Figure 3.3: Pulse waveform, transmit and receive signal versus time

the two targets gets smaller, at some point, the targets magnitude peaks will be superposed. The superposition will result in one peak and the two targets will appear as a single one.

The target resolution $\triangle R$ denotes the minimum difference in distance between two targets required to detect them as two separate targets. For the pulse radar, the target resolution is calculated from the pulse width T_p by $\triangle R = \frac{cT_P}{2}$.

In a real system the transmit and receive peaks are not perfectly rectangular, but due to a limited bandwidth in the transmitter and receiver are smoothened and may contain side-lobes. Usually a pulse shaping filter is used to constrain the spectral output of the transmitter. For this case, the 3 dB width of the shaped pulse is taken as the pulse duration. This definition of resolution also assumes, that the two targets have the same amplitude within the receiver. Otherwise, if one peak is much smaller, it will be masked by the greater peak even for $\triangle R > \frac{cT_P}{2}$.

3.2.3 Range Ambiguity

Another constraint is introduced by the repetition of the pulses with the Pulse Repetition Frequency $PRF = 1/T_{PI}$. If the target echo delay τ is greater than the time between pulses T_{PI}, the echo will be received after the next pulse is transmitted. This will happen for target distances greater than $R_{unamb} = \frac{cT_{PI}}{2}$. If range measurements greater than R_{unamb} are possible, the target range measurement is ambiguous:

$$R = \frac{c\tau}{2} + n \cdot \frac{c}{2PRF} \quad n >= 0$$

3.2.4 Estimation Accuracy

The range estimation accuracy on a point target depends on how accurately the position of the peak within the receive signal can be estimated. The estimation accuracy depends on the signal to noise ratio (SNR). Even for a low SNR of $10dB$, the average range estimation accuracy is much better than the range resolution (3 dB width of the peak).

3.2.5 Pulse Doppler Radar

The target radial velocity introduces a Doppler shift of the echo signal frequency. After down conversion, the frequency of the base band receive signal is identical to the Doppler shift of the HF signal. The coherent mixing process makes it possible to measure the Doppler frequency by observing the complex value of the target's echo signal over time.

The radar receiver as described previously has to be upgraded with a memory to store these complex echo values over many measurements. This is done for every range gate separately. Doing this for multiple cycles, for every range gate there is a sampled time signal available. The sample rate is the PRF. The Doppler frequency can be resolved by doing a spectral analysis over each range gate time signal. With this range-Doppler pulse radar targets can additionally be resolved by their velocities.

3.3 Continuous Wave Radar without Range Resolution

A radar that continuously transmits an electromagnetic wave is called a Continuous Wave (CW) radar. Along with the transmission of the CW signal, the radar continuously listens to backscattered echo signals. The CW radar differs in this from the pulse radar that sends out short pulses and listens to echo replies in-between.

The CW radar measures continuously, so multiple target echoes are additively superimposed within the receive signal. To measure a target's range or to even resolve targets by range, a CW radar needs additional modulation.

The near distance sensors that are used for the radar network described in Chapter 6.2, work according to the CW principle. The sensors use linear frequency modulation (LFM) to measure target range and target Doppler frequency simultaneously.

In the following, a short introduction to the CW modulation is given and the monofrequency CW radar and the FSK CW radar are introduced.

Radars that work according to either of these techniques can not resolve range. In the next section, the LFMCW modulation is introduced and the principles of resolving target range and Doppler with an LFMCW waveform are explained. Finally, the waveform is described that was developed for the sensors of the radar network.

3.3.1 Mono-frequency CW Radar

A CW radar without any modulation is called a mono-frequency CW radar. The waveform is shown in Figure 3.4 together with an example receive signal. The base band receive signal and its FFT transformed squared magnitudes are shown on the right. A target echo is represented in the baseband receive signal as a harmonic oscillation. The frequency of this oscillation depends solely on the Doppler shift due to target motion.

If the signal is processed digitally, the base band time signal is sampled by an A/D converter. The sampling rate should be chosen to unambiguously measure all Doppler frequencies that can occur. Usually, a signal block consisting of many consecutive samples is Fourier transformed and the target detection and frequency measurement is done in the spectral domain.

The mono-frequency CW radar is only able to resolve targets by their velocity, not by their range. This type of radar is used in situations where only the speed of an object is required, for instance it is used by a police radar to check your driving speed or at sports events to measure the speed of a football. This type of radar is neither able to resolve nor estimate target range.

3.3.2 FSK CW Radar

The CW signal has to be modulated to measure target range. The simplest modulation scheme is the frequency shift keying (FSK) modulation. The FSK radar alternately switches the frequency of the transmit signal between two distinct frequencies f_0 and f_1. Switching from f_0 to f_1, the signals wavelength is changed and so the phase of the receive signal is shifted from φ_0 to φ_1. The phase shift $d\varphi = \varphi_1 - \varphi_0$ in the receiver depends on the two frequencies f_0, f_1 and the target range parameter R.

$$d\varphi = \angle\, e^{4\pi\, R\,(f_1 - f_0)/c}$$

The phase shift is measured and used to estimate the target range.

The preferred way to process the FSK receive signal is to use digital signal processing. In the same way as described for the monofrequency CW radar, a consecutive signal block is processed at once. The FSK modulation is usually done by quickly alternating between the two frequencies for

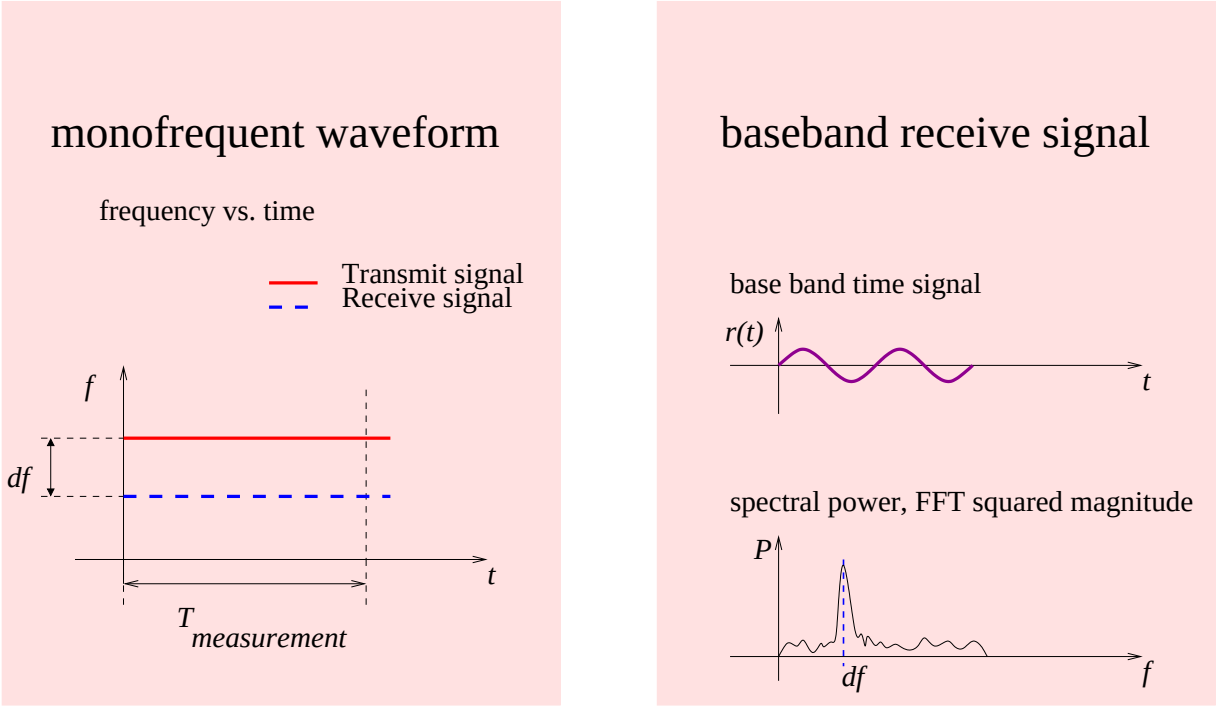

Figure 3.4: Mono-frequency CW waveform and an example baseband signal

each sample taken by the A/D converter. The digitized signal can be interpreted as being two monofrequency measurements that are intertwined. The samples r_{2k} belong to one monofrequency measurement using transmit frequency f_0, the samples r_{2k+1}belong to the measurement using f_1.

The two signals are separated and Fourier transformed. Apart from a phase shift, the two spectra are identical. Target detection is done in the spectral domain. Since the echo signal frequency only depends on the target velocity, the FSK radar can only resolve targets by velocity but not by range. When a target can be resolved, its range can be estimated by the phase shift between the two (complex valued) spectra.

3.4 Linear Frequency Modulation

The linear frequency modulated continuous wave (LFMCW) radar measures the range and Doppler frequency of a target simultaneously. Using a waveform as described in the following, it is possible to resolve multiple targets by range and velocity.

The LFMCW radar transmits a linear frequency sweep from a start frequency f_0 to a stop frequency f_1. This frequency sweep is also called a chirp. The bandwidth of the chirp is the frequency range that is covered by the transmitter: $\Delta f = f_1 - f_0$.

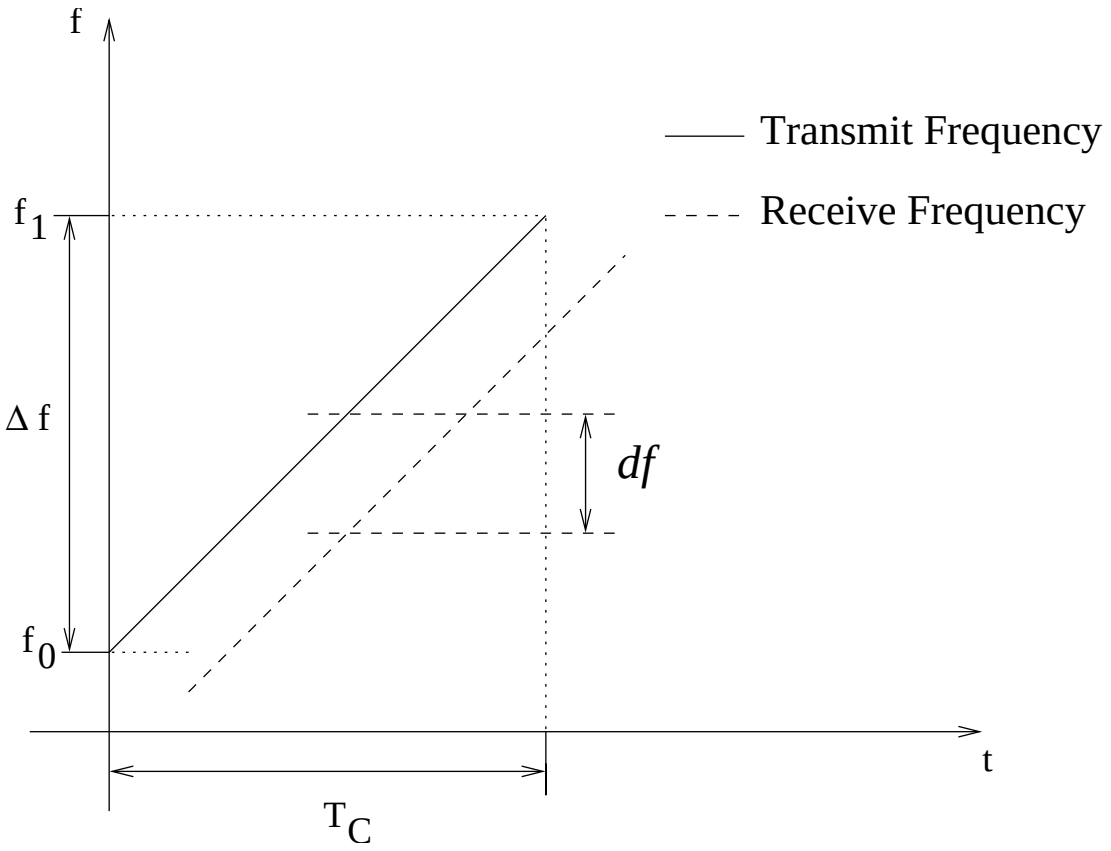

Figure 3.5: Instantaneous frequency of an LFMCW sweep

During the transmission of one sweep, the instantaneous transmit frequency changes linearly with time, as shown in Figure 3.5. The parameters of the transmitted sweep are:

- Start frequency: f_0
- Stop frequency: $f_1 = f_0 + \Delta f$
- Sweep/Chirp duration: T_C

The graph also shows the instantaneous frequency of a receive signal resulting from the echo return of one target. The receive signal is shifted in the frequency direction by the Doppler frequency due to the targets radial velocity. The receive signal is additionally delayed by its propagation delay.

It is important for understanding the CW radar that the receiver down-converts the echo signal to the base band by mixing the receive signal with the currently transmitted signal. In this way, the base band signal will be a harmonic oscillation and its frequency value will be equal to the difference between the current HF transmit and receive frequency from an echo reply.

The frequency difference *df* depends on the Doppler shift and the signal propagation delay. The Doppler frequency depends on the target velocity

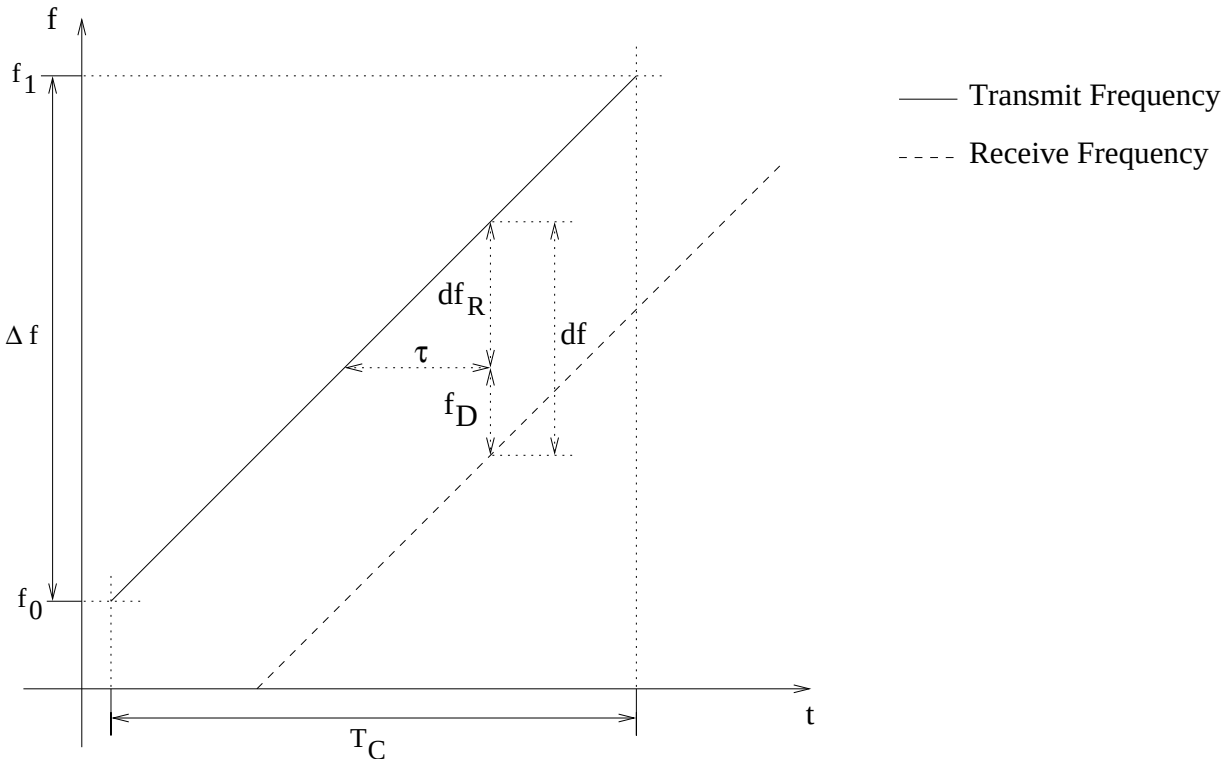

Figure 3.6: Frequency shift due to signal delay and Doppler

v_r:

$$f_D = -\frac{2f_C v_r}{c}$$

The propagation delay τ also results in a frequency shift. The delay τ in turn is directly proportional to the target range:

$$df_R = -\frac{\Delta f}{T_C}\tau = -\frac{\Delta f}{T_C} \cdot \frac{2R}{c}$$

The frequency shifts due to the Doppler effect and due to range simply add up to one complete frequency shift as can be seen in Figure 3.6. The receive signal, down converted to base band, has a frequency value identical to this frequency difference:

$$df = f_D + df_R = -\frac{2f_C}{c}v_r - \frac{2\Delta f}{cT_C}R \tag{3.1}$$

To process the LFMCW base band signal, it is sampled and digitized by an A/D-converter. If there are multiple echo signals from multiple targets, they will be superimposed in the receive signal. To resolve, detect and estimate the involved frequencies a spectral analysis is performed on the base band time signal. For this task a discrete Fourier transform is commonly used.

3.4.1 Measurement of Range and Velocity for a Single Target

It is desired to estimate the targets range R and velocity v_r. However, a single chirp measurement gives only a frequency value df for each target.

This frequency value df is linked to R and v_r through equation 3.1. Since many R,v_r combinations fulfill this equation, R and v_r are said to be measured ambiguously. This dependency between R and v_r for a single chirp measurement can be represented graphically as a straight line in a range-velocity graph, as shown in Figure 3.7. The gradient of the range-velocity line depends on the chirp gradient $\frac{\Delta f}{T_C}$.

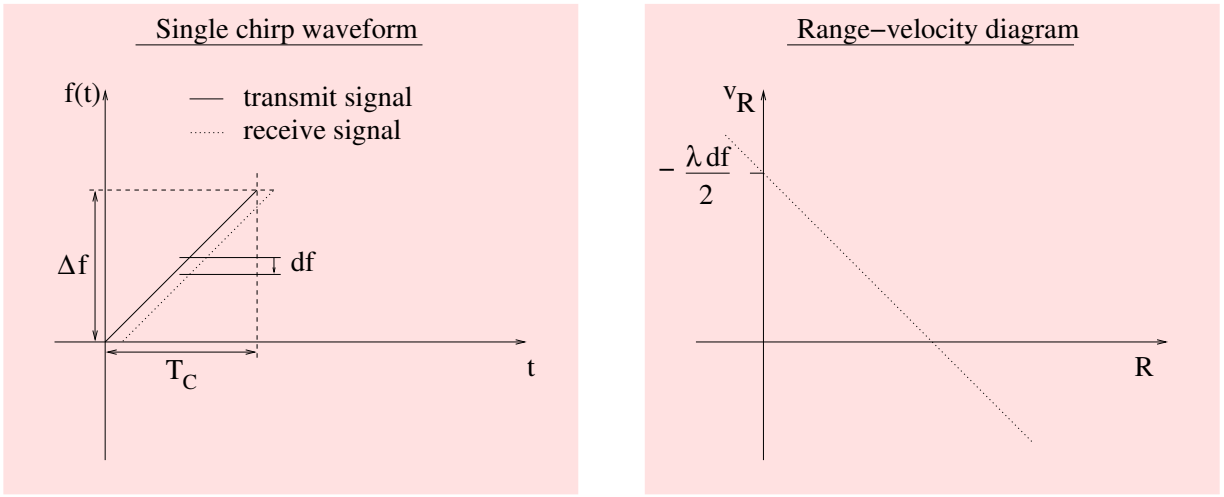

Figure 3.7: Single chirp waveform with positive sweep rate Δf (left) and corresponding R-v_r diagram for a single target measurement (right)

A common technique [Ludloff 2002] uses two chirps with opposite frequency gradients. Represented graphically, two measurements of a target, done with different gradients, produce two lines that are intersecting in one point (Figure 3.8).

Graphically, the target range and velocity is derived by searching for the cross section of the two lines in the graph. Numerically, the two equations from the two chirps measurements have to be solved for R and v_r.

3.4.2 Multiple Target Situations

The technique described above works satisfactory as long as there is only one target. For two targets, there are four cross sections in the range-velocity graph (Figure 3.9). Two of them represent the correct assignments for the two range-velocity pairs. Two of them are a by-product of the real targets.

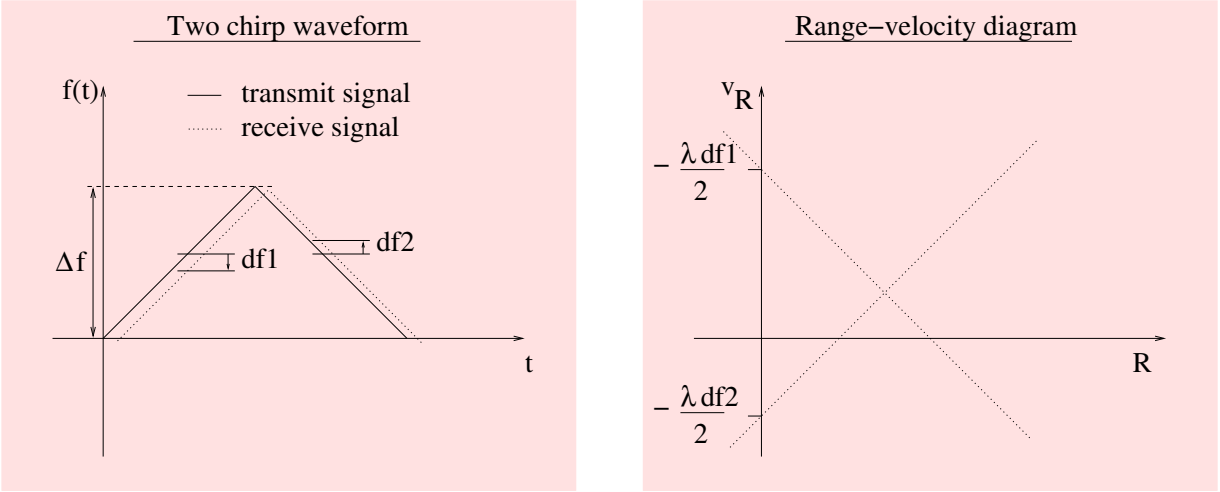

Figure 3.8: Two chirp waveform with sweep rates of opposite sign and corresponding R-v_r diagram for a single target

These wrong combinations are commonly referred to as ghost targets. Some of these wrong combinations could be sorted out in the following processing stages, however, this becomes unreliable and impractical with a growing number of targets as with n targets there are about $n^2 - n$ ghost targets.

3.4.3 Ghost Target Reduction by Using Multiple Chirps

Most of the ghost targets can be filtered out by using more than 2 chirps. In the range-velocity graph, using 4 chirps with different sweep rates, a valid target will produce a cross section with 4 lines intersecting in one point (Figure 3.10). A situation where 4 lines are accidentally intersecting in one point is rare and might easily be handled in further signal processing stages. This technique of reducing the ghost target detections has been published in [Meinecke 1998, Rohling 1998].

A useful waveform consists of 4 chirps. This is a trade-off between the probability of the accidental detection of a ghost target and the measurement time. Chapter 4 explains the algorithms and looks at the performance in detail. A quantitative investigation can also be found in [Meinecke 2001].

Figure 3.11 shows the proposed waveform that is used for the discussed LFMCW near range sensors. The chosen values for the parameters are:

$$f_0 = 76.5GHz$$

$$\begin{array}{ll} \Delta f_{chirp1} = \Delta f & \Delta f_{chirp2} = -\Delta f \\ \Delta f_{chirp3} = \frac{\Delta f}{2} & \Delta f_{chirp4} = -\frac{\Delta f}{2} \end{array}$$

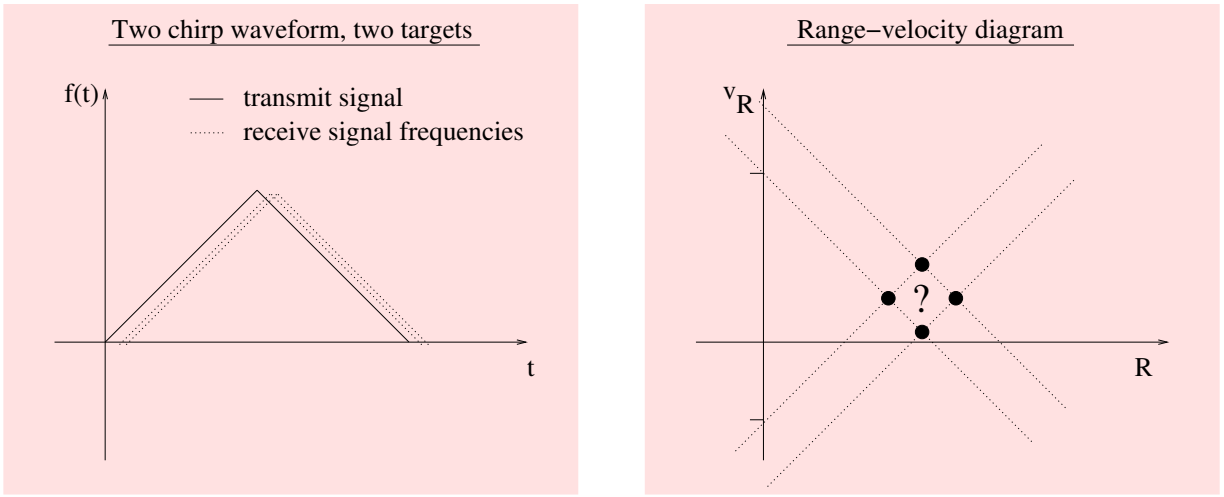

Figure 3.9: Two chirp waveform, corresponding R-v_r diagram for two targets. Two frequencies measured for each chirp yields 4 cross sections

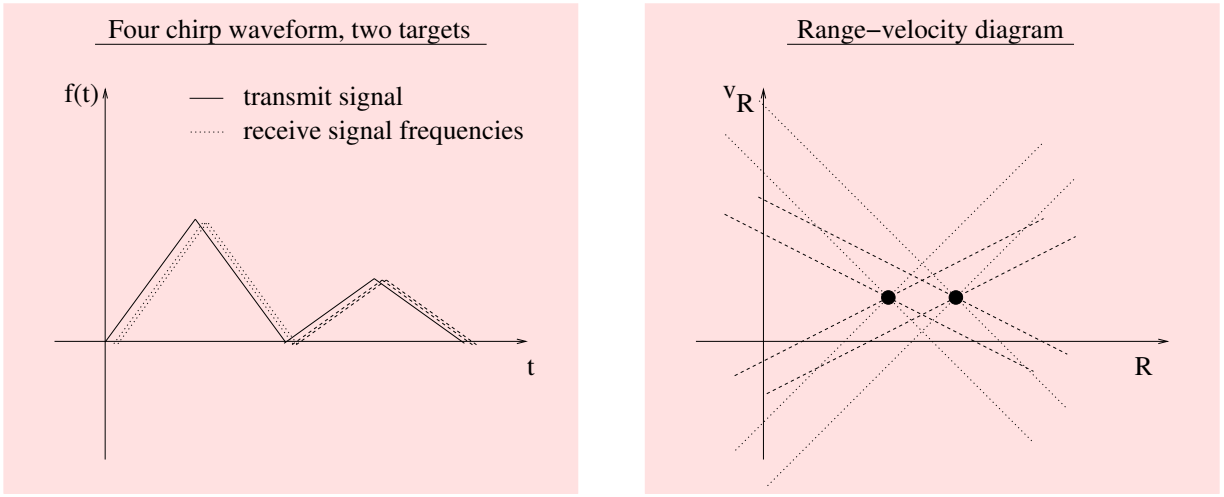

Figure 3.10: Four chirp waveform and corresponding R-v_r diagram for two targets. Using four chirps, there are 4 lines going through the valid cross sections for the real targets.

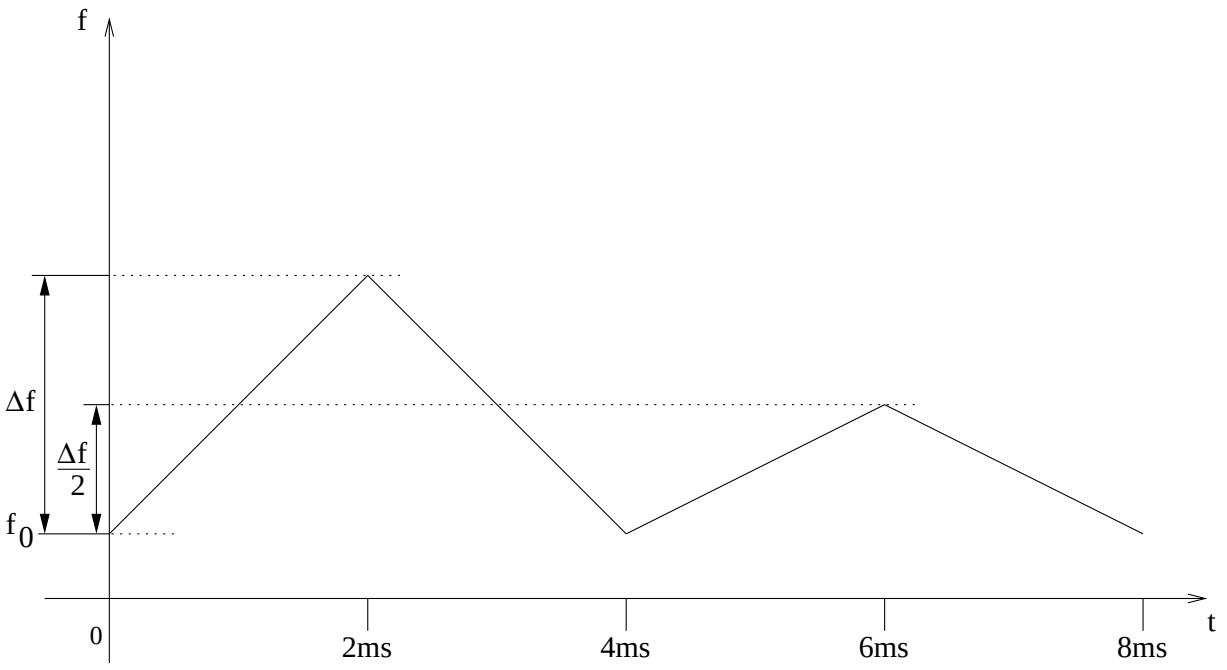

Figure 3.11: Proposed waveform consisting of 4 chirps

$$T_{chirp1} = T_{chirp2} = T_{chirp3} = T_{chirp4} = T_C$$

The parameters $\triangle f$ and T_C are chosen to meet the technical capabilities, where especially the sweep gradient $\frac{\triangle f}{T_C}$ is technically limited and the bandwidth $\triangle f$ is also a frequency allocation issue. Because transient responses occur when changing the frequency gradient, there are intervals at the beginning of chirps that are not used for processing. Because of the currently available hardware the following parameters are chosen:

$$\triangle f = 450MHz$$

$$T_C = 2ms$$

The practically realized waveform is shown in Figure 3.12. The useful bandwidth for the first two chirps is 450 MHz, the last two chirps have half the bandwidth. The transmit signal is shown dashed for the settling time and a flat time, indicating that these intervals are not used for the measurement.

3.4.4 Additional Considerations

Practically all modern LFMCW sensors work according to the stepped LFMCW principle, which is a slight variation of the LFMCW concept.

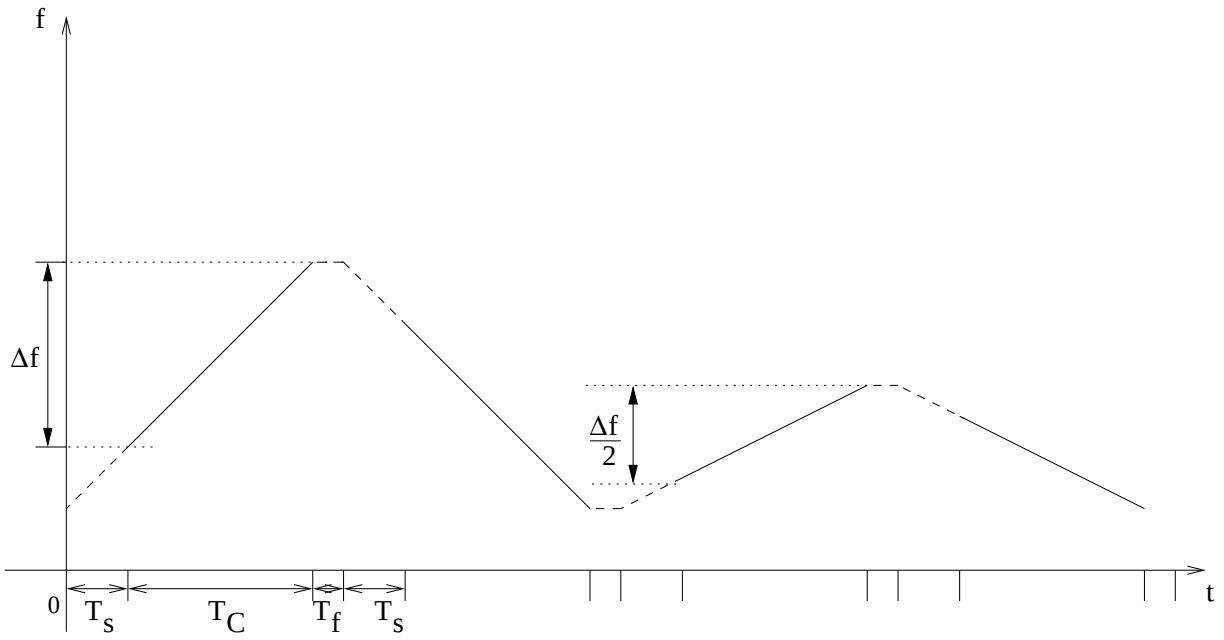

Figure 3.12: Practically realized waveform

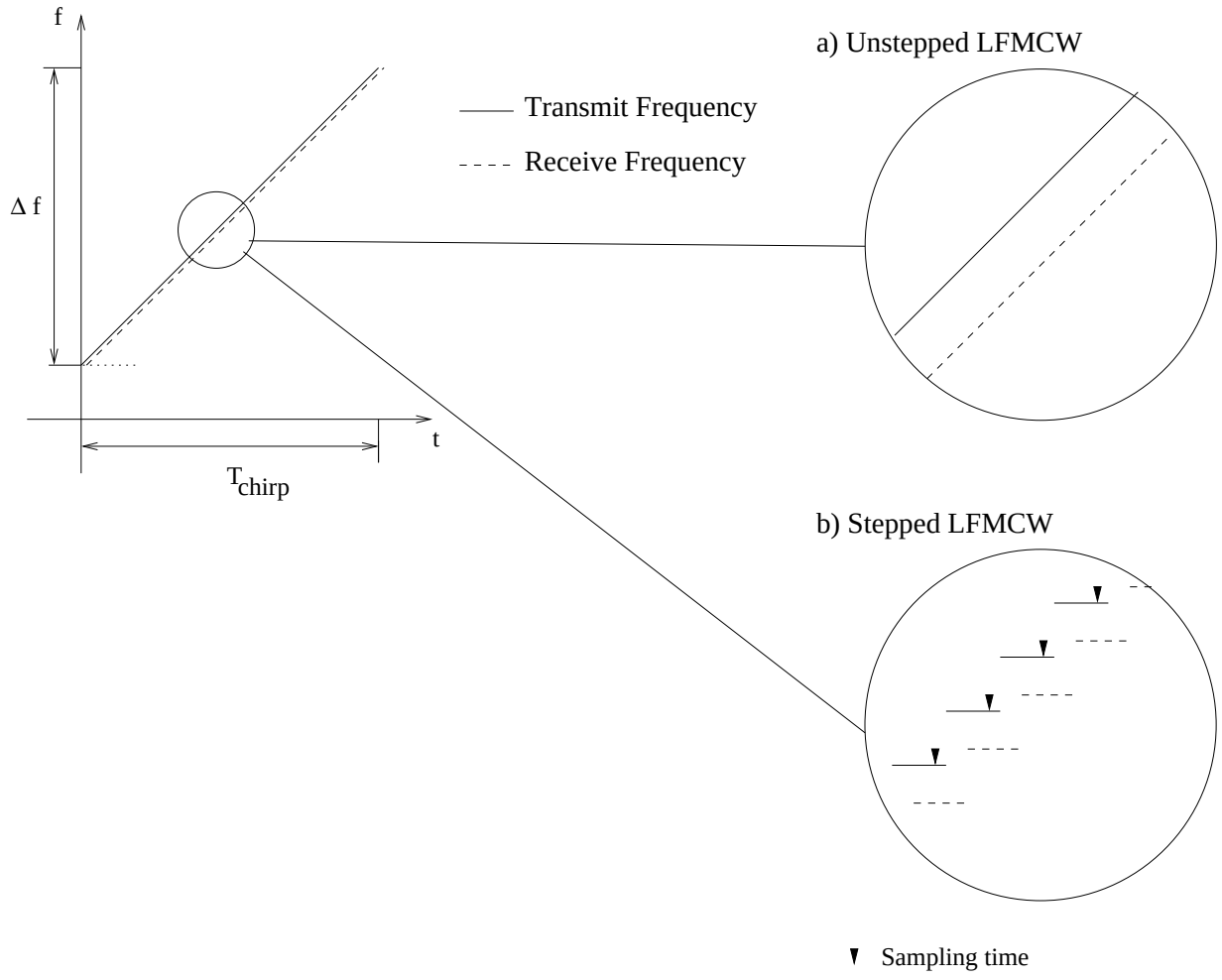

Figure 3.13: Difference between a) un-stepped and b) stepped waveform

A stepped LFMCW radar increases the instantaneous transmit frequency in little quantities instead of using a smooth gradually rising frequency sweep as transmitted by an analog LFMCW radar. The difference is shown in Figure 3.13. The receive signal is sampled in constant intervals determined by the A/D converters clock rate, and the transmit signal is synchronously changed with that sampling rate.

A stepped LFMCW Radar has some technically convenient features as described in [Mende 1999]. As far as the resulting receive signal and the processing is concerned, there is just a minor difference: The starting phase of a targets echo signal in the baseband domain is different to the un-stepped version.

In Appendix A, the down-converted receive signal is analytically determined for both the analog and the stepped LFMCW radar. The results of these calculations are of course consistent with the graphical approach from above in section 3.4. The results are also consistent with the intuitive idea that the stepped waveform will lead to harmonic oscillations of the same frequencies as the analog LFMCW waveform. The signal processing schemes are exactly the same for both the LFMCW and the stepped LFMCW radar. Apart from these results, the equations derived in Appendix A can be used for simulating a (stepped) LFMCW radar front-end.

The stepped LFMCW radar makes it easy to compensate non-linearity in the voltage controlled oscillator (VCO) of the radar front-end. This is done by maintaining a lookup table for driving the VCO control voltage.

When simulating a radar front end, these non-linearities of the VCO can also be incorporated into the simulation. The equations derived in Appendix A can easily be adapted to include nonlinear behavior of the VCO.

However, the LFMCW sensors described in this thesis generate the transmit signal by a digital synthesizer. Therefore, the generated waveform follows the targeted frequency value very precisely, so no additional compensation of non-linearities is necessary in this case.

Chapter 4

Single Sensor Processing

4.1 LFMCW Processing Overview

The preceding chapter introduced the basic concept of a linear frequency modulated continuous wave (LFMCW) radar. It also introduced a useful waveform sequence consisting of four chirps, all with different sweep gradients (Figure 3.12). The signal processing described in this chapter is based on this waveform sequence.

The analog part of the processing consists of the mixer and the analog to digital conversion unit. All further processing is done digitally. An overview of the system design can be seen in Figure 4.1. The proposed digital signal processing consists of two major parts:

1. A spectral analysis to resolve and estimate the frequency values of the echo signals.

2. A frequency to range-velocity algorithm to resolve the desired target parameters from the detected frequencies.

After down mixing and A/D converting the receive signal, the spectral analysis is the first step of digital signal processing. The spectral analysis detects and estimates the frequency components in the receive signal. The analysis is done for the received time signal of each chirp separately. The digitized receive signal is buffered, so that the signal from a complete chirp can be processed at once. The implementation of the spectral analysis is summarized in Figure 4.2.

In multiple target situations the digitized and buffered signal consists of multiple additively superimposed target echoes with different frequencies. In order to resolve these frequencies, an FFT algorithm is used.

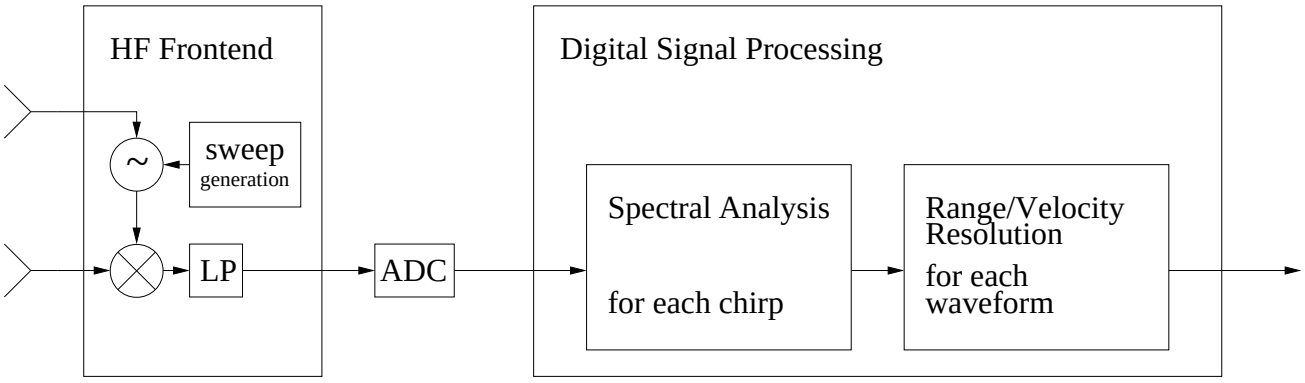

Figure 4.1: Overview of LFMCW sensor

Prior to the FFT processing the time domain signal is windowed. Multiplying the time domain samples by a window function is commonly done to reduce the side lobes of the spectral peaks.

The squared magnitudes from the FFT bins are an estimate of the spectral power. In this power spectrum, targets are represented by peaks, see Figure 4.3. This representation is very similar to a pulse radar measurement which is divided into range gates. Because of this similarity, the further processing strategies for detecting peaks in the measured signal are classical pulse radar processing techniques.

To detect the peaks contained in the spectrum, a constant false alarm rate (CFAR) algorithm is used. The algorithm separately compares the signal power in each bin to an adaptive threshold. For each bin whose power value is above the threshold, the algorithm decides that the bin signal corresponds to a target and writes the index of the bin to a detection list. This entry gives information about the frequency of that echo signal in integral multiples of the FFT bin width.

A center of gravity algorithm is used to estimate the exact frequency value of the detected peaks on a sub-bin level.

The final stage is the target range-velocity processing. While the previous stages process each chirp separately, the range-velocity processing combines all four chirp measurements to estimate target range and velocity from the frequency measurements.

The following sections describe the parts of the spectral analysis and the range-velocity processing in detail.

4.2 Windowing and FFT

The sampled time domain signal is expected to consist of one or multiple target echos, each adding a specific frequency component to the signal. The

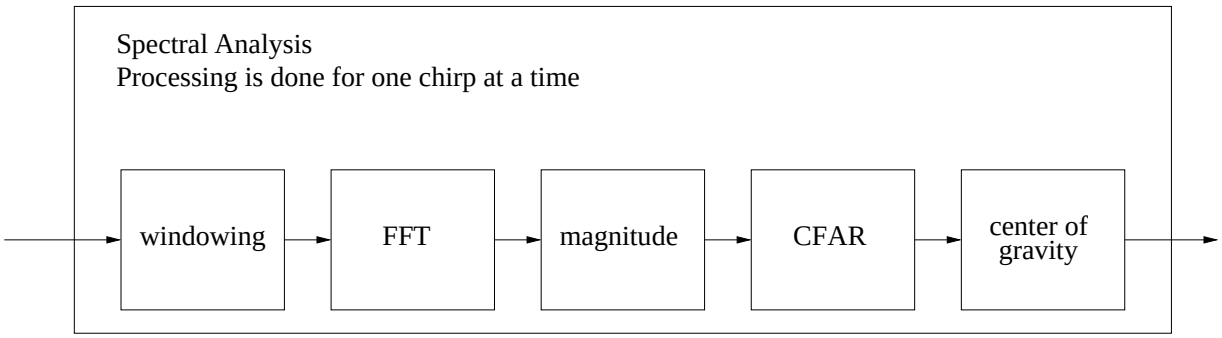

Figure 4.2: Overview of spectral analysis

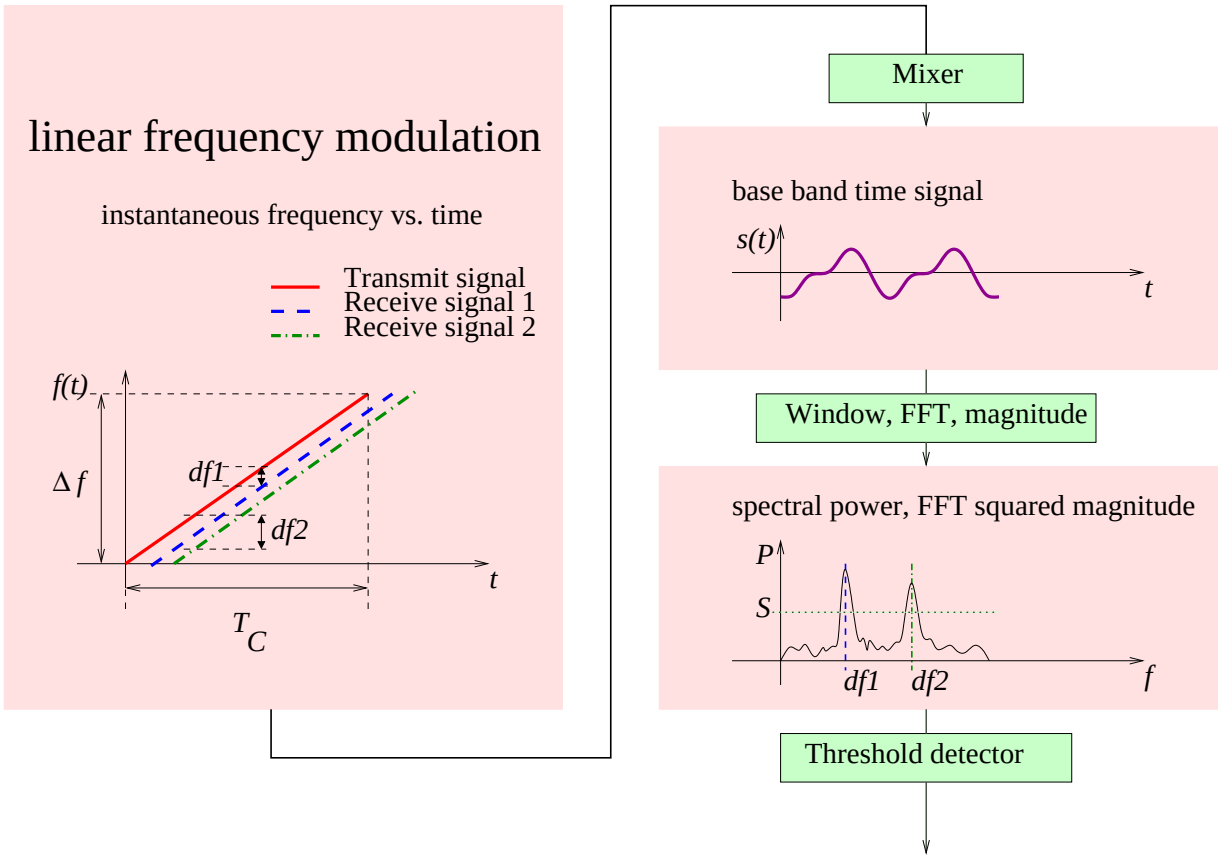

Figure 4.3: Single chirp, baseband signal, and its corresponding spectral power estimate

goal of the spectral analysis is to detect these frequency components. To achieve this, the discrete Fourier transform (DFT) translates the sampled time signal into the spectral domain. The commonly used algorithms are a radix-2 or radix-4 fast Fourier transform (FFT).

The resolution capability of the DFT is given by the observation time window of size T_C and is usually defined as $1/T_C$. For the LFMCW processing, T_C is the duration of the chirp signal. The value $1/T_C$ is commonly referred to as the size or width of a frequency bin.

A finite time segment of a harmonic oscillation is transformed into a sinc-function by the DFT. A spectral peak of a single point target appears as a squared sinc-function in the power spectrum. If two targets with different amplitudes are close to each other, the higher amplitude target can mask the lower amplitude target with its side lobes. To reduce the side lobes of the target peaks, a window function is used. The window function is multiplied with the receive signal block prior to performing the DFT. A side effect of using a window function is a decrease of spectral resolution to values higher than the bin size. Choosing a window function involves making a tradeoff between the width of the main lobe and the attenuation of the side lobes. The Hamming window is commonly chosen. The Hamming window has a side lobe reduction of a little more than 40 dB.

In the table below, some window functions are listed. The rectangular window is implicitly used, when the FFT is processed without any additional window function.

Window	Peak to side lobe level/dB	3dB bandwidth/bin	6dB bandwidth/bin
Rectangular	-13	0.89	1.21
Hanning	-31	1.44	2.00
Hamming	-41	1.31	1.82
Blackman	-57	1.65	2.30

Table 4.1: Common window functions

4.3 Detection

In the preceeding section, the first steps of the spectral analysis were described. The result of the processing is a power spectrum calculated from each chirp receive signal. Within the spectrum the targets appear as peaks. The detection algorithm searches for these peaks in the spectrum.

Detection is performed on each spectral bin separately. The detection algorithm decides whether the power estimate x of a particular bin is indicating a target echo or is due to measurement noise or clutter. This is done by comparing the power estimate x to a threshold S. Figure 4.3 shows a sample signal together with a threshold. If the signal power lies above the threshold, a decision for a target in this bin is made.

The detection task can be understood as a binary hypothesis testing problem. It is assumed that the system of interest can have two different states. The task is to choose between two hypotheses about the current system state (H_0,H_1) from examining an observed measurement x.

In the radar detection case, one hypothesis H_0 refers to the case where only noise is received and there is no target measured. The second hypothesis H_1 refers to the case where the measured signal power x is due to a target echo, additively superposed by noise:

- H_0: no target
- H_1: target present

Detection theory provides detectors that are optimal in terms of some given criterion. Some of the basic detectors are the maximum likelihood detector, the maximum a posteriori detector, and the Neyman Pearson detector. For all these detectors, it is assumed that some probabilistic information on the system state and the corresponding measurements x is available. Commonly, the probabilities of interest are:

- conditional probability densities $p(x|H_0)$ and $p(x|H_1)$
- a priori probabilities of the hypotheses $p(H_0)$ and $p(H_1)$

For the radar detection task, the distribution functions can be stated while the a priori probabilities are not known. Also, the conditional probability density $p(x|H_1)$ can only be modeled for a specific target. In this situation, the Neyman-Pearson detector is useful. For the Neyman-Pearson criterion, the following two probabilities are considered:

- Detection probability P_d: Probability of correctly choosing H_1.
- False alarm probability P_{fa}: Probability of choosing H_1 when actually H_0 was true.

The Neyman-Pearson criterion can be stated with the above probabilities:

- maximize P_d while not exceeding P_{fa} for a given value $P_{fa} \leq \alpha$.

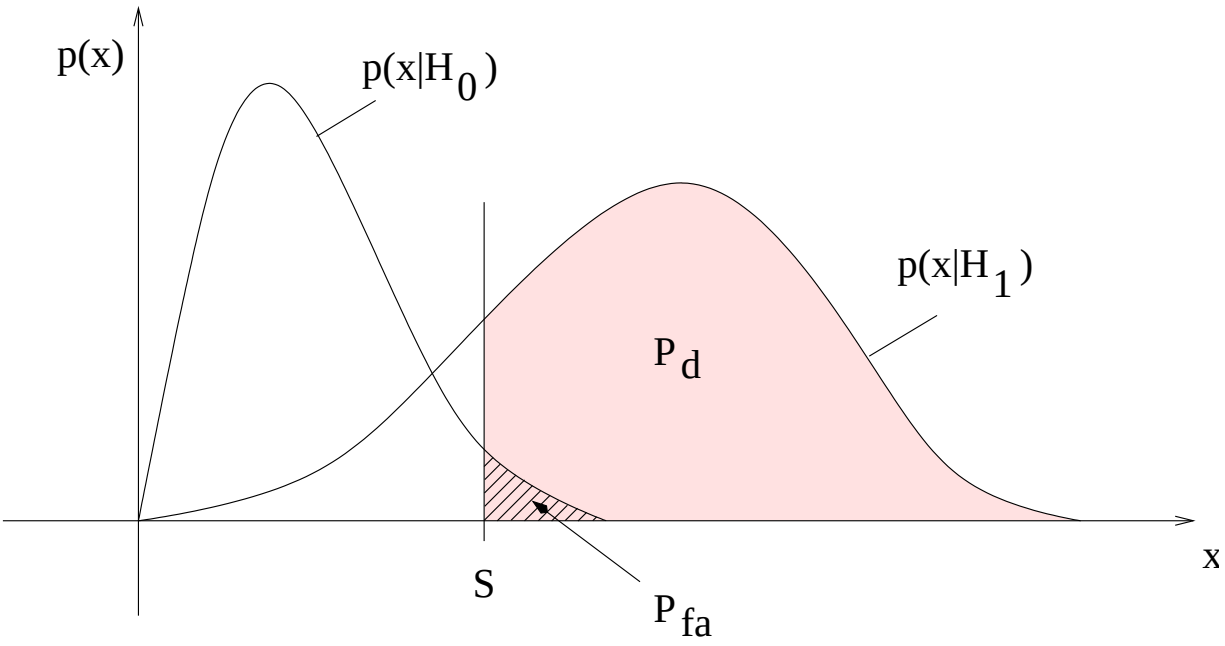

Figure 4.4: Probability distributions for both hypotheses; detection and false alarm rates for a threshold S can be graphically derived

For the radar detection task, Figure 4.4 shows the distribution functions for the two hypotheses. The derivation of these distributions is examined further in the next subsection. For H_0, the measurement is modeled by a Rayleigh distribution, for H_1 it is modeled by a Rice distribution. In this case, the likelihood ratio $l(x)$ is a monotonic function of x, which can easily be shown analytically. A detection decision can be made by comparing the measurement value directly with a threshold S. The Neyman-Pearson detector is then given by:

- choose H_0 if $x < S$
- choose H_1 if $x > S$

In this case, the detection- and false alarm- probabilities can be stated in the following way:

- $P_d = \int_S^\infty p(x|H_1)dx$
- $P_{fa} = \int_S^\infty p(x|H_0)dx$

The integration of the two distributions can be visualized graphically, as can be seen in Figure 4.4. Appendix B shows that indeed the threshold detector is optimal in the sense of the Neyman Pearson criterion.

4.3.1 Determination of the False Alarm Rate

The above section introduced the basic threshold detector and the Neyman-Pearson detector. It was also shown that the Neyman-Pearson criterion is very suitable for the radar detection problem. This leaves the task of obtaining a useful estimation of the conditional distribution function for the target-with-noise hypothesis $p(x|H_1)$ and for the noise-only hypothesis $p(x|H_0)$.

The noise originates from received clutter and from within the receivers circuitry. Without additional information about the noise, the noise hypothesis is modeled as a white Gaussian noise process. Assuming a complex demodulator and a independent Gaussian noise in each channel with power N, the output of the complex demodulator will be random values with a Rayleigh distribution $p(x|H_0) = \frac{x}{2\pi N} e^{-\frac{x^2}{2N}}$. The false alarm rate is simply derived by integrating the Rayleigh distribution from the threshold into infinity:

$$P_{fa} = \int_S^\infty \frac{x}{N} e^{-\frac{x^2}{2N}} dx = e^{-\frac{S^2}{2N}}$$

As an example, for a false alarm rate of $P_{fa} = 10^{-4}$ the threshold should be set to $S \approx 4.3\sqrt{N}$. However, to achieve a specific false alarm rate by adjusting the threshold, the noise power N has to be known. This is initially not the case and the noise level has to be estimated during the measurement.

4.3.2 Determination of the Detection Rate

The target hypothesis can be modeled to determine the detection probability, but this is not needed to dimension the Neyman-Pearson detector. The presence of a target can be modeled by the constant target signal amplitude A and additively superposed noise with power N. In case of a two channel mixer, the distribution is a Rice distribution.

$$P_d = \int_S^\infty p\left(x|H_1\right) dx$$

4.3.3 Detection Rate for Fluctuating Targets

In reality, the target usually consists of multiple elementary reflectors, whose echoes are additively superimposed in the receive signal. Under these assumptions, Swerling has created target models originally used for air surveillance radar systems ([Swerling 1954]). Furthermore, it is assumed that many elementary reflectors of the target are received in the same resolution cell. These elementary reflections have different amplitudes and phases

and interfere with each other. If there is one dominant reflector and multiple less intense reflectors, a rice distribution of the target amplitude is expected. In the case that the targets elementary reflectors are reflecting the radar signal with about the same intensity, the Rayleigh distribution is expected as the special case of the Rice distribution.

For noise additively superposed on a fluctuating target whose signal magnitude A is Rayleigh distributed with an average power of A_0^2 the determination of the detection probability is not trivial and very lengthy. It can be found in [Levanon 1988]. The result is surprisingly simple:

$$P_d = (P_{fa})^{\frac{1}{1+SNR}}$$

Where $SNR = \frac{A_0^2}{2N}$ is the target average signal to noise ratio.

The detection rate can only be stated when the target SNR is known. This is generally not the case because the target radar cross section is not known a priori. However, the above determination can be used for specification and comparison of radar systems. In this case, the minimum SNR is specified for which a target can be detected with a given probability.

However, the determination of the false alarm rate from the last section can be practically used. The Constant False Alarm Rate (CFAR) techniques described in the following section estimate the noise level. The noise estimate is used to set the threshold of the detector to keep the false alarm rate constant.

4.4 CFAR Techniques

Constant false alarm rate (CFAR) detectors have been used in radar systems for a long time. As described above, the Neyman-Pearson detector keeps the false alarm rate at a specified value. But to adjust the threshold of the detector, the noise power has to be estimated. A detector that estimates the noise power and adaptively adjusts the threshold to maintain a given false alarm rate is called CFAR detector.

The observation area can contain clutter objects that produce clutter noise in the receiver. The noise power then has to be measured for each observation and the detectors threshold level has to be set adaptively. Also the clutter conditions can change locally within the observation area. It is therefore very useful to estimate the current noise level only in a specific neighborhood around the cell under test.

The resulting techniques are called constant false alarm rate (CFAR) techniques. The CFAR techniques are based on the estimation of the noise power within the range cell under test by looking at the power values of its

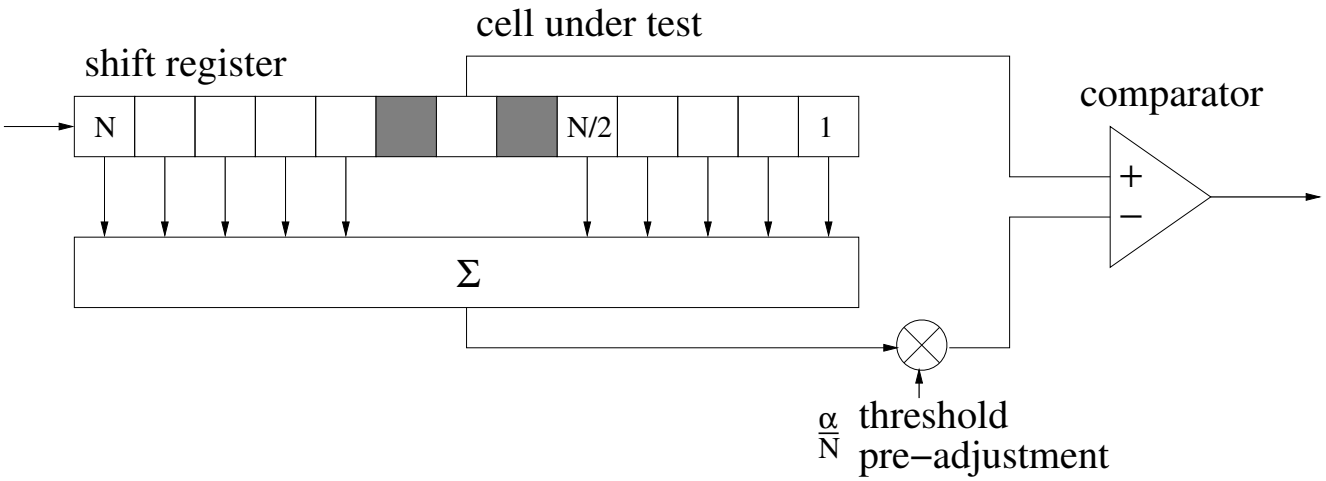

Figure 4.5: Cell Averaging (CA) CFAR

neighboring bins. The estimated noise level is used to adjust the threshold level of the Neyman-Pearson detector. The threshold level is usually set about 10dB above the noise estimate, the exact value of this pre-adjustment factor is dependent on the targeted false alarm rate.

As the quality of the noise estimation is very crucial to the overall performance of the detector, many different CFAR algorithms have been developed over the years. Fundamentally most important are the cell averaging CFAR and the ordered statistics CFAR. However, there exist many more algorithms that tweak the performance of the noise estimation for specific applications.

4.4.1 CA-CFAR

The most basic CFAR algorithm is the Cell Averaging (CA) CFAR, which is illustrated in Figure 4.5. It moves a sliding window over the range gates. The cell in the middle of the window is the cell under test. For detection, its power level will be tested against the estimated noise level. The N neighboring range cells that are left and right of the cell under test are used for this noise estimate by averaging their power values. The closest left and right neighbors are usually excluded from the noise measurement. This is done because a target peak will generally not fall in exactly one range gate, and without a guard interval the noise estimate would be influenced by the target echo signal.

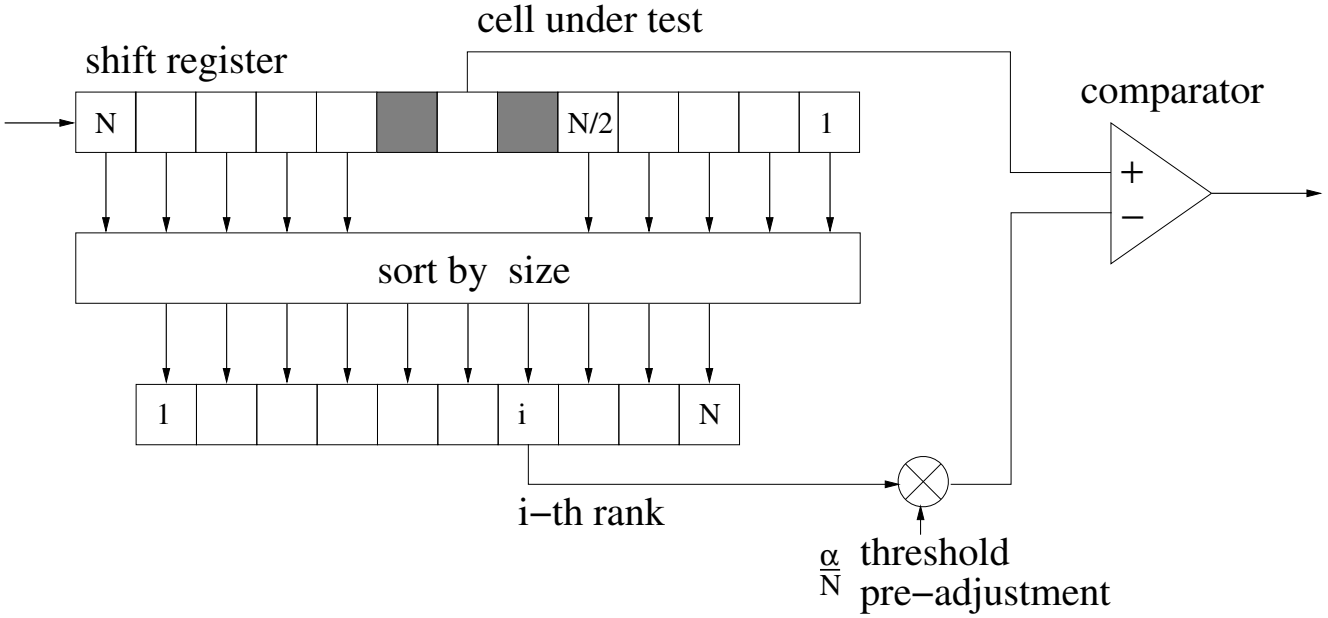

Figure 4.6: Ordered Statistics (OS) CFAR

4.4.2 OS-CFAR

The CA-CFAR detector estimates the noise optimally under the assumption that there are no target signals in the cells used to estimate the noise level. In multiple target situations however, there might fall multiple targets into a CFAR window. In this case, the resulting noise estimate is increased, and the sensitivity of the detector is reduced.

The Ordered Statistics (OS) CFAR was developed [Rohling 1983] to avoid this disadvantage. By using a rank order filter to get an estimate of the noise level, the estimate is only lightly influenced by multiple targets in the CFAR window as long as the rank taken as an estimate still holds a noise value. The rank order filter is not an optimal noise estimator in the ideal case of white uncorrelated noise. However, the OS-CFAR greatly outperforms the CA-CFAR in multiple target situations and also in situations with slightly extended targets. Figure 4.6 shows a block diagram of the OS-CFAR.

A detailed description of all the major CFAR algorithms is given in [Ludloff 2002].

4.5 Frequency Estimation

The detection algorithm, described in the previous sections, produces a frequency list. The list contains the indices of the frequency bins in which

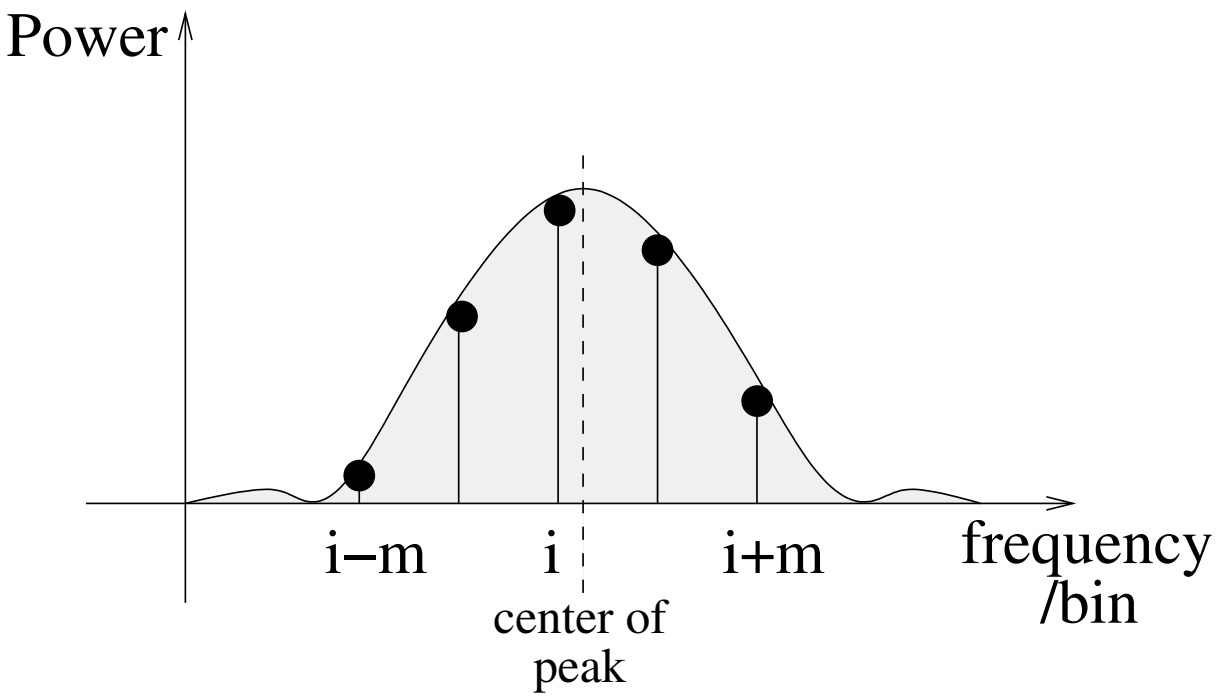

Figure 4.7: The center of the sampled peak is calculated by the Center of Gravity algorithm

targets were detected. These bin indices give the target echo frequency in integral multiples of the DFT frequency bin width. A more precise estimate of the peak frequency values is desired for most applications in order to get precise information on the target range and radial velocity parameters. Specifically, the radar network trilateration algorithms need a very precise range and radial velocity estimation.

The commonly used technique to estimate a peak center position is called "center of gravity" (COG). To estimate the center frequency, the algorithm is given the index of a bin a target was detected in. If more than one neighboring bin has a power above the threshold, the detection only reports the bin with the local maximum. The COG algorithm uses this bin with the maximum power value and its m left and m right neighbors. In the following, the frequency estimate $\hat{f}$ is normalized to the DFT bin size.

$$\hat{f} = \frac{\sum_{k=-m}^{m} (i+k)\, P_{i+k}}{\sum_{k=-m}^{m} P_{i+k}}$$

Where P_{i+k} is the estimated signal power in the $(i+k)$th bin. As can be seen in the above equation, the bin indices are simply weighted by the bins

power values.

This algorithm shows a good performance, compared to other algorithms, while having a low calculation complexity [Ludloff 2002]. It works well under the assumption that the peak does not interfere with other peaks, so that the power values used to weight the positions of the bins are only containing signal power from the examined peak. The higher the number $n = 2m+1$ of bins evaluated is, the more the peaks have to be separated in the spectrum in order to get a correct frequency estimate. Therefore, the number m is usually set very small for radar applications where the target density is expected to be high. The implemented COG algorithm uses one left and right neighboring bin ($m = 1$) to minimize errors due to multiple interfering peaks.

4.6 Range of Observable Frequency Values

The received echo frequencies depend on the target range and radial velocity according to equation 3.1. The range of frequencies that are observed in the receive signal depends on the maximum target range and the minimum and maximum radial velocity that can occur. The analog part of the radar has to let pass all frequencies that need to be detected.

Through the sampling rate $f_s = 1/T_a$ of the time domain signal, the size of the representable spectrum within the digital processing is determined. The Fourier transform represents the signal in the spectral domain with frequencies from 0 to $f_s/2$ if the time domain signal is real valued. If the time domain signal is complex valued, the representable spectrum is of double size and it contains frequencies from $-f_s/2$ to $f_s/2$. This frequency range is called the unambiguous frequency measurement range.

In the case of a complex valued input signal, a signed frequency value is obtained. It can be distinguished whether the frequency shift during the radar measurement is positive or negative. A single channel receiver only produces a real valued signal. In this case, the sign of the frequency value is lost and the unambiguous frequency interval is half the size of its complex counterpart. Since positive and negative frequency shifts can occur within the measurement, the single channel spectrum is ambiguous concerning the sign of the frequency:

$$f_d = \pm f_m$$

If a single channel time signal is processed, both alternatives have to be considered during the range-velocity processing.

The analog signal can be under-sampled. In this case, if a signal with a frequency f_m is measured within the spectrum, all frequencies $f_{d,k} =$

$f_m + kf_s$ have to be considered, for any $k \in \mathbb{Z}$ that gives a frequency within the possible range of frequencies in the analog signal.

As can be seen from the Nyquist theorem, for an optimal signal to noise ratio, the sampling rate should be adapted to the band of possible frequencies in the analog signal. This is because not only the frequencies outside the unambiguous measurement interval are folded into this interval, but also the noise components with higher frequencies add up to the noise in the unambiguous measurement interval.

4.7 Frequency to Range-Velocity Processing

The range-velocity processing stage creates a list of targets and their range-velocity estimates. This is done by processing the list of target frequency detections of each chirp in the waveform. Together with the spectral analysis, this stage makes the basic LFMCW processing complete.

The estimation of range-velocity parameters is based on the relation between a targets measured frequencies f_i and the target range R and radial velocity v_r through the parameters of chirp i. These chirp parameters are average frequency $f_{C,i}$, bandwidth Δf_i, and duration $T_{C,i}$:

$$f_i = -\frac{2f_{C,i}}{c} v_r - \frac{2\Delta f_i}{cT_{C,i}} R \tag{4.1}$$

Where, in the above equation, c is the speed of light. In most cases it is also convenient to work with frequencies normalized to the spectral bin size: $f_{n,i} = T_{C,i} \cdot f_i$.

4.7.1 Precalculation of the Frequency Equations

The two factors preceding the target range and velocity in the above equation can be combined into two constants:

$$f_i = a_i v_r + b_i R_0 \tag{4.2}$$

Prior to the range-velocity processing the constants can be precalculated. The factors can be combined into a precomputed measurement matrix M. For a waveform with 4 chirps, it is a 4 by 2 matrix.

$$M = \begin{pmatrix} a_0 & b_0 \\ a_1 & b_1 \\ a_2 & b_2 \\ a_3 & b_3 \end{pmatrix} \tag{4.3}$$

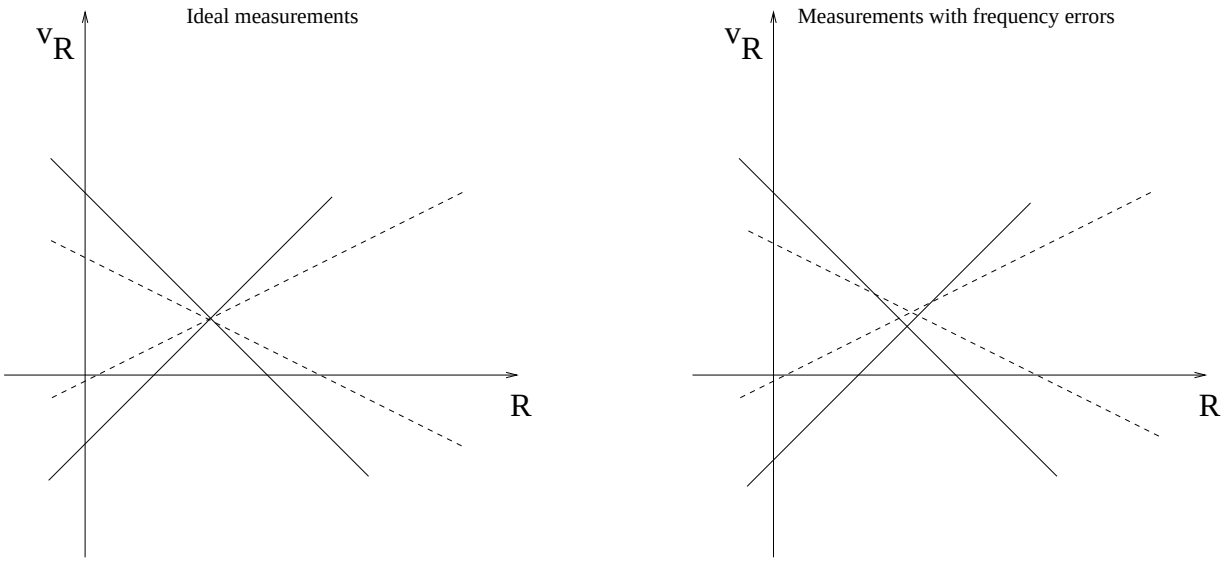

Figure 4.8: Range-Doppler diagram. Due to frequency estimation errors, the lines do not intersect exactly in one point.

With the definition above, the (ideal) relation between measurements for the 4 chirps and the target states can be written in vector form with frequency measurement vector $\vec{f}$ and target state $\vec{t}$:

$$\vec{f} = M\vec{t} \tag{4.4}$$

4.7.2 Range-Velocity Processing for a Single Target

The connection between the target echo frequencies $\vec{f}$ for the four chirp measurements and the target range and velocity is described by Equation 4.4. However, the frequency measurements $\vec{f_k}$ are generally not ideal and differ from the ideal measurements by the measurement error. Equation 4.4 is extended to account for the measurement error:

$$\vec{f_k} = M\vec{t} + \vec{e}$$

If these measured frequencies are plotted into a range-Doppler diagram, the lines will not perfectly intersect in one point as shown in Figure 4.8.

To estimate the target parameters $\vec{t} = \begin{pmatrix} v_r \\ R \end{pmatrix}$ from the measured frequencies $\vec{f_k}$, the minimum mean square error (MMSE) criterion can be used:

$$\widehat{\vec{t}} = \left(M^T M\right)^{-1} M^T \vec{f_k}$$

The MMSE criterion minimizes the error between measured frequencies and frequencies expected for the MMSE position estimate. The error vector can be estimated by:

$$\vec{e} = \vec{f_k} - \widehat{\vec{f}} = \vec{f_k} - M\widehat{\vec{t}} = \vec{f_k} - M\left(M^T M\right)^{-1} M^T \vec{f_k}$$

The mean square error is estimated by:

$$\vec{e}^T\vec{e} = \left(\vec{f_k}^T - \vec{f_k}^T M\left(M^T M\right)^{-1} M^T\right)^T \left(\vec{f_k} - M\left(M^T M\right)^{-1} M^T \vec{f_k}\right)$$

$$\vec{e}^T\vec{e} = \vec{f_k}^T\vec{f_k} - \vec{f_k}^T M\left(M^T M\right)^{-1} M^T\vec{f_k}$$

The MMSE criterion does not depend on the knowledge about the properties of the frequency error. If the frequency estimation error was assumed to be distributed Gaussian and the variances are known, also the minimum variance criterion could be applied. Due to the lack of precise information on the frequency errors due to clutter and interference with other targets, this would only increase the performance in simple synthetic situations.

4.7.3 Range-Velocity Processing in a Multiple Target Environment

In a multiple target scenario, there are generally multiple frequency detections in each chirp. A detected frequency in one chirp has to be assigned to the corresponding frequency detection in another chirp. For each detected target, a group of four frequencies has to be found, one frequency from each chirp.

Therefore, the task of the range-velocity processing can be described as a data assignment process. The task is to find the combinations of frequencies that make up each target.

Within each chirp i, a number of n_i frequencies are detected. These frequency values are denoted as $f_{i,k}$ for $0 \leq k < n_i$.

If there is a target with state (v_r, R) that is detected in all chirps of the waveform, there will be a frequency in each chirps frequency list that fulfills the equation derived above:

$$f_{i,k} = a_i v_r + b_i R$$

With the proposed waveform, four frequencies, one from each of the four chirps, give four equations that can be combined to a linear system of equations:

$$\overrightarrow{f_{\vec{k}}} = \begin{pmatrix} f_{0,k_0} \\ f_{1,k_1} \\ f_{2,k_2} \\ f_{3,k_3} \end{pmatrix} = \left(\vec{a}, \vec{b}\right) \begin{pmatrix} v_r \\ R \end{pmatrix} = M \overrightarrow{t} \tag{4.5}$$

If the frequency estimates are perfect, we only need to look for the right combinations $\vec{k} = (k_0\, k_1\, k_2\, k_3)'$ so that the equation system is solvable. However, there is no ideal measurement, and the measured frequency values contain estimation errors. In the general case, the above equation system is not solvable exactly.

Taking this into consideration, a useful assignment strategy has to find the combinations of frequencies that are likely to constitute a target. A possible way is to estimate the target parameters R, v_r from every combination of frequencies, using the minimum mean square error (MMSE) criterion, and only accepting combinations that are within a certain mean square error limit.

$$\widehat{\overrightarrow{t}} = \left(M^T M\right)^{-1} M^T \overrightarrow{f_{\vec{k}}} \tag{4.6}$$

The error between measured frequencies and frequencies expected for the MMSE position estimate can be calculated as shown for the single target case in the preceding section.

The assignment strategy described above takes into account all possible combinations and verifies each frequency combination individually. The number of all possible combinations is $\prod_i n_i$. If $n_i \approx N_C$, the calculation complexity is about N_C^4. In practice, this number is very high. As there is limited processing capability available, a modified approach is taken that calculates possible target ranges and velocities from two chirps and iteratively tests the combination with the frequencies of the remaining chirps once at a time. This leads to a complexity of $\approx N_C^3$.

The latter approach solves the assignment task in two steps. First, target hypotheses are set up and secondly, these hypotheses are validated by the remaining chirps. This approach was graphically shown for the measurement of two targets in Figures 3.9 and 3.10 on page 33. In this example four possible combinations can be set up using two chirps. These combinations have to be checked with the measurements from the remaining two chirps.

The check of a single frequency is done by defining a gate around the expected value and testing if the measured frequency is within that gate. The complete practical algorithm is described in Algorithm 1.

Additionally, all four frequencies of a validated target hypothesis can be used to make a final MMSE estimate of the target range and velocity using equation 4.6.

Algorithm 1 Cross-section algorithm

1. Take one frequency measurement from each of the first two chirps of the waveform and set up a target hypothesis with target parameters (v_r, R):

$$\left| \begin{array}{l} f_i = a_i v_r + b_i R \\ f_k = a_k v_r + b_k R \end{array} \right| \Leftrightarrow \left| \begin{array}{l} v_r = \frac{b_k f_i - b_i f_k}{b_k a_i - b_i a_k} \\ R = \frac{a_k f_i - a_i f_k}{a_k b_i - a_i b_k} \end{array} \right| \quad (i = 0; k = 1)$$

2. To decide if a frequency from the third chirp matches the hypothesis for a target at $(v_r; R)$, the expected frequency for the third chirp is calculated by:

$$f_i = a_i v_r + b_i R \quad (i = 2)$$

3. The expected frequency f_i is compared to all measured frequencies $f_{2,k}$ of the third chirp. If the nearest measured frequency is within a certain gate around the expected frequency, the hypothesis is in agreement with the measurements of the third chirp.

4. The same will be done with the fourth chirp by deriving the expected frequency for this chirp:

$$f_i = a_i v_r + b_i R \quad (i = 3)$$

5. A target hypothesis is validated, if measurements in both the remaining chirps are in agreement with it.

6. Start from beginning until all frequency combinations from chirps 0 and 1 are calculated and tested

4.7.4 Considerations on Quality of Target Detection

As mentioned before, the complete algorithm can be understood as a two step task: first create the target hypotheses, next find the hypotheses that are correct. The validation is done with a gate, so that the difference between expected and measured frequency has to be smaller than a certain limit. With this algorithm in mind, it is found that there is a possibility for a missed detection if

a) a frequency detection is missed in one or more chirps,

b) the frequency estimates of the last two chirps used for verification do not fall in the gates because of frequency estimation errors.

There is a possibility for a false alarm if

a) accidentally four false alarms make up a hypothesis that is validated (very rare: $p_{fa,total} = p_{fa}^4$)

b) a combination of four correctly detected frequencies - actually belonging to different targets - makes up a hypothesis that is validated.

c) a combination of correctly detected frequencies from other targets together with false alarms makes up a hypothesis that is validated.

A false detection according to point b) is referred to as a ghost target. Point b) is the most important source of false detections since these false detections can occur over a long period of time. In contrast, a false detection because of a) or c) incorporates at least one false frequency detection. A false frequency detection is due to random noise and appears only sporadically and so is easily filtered out by the following network processing stages.

Chapter 5

Improved LFMCW Processing

The near distance sensors described in this thesis are required to measure the target range with a high accuracy in the order of 3 cm. Therefore, all assumptions made for the described signal processing techniques should be revised in order to optimize the range measurement performance in real environments.

In the following two sections, two aspects are considered to improve the measurement accuracy of the near distance sensor:

- In order to estimate the target range and radial velocity with high accuracy, the frequencies of the target echoes within each chirp measurement have to be measured precisely. To optimize frequency estimation accuracy, an adaptation of the center of gravity (COG) algorithm for cluttered target scenarios is proposed in Section 5.1.
- Another inaccuracy is due to the target movement between the four chirp measurements of a waveform. Section 5.2 proposes a scheme for the compensation of target motion during the measurement.

Also the range-velocity processing benefits from a highly precise frequency measurement. Because the frequency validation is done by the nearest neighbor and gating techniques, smaller frequency errors allow the gate size to be smaller. It is important to say that both techniques can improve the performance of the sensors virtually without any additional computational costs.

Another important requirement of the radar network is a steady target detection in all sensors. A simulation in Section 5.3 shows that the detection

rate depends strongly on the number of targets in the scene. The results indicate that a target tracker in each single sensor is mandatory. Section 5.4 introduces two tracking techniques:

- Standard tracker with Range / velocity measurement to track assignment. This tracker is fed by the target lists generated by the LFMCW range-velocity processing algorithm.
- Improved tracker with direct frequency measurement to track assignment. This tracker is integrated into the LFMCW range-velocity processing algorithm.

The improvements described in this chapter make the near distance sensors useful for the radar network application.

5.1 Center of Gravity Algorithm with Compensation

The center of gravity (COG) algorithm was originally formulated for continuous signals. In this case, the algorithm precisely estimates the center of an arbitrary but symmetric peak. Using the COG algorithm on a sampled signal, there is a systematic error, especially when the signal additionally contains noise. In a radar network the requirements for single sensor measurement accuracy are very high, and all systematic errors should be corrected.

The systematic error is introduced by the sampling of the signal; it is higher the more sparsely the peaks are sampled in relation to the width of the peak. Therefore, the correction depends on both the spectral sampling rate and the expected shape of the peaks. In the case of the continuous wave processing, the shape of the Fourier transformed window function can be assumed. This implies that a point target with no extension is measured.

The reason for the COG estimate differing from the actual position of the frequency peak is visualized in Figure 5.1. The two plots in the upper row (plots 1A and 1B) show that the more sparsely a peak is sampled, the less its correct symmetry is conserved. The row at the bottom shows the same situation but with a superimposed constant signal. In this case, the symmetry axis and so the frequency estimate is moved into the direction of the middle of the evaluation window. For a time signal with additively superimposed white noise, the frequency estimate is biased towards the middle of the center bin.

To compensate the COG algorithm, a simulation is done to determine the frequency estimation error. This is done for the two cases, without noise

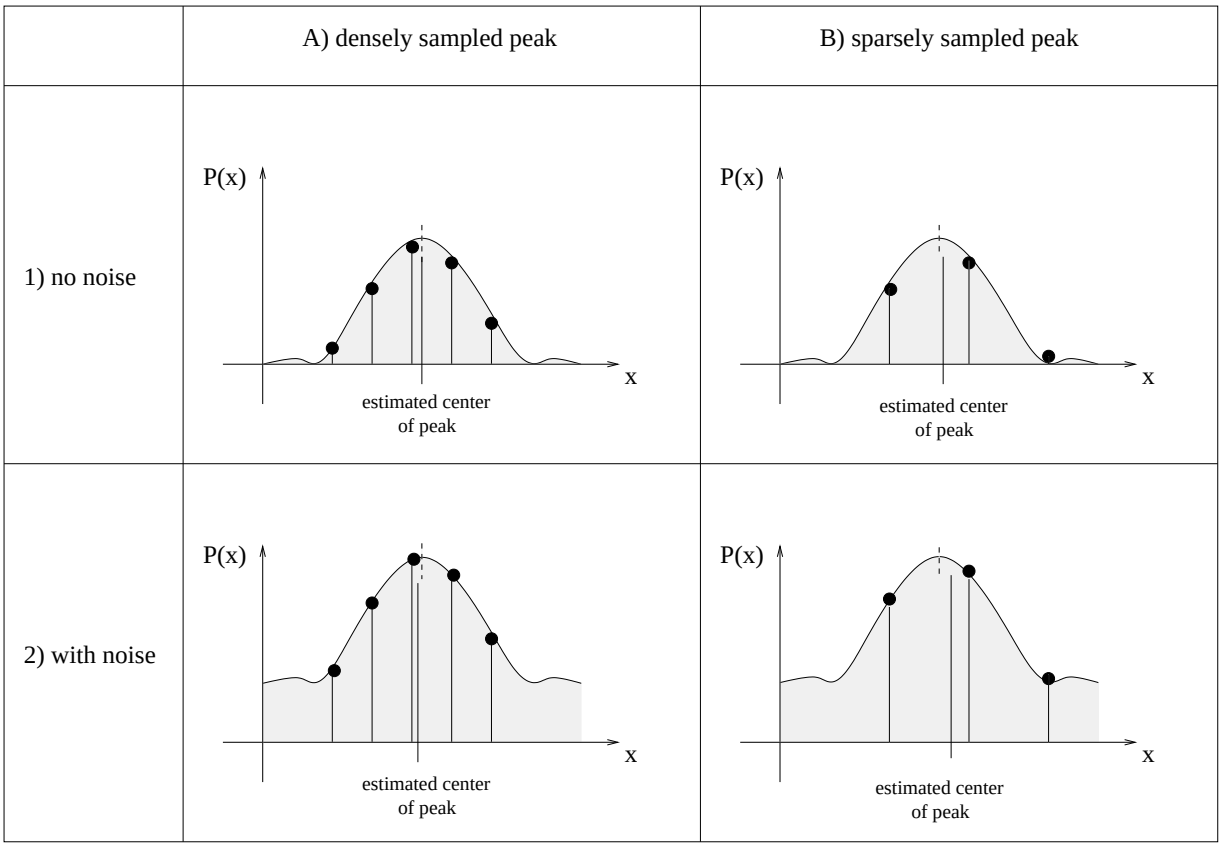

Figure 5.1: Center of gravity algorithm on different sampling rates and noise levels

and with additional noise in the spectrum. It will be shown that the COG algorithm can be sufficiently compensated by a simple correction factor. This factor depends on the noise level in the spectrum.

5.1.1 Model of the Estimation Error

Figures 5.2 and 5.3 show the un-compensated COG frequency estimate versus the actual frequency in the range of $\pm\frac{1}{2}$ frequency bin. The frequency estimate is plotted for some window functions. It can be seen that in the case where additional noise is absent, the center of a windowed peak is well estimated, and the curves approximate the ideal straight line of gradient one. Only the curve for the rectangular window shows a great deviation. The COG algorithm behaves worst on the rectangular window because this window produces the thinnest spectral peak.

The estimated versus actual frequency plots can be obtained by creating a complex oscillation for frequency values of $f_{n,a} = [-0.5\,,\,0.5]$ normalized to the bin width. This oscillation is multiplied with the window function w and from this signal the Fourier transformed spectral samples S_k are determined:

$$S_k = \sum_{i=0}^{N_W-1} w(i)\, e^{2\pi j (f_{n,a}-k)\frac{i}{N_W}}$$

Where N_W is the signal and window size and $f_{n,a}$ is the actual frequency offset normalized to the bin size. The center of gravity algorithm is now used on the squared magnitudes of these samples:

$$\hat{f}_n(f_{n,a}) = \frac{\sum_{k=-m}^{m} k\,|S_k|^2}{\sum_{k=-m}^{m} |S_k|^2}$$

Where m is the number of left and right neighbors to be included in the estimate. This is the function plotted for some window functions in Figures 5.2 and 5.3. The algorithm can be compensated simply by multiplying its output with a correction factor. The quotient of actual and estimated frequency is used as the correction factor:

$$C(f_{n,a}) = \frac{f_{n,a}}{\hat{f}_n}$$

As shown above, $C(f_{n,a})$ can approximately be assumed to be a constant value in the case, a window function is used ($C(f_{n,a}) = C_{COG}$). To calculate the corrected COG estimate $\hat{f}_{c,n}$, the uncorrected estimate is simply multiplied by the correction factor:

$$\hat{f}_{c,n} = C_{COG}\,\hat{f}_n$$

5.1.2 Determination of the Correction Factor

To obtain the value of the constant correction factor C_{COG}, either the value $C(1/2) = C(-1/2)$ or the value that minimizes the mean square error can be used. Using the mean square error criterion, the error is minimized which is introduced by using the constant factor C_{COG} instead of $C(f_{n,a})$. It can be assumed that the actual frequency $f_{n,a}$ is equally distributed within the range of a frequency bin $f_{n,a} = [-1/2\,,\,+1/2]$. The correction factor is determined which minimizes the mean square error $E\left(\left(f_{n,a} - C_{COG}\hat{f}_n\right)^2\right)$. The indices on the frequency variables are omitted in the following equations for the reason of clarity.

$$MSE = \int_{-1/2}^{+1/2} \left(f - C_{COG}\,\hat{f}(f)\right)^2 df$$

The derivation with respect to C_{COG} is determined and is set to zero:

$$0 = \int_{-1/2}^{+1/2} \left(-2\,f\,\hat{f} + 2C_{COG}\,\hat{f}^2\right) df$$

$$C_{COG} = MMSE = \frac{\int_{-1/2}^{+1/2} \left(f \cdot \hat{f}(f)\right) df}{\int_{-1/2}^{+1/2} \left(\hat{f}^2(f)\right) df}$$

With the above equation, the correction factor can be numerically calculated. In the described case, the signal is free of noise and the correction factors are quite small. Table 5.1 lists the factors for some window functions when using the center bin and its next left and right neighbors ($m = 1$). Using no window function (which implies using a rectangular window), the assumption of the COG estimation having a linear error produces quite significant deviations. In this case it is advantageous to oversample the signal or to use a polynomial for correction.

Window function	Correction factor $C_{COG} = C(1/2)$	Correction factor $C_{COG} = MMSE$
Rectangular	1.19	1.56
Hamming	1.03	1.02
Hanning	1.06	1.04
Blackman	1.19	1.16

Table 5.1: Correction factors for the center of gravity algorithm weighting 3 bins ($m = 1$).

5.1.3 COG Correction for a Noisy Signal

If the examined signal contains noise, the expectation value of the estimated frequency can also be determined by simulations. The results are shown in Figure 5.4 for a signal to noise ratio (SNR) of 12 dB and in Figure 5.5 for an SNR of 20 dB. The algorithm weights 3 bins ($m = 1$) to obtain the frequency estimate. The use of a Hamming window is assumed. The plots show the expectation value and the standard deviation of the estimate depending on the actual frequency. From these plots it can be seen that the estimate of the center of gravity algorithm is biased. It is desired to adjust the correction factor to the SNR in order to obtain an unbiased estimate.

Conveniently, the expectation of the frequency estimate still depends approximately linearly on the actual frequency for all noise levels of interest. Figure 5.6 shows the correction factor C_{COG} used to obtain an unbiased frequency estimation. This factor depends on the SNR and is also calculated under the assumption of using a Hamming window. The correction function can be approximated by:

$$C_{COG} = 1.03 + 3.8\frac{1}{SNR} \tag{5.1}$$

5.1.4 COG Simulation Results

Measurements show that for an LFMCW radar with a sweep bandwidth of 450 MHz the range estimation accuracy can be in the range of $3\,cm$ for a strong reflecting point target even without tracking. A range difference of $3\,cm$ roughly corresponds to a frequency difference of a tenth of the frequency bin size before the intersection analysis. Although this estimation accuracy is high, the difference between uncorrected COG estimation and the ideal value are still negligible in the case of a high SNR and when using a Hamming window, even when only taking into account the center bin and one left and right neighbor ($m = 1$).

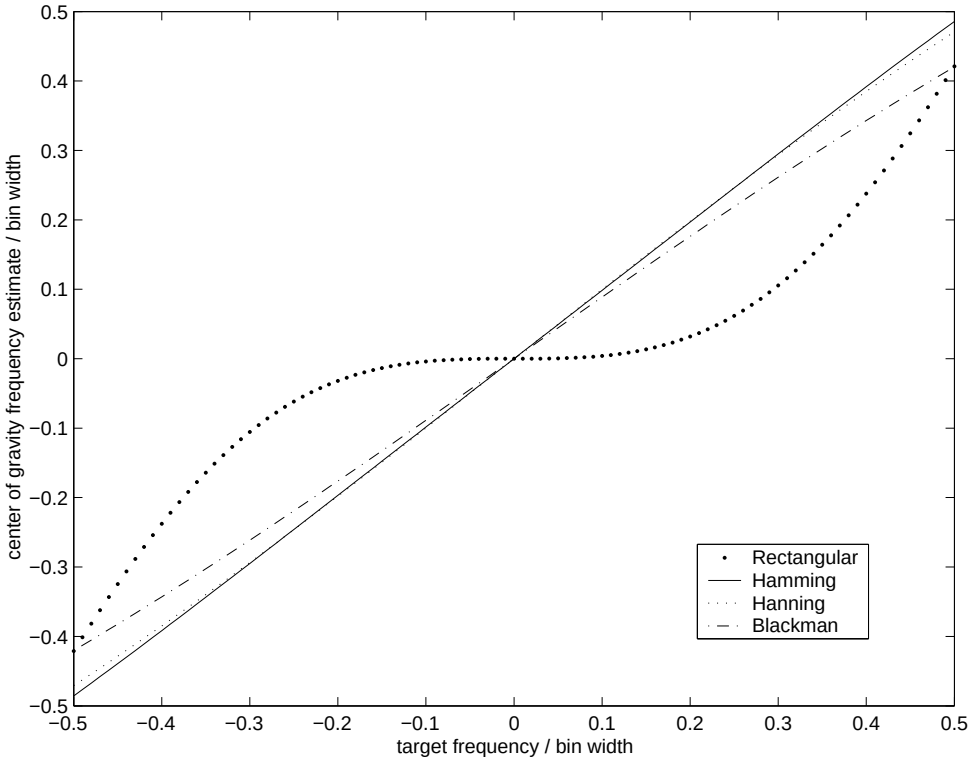

Figure 5.2: Center of gravity algorithm weighting 3 bins ($m = 1$). The frequency estimate is plotted against the actual frequency. The results for four different window functions are shown.

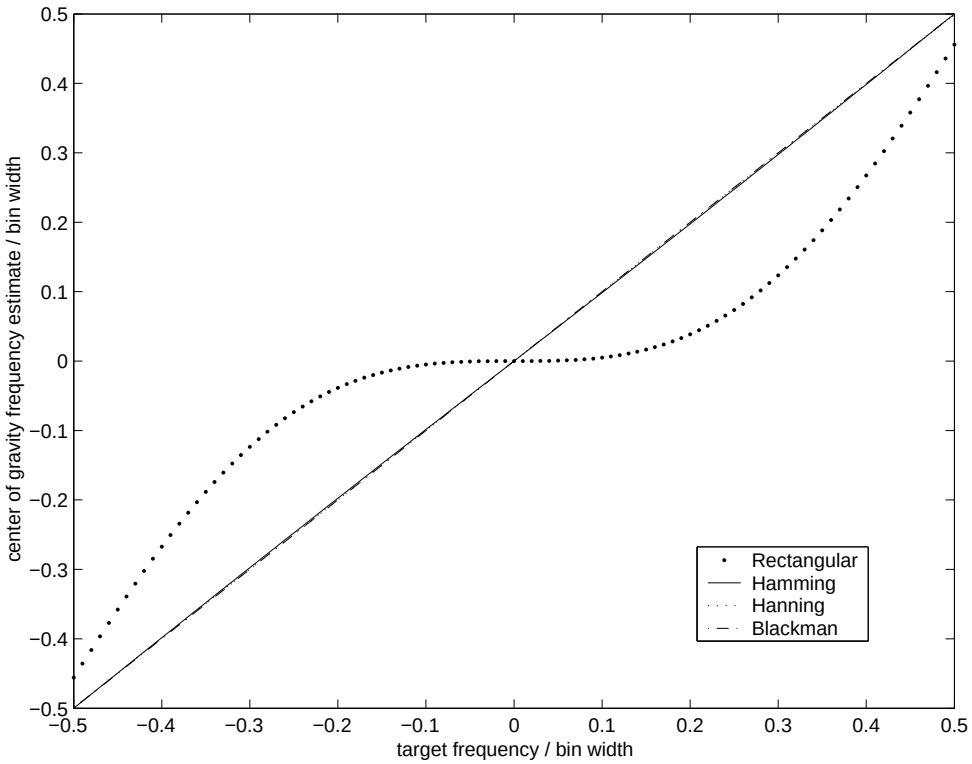

Figure 5.3: Center of gravity algorithm weighting 5 bins ($m = 2$). (Rectangular window behaves worst)

However, when the target signal has an SNR of less than 20 dB, the frequency estimation correction becomes relevant. If a correction factor for a high SNR is chosen and the actual target signal has a low SNR, the frequency estimate is biased towards the center of the nearest bin. A tracking filter will not improve the frequency estimation result beyond the bias.

One way to improve the performance is to chose a COG correction factor that is optimal for the expected average SNR. In this case the COG algorithm is over-compensated when processing a signal with high SNR and the algorithm is under-compensated when processing a signal with an SNR lower than the average.

Another, better way is to use the CFAR noise estimate to adaptively adjust the compensation using the approximation given above in Equation 5.1. If the CFAR estimates are available, there is practically no additional computational effort.

5.2 Compensation of Target Movement

The movement of a target can be neglected during the measurement time of a single chirp. However, during the measurement cycle of a complete

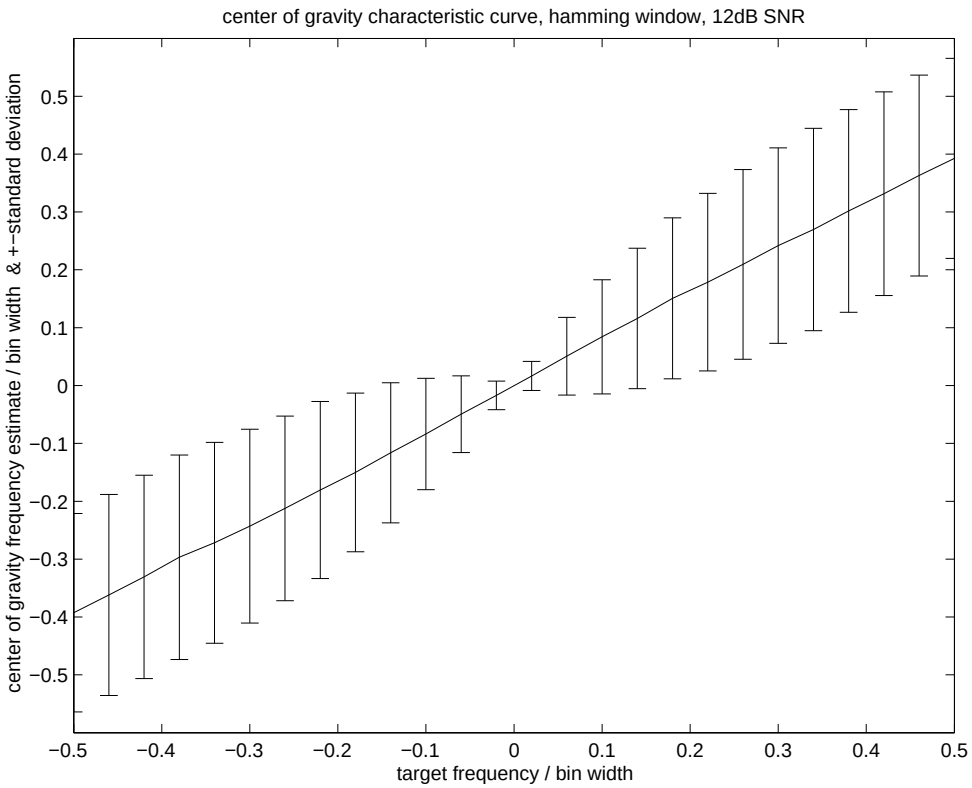

Figure 5.4: Expectation value and standard deviation of the frequency estimate when the COG algorithm is weighting 3 bins. A Hamming window and an SNR of 12 dB is used.

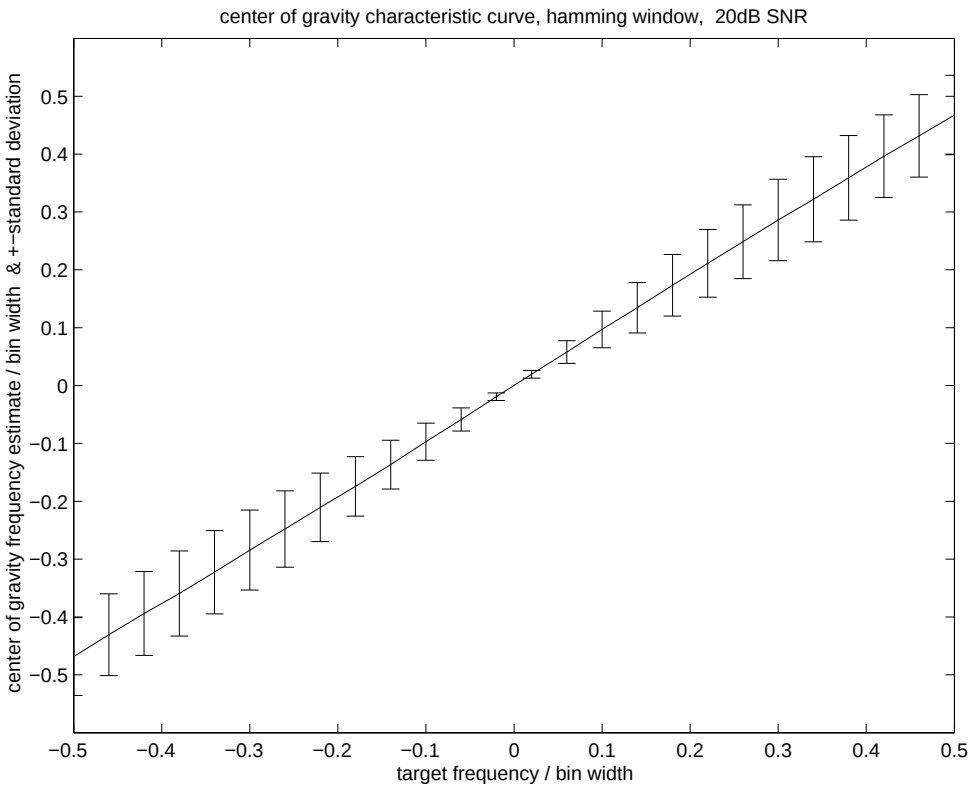

Figure 5.5: Expectation value and standard deviation of the frequency estimate when the COG algorithm is weighting 3 bins. A Hamming window and an SNR of 20 dB is used.

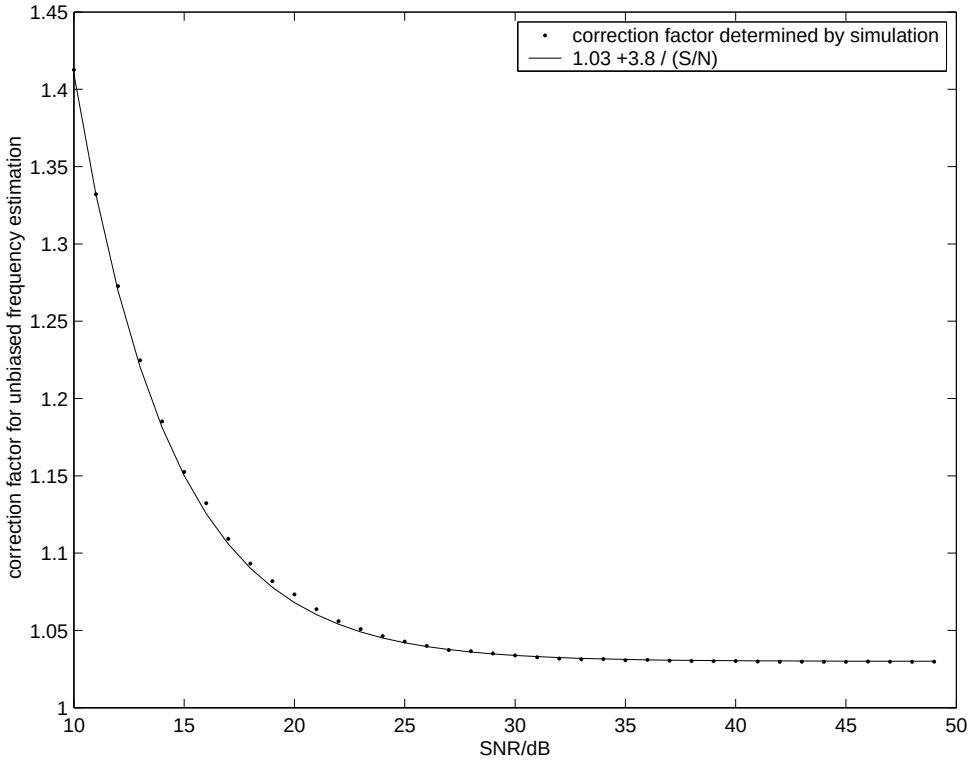

Figure 5.6: COG correction factor to achieve an unbiased frequency estimation versus SNR. 3 bins are weighted, a Hamming window is used.

waveform consisting of multiple chirps, a moving target has a different range for each chirp measurement. Depending on the system parameters, this difference can reach the value of the radars range resolution parameter (For example: $10ms \cdot 50m/s = 0.5\text{m}$) and therefore should be taken into account.

The starting point for the compensation of movement is the standard LFM frequency equation (Equation 4.1) which is repeated here:

$$f_i = -\frac{2f_{C,i}}{c}v_r - \frac{2\Delta f_i}{cT_{C,i}}R$$

To account for the target motion, the measurement time t_i of the ith chirp is defined as the time in the middle of the chirp measurement:

$$t_i = \frac{t_{i,chirpstart} + t_{i,chirpstop}}{2}$$

Assuming four chirps at times $t_0 ... t_3$, the reference time of a waveform is defined as the time point in the middle of the waveform:

$$t_{waveform} = \frac{t_0 + t_1 + t_2 + t_3}{4}$$

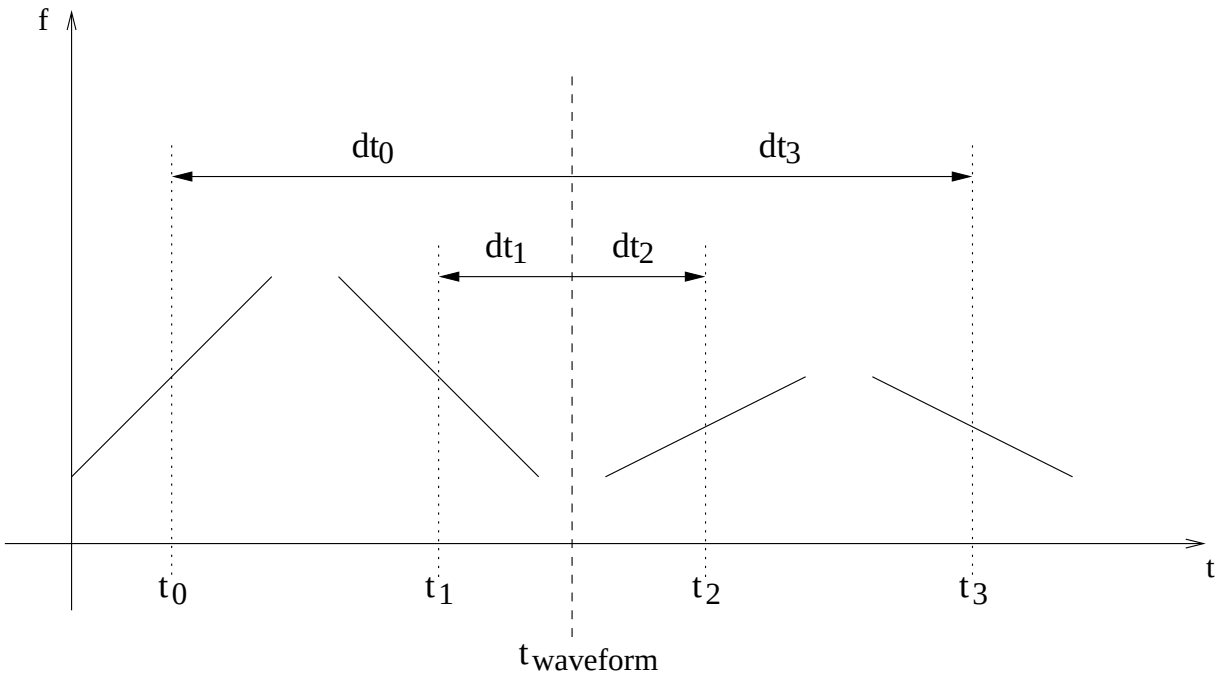

Figure 5.7: Reference times for the compensation of target movement

The relative chirp time dt_i is now defined as the time relative to the waveform reference time:

$$dt_i = t_i - t_{waveform}$$

The times defined above are shown in Figure 5.7.

Implying linear movement, the momentarily range of a target for the measurement time of chirp i is:

$$R_{chirp\,i} = R_0 + v_r dt_i$$

The LFM frequency equation can now be extended to account for the target movement during the measurement:

$$f_i = -\frac{2f_{C,i}}{c} v_r - \frac{2\Delta f_i}{c T_{C,i}} (R_0 + v_r dt_i)$$

$$f_i = -\left(\frac{2f_{C,i}}{c} + \frac{2\Delta f_i}{c T_{C,i}} dt_i \right) v_r - \frac{2\Delta f_i}{c T_{C,i}} R_0$$

The range parameter R_0 is now referring to the reference time $t_{waveform}$.

As shown in the preceding chapter, the coefficients within the chirp frequency equations can be precalculated prior to execution of the range-velocity processing:

$$f_i = a_i v_r + b_i R_0$$

The compensation of target movement does not change the structure of the linear equation system but only its coefficients. Thus, the compensation comes with no computational cost.

Using this compensation, a notable improvement can be seen in practical experiments with high relative velocities but small assignment gate sizes.

5.3 Simulation of a Multiple Target Scenario

The first section of this chapter introduced a method to improve the frequency measurement accuracy. The second section showed that the target movement during the four chirp measurements can easily be compensated. For both improvements shown above, the interrelation between target state and measurement is modeled more accurately. This way, both methods do increase the range velocity measurement accuracy. It is also very important that an increased frequency measurement accuracy makes the assignment of frequencies to target range-velocity measurements more accurate. Using a more accurate measurement model and still performing the frequency assignment with same gate size, the probability of a correct validation of a target hypothesis increases.

The measurements (Chapter 10) show a good performance of the LFMCW radar sensor in single target situations. However, in multiple target situations, interferences between targets will cause missed detections and measurement errors on a target frequency in one or multiple chirps. Especially for the discussed short range sensor with a wide antenna beam, more targets are observed compared to systems with small antenna beams. In this section, the detection probability is examined for multiple target situations. For this simulation, point targets are assumed.

As described in Section 4.7, the range-velocity processing is practically done by creating hypotheses from the measurements of the first two chirps. For each of these hypotheses the frequency measurements for the remaining two chirps are predicted and compared to the actual measurement data. If actual frequency measurements are within a gate around the predicted frequencies, the hypothesis is validated. The size of the validation gate influences the tradeoff between detection and false alarm rate of the detector. Specifically, decreasing the gate size reduces false alarms but also reduces detection rate.

To get an idea of how the quantitative performance of the target hypothesis validation algorithm depends on the number of targets and how it depends on the gate size, a simulation of ideal multiple point target scenarios was done. Five variations of the validation strategy were tested. These are compared against each other below:

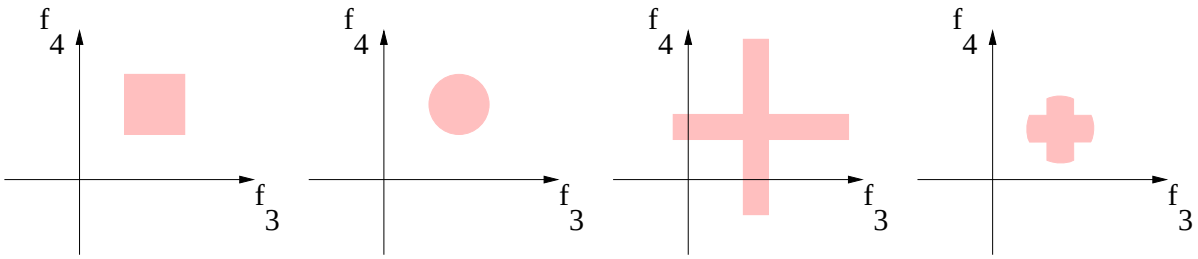

(a) rectangular gate (b) circular gate (c) 1 chirp validation (d) combined algorithms 1 & 2

Figure 5.8: Frequency validation gates for chirps 3 and 4

1. 2 chirp validation with a rectangular gate
First, verify if the best fitting frequency $f_{3,k}$ detected in the 3rd chirp lies within the gate around the expected frequency f_3^*. Second, test the 4th chirp accordingly:

$$|f_{3,k} - f_3^*| < S \wedge |f_{4,k} - f_4^*| < S$$

The frequencies of the third chirp can be plotted against the frequencies of the fourth chirp. If the combined gate for both frequencies is drawn into this plot, it has a rectangular shape (Figure 5.8).

2. 2 chirp validation with a circular gate
Find the best fitting (nearest) frequency measurement for each of the two remaining chirps. Verify if the quadratic sum of the deviations from the expected frequencies is under a threshold:

$$(f_{3,k} - f_3^*)^2 + (f_{4,l} - f_4^*)^2 < S^2$$

In this case the gate can be drawn as a circle in a graph where frequencies of chirp 3 are plotted against frequencies of chirp 4.

3. 1 Chirp validation
Verify if at least in one of the remaining chirps a frequency is detected that lies within the gate around the expected frequency:

$$|f_{3,k} - f_3^*| < \frac{S}{2} \vee |f_{4,k} - f_4^*| < \frac{S}{2}$$

For the comparison, the gate size is divided by 2 to balance the resulting detection rate for the comparison in the following plots.

4. Combined algorithm 1

This is a combination of the third validation strategy with variable gate size S and the second validation strategy with a fixed gate size of $\pm$ one bin:

$$\left[|f_{3,k} - f_3^*| < \frac{S}{2} \vee |f_{4,k} - f_4^*| < \frac{S}{2}\right]$$

$$\wedge$$

$$(f_{3,k} - f_3^*)^2 + (f_{4,l} - f_4^*)^2 < (1\text{bin})^2$$

5. Combined algorithm 2

This is a combination of the third validation strategy with variable gate size S and the second validation strategy with gate size $\sqrt{8}S$:

$$\left[|f_{3,k} - f_3^*| < \frac{S}{2} \vee |f_{4,k} - f_4^*| < \frac{S}{2}\right]$$

$$\wedge$$

$$(f_{3,k} - f_3^*)^2 + (f_{4,l} - f_4^*)^2 < 8S^2$$

The simulation parameters and settings of the first processing stages are as follows:

- A four chirp waveform at 77 GHz is used, each with a duration of 2 ms and with the following bandwidths: 450MHz, -450MHz, 225MHz, and -225MHz.
- The base band receive signal is sampled at a rate of 500 kHz.
- The spectral analysis is done as described in the previous chapters using a Hamming window.
- The gate size for the validation of the target hypotheses is chosen to be between 0.1 and 1.5 FFT bins. For a target to be validated, either all four chirps and/or only three chirps need a frequency detection within a gate around the expected frequency. Compensation of target movement is used.
- About half of the simulated point targets are stationary with a radial velocity of zero and represent stationary objects within the environment. Their range is randomly chosen between 0 and 20m. The remaining point targets are moving with a velocity randomly chosen between -15 m/s and 15 m/s. Their range is also randomly chosen between 0 and 20m.

- Target reflections have the same signal amplitude but have random phase. This way, only interferences between targets lead to missed detections and falsified frequency estimates.

Figures 5.9 to 5.16 show the results from the simulations. The first four figures refer to a simulated scene with a number of 3 stationary and 2 moving targets.

The detection rate (Figure 5.9) and the false alarm rate (Figure 5.10) are plotted against the gate size S. For a comparison of performance, the detection rate is plotted against the false alarm rate in Figure 5.11. It is clearly seen that for any targeted false alarm rate, the first two strategies and the last strategy have a much better detection probability than the remaining two validation strategies.

Figure 5.12 shows the range measurement accuracy versus the false alarm rate. As expected, the accuracy is better for low false alarm rates. The 1 chirp validation and both combined strategies have a better range accuracy than the 2 chirp validation strategy. This is because the frequencies to be used for the range-velocity estimate are chosen more flexibly with the latter three strategies. However only the second combined strategy allows a small improvement in range accuracy while maintaining a good detection rate. Of course, the validation and the selection of frequencies to estimate the target range and velocity can be done separately. Most probably, there are even better adjusted algorithms to optimize the range accuracy.

The 1 chirp validation is shown to present the dramatic improvement of the detection rate when the "2 chirp" criterion is loosened to the "at least 1" criterion. It shows that the target interference quite often prevents an exact frequency measurement from occurring in all four chirps while three chirps do often match the validation criterion. For any given false alarm rate however, the detection rate is always worse for the the 1 chirp validation than for the other strategies.

In practice, the first validation scheme is easiest to implement, because the validation of the two chirps can be done sequentially. Since none of the other strategies performs notably better, the first strategy is used for the described sensor signal processing.

The remaining Figures 5.13 to 5.16 show the results of the same simulation with 5 stationary and 5 moving targets. It can be seen that the doubling of the number of targets leads to a degradation of performance. The severeness of the loss in performance depends on the targeted false alarm rate. The following table shows the (approximate) detection rate for a fixed false alarm rate for the first validation strategy:

N_{fa}	P_d for 5 targets	P_d for 10 targets
10^{-2}	0.55	0.1
10^{-1}	0.84	0.26
1	0.96	0.61

N_{fa} refers to the average number of false detections per processed waveform. For a fixed gate size of 0.2 bin, the following results are made for the first validation strategy:

gate size = 0.2 bin	N_{fa}	P_d
5 targets	$8 \cdot 10^{-3}$	0.53
10 targets	10^{-1}	0.26

The results show that the use of a tracker is necessary to achieve stable target information for the network lateration technique. In the next section, a standard tracker is described and then a direct frequency measurement to track update technique is proposed. The newly proposed technique performs well, even when single chirp frequency detections are missed.

The simulations show no substantial difference in performance among the 2 chirp validation strategies and the second combined algorithm. The separate validation of a target hypothesis and the subsequent selection of the frequencies can improve the precision of position estimation and hence could be investigated further. The implemented radar processing however uses a single sensor target tracking algorithm (Section 5.4). The selection of frequencies to update the state with are done within the tracking, so the estimation accuracy mainly depends on the tracking algorithms.

Measurements (Chapter 10) show that the gate size for accurate estimation of a road vehicle should be around a quarter of the bin size to get about 50 percent of the frequency measurements into the track validation gate. In the simulation, a gate of this size would produce a false alarm rate of 1%-10% per complete measurement cycle. A real situation however contains multiple extended targets with different and varying signal amplitudes. Also, many interfering objects in the surroundings can have signal amplitudes just below the detection threshold. These are not seen in the measurements but influence the detection of the targets of interest. Measurements of real scenarios are shown in Chapter 10.

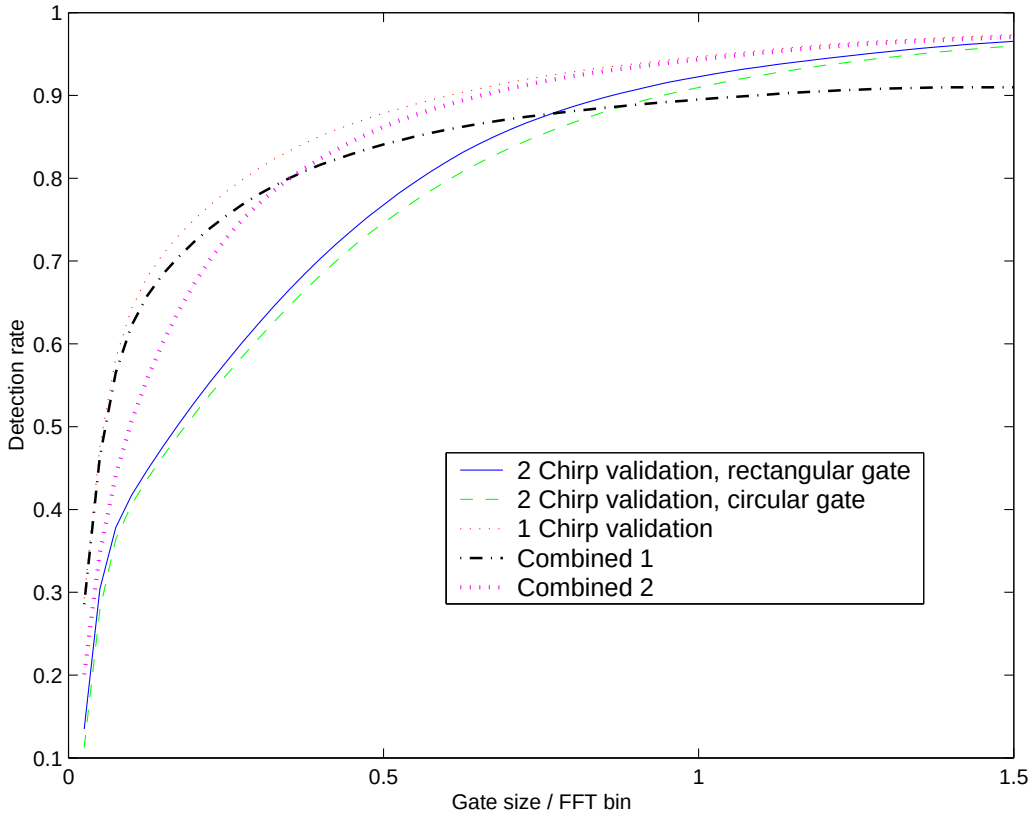

Figure 5.9: Detection rate vs. gate size, 5 simulated targets

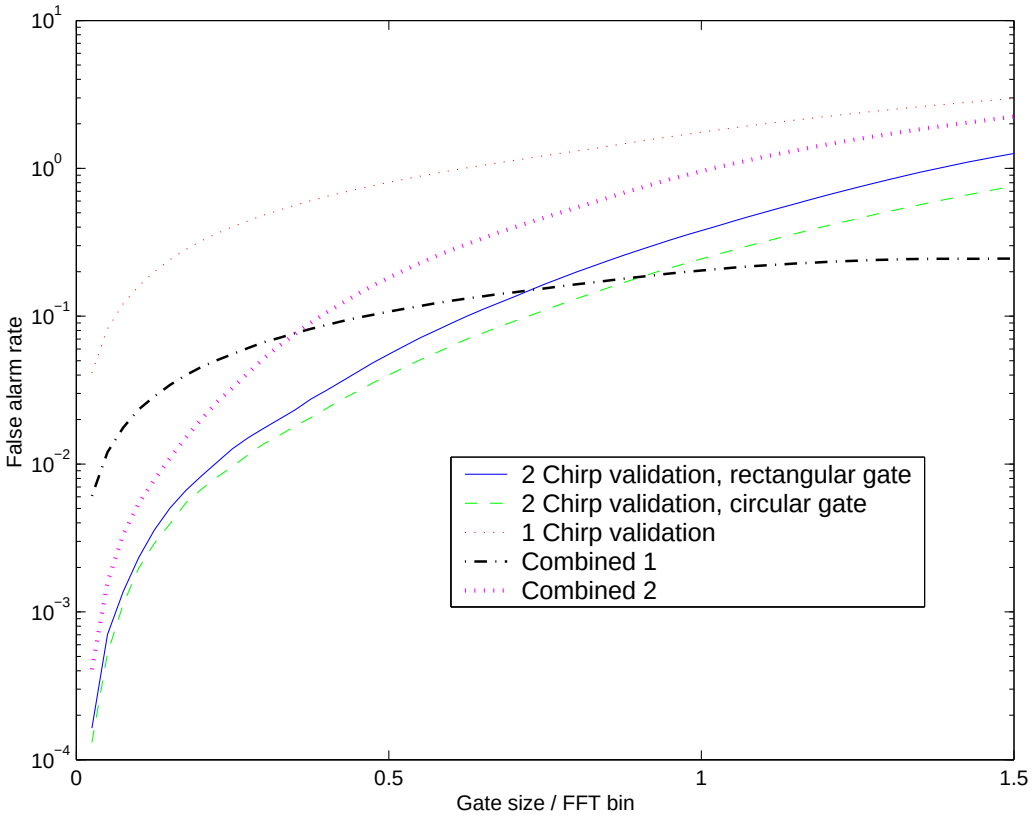

Figure 5.10: False alarm rate vs. gate size, 5 simulated targets

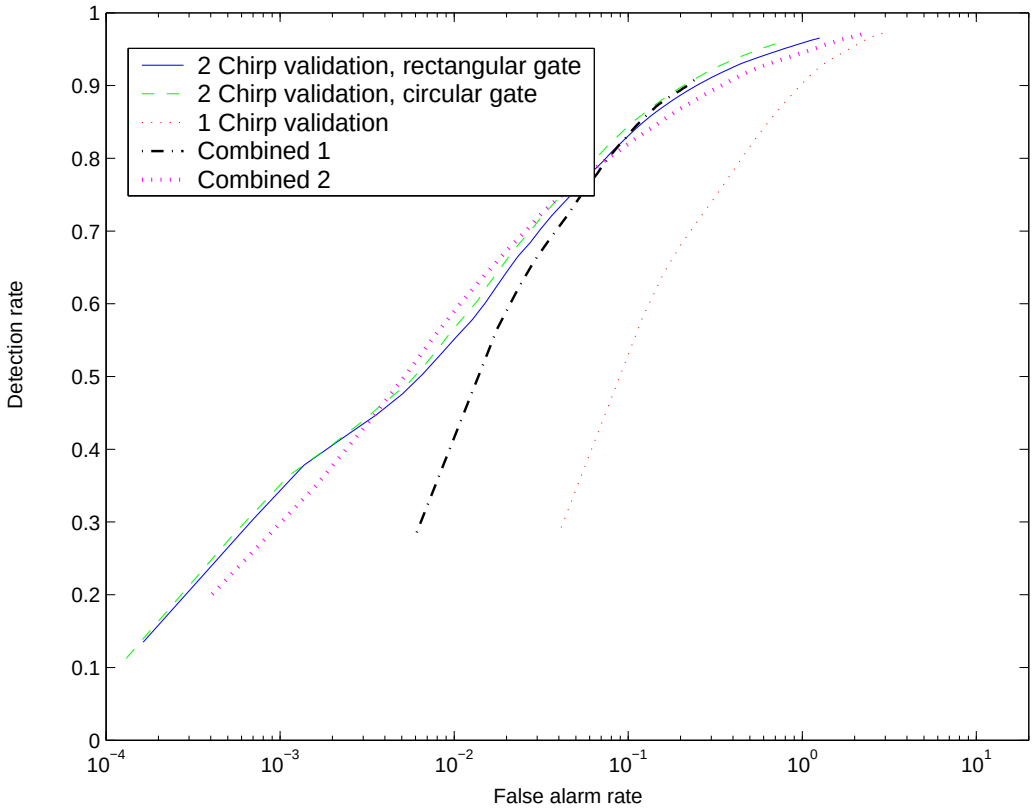

Figure 5.11: Detection rate vs. false alarm rate, 5 simulated targets

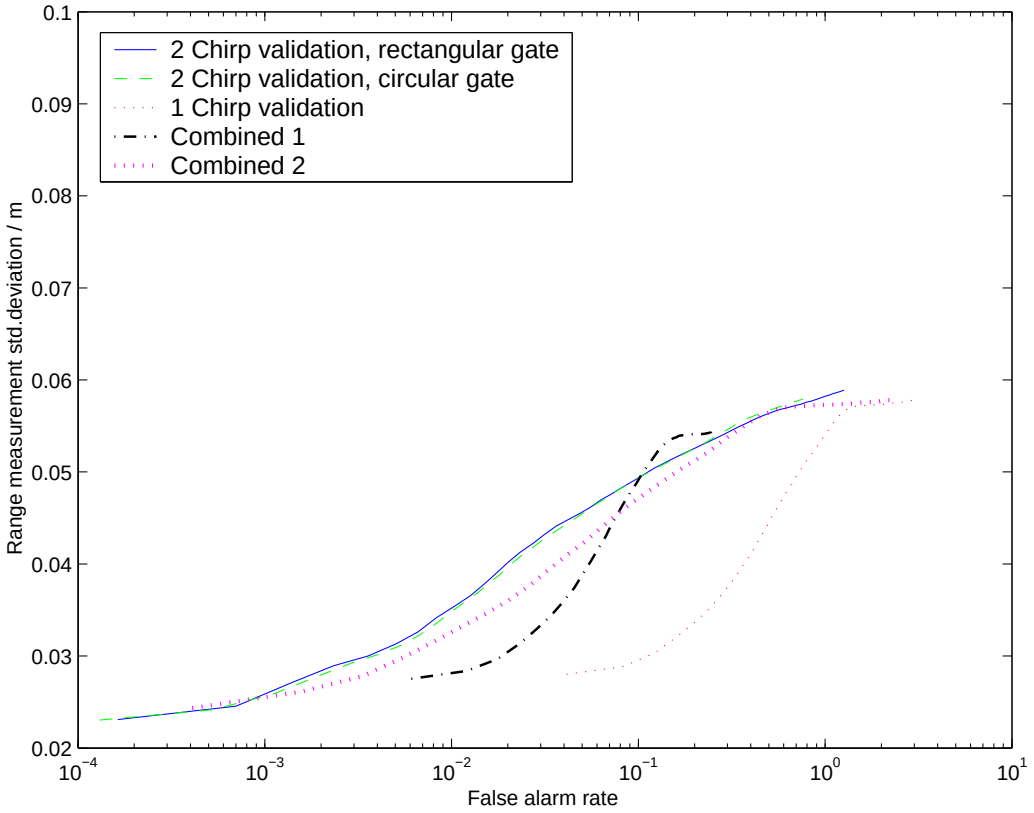

Figure 5.12: Range accuracy vs. false alarm rate, 5 simulated targets

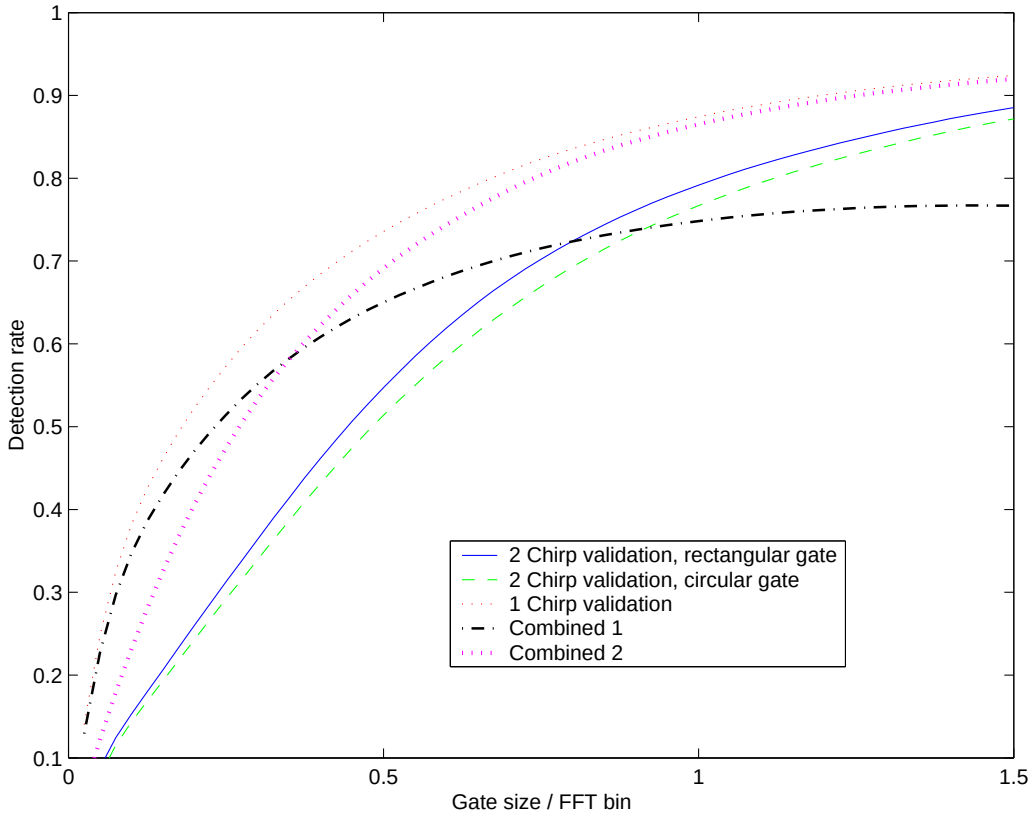

Figure 5.13: Detection rate vs. gate size, 10 simulated targets

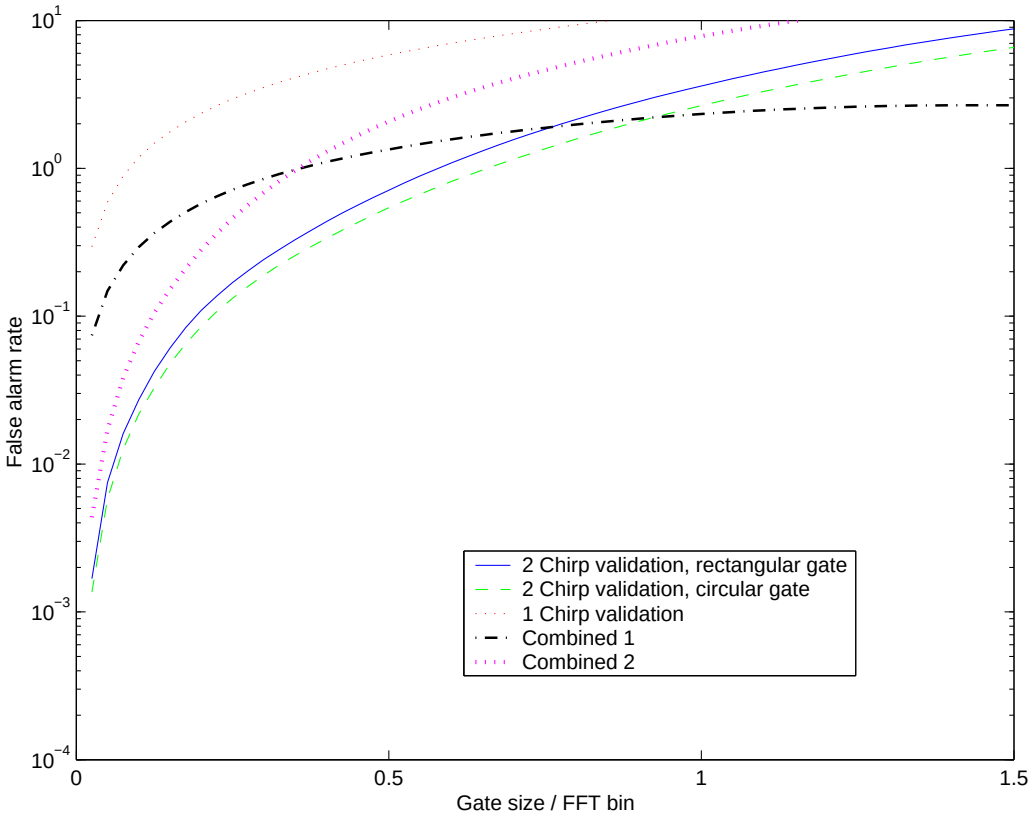

Figure 5.14: False alarm rate vs. gate size, 10 simulated targets

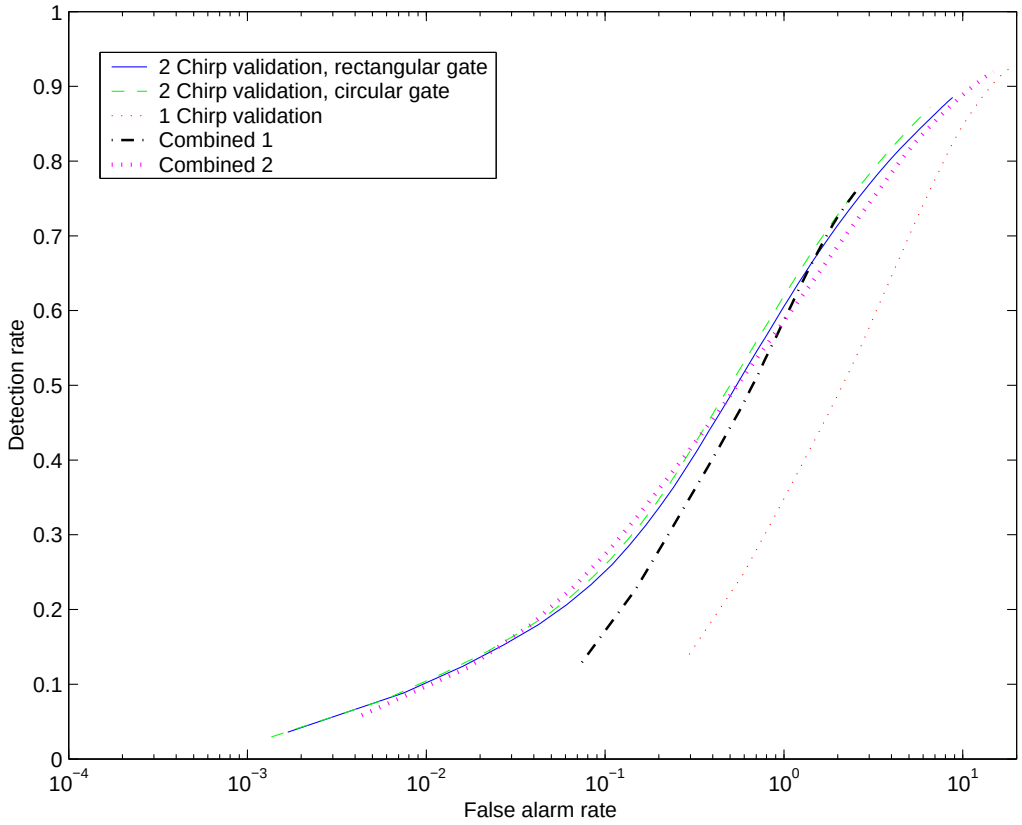

Figure 5.15: Detection rate vs. false alarm rate, 10 simulated targets

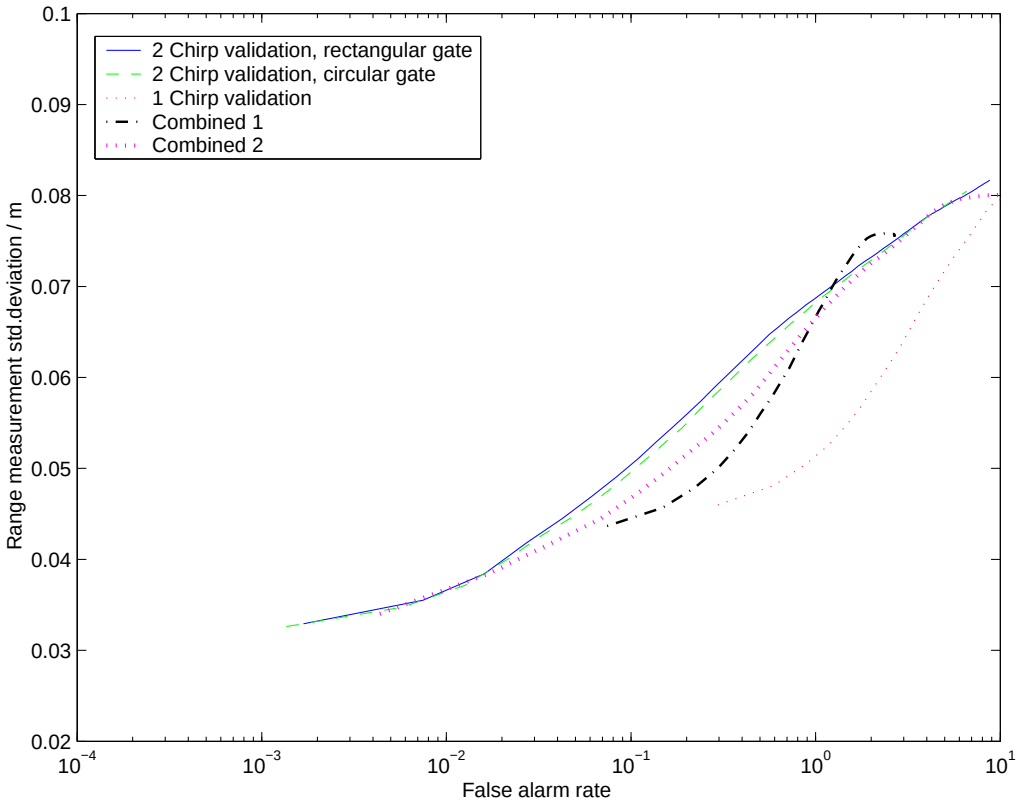

Figure 5.16: Range accuracy vs. false alarm rate, 10 simulated targets

5.4 Single Sensor Target Tracking

The LFMCW processing is greatly affected by the number of targets in the observation area. This can be seen from the simulations in the preceeding section.

To do the network lateration on basis of the single sensor range and velocity estimates an improvement in detection rate is necessary. An option that is presented in this chapter is the employment of a target tracker.

The classical approach is to feed a tracker with the raw range-velocity information of the detected targets. This information is generated from the standard range-velocity processing by cross-sectioning the 4 chirp frequency detections.

The newly proposed system uses a tracker directly updated by the chirp frequency detections. The standard range-velocity processing is still used to find new targets for which new tracks can be initialized.

The classical standalone tracker receives target range and velocity measurements. When in one or more chirps a frequency measurement is falsified due to interferences, the target is not reported to the tracker. If the frequencies are directly used to update the tracker, the remaining, correctly measured target frequencies can still be used for updating the target track. In multiple target situations, the increase of the number of track updates improves the track validation and stability of the active tracks.

In the following, the basic concept of target tracking is described. Thereon, the new direct frequency update technique is presented.

5.4.1 Standard Tracker

A radar tracker maintains a list of target tracks. Each of these target tracks corresponds to a target that is observed by the radar. Literally, the task of the tracker is to keep track of these targets. To accomplish this, the tracker stores information about the target states. The state consists of the target parameter range and optionally can include the target velocity and acceleration. When new radar measurements are available, the tracker assigns each measurement to the corresponding target track and updates the track states with the assigned measurements. Each track gets a unique ID so it can be identified over successive cycles. After the update with measurement data, the track states for the next measurement cycle are predicted by using the equations of motion.

The use of a tracker has multiple advantages:

1. Because the target states are associated over time, the states can be filtered over time to increase estimation accuracy.

2. When there are missed target detections in the preceding signal processing, the tracker can bridge the gaps by reporting a prediction of the target state based on the old measurement information.

3. False alarms can be inhibited by only forwarding target tracks that have already been updated multiple times and so prove to be stable target detections.

The complete tracking algorithm can be separated into two parts:

1. Target state update with measurements

2. Target state prediction for the next measurement cycle

In estimation theory, the predicted state estimate is called the a priori estimate and the updated state is called the a posteriori state estimate. The a posteriori estimate is predicted forward in time and becomes the a priori estimate for the next cycle.

The tracking algorithm is executed once for each measurement cycle. Figure 5.17 shows the overview of a complete tracking cycle. One tracking cycle consists of 6 steps:

1. When new measurements are available, the measurements and the existing tracks are associated.

2. Measurements that can not be associated with existing tracks are used to create new tracks.

3. The states of the existing tracks are updated with the associated measurements.

4. Tracks with nearly identical states are merged in order to reduce processing load.

5. Tracks that were not updated for a specified number of cycles, are deleted.

6. The states of the existing tracks are used to predict the states for the next cycle.

5.4.2 Range-Velocity Measurement to Track Update

The data assignment between measurements and track states has been a broad field for many research activities [Blackman 1999]. Applications for advanced tracking assignment techniques are mostly found in the area of

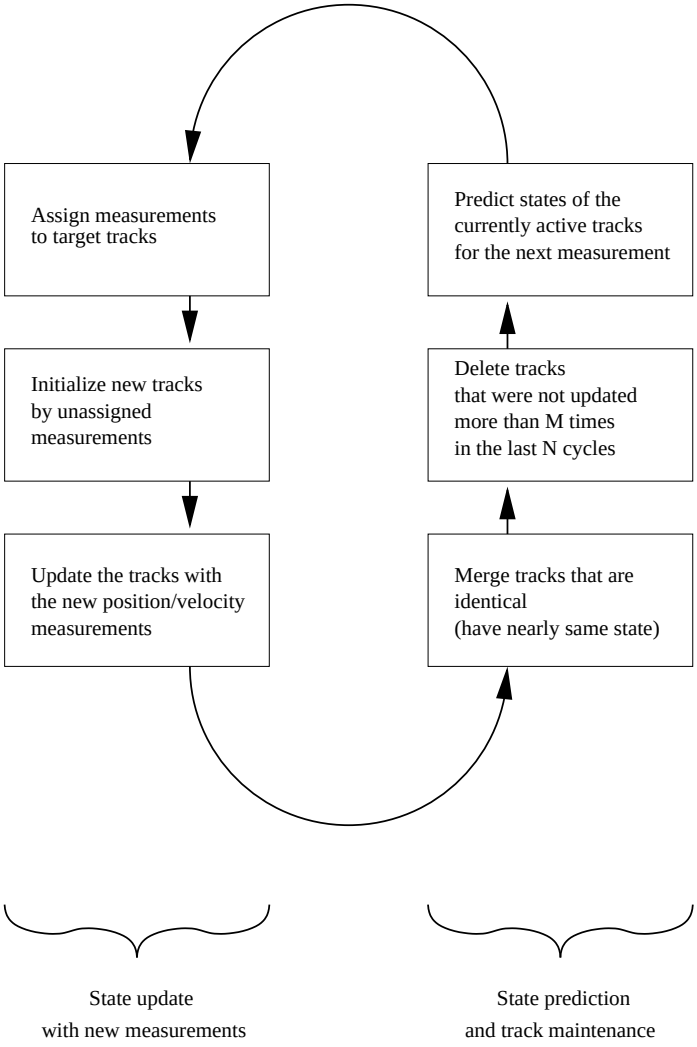

Figure 5.17: Overview of the tracking cycle

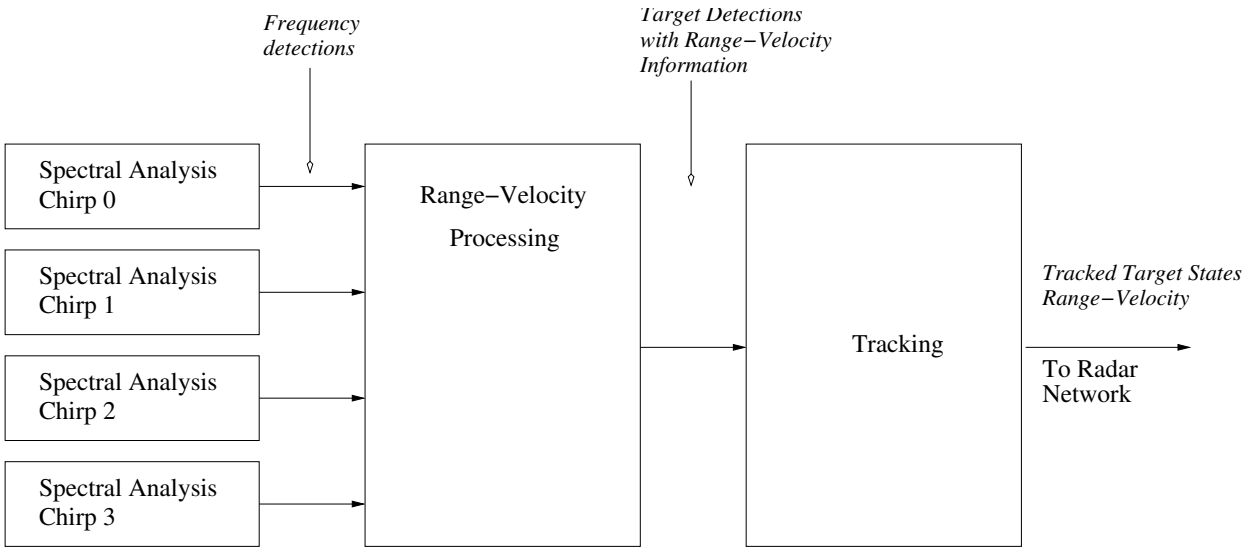

Figure 5.18: LFMCW processing with standard tracker

long range air and sea surveillance systems where the update rate from the radar is relatively low. The lower the measurement update rate the more complicated it is to find the correct associations between successive radar cycles.

The single sensor update rate is relatively high so that for the tracker discussed in this chapter a simple nearest neighbor technique is chosen together with a simple gating mechanism. In the described single sensor tracking algorithm, for each track the frequency measurement is predicted and the nearest actual frequency measurement is selected. Additionally, the error between prediction and measurement is checked. If it is smaller than the predefined gate size, the track is updated by this nearest measurement.

5.4.3 Direct Frequency Measurement to Track Update

The common approach described above is to attach a tracker to the LFMCW processing. This approach can be seen in Figure 5.18. The frequency detections are resolved by the range-velocity processing to obtain targets with range and velocity estimates. These estimates are used as measurements to feed the tracker. Measurement space and track state space are identical.

From the outset, target state estimation with a tracker distinguishes between a target state to be estimated and the measurements that are reported by the radar pre-processing. It also allows the measurement space to be different from the target state space. This is possible as long as the connection between the target state and the corresponding measurements can be sufficiently modeled by a measurement equation.

The proposed tracking strategy directly updates the track with the fre-

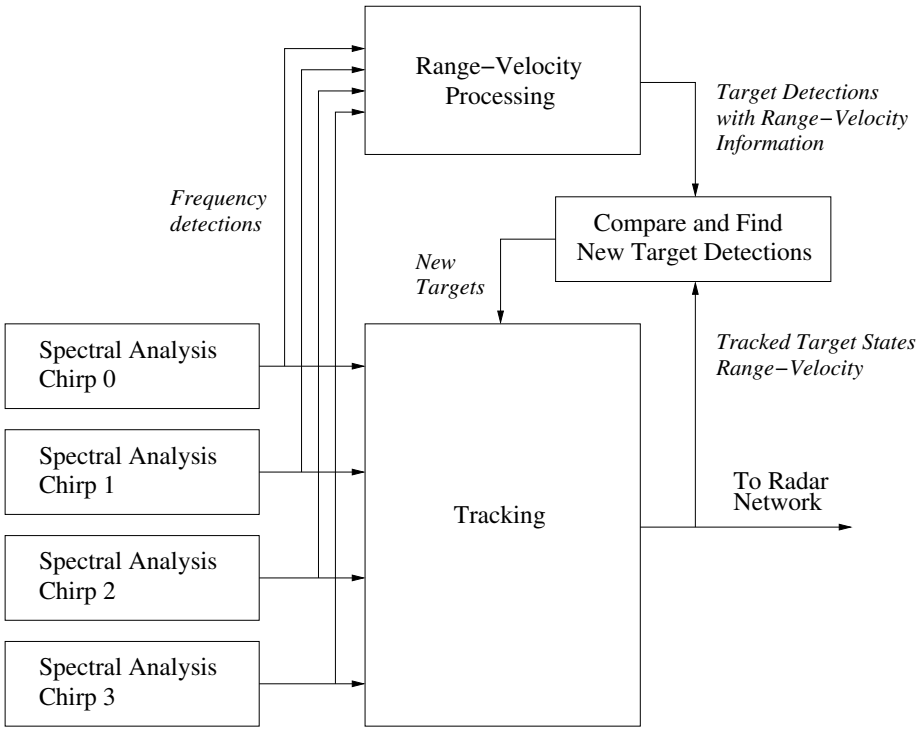

Figure 5.19: LFMCW processing with direct frequency track update

quency measurements from all four chirps. Because the tracker can not detect new targets, the standard range-velocity processing is performed additionally. The range-velocity processing results are compared to the tracked target states to find new targets.

5.4.4 Implementation of the Single Sensor Tracking

The tracker estimates the target states, range R and radial velocity v_r. For each existing track, the state is predicted from the previous state for the current measurement cycle. This is done by the equation of motion:

$$\hat{R}_n^* = \hat{R}_{n-1} + \hat{v}_{r,n-1} T_{cycle}$$

$$\hat{v}_{r,n}^* = \hat{v}_{r,n-1}$$

Since the target acceleration is not included in the track state, the velocity remains unchanged. From the prediction of the state, a prediction of the measurement data is calculated:

$$\begin{pmatrix} \hat{f}_0^* \\ \hat{f}_1^* \\ \hat{f}_2^* \\ \hat{f}_{3,}^* \end{pmatrix} = M \begin{pmatrix} \hat{v}_{r,n}^* \\ \hat{R}_n^* \end{pmatrix}$$

Where M is the LFMCW measurement matrix (Equation 4.3). This measurement prediction is used to find the best fitting (nearest) measurements - one frequency value from each chirp. If the nearest neighboring frequency lies within a specific gate around the expected frequency, this measurement is included to be used for the state update.

For the state update and prediction, a Kalman filter (Section 6.5) can be used. In this case, a simple recursive alpha filter was chosen. Each frequency measurement that is available for the update is used. If no frequency measurement is available from a chirp, the prediction is used for the update. The resulting four frequencies - some of them predictions, some of them actual measurements - are transformed back to the target state space:

$$\begin{pmatrix} \hat{v}^{\circ}_{r,n} \\ \hat{R}^{\circ}_{n} \end{pmatrix} = M^{-1} \begin{pmatrix} \hat{f}_0 \\ \hat{f}_1 \\ \hat{f}_2 \\ \hat{f}_{3,} \end{pmatrix}$$

The new target state is a linear combination from the state prediction and the new state estimate, generated as described above.

$$\begin{pmatrix} \hat{v}_{r,n} \\ \hat{R}_{n} \end{pmatrix} = (1-\alpha) \begin{pmatrix} \hat{v}^{*}_{r,n} \\ \hat{R}^{*}_{n} \end{pmatrix} + \alpha \begin{pmatrix} \hat{v}^{\circ}_{r,n} \\ \hat{R}^{\circ}_{n} \end{pmatrix}$$

The value for the coefficient α is chosen to be very high, for instance $\alpha = \frac{3}{4}$. If the new state estimate is a result from four new frequency measurements, the new state estimate is nearly completely determined by the measurement. The tracks are filtered only lightly for the succeeding network processing stages. The final filtering takes place in the network tracker.

If there are one or more chirps with no suitable measurements, the predicted measurements are used to fill up the missing values. In this case, the prediction has an increasing influence on the new state estimate.

Algorithm 2 summarizes the steps of the proposed pre-tracking technique.

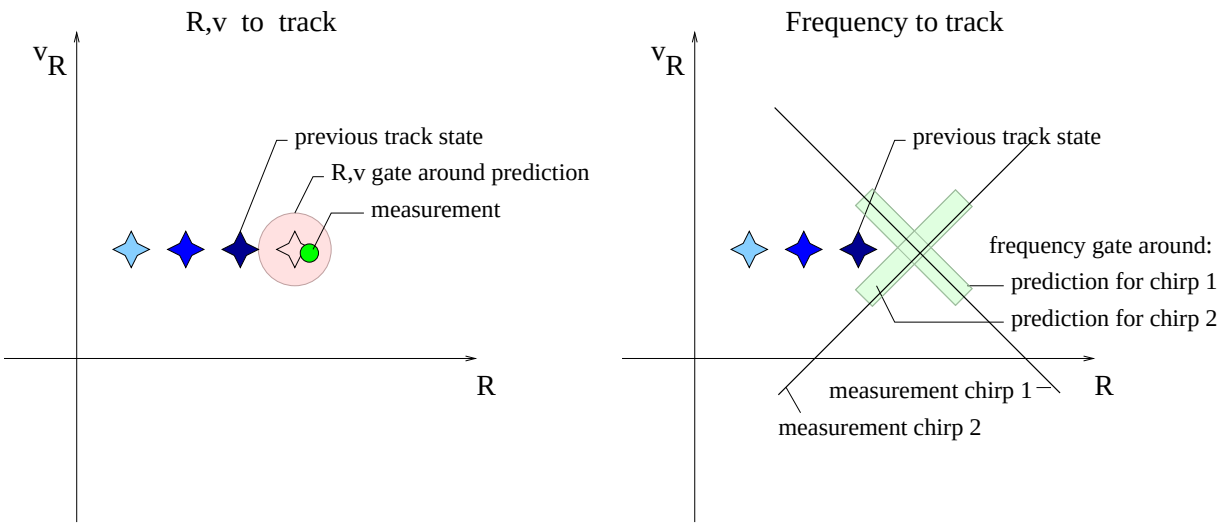

Figure 5.20: LFMCW Tracking: R, v_r-measurement to track assignment (left), frequency to track assignment (right)

Algorithm 2 LFMCW pre-tracking with direct frequency to track update

1. Perform cross sectioning algorithm
2. Find target estimates in the results of the cross sectioning algorithm that are not corresponding to any existing target track. Initiate new tracks with these target estimates.
3. Update tracks directly by the available frequency measurements of the single chirps.
4. Output target list.
5. Move forward track states by the equation of target movement: $R_{n+1} = R_n + v_{r,n} T_{waveform}$.
6. When new measurements are available, start the next cycle.

Chapter 6

Measurement of the Target Position

In this chapter, techniques of measuring the target position are introduced. The classical techniques measure the target angular position, which together with the target range measurement gives complete information about the target position. The target range is measured according to the pulse or CW principles that were introduced in the previous chapters. This chapter first introduces the classical techniques of measuring the target azimuth. Thereon, the concept of radar networks and the trilateration principle is explained.

6.1 Classical Measurement of Target Azimuth

Classical techniques measure the target angle and the target range separately. Commonly, the relative target position in the three dimensional space is specified with one range coordinate and two angular coordinates (azimuth and elevation). Before presenting the classical techniques, the terms azimuth and elevation are defined in the following.

6.1.1 Definition of Azimuth and Elevation

Within the field of navigation, the target position is often presented as a set of range and angle values. This is also the natural representation for many radar systems since target range and angle are measured separately utilizing different effects of the wave propagation. Within navigation, a target position, relative to an observer, is fully described by the value triplet

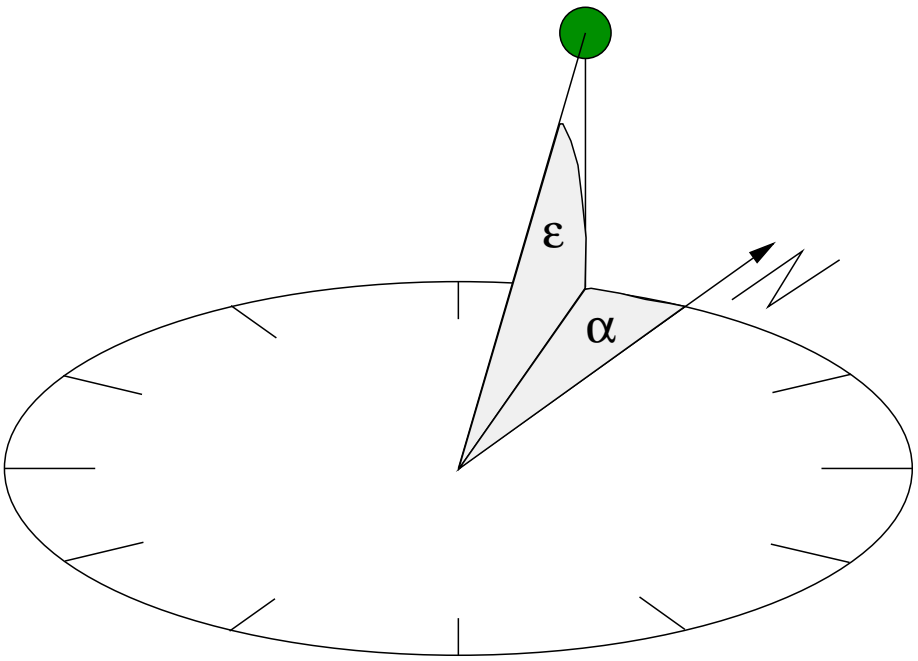

Figure 6.1: Classical definition of azimuth α and elevation ε

range, azimuth angle, and elevation angle. The following definition for azimuth and elevation angle can be found in many dictionaries:

> The azimuth angle is defined as the compass bearing, relative to true (geographic) north, of a point on the horizon that is directly beneath the observed object. As seen from above the observer, compass bearings are measured clockwise in degrees from north.
>
> The elevation angle of an observed object is determined by first finding the point on the horizon directly beneath the observed object, and then measuring the angle between the line going through the observer and this point and the line going through the observer and the observed object.

The definition is visualized in Figure 6.1. In contrast to the above definition, in the following chapters azimuth and elevation are defined as angles relative to the orientation of the radar's coordinate system and the angles are measured anti-clockwise.

6.1.2 Azimuthal Scanning Technique

The most intuitive and familiar technique used to measure the angular position of a target is to scan the observation area in azimuthal direction. Figure 6.2 shows the rotating radar antenna that can be seen at Heathrow

Figure 6.2: Radar antenna at Heathrow airport

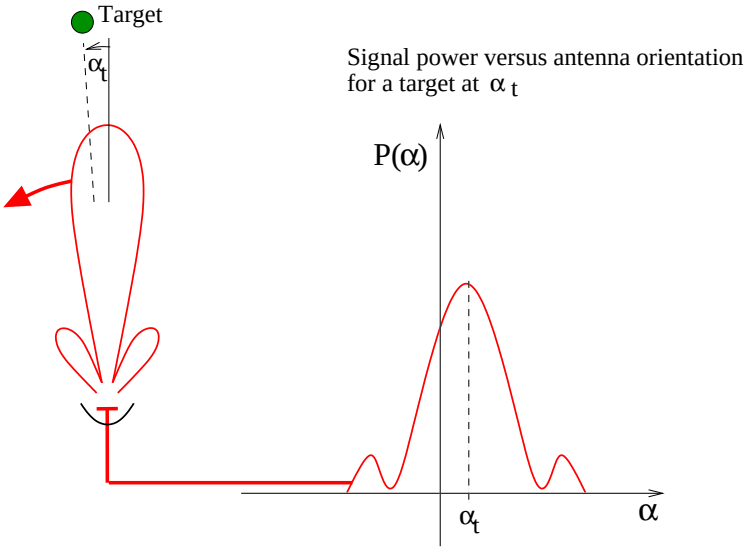

Figure 6.3: Azimuthal scanning principle

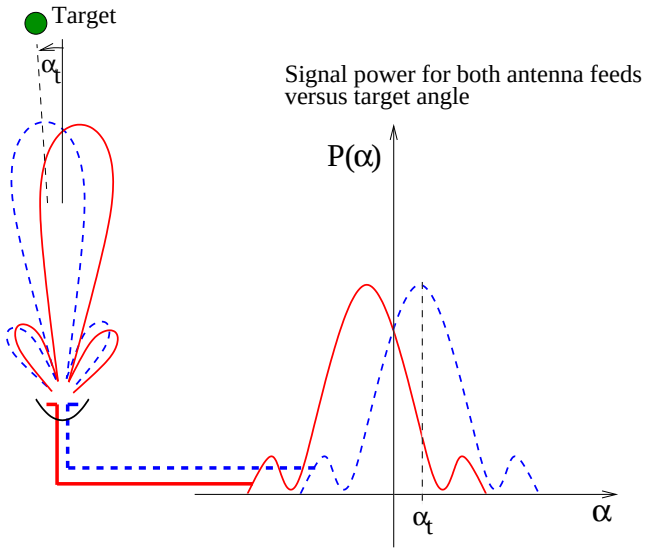

Figure 6.4: Monopulse principle

airport. The radar shown uses a mechanically rotating antenna with a highly focused antenna beam. The radar system scans the observation area in the azimuth angle by doing multiple measurements, each measurement at a different orientation of the antenna. This technique also allows the radar to resolve targets by their azimuth angle if the angular separation is greater than the 3 dB width of the scanning antenna. Figure 6.3 shows measurements of the target echo power while rotating the antenna during the complete measurement sequence. The plot shows the signal power over the azimuth angle of the antenna orientation. The shape of a target peak only depends on the shape of the antenna beam. To precisely estimate the target azimuth position, the center of gravity algorithm can be used. The center of gravity algorithm is described in Sections 4.5 and 5.1 for the LFM frequency estimation.

The described technique of measuring the target azimuth is the most basic technique and can be found in every introductory book on radar.

6.1.3 Monopulse Technique

Another technique to measure the target azimuth is the monopulse technique. Within the field of automotive radar, this technique is preferred over the scanning technique because it does not involve moving parts. The monopulse technique also utilizes the principle of antenna directivity. Figure 6.4 shows the monopulse principle. The radar signal is transmitted over one transmit antenna and is received over a receive antenna system with two antenna beams whose directions are slightly rotated relative to each other.

Both antenna receive signals are processed, and for each target the signal power values from both antenna beam directions are compared. The ratio of the two signal powers depends on the target azimuth. A simple calculation retrieves an estimate of the azimuth value. The monopulse technique got its name from its advantageous characteristic of being able to estimate the target azimuth within one single measurement (pulse). Technically, one receive antenna is used that has multiple feeding points.

The estimate of the target angle α is calculated from the two measurements of target signal power. Assuming that the antenna beams are shaped like a Gaussian bell-shaped curve, a simple equation can be derived to obtain the estimate. For the calculation, it is assumed that the two antenna beams both have the same 3dB width of $\Theta_{3\text{dB}}$ and that they are rotated 2ϑ against each other.

$$P_1 = e^{-a(\alpha+\vartheta)^2} \qquad P_2 = e^{-a(\alpha-\vartheta)^2}$$

$$\frac{P_1}{P_2} = e^{-a(\alpha+\vartheta)^2+a(\alpha-\vartheta)^2}$$

$$\frac{P_1}{P_2} = e^{-4a\alpha\vartheta}$$

$$\alpha = -\frac{1}{4a\vartheta} ln\left(\frac{P_1}{P_2}\right)$$

Where $a = \frac{4ln2}{\Theta^2_{3\text{dB}}}$.

With the digital signal processing capabilities available today, the target angle as a function of the quotient of the signal attenuation can be looked up in a precalculated table. This look-up table is precalculated based on measurements of the actual antenna characteristics.

The observation area for a monopulse receive antenna depends on the beam width and orientation of the receive antenna beams. To be able to estimate a correct target azimuth angle, both antenna beams need to receive the target signal within their main lobes. Therefore, the single antenna main lobes should overlap significantly. To extend the observation area, three options are available:

1. Widen antenna beams and increase angle between beams.

2. Rotate the antenna system and perform additional scanning.

3. Use more than two antenna beams.

The monopulse technique was originally used in military air surveillance systems to continuously track the target with the radar antenna beam. Detailed information on monopulse techniques can be found in many radar textbooks [Levanon 1988, Ludloff 2002]. Also, research within the field of automotive radar has been done [Wagner 1997, Klotz 2002].

6.1.4 Sequential Lobing Technique

A technique closely connected to the monopulse technique is the sequential lobing technique. The sequential lobing technique switches between two or multiple antenna beams rather than receiving and processing all receive antennas in parallel. The advantage is to have a reduced complexity, since only one receiver circuitry is used. The drawback lies in the fact that target fluctuations over time lead to errors in the estimation of the target angle.

6.2 Advantages of Position Estimation with a Radar Network

All three techniques described above use the antenna directivity to estimate the target angular position. The target range and radial velocity can be measured by the standard techniques of a pulse or LFMCW radar. Together, target range and target azimuth give information about the target position. In the field of automotive radar, the target elevation is usually not considered.

Each of the techniques described has its advantages and disadvantages. However, it is also important to consider the targeted observation area. When dealing with advanced automotive applications, where the observation of the complete surroundings of a car is desired, a high number of sensors around the car is needed. All sensors need to have a high number of beams to measure the targets angular position by means of sequential lobing or monopulse techniques. The azimuthal scanning technique has another drawback. A mechanically rotated antenna is not considered to be advantageous for rough automotive environments. Additionally, for some applications, the need for a high measurement update rate sets high demands on the system specifications, leading to high complexity and cost.

A radar network takes a completely different approach to the measurement of the target position. Radar networks are based on lateration techniques that use trigonometry to estimate a targets position. The lateration uses the range measurements of multiple distributed sensors to estimate the

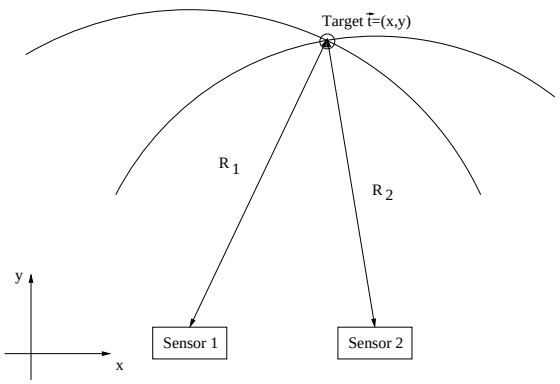

Figure 6.5: Trilateration of one target

target position, while the single sensors themselves do not need to perform an angular position estimation. The advantage is that the sensor hardware requirements and the costs are much lower.

In the next section, the concept of trilateration and the underlying processing algorithms are introduced. The following chapter shows a basic strategy for implementing a network signal processing system. Building on this straightforward processing, advanced signal processing concepts are proposed that optimize the network processing for LFMCW sensors.

6.3 Trilateration

The trilateration technique uses range and optionally also velocity measurements from distributed sensors to estimate the targets position.

The technique of trilateration can be demonstrated graphically by drawing a sensor's range measurement R as a circle with radius R around the sensor. This circle represents all possible positions where the target could be located. If a target is correctly measured by two sensors, two circles can be drawn that intersect at the target position. This is shown in Figure 6.5.

Given a single target with position $\vec{t}$, the ideal range measurements R_1, R_2 of two sensors with positions $\vec{s}_1$, $\vec{s}_2$ can be specified by the theorem of Pythagoras:

$$\left| \begin{array}{l} R_1 = \left|\vec{s}_1 - \vec{t}\right| \\ R_2 = \left|\vec{s}_2 - \vec{t}\right| \end{array} \right|$$

To simplify the calculations, let the first sensor be placed in the coordinate center $\vec{s}_1 = \begin{pmatrix} 0 \\ 0 \end{pmatrix}$ and the second sensor on the x-Axis $\vec{s}_2 = \begin{pmatrix} d \\ 0 \end{pmatrix}$. With a simple shift and rotation, an arbitrary sensor setup can satisfy these

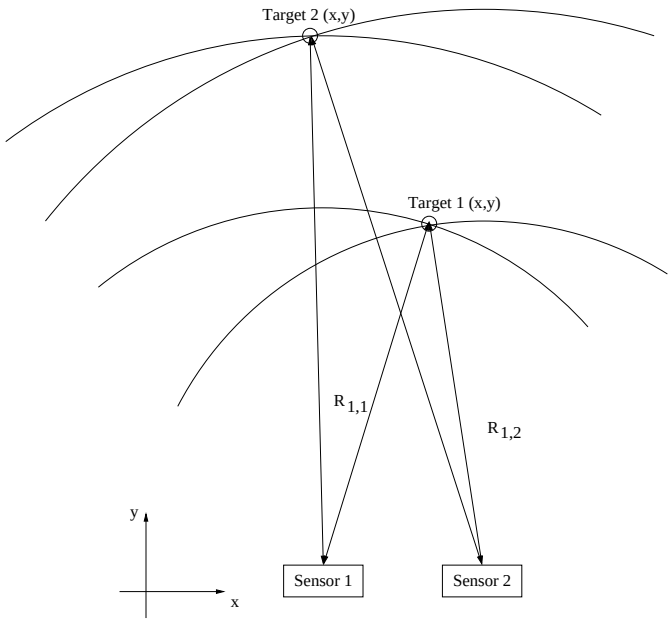

Figure 6.6: Trilateration of well separated multiple targets

constrains. Using these constraints, the two equations can easily be solved for $\vec{t}$:

$$\left| \begin{array}{ll} R_1 = & \sqrt{t_x^2 + t_y^2} \\ R_2 = & \sqrt{(d - t_x)^2 + t_y^2} \end{array} \right|$$

$$\Leftrightarrow \left| \begin{array}{ll} t_x = & \frac{R_1^2 - R_2^2 + d^2}{2d} \\ t_y = & \pm\sqrt{R_1^2 - t_x^2} \end{array} \right| \tag{6.1}$$

Usually, only one solution is wanted. If the sensor's antenna beams are looking in the direction of the y-axis, only a target position with positive y-coordinate is valid. The visualization of the trilateration technique is very similar to the LFMCW technique of range-velocity processing. The obvious difference is that the trilateration is represented by intersecting circles while the LFMCW range-velocity processing is represented using straight lines. The advantage of circles can be seen in Figure 6.6: Multiple targets do not necessarily produce ambiguities when assigning the ranges to the targets. Ambiguities only appear if the range differences between targets, seen from different sensors, are smaller than the distance between the sensors ($|R_1 - R_2| < d$).

Using LFMCW sensors for trilateration the sensors also provide information on the target's radial velocity. Having the target position precomputed as shown above, the target velocity $\vec{v_t}$ is related to the radial target velocities

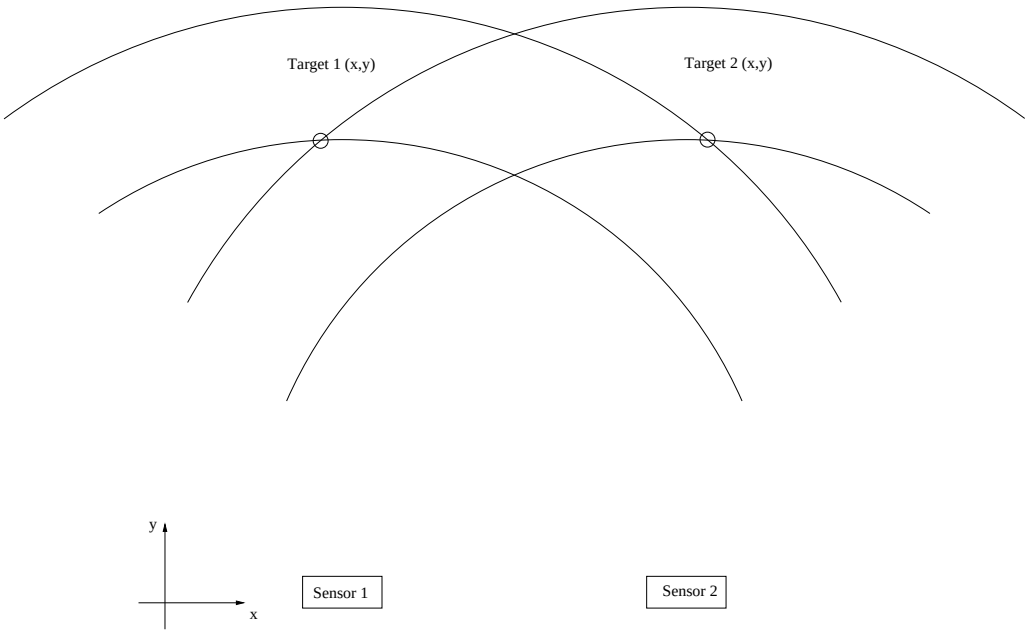

Figure 6.7: A situation which can not be resolved by two sensors

v_{ri} (measured from sensor i) by:

$$v_{ri} = \frac{\left(\vec{t} - \vec{s_i}\right) \vec{v_t}}{\left|\vec{t} - \vec{s_i}\right|} = \vec{r}_{in}\vec{v_t} = r_{inx}v_x + r_{iny}v_y$$

Where $\vec{r}_{in}$ is introduced as the normalized vector between sensor i and the target. With known target position and radial velocity measurements, the target velocity can be calculated:

$$\begin{pmatrix} v_x \\ v_y \end{pmatrix} = \frac{1}{r_{1nx}r_{2ny} - r_{1ny}r_{2nx}} \begin{pmatrix} r_{2ny} & -r_{1ny} \\ -r_{2nx} & r_{1nx} \end{pmatrix} \begin{pmatrix} v_{r1} \\ v_{r2} \end{pmatrix} \tag{6.2}$$

When two target ranges are close to each other, invalid intersections can appear. Such a situation is shown in Figure 6.7. Similar to the LFMCW processing, these invalid cross-sections are called ghost targets. Analogous to the increase of chirps in the LFMCW waveform, the number of sensors can be increased. A target measured with four sensors yields an intersection of four intersecting circles. This is shown in Figure 6.8. The valid intersections are distinguished from the ghost targets by the number of range-circles contributing to an intersection.

With one target measurement from each of the $N = 4$ sensors, a system with N equations can be set up for the target position and for the target

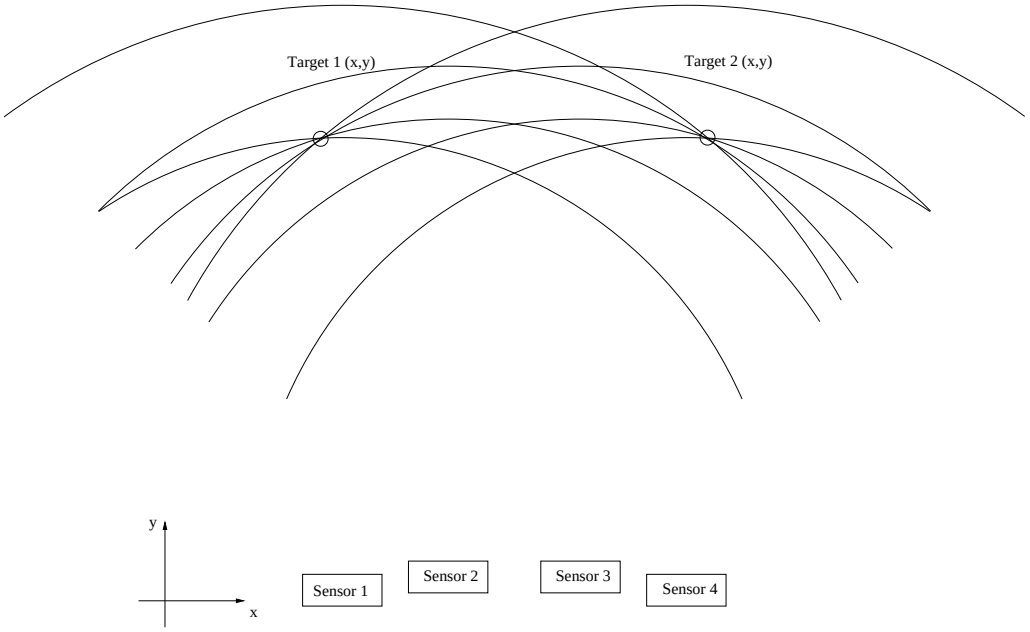

Figure 6.8: Using four sensors to resolve targets with similar ranges

velocity:

$$\vec{R}(\vec{t}) = \begin{pmatrix} \left|\vec{t} - \vec{s_1}\right| \\ \left|\vec{t} - \vec{s_2}\right| \\ \vdots \\ \left|\vec{t} - \vec{s_N}\right| \end{pmatrix} \tag{6.3}$$

$$\vec{V}_r(\vec{t}) = \begin{pmatrix} r_{1nx} & r_{1ny} \\ r_{2nx} & r_{2ny} \\ \vdots & \vdots \\ r_{Nnx} & r_{Nny} \end{pmatrix} \vec{v} \tag{6.4}$$

Again, r_{inx} and r_{iny} are the components of the normalized distance vector between sensor i and the target.

The equation system $\vec{R}\left(\vec{t}\right)$ is non-linear and also overdetermined in the case of more than two sensors contributing a range measurement. To estimate the target position $\vec{t}$, an iterative algorithm like the Gauss-Newton algorithm can be used. This operation produces a target position estimate according to the minimum mean square error (MMSE) criterion.

Although both equation systems can be solved together, it is computationally less expensive to get an estimate of the position $\hat{\vec{t}}$ and then solve the second equation system $\vec{V}_r(\hat{\vec{t}}, \vec{v})$, that is linear when $\hat{\vec{t}}$ is used as a constant estimate for $\vec{t}$. This approach is suboptimal compared to solving the two

systems $\left| \begin{array}{c} \vec{R}_i\left(\vec{t}\right) \\ \vec{V}_i\left(\vec{t},\vec{v}_r\right) \end{array} \right|$ together. Simulations with practical system parameters show that the loss in accuracy is negligible.

6.4 Gauss-Newton Algorithm

The trilateration equation system is nonlinear and it is overdetermined in the case that more than two sensors contribute a measurement to the target estimation. For this case, a basic approach is to find the best estimate according to the MMSE criterion. The error in the measurement space is defined as:

$$\vec{e} = \vec{R}_m - \vec{R}\left(\hat{\vec{t}}\right) = f\left(\hat{\vec{t}}\right)$$

Where $\vec{R}_m$ is the measurement data vector and $\vec{R}\left(\hat{\vec{t}}\right)$ is the expected measurement for a target estimate $\hat{\vec{t}}$. The sum of the squared vector elements is to be minimized:

$$\min_{\vec{t}}\left(\vec{e}^T\vec{e}\right) = \min_{\vec{t}}\left(\vec{f}\left(\vec{t}\right)^T\vec{f}\left(\vec{t}\right)\right)$$

The Gauss-Newton algorithm performs multiple iterations of linearizing the equation system at some approximated solution $\vec{t}_i$ and iteratively approaching the MMSE solution $\hat{\vec{t}}^*$. Important for stability and a fast convergence to the solution is the starting point of the search $\vec{t}_0$. For the trilateration, a good starting point can be obtained by intersecting two sensor measurements by basic trigonometry as shown above. Using this starting point, the Gauss-Newton algorithm is fast and stable enough for the radar trilateration processing. The Gauss Newton algorithm is described in Algorithm 3.

For the trilateration application, the Gauss-Newton algorithm has to linearize the trilateration equation system (6.3) at point $\vec{t}_0$. The matrix of the linearized system (at point $\vec{t}_0$) is called the Jacobian matrix $J = \frac{\partial\vec{R}(\vec{t})}{\partial\vec{t}}\left|\vec{t_0}\right.$. Starting from the nonlinear system $\vec{R}(\vec{t})$, the Jacobian can be calculated as follows:

$$\vec{R}(\vec{t}) = \begin{pmatrix} \left|\vec{t}-\vec{s_1}\right| \\ \left|\vec{t}-\vec{s_2}\right| \\ \vdots \\ \left|\vec{t}-\vec{s_N}\right| \end{pmatrix} = \begin{pmatrix} \sqrt{\left(t_x-s_{1x}\right)^2+\left(t_y-s_{1y}\right)^2} \\ \sqrt{\left(t_x-s_{2x}\right)^2+\left(t_y-s_{2y}\right)^2} \\ \vdots \\ \sqrt{\left(t_x-s_{Nx}\right)^2+\left(t_y-s_{Ny}\right)^2} \end{pmatrix}$$

Algorithm 3 Gauss Newton

Task: Find the MMSE solution for: $\vec{f}_m = \vec{f}\left(\vec{t}_i\right)$

1) Start with first iteration $i = 0$, get some initial estimate $\vec{t}_0$.

2) Linearize the equation system at the current approximation $\vec{t}_i$ by calculating $\vec{f}_i = \vec{f}\left(\vec{t}_i\right)$ and the Jacobian matrix for $\vec{f}$ at $\vec{t}_i$:

$$J_i = \frac{d\vec{f}}{d\vec{t}} = \begin{pmatrix} \frac{\partial f_0}{\partial t_x} & \frac{\partial f_0}{\partial t_y} \\ \frac{\partial f_1}{\partial t_x} & \frac{\partial f_1}{\partial t_y} \\ \frac{\partial f_2}{\partial t_x} & \frac{\partial f_2}{\partial t_y} \\ \frac{\partial f_3}{\partial t_x} & \frac{\partial f_3}{\partial t_y} \end{pmatrix}$$

3) Solve the linear problem $\vec{f}_m = \vec{f}_i + J_i\vec{dt}$ for the MMSE criterion:

$$\vec{dt} = \left(J_i^T J_i\right)^{-1} J_i^T \left(\vec{f}_m - \vec{f}_i\right)$$

4) Generate a new approximation:

$$\vec{t}_{i+1} = \vec{t}_i + \vec{dt}$$

5) Test for the break condition, if $\left|\vec{dt}\right|^2 < \lambda$ the algorithm has finished.

6) Increment i, start next iteration at step 2.

$$\frac{\partial \vec{R}(\vec{t})}{\partial \vec{t}}\Big|_{\vec{t_0}} = \begin{pmatrix} \frac{t_{0x}-s_{1x}}{\left|\vec{t_0}-\vec{s_1}\right|} & \frac{t_{0y}-s_{1y}}{\left|\vec{t_0}-\vec{s_1}\right|} \\ \frac{t_{0x}-s_{2x}}{\left|\vec{t_0}-\vec{s_2}\right|} & \frac{t_{0y}-s_{2y}}{\left|\vec{t_0}-\vec{s_2}\right|} \\ \vdots & \vdots \\ \frac{t_{0x}-s_{nx}}{\left|\vec{t_0}-\vec{s_N}\right|} & \frac{t_{0y}-s_{ny}}{\left|\vec{t_0}-\vec{s_M}\right|} \end{pmatrix} \tag{6.5}$$

With the known target position, the velocity is calculated by the linear system (6.4). It is very convenient that this linear system and the above Jacobian of the nonlinear system (6.3) have the same matrix.

As far as calculation speed and numerical stability is concerned, there are better algorithms than the Gauss-Newton algorithm to solve this nonlinear equation, but these factors are not considered in this thesis. Concerning the estimation quality, no noticeable difference between algorithms is observed within a practical radar application.

6.5 The Kalman Filter

To increase the accuracy of the target parameter estimates, the measurements can be filtered over time. A significant improvement of accuracy can be obtained because the observed targets obey the physical laws of motion. The Kalman filter is model-based and very suitable for this application, provided that some preconditions are met.

The Kalman filter distinguishes between the state of a process and the observable values. The process state is not accessed directly but measured indirectly over a measurement process. Both, the state process and the measurement process are modeled by linear equations. The extended Kalman filter allows the use of nonlinear equations and so greatly extends the scope of possible applications. The extended Kalman filter is used for the improved network processing algorithms in Chapter 8.

6.5.1 The Linear Kalman Filter

The original linear Kalman filter is a model based state estimator. The filter is optimal in the sense that it minimizes the variance of the error of the estimated state. The Kalman filter is the optimal estimator for a large class of problems including those in the field of radar.

The original Kalman filter uses discrete data as input, and it is implemented as a recursive algorithm that only needs the current state to be stored. These two properties made the Kalman filter very popular for digital signal processing. The filter was first described in 1960 by R.E.Kalman [Kalman 1960].

As mentioned above, the linear Kalman filter is based on some assumptions about the problem. The first is, that the system process state at time step k can be stated as a vector x_k and the system process can be modeled by a simple difference equation:

$$x_k = Ax_{k-1} + w_{k-1}$$

Where A is the process matrix and w_k is the process noise that combines all nondeterministic (or not modeled) influences on the state.

The internal system state x_k is not observed directly. Instead, the system output z_k is measured. Obtaining the measurement z_k is modeled by:

$$z_k = Hx_k + v_k$$

Where H is the measurement matrix and v_k is the measurement noise.

Both random variables, w_k and v_k are assumed to be independent of each other and to have normal probability distributions with the following

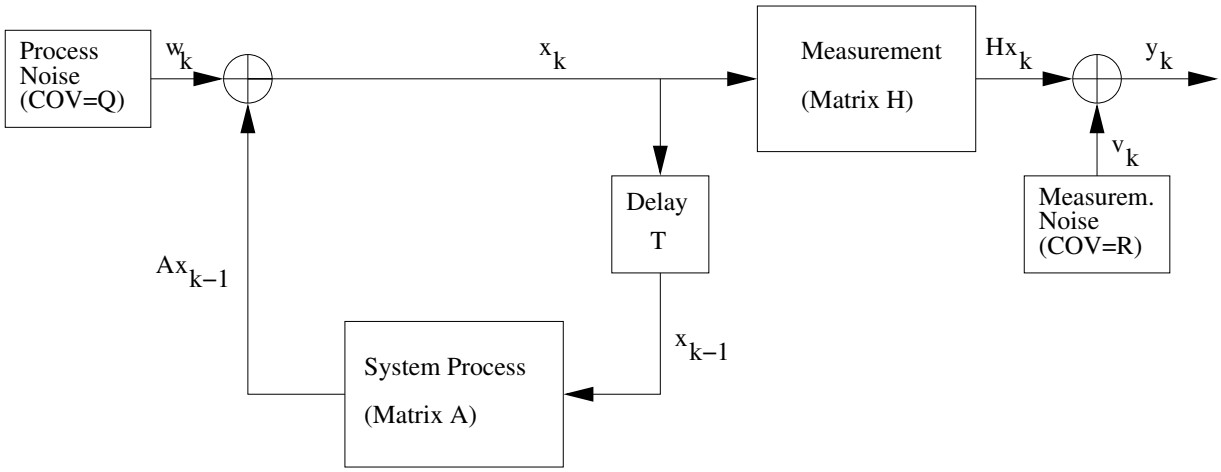

Figure 6.9: System model for the Kalman filter

(known) covariance matrices:

$$E(w_k w_k^T) = Q$$

$$E(v_k v_k^T) = R$$

This system model is illustrated in Figure 6.9.

The Kalman filter uses this system model to estimate the process state. At time step k the process is at state x_k and the measurement vector z_k is observed. At this step, two state estimates can be distinguished: the a priori state estimate $\hat{x}_k^*$ that is determined without knowledge of the new measurement, and the a posteriori estimate $\hat{x}_k$ that includes knowledge of the measurement z_k. The covariances of the a priori and a posteriori estimation error are defined as:

$$P_k^* = E\left((x_k - \hat{x}_k^*)(x_k - \hat{x}_k^*)^T\right)$$

$$P_k = E\left((x_k - \hat{x}_k)(x_k - \hat{x}_k)^T\right)$$

The goal of the Kalman filter is to minimize the error variance of the a posteriori estimate:

$$\min\left((x_k - \hat{x}_k)^T (x_k - \hat{x}_k)\right)$$

It can be proven [Kalman 1960] that the following linear equation minimizes the error:

$$\hat{x}_k = \hat{x}_k^* + K_k(z_k - H\hat{x}_k^*) \tag{6.6}$$

In the above equation, the difference $(z_k - H\hat{x}_k^*)$ between actual and predicted measurement is called the measurement innovation. The matrix K

is called the Kalman gain. Its value is calculated to minimize the error variance of the a posteriori state estimate:

$$K_k = P_k^* H^T \left(H P_k^* H^T + R \right)^{-1} \tag{6.7}$$

The covariance matrix of the new a posteriori state estimate is:

$$P_k = (I - K_k H) P_k^* \tag{6.8}$$

Where I is the unitary matrix. The following algorithm shows all steps of the Kalman filter loop. The steps can be grouped into an initialization part and two main parts: the corrector and the predictor.

Algorithm 4 The recursive Kalman algorithm.

Initialization

1. Start with an initial state estimate $\hat{x}_0^*$ and its covariance matrix P_0^*. Set k to zero.

First Part: Corrector

2. Obtain the measurement data vector z_k, its covariance R and the process covariance Q.

3. Build the Kalman gain K_k (Equation (6.7)) and estimate the a posteriori probability $\hat{x}_k$ and its covariance matrix P_k with equations (6.6) and (6.8).

Second Part: Predictor

4. Increment k.

5. Calculate the state prediction which is the a priori estimate for the next step: $\hat{x}_k^* = A\hat{x}_{k-1}$

6. Calculate its covariance: $P_k^* = AP_{k-1}A^T + Q$

7. When the next measurement z_k is available, go back to step 2.

The original Kalman state prediction includes a term for a known (additively superimposed) influence on the state: $\hat{x}_k^* = A\hat{x}_{k-1} + Bu_k$. The second term does not influence any other Kalman filter equations. More details can be found in [Sorenson 1970].

6.5.2 The Extended Kalman Filter

The extended Kalman filter (EKF) is the extension of the linear Kalman filter to nonlinear systems and nonlinear measurement equations. The EKF uses nonlinear system equations and linearizes these equations for each filter step. Linearization is done at the current estimate of the state.

The extended Kalman filter uses the following nonlinear state difference equation:

$$x_k = a\left(x_{k-1}, w_{k-1}\right)$$

Also the measurement equation is given as a nonlinear function:

$$z_k = h\left(x_k, v_k\right)$$

For the linear Kalman filter, the process matrix A is used for the state prediction and the update of the state error covariance matrix. The extended Kalman filter uses $a(x_k, 0)$ for the state prediction and the Jacobian A_k of $a(x_k, w_k)$ for the update of the state error. The Jacobian A_k is the partial derivation of $a(x, w)$ with respect to x at the currently estimated position $\hat{x}_{k-1}$:

$$A_k = \frac{\partial a}{\partial x}(\hat{x}_{k-1})$$

Accordingly, instead of the measurement matrix H, the Jacobian of the measurement function $h(x, v)$ is used. The Jacobian H_k is the partial derivation of $h(x, v)$ with respect to x at the currently best estimate $(\hat{x}_k^*, 0)$:

$$H_k = \frac{\partial h}{\partial x}(\hat{x}_k^*)$$

In the presented nonlinear model equations, also the noise vectors w_k and v_k contribute nonlinearly to the state prediction and the measurement vector. Therefore, the linearizations for the noise vectors are considered for the extended Kalman filter:

$$W_k = \frac{\partial a}{\partial w}(\hat{x}_{k-1})$$

$$V_k = \frac{\partial h}{\partial v}(\hat{x}_k^*)$$

The original Kalman filter prediction and update equations, described in the previous section, are modified to take into account the nonlinear influence

of the noise vectors. Within the calculation of the Kalman gain, the noise covariance is transformed by Jacobian V_k:

$$K_k = P_k^* H_k^T \left(H_k P_k^* H_k^T + V_k R_k V_k^T \right)^{-1}$$

The a posteriori state update equation is changed, because the measurement innovation can be calculated directly from the nonlinear measurement equation:

$$\hat{x}_k = \hat{x}_k^* + K_k \left(z_k - h \left(\hat{x}_k^*, 0 \right) \right)$$

The calculation of the a posteriori covariance remains unchanged:

$$P_k = \left(I - K_k H_k \right) P_k^*$$

The state prediction can be calculated by the nonlinear update function, the estimate is calculated with the (unknown) noise vector set to its expected value:

$$\hat{x}_k^* = a \left(\hat{x}_{k-1}, 0 \right)$$

The covariance of the predicted state includes the transformation of the measurement noise variance by Jacobian W_k:

$$P_k^* = A_k P_{k-1} A_k^T + W_k Q_k W_k^T$$

6.6 Multilateration with Synchronized Networks

6.6.1 Multistatic Radar Network

The multilateration technique is an extension of trilateration procedure. The technique is based on a network of multiple sensors that are able to do multistatic measurements. In a multistatic measurement one station is transmitting while other stations located at different positions are receiving. This technique is known from aeronautical and military applications [Willis 1991].

An automotive radar network with four multistatic sensors can alternately switch one of the four sensors to transmit mode while all four sensors are in receive mode. In such a network, a multistatic sensor has to be able to receive and process the signal not only originating from its own transmitter, but also from the other sensors transmitters. In order to accomplish this in practice the sensors have to be synchronized precisely.

The advantage of a synchronized network lies in the increased number of signal paths that are measured. While a 4 sensor network with monostatic sensors can measure 4 signal paths, a network with four multistatic sensors can measure 16 signal paths from which 10 are different.

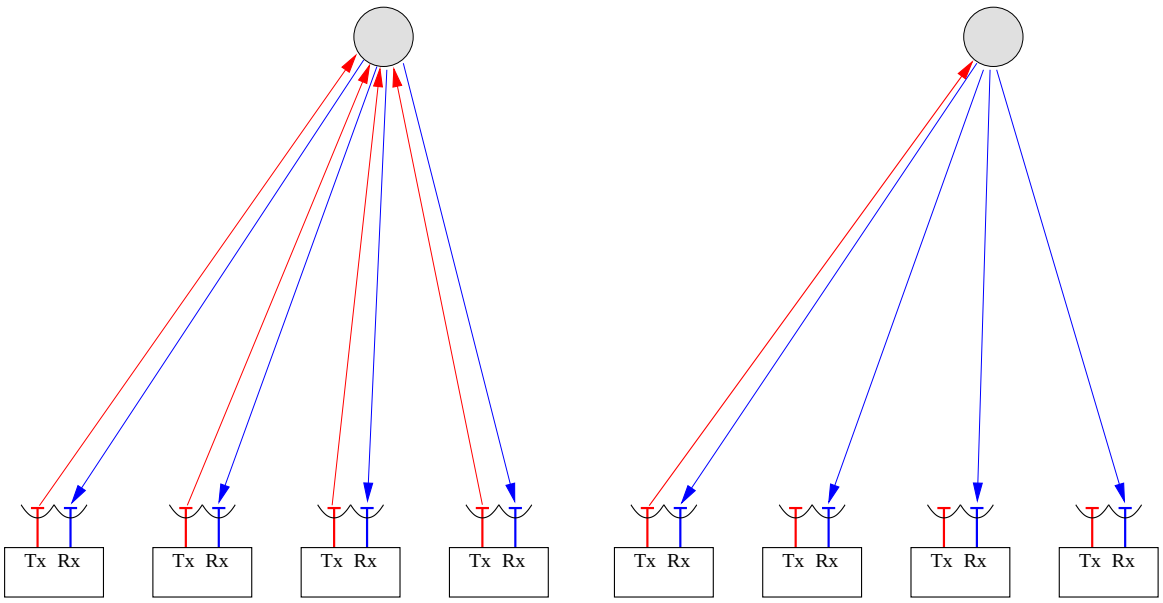

(a) monostatic (b) multistatic

Figure 6.10: Radar network with (a) monostatic and (b) bistatic measurement

6.6.2 Multilateration Algorithm

The multilateration algorithm is merely an extension to include the additional signal paths. In order to include these paths, a slight change in nomenclature is made. With trilateration, the signal propagation delay τ_i from sensor i to the target and back to the sensor directly corresponds to the target range:

$$R_i = \tau_i \frac{c}{2}$$

In contrast to this, the multistatic measurement measures the propagation delay between the transmitting sensor i to the target and back to a receiving sensor j:

$$D_{i,j} = R_i + R_j = \left|\vec{t} - \vec{s_i}\right| + \left|\vec{t} - \vec{s_j}\right|$$

The same applies to the single sensor velocity measurements:

$$v_{i,j} = v_{ri} + v_{rj} = \frac{\left(\vec{t} - \vec{s_i}\right)\vec{v_t}}{\left|\vec{t} - \vec{s_i}\right|} + \frac{\left(\vec{t} - \vec{s_j}\right)\vec{v_t}}{\left|\vec{t} - \vec{s_j}\right|}$$

Using this definition, the trilateration is a special case of the multilateration, measuring only those signal paths, for which the receiving sensor is also the transmitting sensor:

$$R_i = \frac{1}{2} D_{i,i}$$

Equivalently to the trilateration case, the multistatic measurements are related to the target position via a nonlinear equation system. The multilateration equation system can also be solved by the Gauss Newton algorithm. Because of the relation $D_{i,j} = R_i + R_j$ there is a simple linear connection between the trilateration equations and the multilateration equations:

$$\vec{D} = M\vec{R}$$

$$\begin{pmatrix} D_{0,0} \\ D_{0,1} \\ D_{0,2} \\ D_{0,3} \\ D_{1,0} \\ D_{1,1} \\ D_{1,2} \\ D_{1,3} \\ D_{2,0} \\ D_{2,1} \\ D_{2,2} \\ D_{2,3} \\ D_{3,0} \\ D_{3,1} \\ D_{3,2} \\ D_{3,3} \end{pmatrix} = \begin{pmatrix} 2 & & & \\ 1 & 1 & & \\ 1 & & 1 & \\ 1 & & & 1 \\ 1 & 1 & & \\ & 2 & & \\ & 1 & 1 & \\ & 1 & & 1 \\ 1 & & 1 & \\ & 1 & 1 & \\ & & 2 & \\ & & 1 & 1 \\ 1 & & & 1 \\ & 1 & & 1 \\ & & 1 & 1 \\ & & & 2 \end{pmatrix} \begin{pmatrix} R_0 \\ R_1 \\ R_2 \\ R_3 \end{pmatrix} \tag{6.9}$$

This can be utilized to reduce the calculation complexity solving the multilateration equation system.

To theoretically determine the position estimation performance of a radar network, the accuracy measuring a point target is usually referenced. The measured ranges are assumed to have an additively superposed uncorrelated Gaussian error. Comparing the trilateration and multilateration technique by the theoretical analysis shows that both techniques result in approximately the same performance. This is not surprising, since only the signal paths are combined in a slightly different way. The result can be found analytically by examining the connection between trilateration and multilateration through equation 6.9 and determining the relation between covariance matrix $E\left(\vec{R}\vec{R}^T\right)$ and $E\left(\vec{D}\vec{D}^T\right)$.

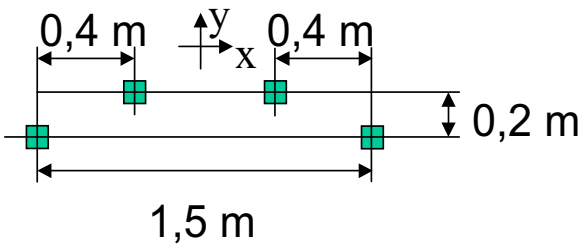

Figure 6.11: Example network configuration with 4 sensors

The incorporation of multistatic measurement principles was proposed to take advantage of the increased number of aspect angles on an extended target without increasing the number of sensors. Furthermore, the characteristics of the target reflections are different for a multistatic measurement compared to a monostatic measurement.

To investigate the advantages of multistatic measurements, the European project RadarNet has set itself the target of incorporating a multistatic measurement mode into a radar network [Lübbert 2002]. Within this project, there has been much progress made in the implementation of the multistatic measurement technique, which demands a highly precise synchronization of the sensor local oscillators. Synchronization has to be precise, so that for the time of a complete chirp signal, a sensor can coherently mix down the signal of another sensor. Successful measurements were done in the laboratory, measurements of actual traffic scenes are expected in the future.

6.7 Requirements on the Single Sensors

From the lateration principle it follows that the single sensor range accuracy needs to be very high to achieve good angular measurement results [Klotz 2002]. To obtain a rough approximation of the position error, an example network configuration with four sensors is used as shown in Figure 6.11.

When the target to be measured is located far from the sensor network compared to the distance between the single sensors, the target position can approximately be decomposed into a range and a tangential component. The range between target and network center is approximately the mean target range measured from the single sensors. The tangential component is derived from the difference between each sensors target range measurement. The estimation accuracy of the range component is of the order of the single sensor range accuracy, which is high in the investigated system. In contrast,

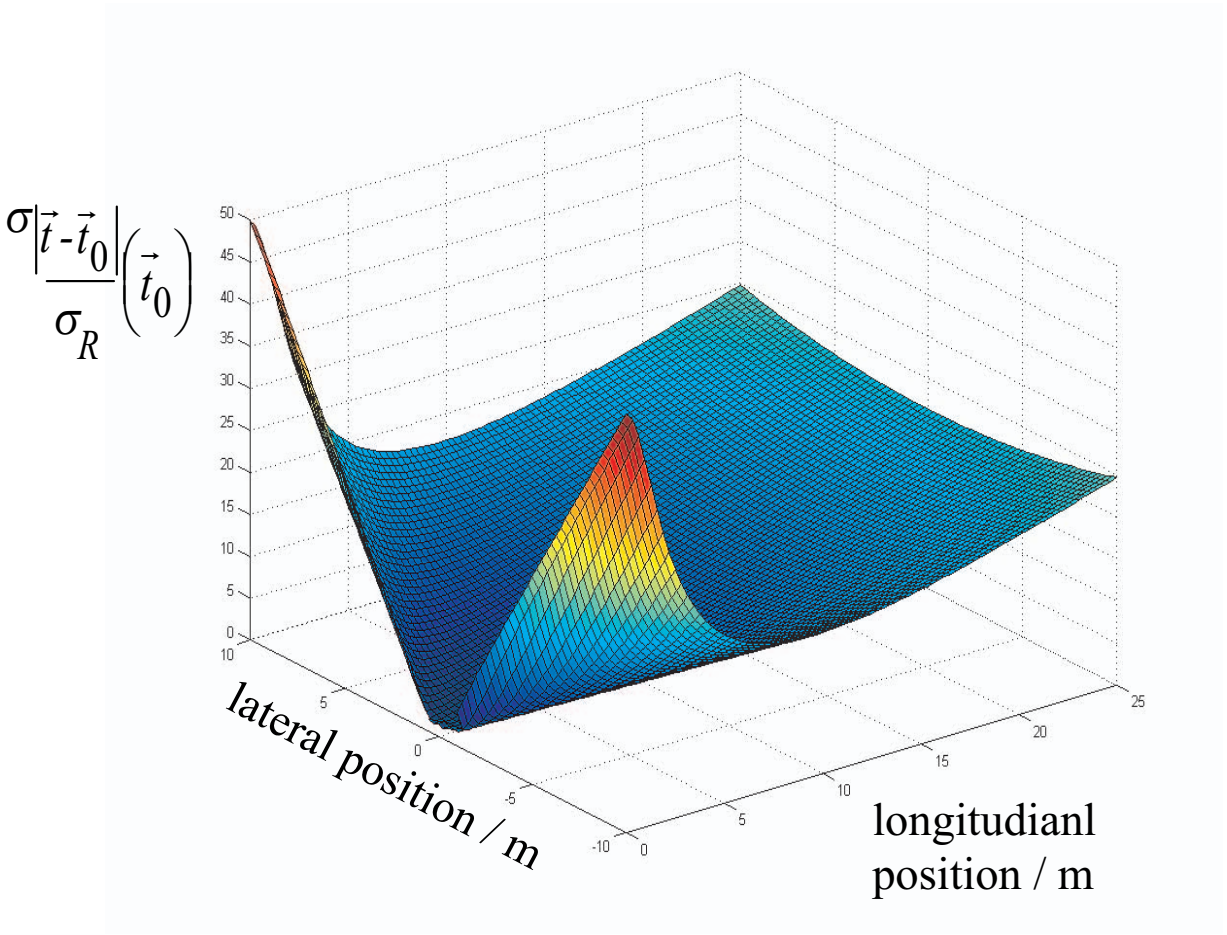

Figure 6.12: Accuracy of position estimation in relation to the single sensor range accuracy.

the accuracy of the tangential component can be very much lower.

The deviation $\sigma_{tang.}$ of the tangential component of the position estimate depends approximately linearly on the deviation σ_R of the single sensor range estimate. This holds true for small deviations where the relationship between target position $\vec{t}$ and range measurements R_i can be approximated by a linear equation system. Furthermore, the tangential deviation $\sigma_{tang.}$ is approximately equal to the deviation $\sigma_{|\vec{t}-\vec{t_0}|}$ of the magnitude of the position error vector. The factor $\frac{\sigma_{|\vec{t}-\vec{t_0}|}}{\sigma_R}$ is plotted in Figure 6.12. The factor is depending on the actual target position $\vec{t_o}$. For a target 25m in front of the sensor network, this factor is 20. This means that for a single sensor range accuracy of 2.5 cm, the tangential component of the position estimate has an accuracy of half a meter. The plot was created using the trilateration equation linearized at position $\vec{t_o}$ and inverted as done in the solution of the trilateration equations described in Section 6.4.

The next important ability of interest is the resolution of targets with nearly same distances but different azimuth positions. For this, the single sensors are required to have a very high range resolution capability. In a dynamic traffic scenario with relative movement between targets and radar, a high resolution in velocity can assist the process of resolving targets with different angular positions. In a dynamic scenario, target fluctuations also appear, so that closely neighboring targets are likely to be measured with different signal amplitudes in each cycle. This effect can be used to resolve closely neighboring targets over time.

Real physical range resolution is directly determined by the used bandwidth. The amount of bandwidth available is not only a technical issue or a question of cost. This is also a regulatory issue of frequency allocation. The 77 GHz frequency band is very likely to provide a full 1 GHz of bandwidth which can be used for automotive applications. The LFMCW single sensors in the underlying project have a sweep bandwidth of 450 MHz which gives a practical range resolution of about half a meter when using an FFT and a window function (Section 4.2). This is a much poorer resolution than was available in previous 24 GHz systems [Klotz 2002].

Chapter 7

Classical Radar Network Signal Processing

In Chapter 6 the relation between the range measurements of one target and its position estimation in Cartesian coordinates is described. It is shown how to solve the trilateration equations which form a nonlinear and overdetermined system. An important capability of automotive radar systems is the resolution of multiple targets within the observation area. When the measurement data space is different from the estimation space, resolving multiple targets is often not trivial as can also be seen in the previously described LFMCW signal processing methods. The resolution of multiple targets is done by the data assignment stage of the network processor.

In this section, a straightforward implementation of the network signal processing is described, as introduced in [Klotz 2002]. This implementation can be separated in three major processing modules as shown in Figure 7.1. These modules are:

1. Data assignment,
2. Trilateration,
3. Target tracker.

The data assignment module receives target lists from the attached single sensors. These lists contain target detections together with the corresponding target range and radial velocity information. These ranges and radial velocities are assigned to one or multiple target hypotheses.

The trilateration module receives the target hypotheses as a set of multiple ranges together with a coarsely pre-estimated position. The trilateration

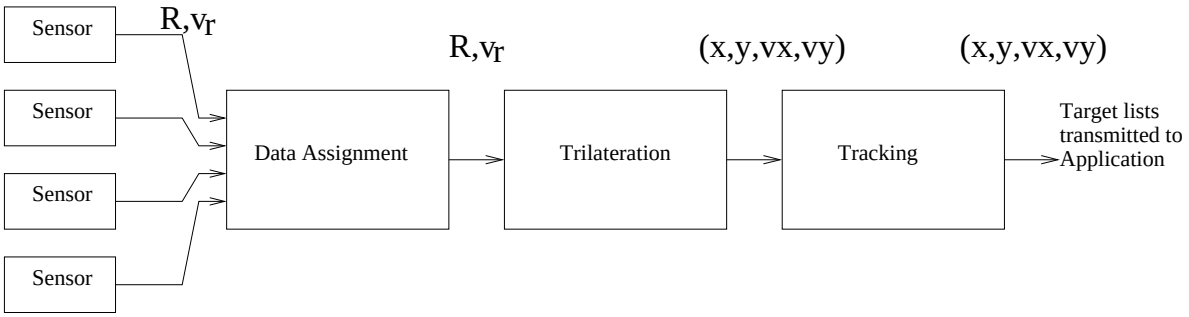

Figure 7.1: Straightforward network processing

module combines these ranges and estimates the target position and velocity in 2 dimensional Cartesian coordinates.

The tracker receives the trilaterated position and velocity estimates. It tries to assign all these target position-velocity measurements to the currently active tracks. If some measurements could not be assigned, they are used to initiate new tracks. The output of the tracking module is a tracked target list with target position and velocity information.

In the described straightforward network processing method there are two assignment algorithms, one to assign a range from each sensor to a target for lateration, one to assign the laterated target positions to target tracks.

7.1 Data Assignment

The data assignment module searches for combinations of range-velocity measurements that are likely to represent a target. For this, there are m_i range-velocity measurements available from each sensor $i = 0..3$. Let $(R_{i,k}; v_{r\,i,k})$ be the kth range-velocity measurement from sensor i. For an ideal measurement of a point target with the state $\begin{pmatrix} \vec{t} \\ \vec{v}_t \end{pmatrix}$, a valid combination k_0, k_1, k_2, k_3 of ranges has to fulfill the trilateration equations:

$$\begin{pmatrix} R_{0,k_0} \\ R_{1,k_1} \\ R_{2,k_2} \\ R_{3,k_3} \end{pmatrix} = \vec{R}(\vec{t}), \qquad \begin{pmatrix} v_{r\,0,k_0} \\ v_{r\,1,k_1} \\ v_{r\,2,k_2} \\ v_{r\,3,k_3} \end{pmatrix} = \vec{V}(\vec{t}, \vec{v}_t)$$

For real measurement data, the range-velocity values contain a frequency estimation error. As shown in section 6.4 above, the Gauss-Newton algorithm can be used to obtain a good estimation $\hat{\vec{t}}$ of the target position. Within the Gauss-Newton algorithm, the error $\vec{e}$ between the real measurement and

the expected measurement for the estimation of $\hat{\vec{t}}$ is available. This error can be used to approximate the mean square error (MSE) of the estimate:

$$MSE \approx \vec{e}^T \vec{e}$$

The MSE is a good criterion to validate an assignment hypothesis. Equivalently to the LFMCW frequency assignment, the MSE can be calculated for all possible combinations and a hypothesis is validated if the MSE is below a limit.

However, in comparison with the LFMCW processing method, checking all hypotheses is computationally very expensive. Again, the approach can be taken to first set up some target hypotheses and then test them. The hypotheses are set up with the range-velocity measurements from two sensors. In this case, the target positions can be calculated directly from equations 6.1 and 6.2.

If only one pair of sensors is used to set up the hypotheses, a missed detection in one of these sensors completely prevents the recognition of this target. To avoid this, other combinations of sensor pairs are additionally used to set up target hypotheses. This is rather more important for the trilateration than for the LFMCW cross-sectioning, because target fluctuations are much less correlated between the four sensors than in different chirps from one sensor.

After setting up the hypotheses, it is checked which of the hypotheses are in agreement with the remaining sensor measurements. This is done by calculating the range and radial velocity measurements expected for the remaining sensors. These expected measurements are compared to the actual measurements. If the remaining sensors have a measured range-velocity pair that lies within a certain gate around the expected values, the hypothesis is validated. In Figure 7.2 a target hypothesis, generated from sensors 1 and 4 is shown. The gate for acceptable range estimates from sensor 2 is drawn as a thick circle going through the target hypothesis and having its center at the location of sensor 2. A range measurement is shown within this gate.

Also the radial velocities can be used to verify a hypothesis. The radial velocity gate cannot be visualized in the way the range gate is.

In the LFMCW cross-sectioning algorithm it is advantageous to first remove all target hypotheses that have illegal or out of bound range and velocity estimates. Similarly, there are constraints for the trilateration case as was already mentioned in section 6.3. The constraints are:

- $\text{abs}\left(R_{i,k_i} - R_{j,k_j}\right) < d_{s_i,s_j}$ meaning that the range measurements from two sensors only intersect if their difference in range is smaller than the distance d_{s_i,s_j} between the two sensors s_i and s_j.

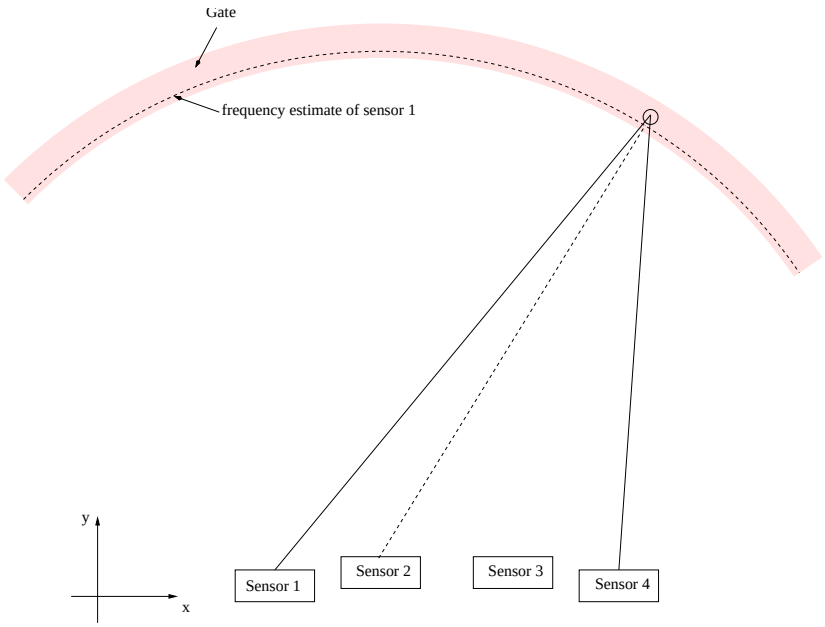

Figure 7.2: Gate for range to target association

- The lateral component of the velocity estimate is checked for very high velocities. If two measured range-velocity pairs are not coming from the same target, they can have very different radial velocities. Because the distance between the sensors is usually small compared to the distance of the sensors to the target, the resulting target velocity estimate has a very high magnitude of some hundreds of meters per second.

- Target positions outside the observation area can be discarded.

As in the LFMCW case, the complete algorithm can be understood as a two step task: first create the target hypotheses, next, detect the hypotheses that are correct. A target hypothesis is validated if the difference between expected and measured range (and velocity) is below a certain limit. Equivalently, the reasons for a missed detection are:

a) One or more single sensor detections are missing.

b) The error on the sensors' range-velocity estimates are too high.

There is a false alarm, if:

a) Accidentally four false alarms form a hypothesis that is validated. (very rare, negligible)

b) A combination of some correctly detected ranges with false alarms constitutes a validated hypothesis.

c) A combination of correctly detected ranges, belonging to other targets, constitutes a validated hypothesis. (Referred to as a ghost target)

Point c) is again the most important source of network false alarms since the single sensor false alarms from the processed range-velocity lists are due to random noise. Sporadic false alarms are easily filtered out by the tracking stage. Ghost targets do not have the characteristics of random noise and can exist over a period of time. Therefore, the probability of ghost targets should be kept very small in the network processing.

As in the LFMCW cross-sectioning case, we can adjust two kinds of parameters to optimize the algorithm performance to our needs:

- The number of detected single sensor range-velocity pairs in accordance with the target hypothesis, as needed to validate the hypothesis.

- The size of the gate used to check the hypothesis against a sensor measurement.

The target scattering behavior could be simulated for many different target types. However, the use of real measurements is preferred for evaluation of the network processing, since the wave propagation effects are very complex and not completely foreseeable. Measurement results are presented in chapter 9.

7.2 Lateration Processing

The principle of the lateration technique was described in section 6.2. The trilateration module receives sets of range and velocity pairs and solves the nonlinear trilateration equations 6.3 and 6.4.

The target position and velocity data is delivered to the tracking module. For the Kalman filtering, an estimate on the covariance matrix of the measurement error is needed. This matrix can be approximated from the estimated single sensor measurement errors and the linearization of the trilateration equation (equation 6.5). The error in range measurement from sensor i is given by:

$$e_{R_i} = (\hat{R}_i - R_i)$$

The range errors from sensors $i = 0..3$ are combined to an error vector:

$$\vec{e} = (\hat{\vec{R}} - \vec{R})$$

It is assumed that the measurement errors are uncorrelated between sensors, so the covariance matrix of $\vec{e}$ is a diagonal matrix:

$$E\left(\vec{e}\vec{e}^T\right) = \begin{pmatrix} \sigma^2_{R_0} & & \cdots & 0 \\ & \sigma^2_{R_1} & & \vdots \\ \vdots & & \sigma^2_{R_2} & \\ 0 & \cdots & & \sigma^2_{R_3} \end{pmatrix}$$

To obtain the covariances of the position estimate, this range error covariance matrix is transformed by the inverse of the linearized trilateration equations:

$$E\left(\vec{e}_t\vec{e}_t^T\right) = \left(J^{-1}\right)^T E(\vec{e}\vec{e}^T)J^{-1}$$

For the implementation of the signal processing, the single sensor range error is assumed to have a constant variance that is of the same size for all sensors: $\sigma^2_{R_i} = \sigma^2_R$ for $i = 0..3$. If the single sensor signal processing is producing estimates of the error variances, these can be used for the calculation of $E\left(\vec{e}_t\vec{e}_t^T\right)$ without additional processing effort.

The Jacobian J and its inverse is calculated during the trilateration, so the computation of the estimation error covariance matrix comes at the cost of a matrix by diagonal matrix multiplication.

7.3 Target Tracking

In radar signal processing, the main reason for tracking the target detections is to create an association between measurements made at different times. In other words, the tracker is used to keep track of the once detected targets. Each initiated track receives a unique identifier and so the measurements are associated over time by their corresponding track IDs. This association over time makes some additional techniques possible that are commonly used in radar tracking.

A tracking filter is used to filter the measurements assigned to a track over time to increase the measurement accuracy. An increased accuracy is not only helpful for the recipient of the target list but also helpful for the tracking process itself, especially the assignment of measurements and tracks.

Another advantage of keeping track of the targets is that losses of detections for short times can be bridged by the tracker. In case of a missed

detection, the current target state is estimated by the previous state. The prediction is usually done within the tracking filter.

As already described for the single sensor tracking in Section 5.4, the tracking cycle consists of 6 steps. The major parts of the tracker are:

- New measurements are associated with the existing target tracks.
- The track states are updated with the associated measurements.
- The track states of the next cycle are predicted.

To pick up new targets, the tracker additionally needs to initialize new tracks by measurements that could not be assigned to existing tracks. Furthermore, tracks have to be deleted if they are not updated by new measurements for a given time. Tracks with nearly identical states are merged in order to reduce processing load. Figure 7.3 gives an overview of the tracking algorithm.

The implemented tracking algorithm uses a Kalman filter for state update and state prediction. The association of new measurements and tracks is discussed in the following section.

7.3.1 Association of Measurements and Tracks

When new measurements arrive, the tracker first performs an association between the new measurements and the existing tracks. The basis of finding the best association is usually the likelihood criterion. In the case investigated, the measurements are the 2-D Cartesian coordinate position estimates from the trilateration. If the measurement errors are assumed to be normally distributed and also the errors of the two coordinates have the same variance and are uncorrelated, the likelihood ratio between different assignments is identical to the nearest neighbor criterion.

There are three major strategies to associate the new measurements with the existing tracks:

- Using a "Measurement to Track" assignment strategy, each measurement is assigned to the most likely (nearest) target track. This track will be updated by the measurement. A track might receive multiple measurements.
- Using a "Track to Measurement" assignment strategy, each target track is compared to the measurements. The track is assigned to and updated with the most likely measurement. A measurement might be used to update multiple tracks.

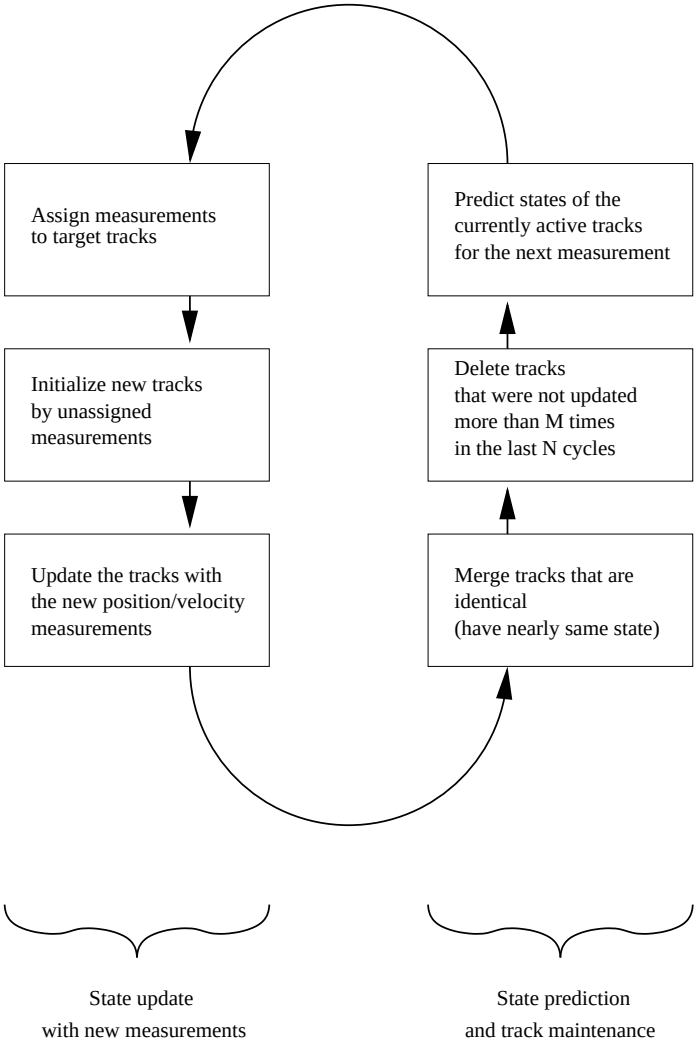

Figure 7.3: Complete cycle of the tracker, repetition of Figure 5.17.

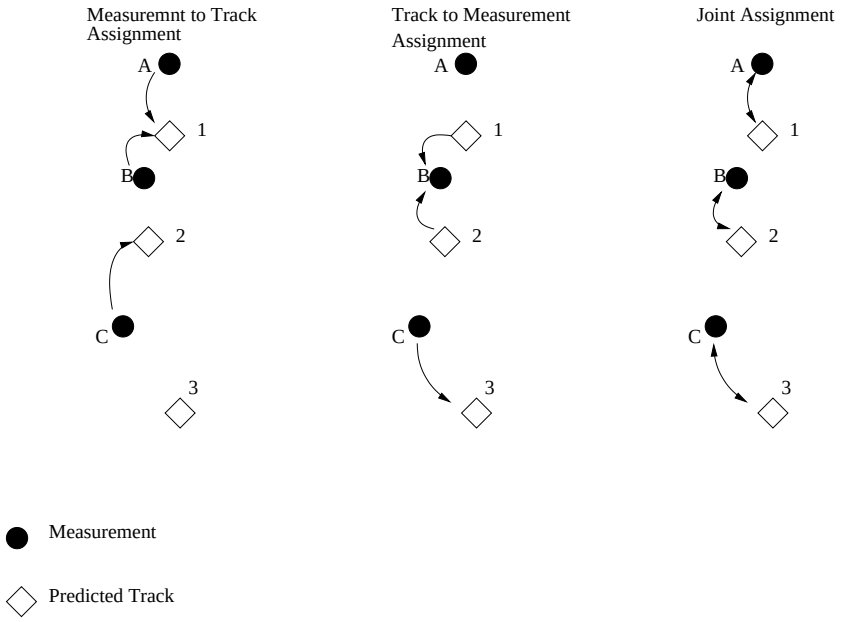

Figure 7.4: Assignment strategies

- A joint probabilistic assignment technique determines all possible combinations for assigning the measurements of one cycle to the tracks and determines the maximum likely combinations. The Joint Probabilistic Data Association (JPDA) does not make hard decisions but weights all possible assignments. The track states are updated with all measurements in a weighted manner. The Multiple Hypothesis Tracking (MHT) carries along all possible assignment combinations over a sequence of measurement cycles and so creates a tree of possible assignments. Very unlikely hypotheses are culled to thin out the growing tree of assignment combinations.

As can bee seen from Figure 7.4, the three strategies can produce three different association results. However, the shown example is a very special situation. The targets are very close to each other in comparison to the magnitude of the error between measurements and track predictions.

The JPDA and MHT have great advantages when dealing with low measurement update rates in air and sea surveillance radar systems. In the case of low update rates, the track prediction becomes a major source of error. However, the discussed radar network has a high update rate compared to the speed and the maneuverability of the targets. The measurement error and the prediction error generally will be smaller than the resolution capability of the sensors.

The discussed LFMCW sensors are able to resolve by velocity, targets with different velocities can be resolved even when they are close to each

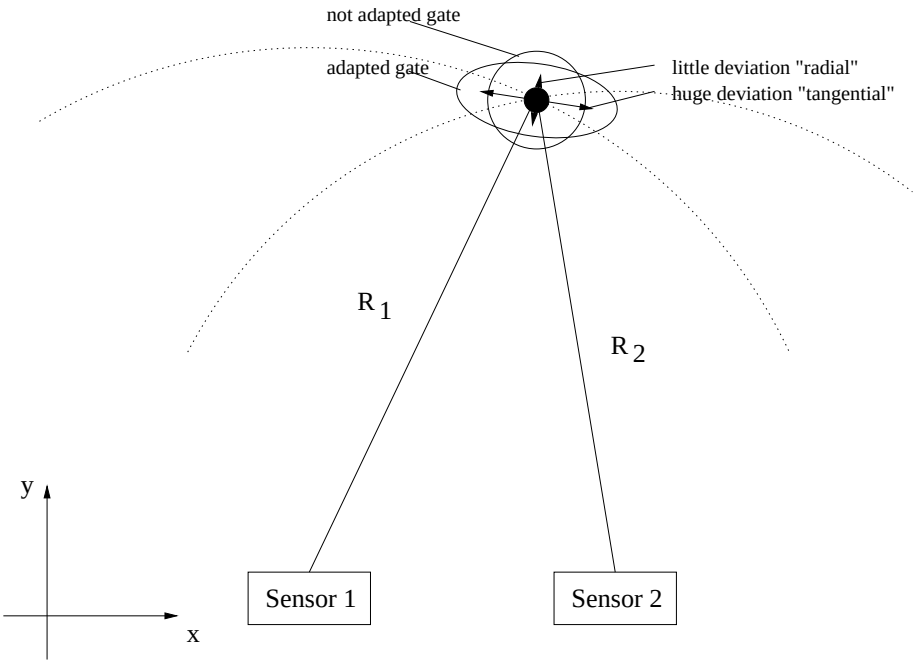

Figure 7.5: Estimation variance

other. The velocity estimate can be used in the validation process. In any other case, the targets interfere and the sensors cannot resolve the targets correctly. In this situation, a correct target position estimation is not possible by the trilateration technique.

For these reasons, a simple track to measurement assignment is chosen for the discussed radar network. The assignment uses the nearest neighbor technique with a weighted distance metric. An additional validation gate is used to prevent obviously wrong assignments.

7.3.2 Weighted Distance Metric and Adaptive Gate Size

The trilateration estimates position and velocity with very different accuracy in the two directions radial and tangential from the radar network. When measurements and track states are in Cartesian coordinates, an adaptive distance metric and gate can together improve the performance of the data association greatly.

The following proposal uses the approximated variances of the measurement error and the tracks measurement prediction error to determine a weighted distance between actual and the predicted measurement.

The assumption made for this is that the measurement and state errors are normally distributed random variables, an assumption that is done all throughout Kalman track filtering.

Define z_p, R_p as the tracks measurement prediction and its error covariance and z_m, R_m as a measurement and its error covariance matrix. In terms of Kalman filtering, the error between actual and predicted measurement is called the innovation:

$$v = z_p - z_m$$

The covariance of the innovation is:

$$S = R_p + R_m$$

The weighted norm d of the innovation can be used as the likelihood of a correct association or the distance between the measurement and the prediction:

$$d^2 = v^T S^{-1} v$$

7.3.3 Track Validation and Deletion

The tracking algorithm is not an end in itself but delivers information about the target tracks to the application. This was omitted in the previous description of the tracker. A snapshot of the currently existing tracks and their state estimates is regularly transmitted to the application of the radar system. Since a false alarm instantly initiates a new track and the transmission of false alarms is usually not wanted, a track validation scheme is needed. The implemented validation scheme is a classical M out of N detector. A track is validated when it has received M_v updates in the last N_v cycles.

Tracks that are not updated regularly are deleted. The deletion criterion is again stated by an M out of N detector. For the track deletion, it is advantageous to consider the tracks validation state, in order to quickly dispose of the tracks originating from false alarms. Therefore, the implemented tracker distinguishes between validated targets and not validated targets. A track is deleted when it has received:

- M_d updates in the last N_d cycles for a not validated track, or
- M_{dv} updates in the last N_{dv} cycles for a validated track.

The actual values that are optimal depend on the time domain properties of the target fluctuations, the expected false alarm rate and the expected rate and properties of ghost targets. For a cycle period of 25ms the parameters should be around:

- $M_v = 10$ $N_v = 12$

- $M_d = 1$ $N_d = 5$ (After the second cycle)
- $M_{dv} = 2$ $N_{dv} = 20$

With these values, the time scope of the track validation and deletion is not more than half a second. It makes sense to choose higher values for N_{dv} for tracks with low velocity.

7.3.4 Additional Track Validation and Deletion Criteria

After a track is validated it is assumed that the target is actually present. So, if a validated target track receives no more measurement updates it cannot be assumed that the target has simply disappeared. The lack of measurement updates is much more likely to be for one of the following reasons:

1. The target leaves the observation area or is shadowed by another object.
2. The signal is below the detection threshold due to target fluctuations.
3. The tracker has literally lost the track due to measurement errors. These errors cause the target measurements to be out of scope for the data assignment.

As targets do not simply vanish, it does not seem to be pertinent to close a target track as soon as there are no more measurements observed. Inspired by this idea, another criterion for track validation and deletion is proposed that uses the uncertainty of the track state. If it is no longer possible to predict the track state better than a given value, the track is not useful anymore, and can be deleted. Since the Kalman filter maintains an approximation of the state error variance and includes an uncertainty for the system model, the approximated state error variance can directly be used to delete or at least invalidate target tracks.

7.3.5 Target Model of Motion

The tracker predicts the target states for each cycle according to the target equations of motion. In Cartesian coordinates, the equations are linear. Given the state $\vec{x}$ of the target as the combination of target position $\vec{t}$ and

$\vec{v}$ in Cartesian coordinates

$$\vec{x} = \begin{pmatrix} t_x \\ t_y \\ v_x \\ v_y \end{pmatrix}$$

the system matrix $A(dt)$ that models the target motion for a step dt in time is a 4 by 4 matrix:

$$A(dt) = \begin{pmatrix} 1 & 0 & dt & 0 \\ 0 & 1 & 0 & dt \\ 0 & 0 & 1 & 0 \\ 0 & 0 & 0 & 1 \end{pmatrix} \tag{7.1}$$

This equation can directly be used in the Kalman filter state prediction. Usually and within this investigation, the trackers cycle time dt is constant, so $A(dt)$ is also a constant matrix.

Also, the Kalman filter process noise has to be modeled. This noise corresponds to the unknown acceleration of the object. A compromise has to be made between the variance of the state estimates and the ability to track accelerated targets. It has been found that

$$Q = \begin{pmatrix} 0 & 0 & 0 & 0 \\ 0 & 0 & 0 & 0 \\ 0 & 0 & \left(dt \cdot 3\frac{m}{s}\right)^2 & 0 \\ 0 & 0 & 0 & \left(dt \cdot 3\frac{m}{s}\right)^2 \end{pmatrix} \tag{7.2}$$

is a useful tradeoff.

7.3.6 Update Rate of the Tracked Target List

The higher the sensor update rate is, the more data the tracker has available in a segment of time. A higher update rate can either improve the state estimates or makes the tracker react faster to changing target situations. In most cases, the update rate at the output of the tracking filter can be chosen to be lower. It is even conceivable that a specified update rate has to be met. The use of a tracking filter like a Kalman filter makes it very easy to run a different update rate at the output of the tracker than is used at its input. The update clock of the tracker output can even be driven asynchronously from the input. To produce a target list for a specific time, the current state variables of each track are calculated for the desired point in time by the use of the tracker state prediction equation.

With some additional timing information, it is also possible to formally compensate the time that is used for the complete measurement, by transmitting an optimal prediction for the current time. This is much better

than compensating for the measurement time in the application because all the necessary information is already available to the tracker.

7.4 Synchronization between Sensors

The trilateration algorithm has an especially high demand for accurate range information. However, if the range-velocity lists from different sensors are not processed synchronously, the range measurements used for triangulation are not referring to the same point in time. Due to the target movement, there is a discrepancy between range measurements from different sensors and the position estimate contains an additional error. For instance, with a target-list update rate of 25 ms, a vehicle can easily move $25ms * 50\frac{km}{h} \approx 0.35m$ between two measurements. For trilateration, a third of a meter is a significant amount of uncertainty in the range information. Therefore, synchronized processing of the target lists from multiple sensors is essential. There are two methods to achieve correct processing:

1. Process only the target lists that are from the same measurement cycle of a synchronized sensor group.

2. Compensate the Ranges by $R_0 = R_t + v(t_0 - t)$ so that all ranges are referring to the same point in time.

Both methods assume the knowledge of the (relative) time of the measurement for each target list from each sensor. The second method implies a linear movement of the objects.

7.4.1 Implemented Radar Network Synchronization

The synchronization concept of the radar network is shown in Figure 7.6. It consists of a hardware aspect and a software aspect.

The sensor hardware is driven synchronously. Transmission of the waveform is triggered by a central synchronization box. The synchronization box precisely triggers the start of a waveform sequence every 100ms by distributing a synchronization signal to all sensors. Upon the synchronization signal, the sensors start the transmission synchronously and transmit a waveform sequence consisting of 4 waveforms. The second signal that is distributed from the synchronization box to the sensors is a 100 MHz clock signal. This signal is used within each sensor to derive the local timing and clock signals.

The LFMCW signal processing is done on the sensors local signal processing hardware. For this, an interface between the sensor front end and the digital signal processor (DSP) forwards the receive data to the DSP in

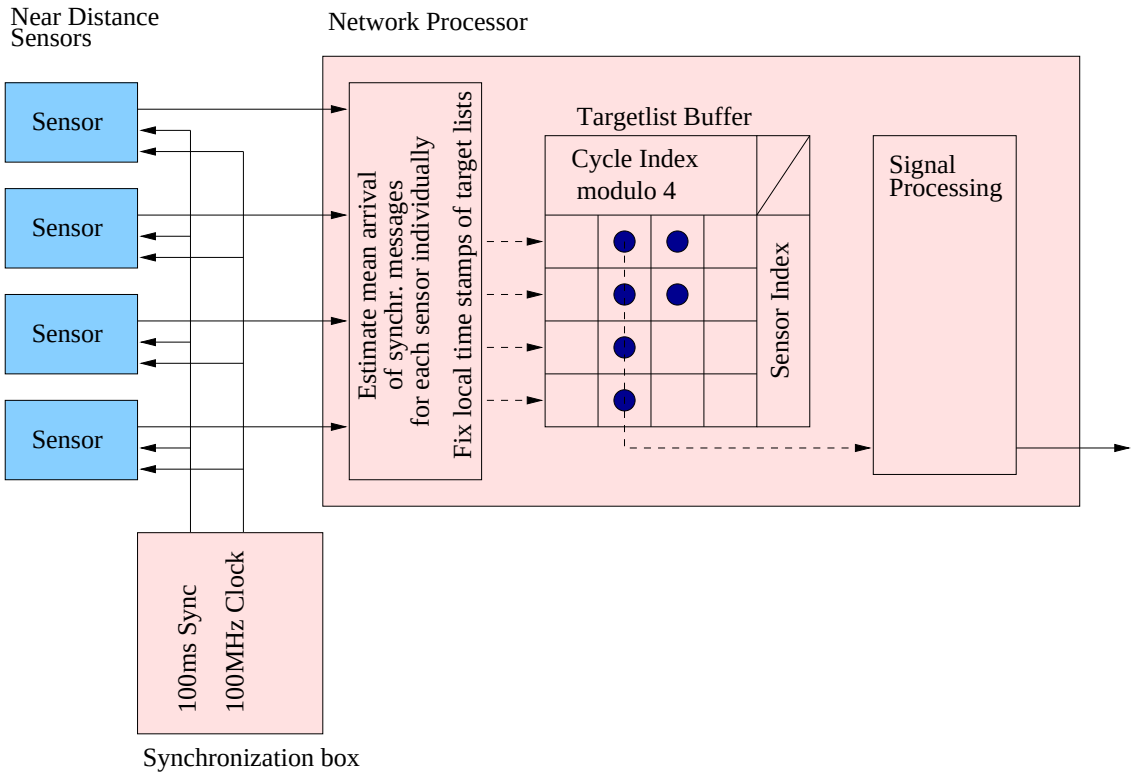

Figure 7.6: Synchronization scheme

a continuous stream of samples. Each transmitted sample is 16 bit wide. 14 bits contain the AD converted receive signal and 1 bit is used as a flag, marking the start of a new waveform sequence. The remaining bit is unused.

The sensors run synchronously and each sensor knows the start of a new waveform sequence and locally counts the numbers of processed waveform-sequences. The target lists transmitted to the network processor are time stamped using this local counter. However, there are two limitations that make an additional synchronization step necessary:

1. As a result of the complex signal processing hardware, it cannot be ensured that after power-up all sensors start exactly from the same waveform sequence. The network processor receives target lists with each sensors local time stamp but does not know precisely at which time each sensor started its counter. There remains an ambiguity of about one waveform sequence (100ms).

2. The sensors are connected to the network processor using an Ethernet link. The network processor is a standard personal computer with standard networking components. Using standard hardware and in this case also using a standard operating system, the latencies of the network connections are unpredictable to the network processing

software. With a high system load, latencies can sometimes reach the order of 100 ms. The network processor can not directly use the target lists time of arrival for resolving the ambiguity of 100ms.

In summary, the waveforms are transmitted and processed synchronously with a very high accuracy. However, the relation between each sensors local waveform sequence counter is not known precisely. In practice, the unknown latencies of the Ethernet connections prevent a direct comparison of each sensor's local sequence counter on arrival at the network processor. For the described situation, the following additional synchronization scheme within the network processing is proposed and has been successfully implemented. It is described in the following.

Additional Target List Synchronization

Each sensor transmits a short synchronization message containing the local sequence count as soon as the sensor recognizes the start of a new sequence. This message is transmitted over the Ethernet link as an out-of-band message alongside with the target lists.

The network processor receives the synchronization messages from each sensor every 100 ms. The network processor creates a statistic about their mean times of arrival. This statistic has a scope of a few seconds.

The synchronization message from sensor i with the sequence count k is received at time $t_{i,k}$. The sensor start time t_0 is defined as the time, the sequence with number 0 has been processed. This sensor start time is estimated by averaging the receive time of the incoming messages:

$$\hat{t_{i,0}} = \frac{1}{k_{stop} - k_{start} + 1} \sum_{k=k_{start}}^{k_{stop}} t_{i,k} - T_{seq} k$$

The relation between the sensors local counters can be identified by comparing the sensor start times:

$$dk_{i,j} = round\left(\frac{t_{i,0} - t_{j,0}}{T_{seq}}\right)$$

The maintenance of this statistic allows a robust synchronization that also accounts for the occasional outliers which are unavoidable when using standard computer hardware and operating systems. For this implementation, it is numerically more accurate to adjust the sensor reference start time to the time scope of the statistic:

$$\hat{t_{i,k_{start}}} = \frac{1}{k_{stop} - k_{start} + 1} \sum_{k=k_{start}}^{k_{stop}} (t_{i,k} - t_{start}) - T_{seq}(k - k_{start})$$

With the knowledge of the relation between the sensors local sequence counters, the target lists can be processed synchronously. For this, the target lists contain the local count l of the corresponding processed waveform:

$$l_i = 4 \cdot k_i + c_i$$

Where c_i is the number of the waveform relative to the start of the sequence for sensor i. For all further processing, the network processor replaces the sensors local waveform count l_i with a count l^* common to all sensors:

$$l^* = l_i - 4 \cdot dk_{i,0}$$

Because of the described network latency, the received target lists are buffered prior to processing. The target list buffer is chosen to hold 4 sets of 4 target lists, in order to buffer 4 target lists from each of the 4 sensors. The target lists are sorted into the buffer according to their waveform index modulo 4. When all target lists for one waveform index $l*$ have been received, the corresponding column from the receive buffer is passed to the signal processing stages.

7.5 Performance Considerations

The performance of the straightforward implementation of the radar network is acceptable in the single target case where a robust detection of the target by the LFMCW sensors is possible. In the multiple target case with a growing number of targets, the detection rate and the probability of an accurate target range and velocity measurement go down. The implementation only works in some situations, for example when the target of interest is the dominant reflector in the scene. This is usually the case for vehicles that have one of their faces oriented perpendicular to the direction of the radar sensors. This situation occurs when following a car on a straight road.

The network processing implementation described above uses a forward data association and trilateration without any memory of the previous targets states. To obtain a good lateration result on a target, at least 3 sensors have to provide accurate range information about this target. Unfortunately, in many multiple target situations the probability for this is very low. The following section describes improved network processing strategies which increase the detection performance and measurement accuracy.

Chapter 8

Improved Radar Network Processing Strategies

The system described in Chapter 6.2 is particularly characterized by the need for a very good target detection rate from the single sensors. The data assignment and trilateration processing works only for targets that are steadily detected by at least 3 sensors. An alternative strategy, introduced in [Oprisan 2002], is to update the track states directly by the single sensor range measurements. In this "range to track" association strategy, the trilateration algorithm is shifted into the measurement update function of the extended Kalman filter. The trilateration equations are directly used as the measurement equation of the extended Kalman filter. In this case, the target track is updated, even when fewer ranges are available than required for a standalone trilateration procedure. Therefore, much more information is used to update the track.

The "range to track" association strategy exhibits better track maintenance than straightforward processing. However, there is still scope for improvement in the estimation accuracy of targets with either a low RCS or in dense multiple target situations. To further improve track stability and estimation accuracy, a third processing strategy is proposed, that uses data directly from the sensors spectral analysis. The detected frequencies of each chirp and each sensor are used to directly update the track states. This strategy is referred to as the "frequency to track" association strategy.

This new strategy shows a remarkable improvement, because a target track of a normal reflecting object is now nearly always updated by every sensor in each measurement cycle. With this strategy, the data assignment can be very selective about the measurements used to update the target

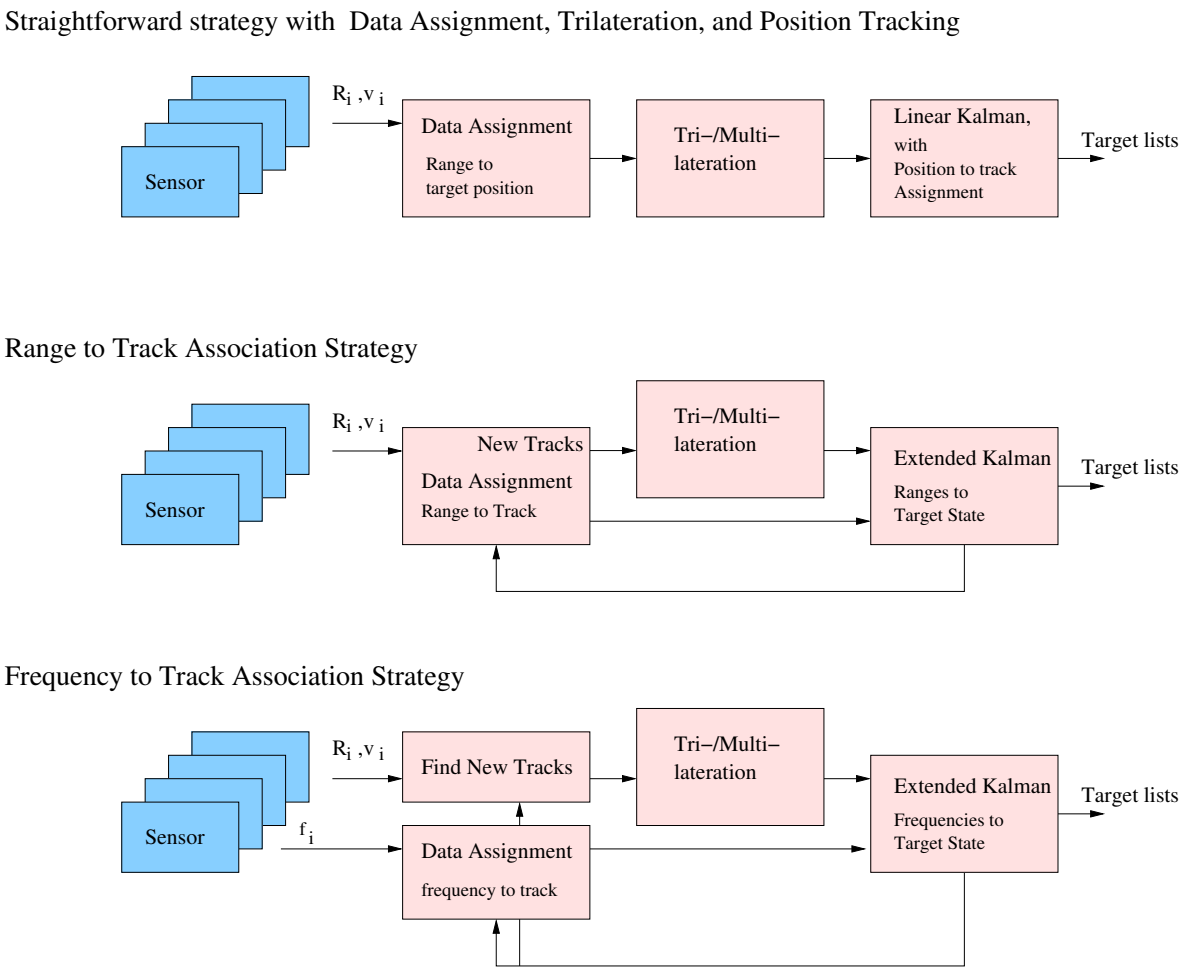

Figure 8.1: The three investigated network processing strategies

state estimates in order to improve position estimation quality. Figure 8.1 shows the three investigated network processing strategies.

8.1 Track Update by Range to Track Association Strategy

The second diagram in Figure 8.1 shows the extended modules and new interaction between these modules for the range to track association strategy. For this strategy, the data assignment directly assigns the ranges to the tracks. After being assigned to their corresponding tracks, the ranges are forwarded to an extended Kalman filter. New target tracks are generated by the standard trilateration algorithm used in straightforward processing.

8.1.1 Adaptation of the Kalman Filter

The straight forward processing strategy uses a linear Kalman filter whose measurement space and target state space are identical. In the case of the advanced range to track strategy, the measurements are related nonlinearly to the target state by the lateration equations 6.3 and 6.4. These equations are used as the measurement equation system for the extended Kalman filter. The state equations do not change and remain linear.

Since the state model remains linear, the state equation 7.1 and the corresponding process noise matrix 7.2 from the linear Kalman tracker can still be used.

The nonlinear measurement equation is linearized at the currently best state estimate. Computationally, this linearization of the measurement equation is identical to one iteration of the Gauss-Newton algorithm (Section 6.4). Therefore, the construction of the Jacobian of the measurement equations can be taken from equation 6.5 which is repeated here, written with the abbreviation $\vec{r}_i = \begin{pmatrix} r_{ix} \\ r_{iy} \end{pmatrix} = (\vec{t}_0 - \vec{s}_i)$ as the distance vector between the position of sensor i and the target position:

$$J_{Rt} = \frac{\partial \vec{R}(\vec{t})}{\partial \vec{t}} \Big| \vec{t_0} = \begin{pmatrix} \frac{r_{1x}}{|\vec{r}_1|} & \frac{r_{1y}}{|\vec{r}_1|} \\ \frac{r_{2x}}{|\vec{r}_2|} & \frac{r_{2y}}{|\vec{r}_2|} \\ \vdots & \vdots \\ \frac{r_{nx}}{|\vec{r}_n|} & \frac{r_{ny}}{|\vec{r}_n|} \end{pmatrix} \tag{8.1}$$

The above matrix is identical to the matrix used to calculate the radial velocities $\vec{V}_R$ from the target velocity $\vec{v}$ assuming the target at position $\vec{t_0}$. Since the relation between $\vec{V}_R$ and $\vec{v}$ is linear, the Jacobian matrix is identical to the measurement matrix:

$$J_{Vv} = J_{Rt} = \frac{\partial \vec{V}_R}{\partial \vec{v}} \Big| \vec{t_0}, \forall v \tag{8.2}$$

The partial deviations of $\vec{V}_R$ with respect to $\vec{t}$ are:

$$J_{Vt} = \frac{\partial \vec{V}_R}{\partial \vec{t}} \Big| \vec{t_0}, \forall \vec{v} \quad = \begin{pmatrix} \frac{v_x r_{1y}^2 - v_y r_{1x} r_{1y}}{|\vec{r}_1|^3} & \frac{v_y r_{1x}^2 - v_y r_{1x} r_{1y}}{|\vec{r}_1|^3} \\ \frac{v_x r_{2y}^2 - v_y r_{2x} r_{2y}}{|\vec{r}_2|^3} & \frac{v_y r_{2x}^2 - v_y r_{2x} r_{2y}}{|\vec{r}_2|^3} \\ \vdots & \vdots \\ \frac{v_x r_{ny}^2 - v_y r_{nx} r_{ny}}{|\vec{r}_n|^3} & \frac{v_y r_{nx}^2 - v_y r_{nx} r_{ny}}{|\vec{r}_n|^3} \end{pmatrix} \tag{8.3}$$

Again, written with the abbreviation $\vec{r}_i = \begin{pmatrix} r_{ix} \\ r_{iy} \end{pmatrix} = (\vec{t}_0 - \vec{s}_{iy})$. The Jacobians are independent from the current velocity estimate, because the relation between radial velocities $\vec{V}_R$ and laterated velocity $\vec{v}$ is linear. The target measurement vector z is implemented as a combination of each sensor's measured range followed by each sensor's measured radial velocity. The target state vector x remains unchanged.

$$z = \begin{pmatrix} \vec{R} \\ \vec{V}_r \end{pmatrix} = \begin{pmatrix} R_1 \\ R_2 \\ R_3 \\ R_4 \\ v_{r1} \\ v_{r2} \\ v_{r3} \\ v_{r4} \end{pmatrix}, \quad x = \begin{pmatrix} t_x \\ t_y \\ v_x \\ v_y \end{pmatrix}$$

If the measurement vector z is defined in this way, the linearization of the measurement equation is constructed by using the Jacobians derived above:

$$\frac{\partial z}{\partial x} = \begin{pmatrix} J_{Rt} & 0 \\ J_{Vt} & J_{Vv} \end{pmatrix} = J_{zx} \tag{8.4}$$

If some measurements are not available, the corresponding rows are deleted from the above matrix.

8.1.2 Adaptation of the Assignment Stage

The network processing concept described in this section uses only one assignment procedure. It directly assigns the ranges to the target tracks, while, in contrast, the straight forward processing strategy has two assignment stages:

- for the trilateration, the range measurements are assigned to target position estimates,
- for the tracker, target position estimates are assigned to target tracks.

The new range to track assignment is an integration of these two separate assignment procedures. It translates between the target position space and the range measurement space as the straight forward trilateration assignment does. It is an assignment of measurements to track state estimates like the straight forward position to track assignment is.

The standard range to target position processing described in the last Chapter is preserved to initialize tracks for new targets. A detailed description of the complete range to track strategy can be found in algorithm 5.

Algorithm 5 Tracking with range to track assignment

---

1. Wait for new range-velocity (R, v_r) measurements. Create measurement predictions $\hat{R}$, $\hat{v}_r$ for all existing tracks. For this, the extended Kalman measurement equations are used.

   For each existing track:

   (a) For each sensor:

      i. Each sensors target list is checked for the measurement closest to the predicted measurement $\hat{R}$, $\hat{v}_r$. The distance between measurement and prediction is calculated by: $D = p^2 \left(R - \hat{R}\right)^2 + q^2 \left(v_r - \hat{v}_r\right)^2$. q and p are parameters compensating for the different error variances on range and velocity measurements.

      ii. From each sensor's target list, the measurement with smallest D is assigned to the track if D is smaller than a predefined gate. Therfore, a measurement can be assigned to multiple tracks, but each track can have only one measurement assignment from each sensor.

      iii. if the measurement is assigned, mark the measurement as "assigned to track".

   (b) Update the track with the assigned measurements using the extended Kalman filter.

2. Perform the straightforward processing with all measurements not marked as "assigned to track". If there are new validated hypotheses, initiate new tracks.

3. Perform the track maintenance as described in section 7.3.3.

4. Update track states for the next measurement cycle by the Kalman filter prediction.

8.2 Track Update by Frequency to Track Association Strategy

A third network signal processing strategy is proposed to further improve the track update rate and position estimation. The newly proposed frequency to track association strategy combines the LFMCW range-velocity processing with the position estimation by lateration. Both subtasks are merged by directly using the frequency estimates to update the target track states. The third diagram in Figure 8.1 on page 124 shows the structure for the new frequency to track association method.

The range to track association strategy, described in the previous section, is used as the starting point. The previously defined measurement vector z contains the ranges and radial velocities from one target. Now, for the frequency to track update, the measurement vector z_f contains the frequency measurements $f_{i,j}$ from all chirps i from all sensors j. The state vector x remains unchanged. These three vectors are shown below:

$$z_f = \begin{pmatrix} f_{1,1} \\ f_{2,1} \\ f_{3,1} \\ f_{4,1} \\ f_{1,2} \\ f_{2,2} \\ \vdots \\ f_{4,n_s} \end{pmatrix}, z = \begin{pmatrix} R_1 \\ R_2 \\ R_3 \\ R_4 \\ v_{r1} \\ v_{r2} \\ v_{r3} \\ v_{r4} \end{pmatrix}, \quad x = \begin{pmatrix} t_x \\ t_y \\ v_x \\ v_y \end{pmatrix}$$

With Equation 4.2 the relation between a frequency $f_{i,j}$ and target range R_j and radial velocity $v_{r,j}$ can be stated:

$$f_{i,j} = a_i v_{r,j} + b_i R_j$$

The relation between frequency measurement vector z_f and range-velocity measurement vector z is linear and can be described by:

$$z_f = A\, z$$

The matrix A is constructed according to the sequence of the elements

defined above for the measurement vectors:

$$A = \begin{pmatrix}
b_1 & 0 & 0 & 0 & a_1 & 0 & 0 & 0 \\
b_2 & \vdots & \vdots & \vdots & a_2 & \vdots & \vdots & \vdots \\
b_3 & & & & a_3 & & & \\
b_4 & & & & a_4 & & & \\
 & b_1 & & & & a_1 & & \\
 & b_2 & & & & a_2 & & \\
 & b_3 & & & & a_3 & & \\
 & b_4 & & & & a_4 & & \\
 & & b_1 & & & & a_1 & \\
 & & b_2 & & & & a_2 & \\
 & & b_3 & & & & a_3 & \\
 & & b_4 & & & & a_4 & \\
 & & & b_1 & & & & a_1 \\
 & & & b_2 & & & & a_2 \\
\vdots & \vdots & \vdots & b_3 & \vdots & \vdots & \vdots & a_3 \\
0 & 0 & 0 & b_4 & 0 & 0 & 0 & a_4
\end{pmatrix}$$

The Jacobian J_{fx} of the Kalman filter measurement function can now be written as a multiplication of A with the previously defined range-to-track update Jacobian J_{zx}:

$$J_{fx} = A\, J_{zx}$$

The frequencies are assigned to the tracks and are forwarded to the extended Kalman filter in the form of sets of frequencies for each track. Additionally, the original range-velocity measurements are evaluated to detect new targets. By means of a normal trilateration, all new likely target hypotheses are calculated and sent to the tracker for initialization of new tracks. New targets are distinguished from targets having existing tracks by comparing the laterated positions to all track state variables.

Chapter 9

Experimental System

This chapter describes the experimental radar network used to test the signal processing concepts investigated in this thesis. The radar network was built up within the European project[1] "A multifunctional radar network (RadarNet)". The complete system consists of four near distance sensors, a central synchronization unit, and the radar network processor. An overview of the system is shown in Figure 9.1. The experimental car shown in Figure 9.2 was equipped with the radar network system at the Technical University of Hamburg Harburg.

Within the RadarNet project several automotive applications have been implemented and tested. The applications interpret the target information generated by the network processor. On the basis of this target information and the state of the vehicle, the applications control the vehicle functions accordingly. The possible interventions range from alerting the driver to applying the vehicle brakes.

9.1 Single Sensor Hardware

The sensor hardware of the network consists of four 77GHz LFMCW sensors of the type described in Chapter 10. They are to operate in the near range of up to 30 meters. The maximum sweep bandwidth of the sensors is 450 MHz while one sweep has a duration of only 2 ms. Using an FFT and a window function (Section 4.2), this results in a practical range resolution of 0.5m and a velocity resolution of 1.5m/s.

[1]The European research project "A Multifunctional Automotive Radar Network" (RadarNet) has been supported by the European Commission under the 5th Framework Programme (project no. IST-14031).

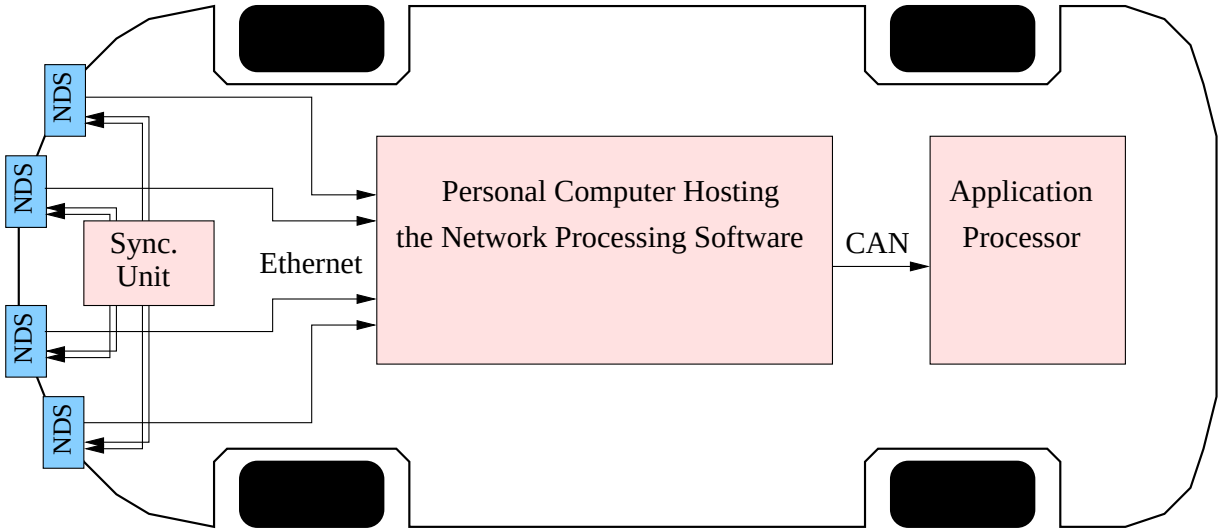

Figure 9.1: Radar network hardware overview

Figure 9.2: Experimental car equipped with the radar network

The internal clock and sweep generation is driven by a central synchronization unit. The unit delivers two signals to the sensors. A 100 MHz clock signal is used to derive the internal clock signal within each sensor. The second signal is a synchronization signal that triggers the start of a waveform sequence every 100 ms. The details of the synchronization concept are described in Section 7.4.1.

Each sensor processes the LFMCW receive signal on its digital signal processing hardware. The resulting target lists contain the target detections and for each target detection, the measured target range and target radial velocity are included. The target lists are transmitted to the central network processor via an 100 MBit Ethernet interface.

For the advanced frequency to track processing strategy, the frequency detections for each chirp are also transmitted to the network processor.

9.2 Network Hardware

The central network processor hardware is a personal computer. It consists of standard components including a four port Ethernet card and a CAN interface. The four near distance sensors are connected to the network processor via the Ethernet interface. To allow a high data-rate for each sensor and to minimize network latencies, each sensor has its own dedicated Ethernet port on the four port Ethernet card.

The network processing software processes the single sensor measurements to obtain a target list with target position information. The target position information is transmitted to the automotive application processor via the CAN interface.

9.3 Sensor Positioning

The sensors are mounted at the front side of the experimental vehicle (Figure 9.2). The observation area is in front of the vehicle with a targeted azimuthal coverage of $\pm$30deg. Figure 9.3 shows the relative positions of the sensors on the experimental vehicle. Since the distance between the outer sensors has the most impact on the accuracy of the target position estimation, this distance should be chosen to be as large as possible.

9.4 Network coordinates

To report targets to the application in Cartesian coordinates, a network coordinate system is introduced. Figure 9.4 shows the origin of the network

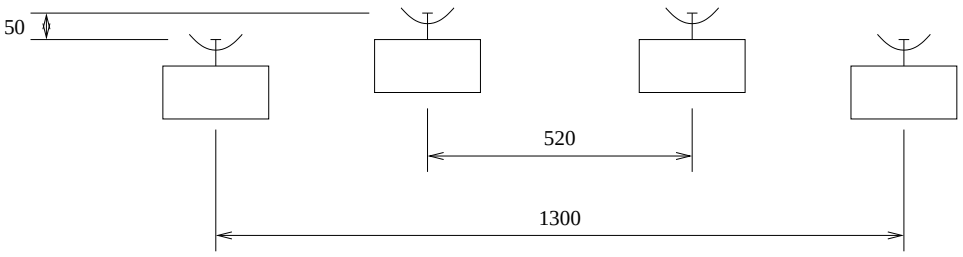

Figure 9.3: Radar network relative sensor positions in millimeters

coordinate system in the center of the sensor setup. The coordinate center can be defined by the N sensor positions ($s_{i,x}$, $s_{i,y}$) within this coordinate system itself:

$$\sum_{i=0}^{N-1} s_{i,x} = 0 \quad \wedge \quad \sum_{n=0}^{N-1} s_{i,y} = 0$$

The network coordinate center can be placed freely at any position on the host vehicle. The above definition of the coordinate center is an arbitrary choice.

Most classical radar systems measure range and azimuth separately. Performance characteristics of range and azimuth measurement are therefore stated separately for these classical systems. With a monopulse radar for example, the accuracy of the range measurement does not directly depend on the target azimuth (and vice versa). The radar network on the other hand estimates the two-dimensional target position by the trilateration technique from only the range measurements of the single sensors. The trilateration technique naturally represents target position estimates in Cartesian coordinates.

Measurement of the target position by the trilateration principle cannot be separated into range and azimuth measurement for near targets. However, if the targets are far away from the radar network - compared to the extension of the network sensor setup itself - the measurement of range and azimuth can approximately be assumed to be separate. In this case it is advantageous to present the characteristics of the target position estimates in polar coordinates.

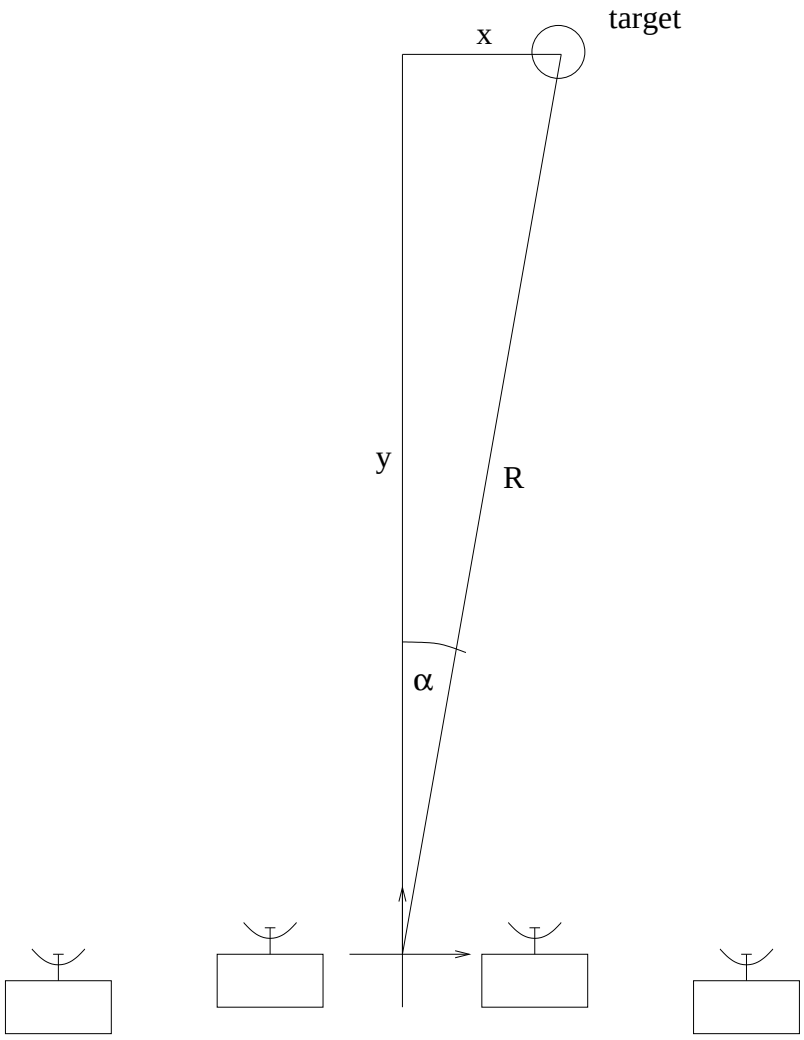

Figure 9.4: Radar network coordinates

Chapter 10

Single Sensor Experimental Results

In this chapter, measurement results for the single LFMCW sensor are shown. These practical measurements are used to verify the signal processing concepts in an environment with complex backscattering properties and the non-ideal properties of a complex radar sensor.

Most analytic investigations of radar systems make use of point target models in which the target radar cross section is assumed to be fluctuating according to a rice distribution. In reality, these target fluctuations are a result of the target spatial extension. If the spatial extension is much smaller than the radar resolution, the assumption of a fluctuating point target is valid. However, with high resolution radar sensors and radar network applications, the target extension is a very important feature to be considered. The following three measurement scenarios are described in the following sections:

- The first measurement evaluates the sensor range measurement performance in a very elementary laboratory setup. A corner reflector is moved towards the sensor and the measured distance is compared to a reference.
- The second measurement is done using an extended target. Measurements are investigated for a passenger car passing the radar sensor. Also the proposed tracking strategy (Section 5.4) is investigated.
- Thirdly, measurement data of a real traffic scenario is used to show the general performance of the sensor. Results are shown for the proposed tracking strategy.

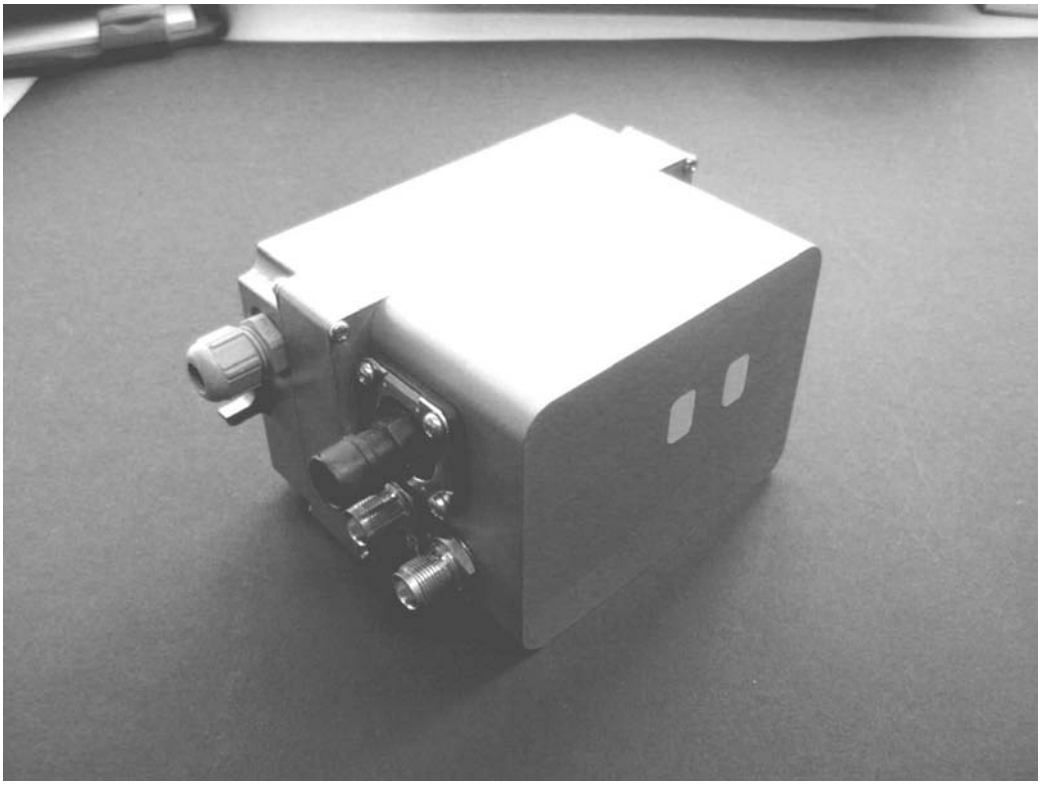

Figure 10.1: Photograph of prototype near distance sensor

Figure 10.1 shows a photograph of the LFMCW near distance sensor that is a part of the experimental radar network. These prototypes work in the 77GHz frequency domain with a maximum sweep bandwidth of 450MHz. The remaining parameters of the used waveform are described in Section 5.3. The transmitted frequency sweeps are generated by a direct sequence synthesizer. This generation technique guarantees the linearity of the sweep and the exact adherence to the specified frequency bandwidth. Thus, no compensation is needed, while for voltage controlled oscillators it is often necessary to compensate the non-linearity of the VCO and deviations of the actual bandwidth of the transmitted sweep.

10.1 Single Point Target Range Measurement

The sensor range accuracy has been tested with a single target at ranges up to 10m. The target is a corner reflector with a radar cross section of 25m^2. During the experiment, the target was moved automatically between a distance of 1m and 10m to the sensor a large number of times. For each target position, a histogram of the measurement errors was recorded.

In Figure 10.2, the measured range errors are plotted as histograms

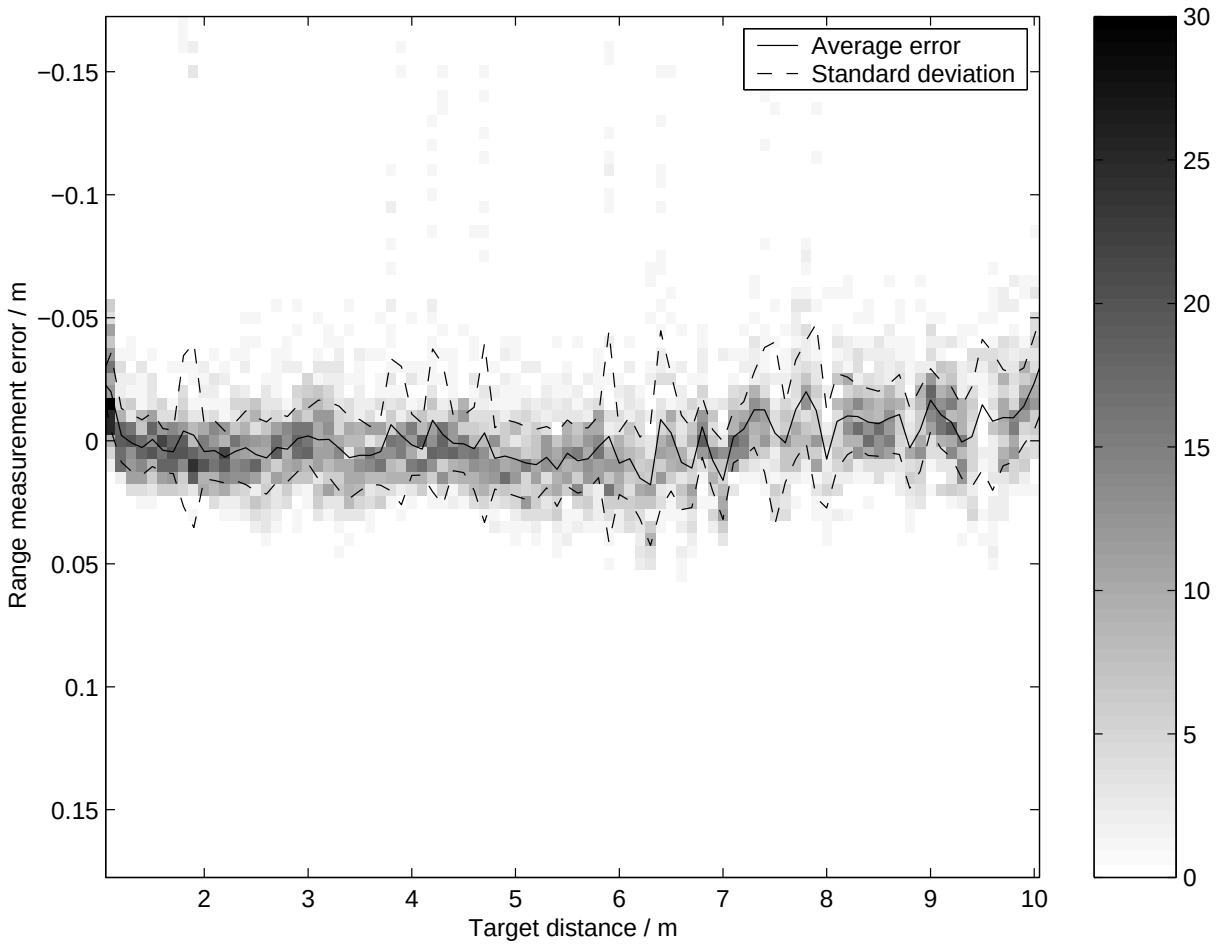

Figure 10.2: Distribution of range error versus target distance

against the target position. The gray scale intensity shows the frequency of occurrence for each measurement error value at each target position. This measurement shows that under good measurement conditions, the sensor measures the range with a standard deviation of less than 3cm.

The measurement shows outliers at some ranges due to obstacles in the measurement room that could not be removed. The detection rate is 100% at the target positions where there is no interference. Apart from these interferences, the question of which range-velocity assignment method to use has no impact on the single target measurement.

10.2 Single Extended Target Range Measurement

Measurements of a car at distances up to 60m have been done. The measured range deviation of the untracked data is near to that of a point target

(under 5cm) for a car oriented in the direction to the sensor. In this case, the reflection of the forward face of the car is measured. A car oriented sideways - exactly perpendicular to the line between radar and target - also has a strong reflection from the foremost parts of the car body. The data presented in this section is from a vehicle that is passing the sensor. The vehicle is not directly oriented towards the network but presents a constantly changing aspect angle.

10.2.1 Deviation of Frequency Measurements

Three plots for the measurement of a passing car are shown in Figure 10.3. The upmost plot shows the tracked range of the passing car over the measurement cycle. The tracker described in Section 5.4.4 is used for this measurement.

There was no reference information of the target position available. Even if the position of the target vehicle were known, it would still not be possible to define a precise reference point on the vehicle that could be used to compare the sensor measurements. Therefore, a different approach is taken to quantify the measurement performance. The velocity of the target vehicle is held constant and the target measurements are tracked. Because of the constant speed, the tracks can be strongly filtered. Using this method, the measurements can be compared relatively to the track prediction. The deviation of the measurements from the prediction gives a good indication of the short term variations of the measurements. It makes visible the measurement noise and range variations due to fast fluctuations of the target signal. However, it does not give information about the absolute measurement error. Also, slow shifts of the reflection center are not detectable.

The lowermost plot in Figure 10.3 shows the deviation of the frequency measurements from the track prediction for all ~250 measurement cycles. The frequency measurements are from the first two chirps of the waveform. It can be seen that the errors are not correlated notably over the measurement time.

The middle plot shows a histogram generated from all deviations of the complete measurement. In this measurement, a frequency of 500Hz corresponds to the spectral bin size. Roughly 50% of the measured frequency values are within a gate of $\pm$ a fourth of the bin size. A spectral bin size of 500 Hz corresponds to a range of 30cm.

10.2.2 Investigation of Proposed Tracking Algorithm

The results presented above indicate a low detection rate using the classical LFMCW frequency to range-velocity assignment technique with small gate

sizes. The probability of all four chirps lying within a gate of ±0.2bin is much lower than 50%. In order to achieve a good detection rate, the gate size has to be chosen higher. This in turn would increase the false alarm rate and reduce measurement accuracy in multiple target situations as shown in Section 5.3.

The estimation accuracy and track stability of the proposed tracker with frequency to track assignment (Section 5.4.4) is shown in the following measurement. For the analysis, the tracks are only lightly filtered as the overall performance of the tracker and the measurement to track assignment is of interest.

The tracker is updated by the frequencies of all chirps that lie within the validation gate. A measurement is used for track update if it is within the assignment gate around the track prediction. A gate size of ±1bin leads to a track update rate of above 90 %. This means that the track is updated with at least 1 frequency measurement in 9 out of 10 measurement cycles. A gate size of ± 0.2 bin still leads to an update rate of 70%. For both gate sizes, the track is maintained throughout all the measurement cycles.

As already stated, there is no absolute reference for the target position. To estimate the error of the tracked range states, the track range states of the complete measurement are fitted by a 5th order polynomial and the polynomial is compared to the estimated track states. A 5th order polynomial was chosen to adapt to slow shifts of the reflection center and/or a slight variation in vehicle speed.

Again, it should be explicitly stated that this is not a valid test for the absolute deviation of the measured range from the vehicle's position since the vehicle position is actually not perfectly known. However, the variance of the state estimate can be compared for the two gate sizes ±1 and ±0.2. Figure 10.4 shows the resulting range deviation for each of the two gate sizes. They differ by a factor of approximately 5.

The results show that a gate size around ±0.2 bin can be used to validate the measured frequencies for the track update. The resulting track update rate of 70% still makes it very possible to keep the track active over the complete measurement. It is a very interesting result that the standard deviation of the range estimate is nearly accurately proportional to the gate size. The chosen tracking algorithm does a good job even though the data assignment is of a simple design.

It should be kept in mind that the shown range deviations can not represent the reflection displacement from a reference position on the vehicle. The center of the reflection depends on the aspect angle on the target. Four range measurements from four distributed near distance sensors do not necessarily measure the same reflection center.

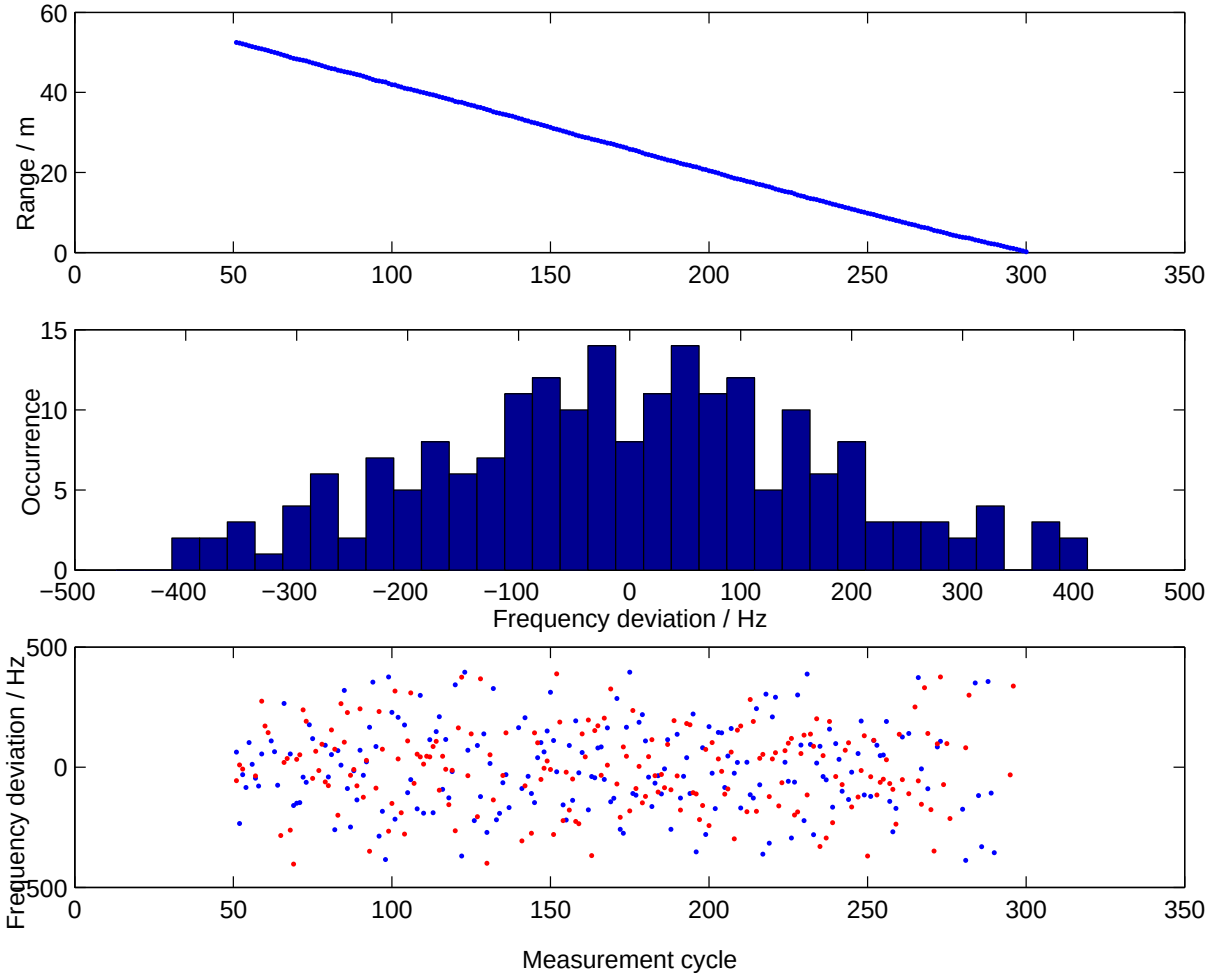

Figure 10.3: Measurement of a passing car
Upper plot: Range track of a passing car.
Lower plot: Frequency deviation over measurement cycle for the measurements of *two* 450MHz chirps
Middle plot: Histogram of the frequency deviation from tracker for complete measurement

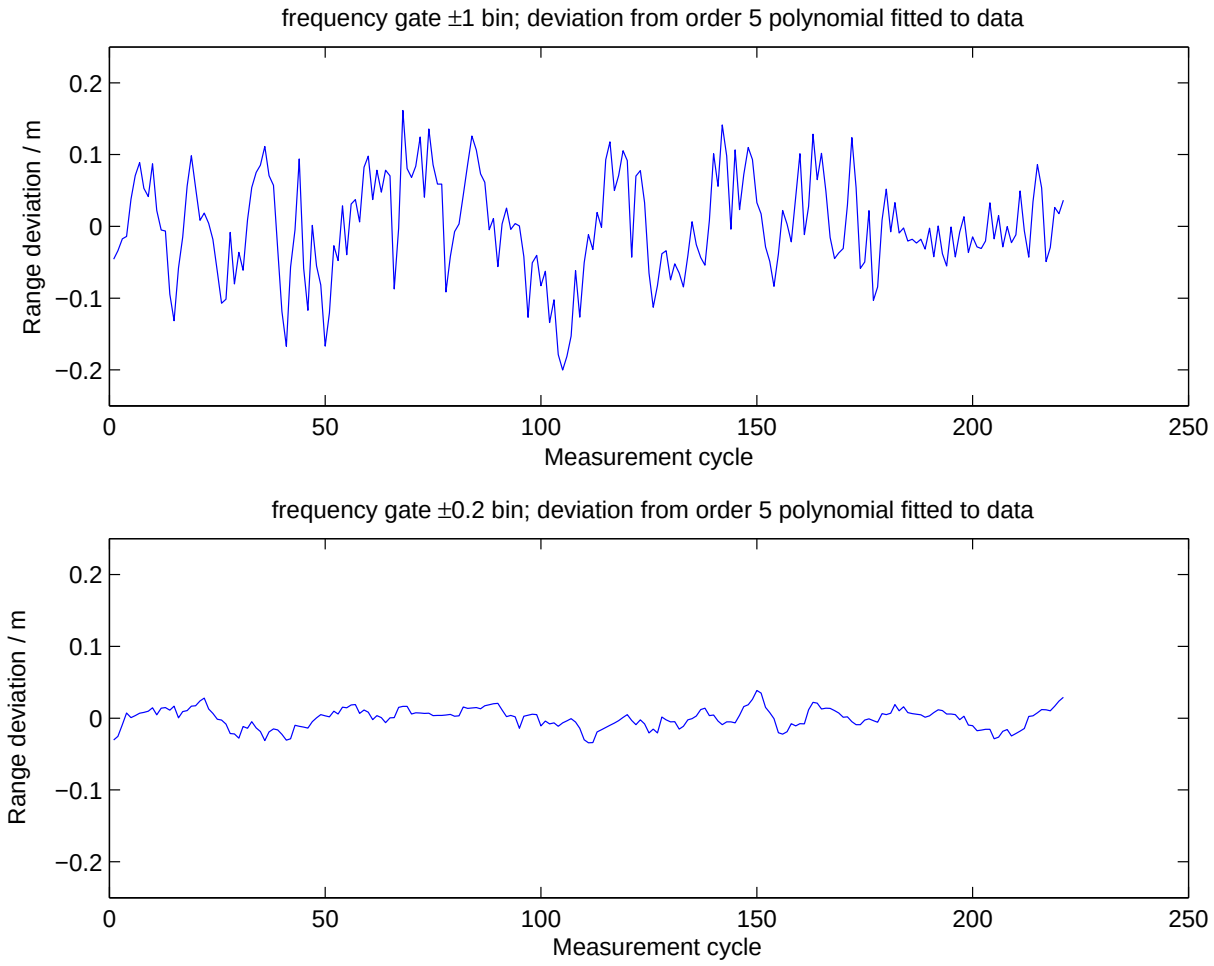

Figure 10.4: Range deviation of tracked state from a 5th order polynomial fitted to data. Frequency gate: ±1bin (upper plot); ±0.2 bin (lower plot)

10.3 Measurement of a Road Traffic Scenario

In this section, the performance of the radar in a road traffic scenario is presented. The radar sensor is placed on a parking space parallel to a two lane street. There are two cars approaching and passing the radar, there is one car moving away from the sensor. The results show the raw target detections of the LFMCW frequency to range-velocity assignment and the target range-velocity estimates from the target tracker.

Three validation methods for the LFMCW processing were selected from the methods presented in Section 5.3. In Figures 10.5 to 10.10, detections of stationary targets ($|v_r| < 0.2\frac{m}{s}$) are shown as crosses, detections of moving targets as dots. For the stationary target detections it is not possible to clearly identify if it is a wrong detection because there are many objects in the scene. Since there were only three moving objects, false detections with a non-zero radial velocity are easily identified.

The gate size of the validation methods is a parameter of major interest. This parameter controls the tradeoff between detection probability and false alarm rate of the sensor signal processing. Results are shown for gate sizes of ± 0.1 bin and ± 0.2 bin. All results shown in the figures were created from the same (recorded) measurement data.

The results of the single sensor tracking are shown as lines in the same plots. The direct frequency to track method is used that was described in Section 5.4.4. The tracker uses another validation gate to directly assign the frequencies to the target tracks. The size of this gate is set to be equal to the gate size used in the range-velocity processing. The two validation gates influence different aspects of the signal processing. While the upholding of the target tracks depends on the tracking assignment, the track initiation depends on the standard range-velocity processing.

From the first figure (Figure 10.5) it can be seen that a gate size of ± 0.1bin results in a low detection quality using the 2 chirp validation technique with a circular gate. This is consistent with the previous results. Despite the small gate size, there are some obvious false detections. This is typical for an urban environment where numerous objects are within the observation area. For a standalone sensor, a tracker is mandatory in order to reject these false detections. To some extend, the tracker is able to initiate and validate the three target tracks, even when using the small gate of size ± 0.1bin.

The next two figures show the combined validation method which allows one chirp measurement to be falsified to some degree (Section 5.3.) The track initiation is already useful. The validation method does not change the frequency assignment of the tracker, so the tracks are still unstable due to the small gate size.

In previous sections, a gate size of ±0.2bin was shown to be a useful choice in case of an extended target and also in multi-target situations. This can be approved by the measurement results shown in Figures 10.8 to 10.10. The simulations showed that the performance of the 2 chirp validation method is always better when comparing detection rates for a fixed false alarm rate. Figure 10.8 shows a sufficient detection performance for a fast track initiation. The gate size of ±0.2bin is also sufficient for the frequency to track assignment to steadily maintain the target tracks.

The results show that a stable tracking of the three vehicles is possible. A few false alarms from the sensors are negligible for the radar network application. That is because the radar network processor can only form a target track when it receives consistent updates on a target from multiple sensors. Optimized strategies of track validation are not considered further in this section. A further optimization of the track validation should be investigated to reduce false track initiations for standalone LFMCW sensors.

10.4 Discussion of Results

The LFMCW processing using a waveform of four chirps is a well known concept in automotive radar [Meinecke 2001, Mende 1999]. It is a technique enabling the simultaneous measurement of a targets range and Doppler frequency with a very simple CW radar front-end. With this technique it is also possible to resolve multiple targets in many situations.

In radar signal processing, a major characteristic taken advantage of is the dynamics of the target scenario. In a dynamic target scenario the target states are constantly changing and so also the measured echo frequencies are different for each measurement cycle. Target fluctuations also add to the variation of the measurements. Each measurement is unique and moving targets interfere only for a short time in one chirp. These effects make it possible to guarantee a high probability of a target detection after some measurement cycles.

It was shown in [Meinecke 2001] that a standard algorithm can be applied to far distance sensors. This classic concept will produce useful results for applications like automotive cruise control (ACC) systems. There are two differences when using LFMCW near distance sensors in a radar network instead of using an LFMCW far distance sensor:

1. The target density per unit range is much higher because of the shape of the observation area.

2. The requirements for the range accuracy are much higher.

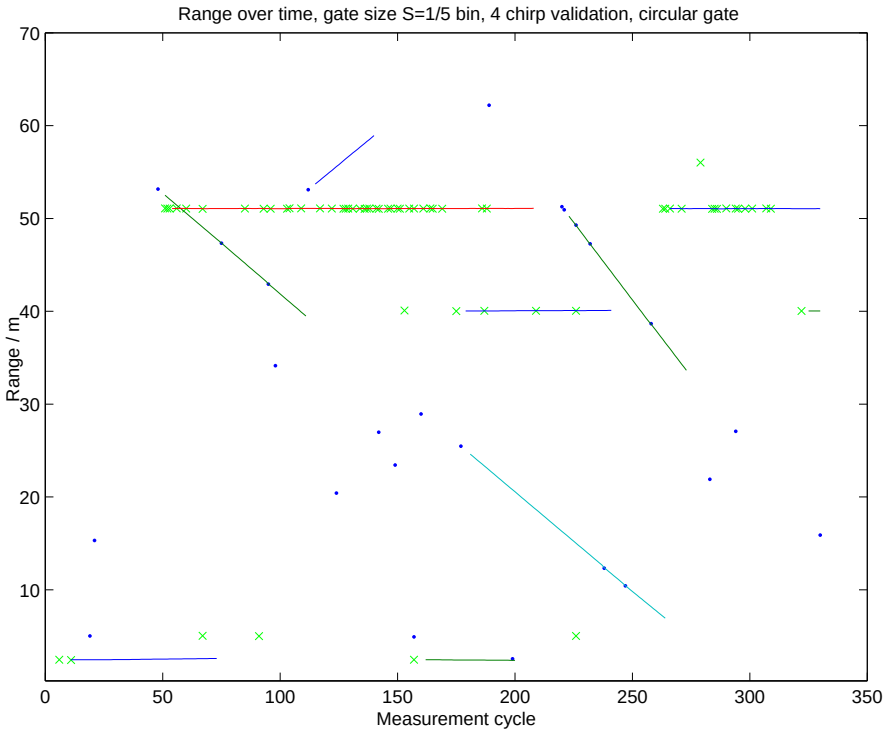

Figure 10.5: Range measurements and track states of a road traffic scenario. *2 chirp validation, circular gate, gate size* $S = \pm 0.1$bin

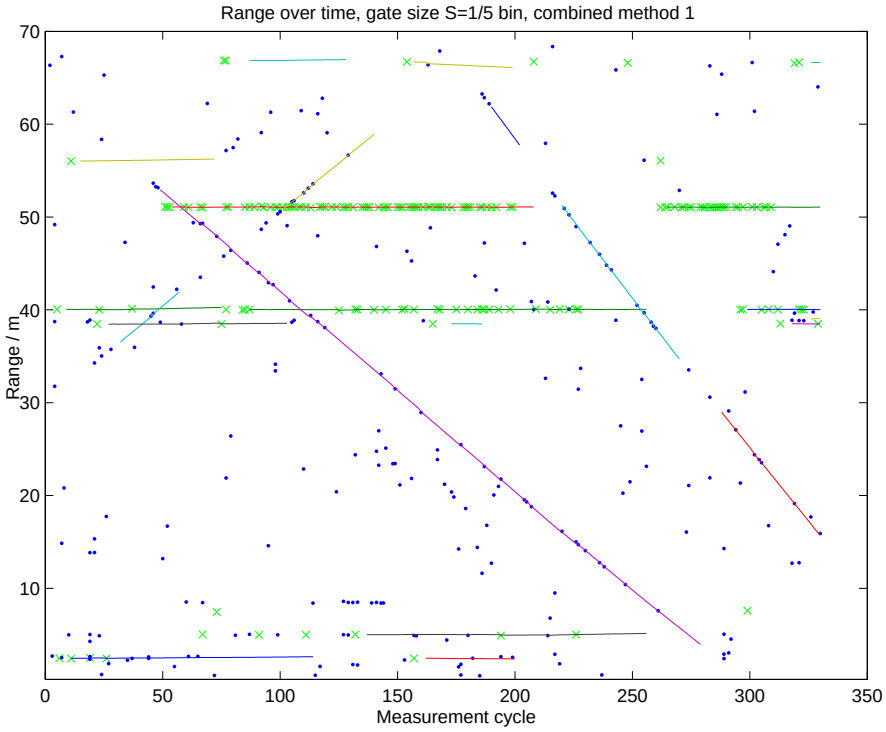

Figure 10.6: Range measurements and track states of a road traffic scenario. *First combined validation method, gate size* $S = \pm 0.1$bin

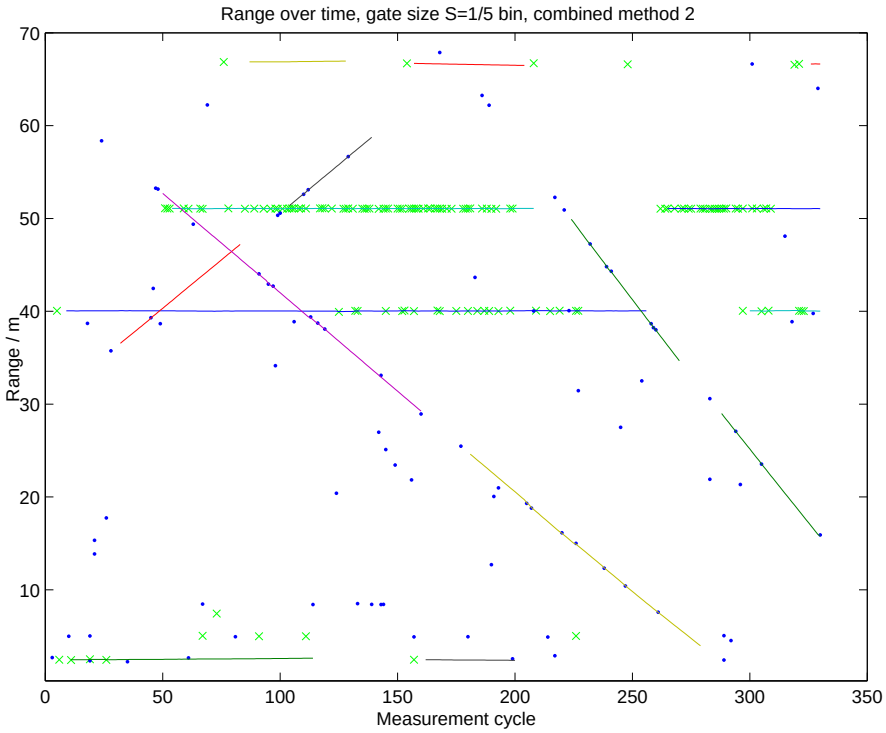

Figure 10.7: Range measurements and track states of a road traffic scenario. *Second combined validation method, gate size* $S = \pm 0.1$bin

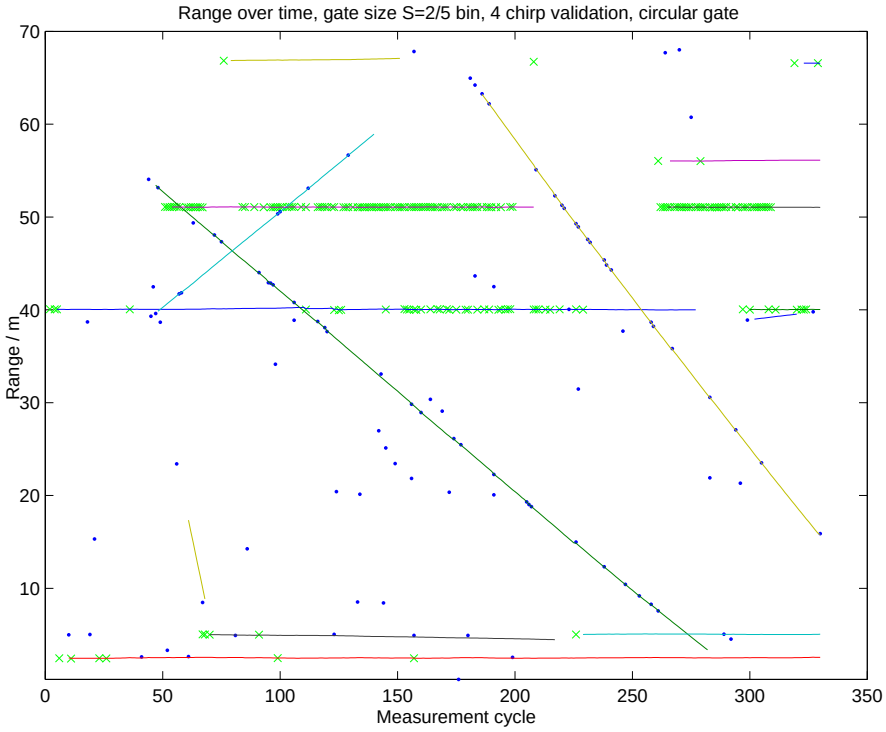

Figure 10.8: Range measurements and track states of a road traffic scenario. *2 chirp validation, circular gate, gate size* $S = 0.2$bin

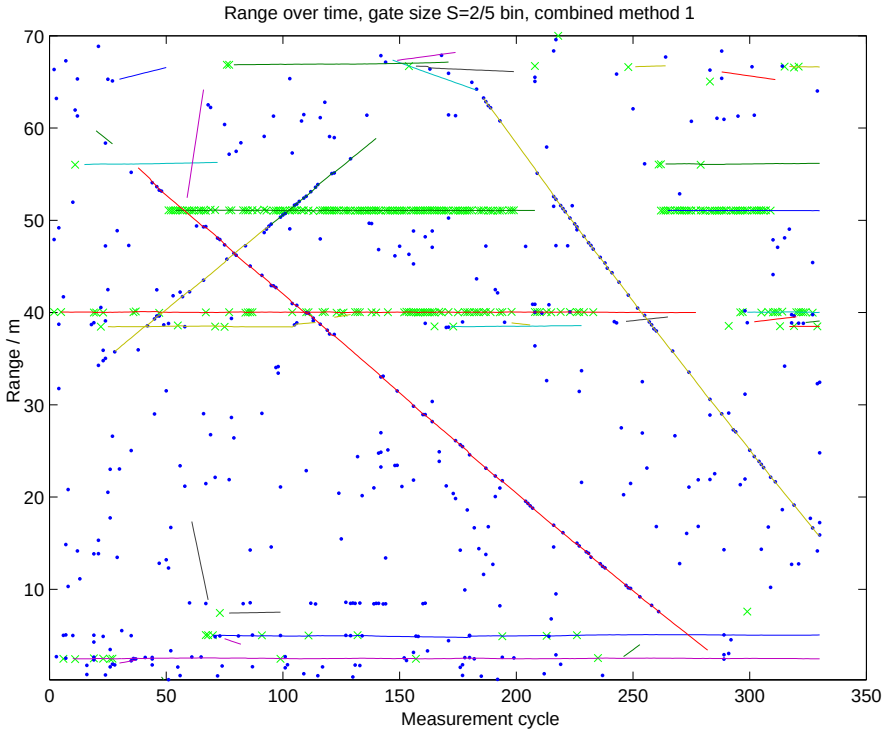

Figure 10.9: Range measurements and track states of a road traffic scenario. *First combined validation method, gate size* $S = 0.2$bin

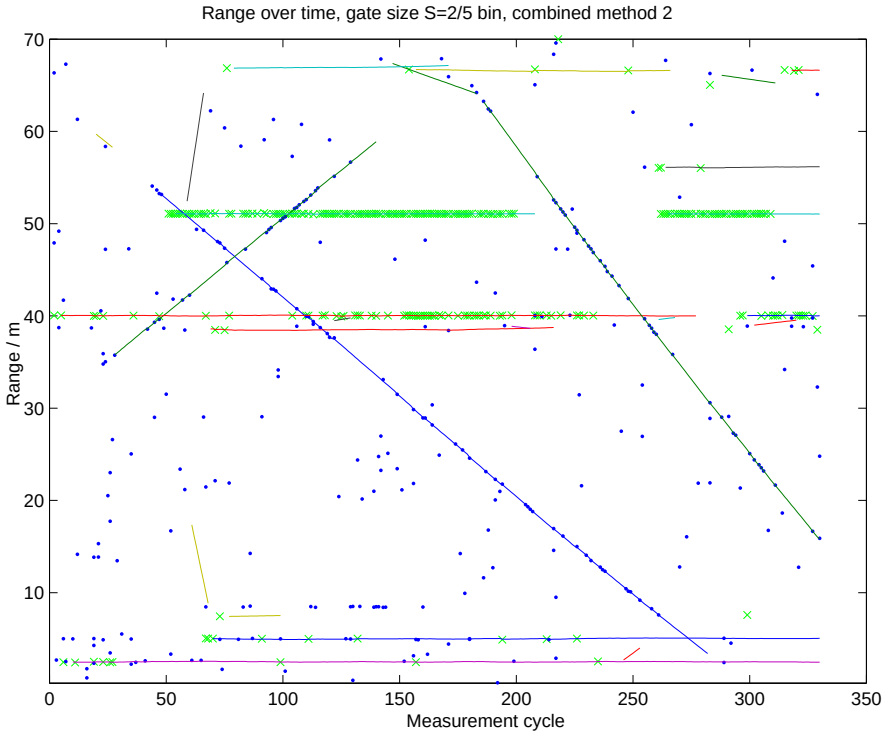

Figure 10.10: Range measurements and track states of a traffic scenario. *Second combined validation method, gate size* $S = 0.2$bin.

While an automotive far distance sensor (FDS) operates with an observation range of up to 200m with multiple small antenna beams, a near distance sensor (NDS) has a wide antenna beam and only a small maximum range up to 30m. It was shown that the basic processing commonly used for an FDS has to be modified for an NDS because of the higher target density per unit range.

The single sensor LFMCW processing algorithm produces target detections and parameter estimations that are the basis of the radar network lateration techniques. These techniques need a high target detection rate and a good accuracy of the range measurements in order to produce good lateration results.

It was shown in this chapter that in situations with multiple targets, especially when many surrounding objects interfere with the targets to be detected, a small gate size (about ± 0.2 bin) has to be chosen for the range-velocity processing to get useful values for the false alarm rate. A small gate size is also very useful to achieve a good accuracy.

However, the small gate size will result in a small detection rate at the output of the range-velocity processing algorithm. The proposed single sensor tracking directly uses the frequency detections of the chirps to update the target tracks. This approach improves the stability of the target tracks significantly, because the tracks are updated even when detections in single chirps are lost due to target interferences.

The measurement results from the last section show, that with the proposed signal processing scheme, it is realistic to use the LFMCW modulation technique also in multiple target situations with many interfering objects while maintaining a good range estimation accuracy.

Chapter 11

Radar Network Experimental Results

This chapter presents experimental results from the complete radar network. The results show the performance, a radar network is able to achieve even with a sensor range resolution of only$\approx$ 0.5m. This is much less resolution than other test systems [Klotz 2002] have.

In the first section, test results for single point targets are shown to illustrate the achievable position estimation accuracy in an ideal situation. These tests also verify the basic functionality of the radar network.

The second section presents the results of measuring a single extended target moving in front of the radar network. These results will be used to assess whether the principle of position estimation by lateration techniques with the described system parameters is applicable to extended targets.

In the third section, the azimuth accuracy is analyzed for extended targets that are not oriented in the direction of the radar network. Measurement data are investigated for vehicles driving along a road. The radar network is positioned next to the road, so that the target vehicles are oriented and moving in a direction different to the radar network orientation.

The fourth section presents the results of a typical urban stop and go scenario. The test vehicle equipped with the radar network is driven through a two lane street following another vehicle. The purpose of this experiment is to check for the practical usability and the limits of the presented radar network.

11.1 Single Point Target Detection and Position Measurement

The experiment to measure a single point target is done for two reasons. It proofs the basic functionality of the lateration concept. It also shows the achievable position estimation accuracy under best conditions.

In Figure 11.1, two experimental setups are sketched. In the first setup, a corner reflector is moved back and forth in front of the radar network. The target range, defined as the distance between target and network coordinate center, is generated from the trilateration position estimation and compared to the reference range. In the second setup, the lateral position of the corner reflector is changed. The target azimuth, defined as the angle between target distance vector and network y-axis, is generated from the trilateration position estimation and compared to the reference angle.

In both experimental setups, the corner reflector is moved automatically, and the measured values are plotted against the reference values. Figures 11.2-11.4 show the experimental results of the single target measurements of target range and target azimuth.

The single point target experimental results show an extraordinary precision in range and azimuth accuracy. Since the scene contains only one stably detected target, the chosen network processing strategy does not alter the results. The network range accuracy is better than 1.5cm. As expected, the network range accuracy is better than the single sensor accuracy. This is because four single sensor range measurements are combined in the position estimate. The accuracy of the tracked target angle is much better than 2 degrees. These measurements thus show the basic functionality of the radar network.

The network processing system provides an accurate and unbiased estimate of the target position. The experimental setup includes a system to automatically move the test reflector. The system provided a reference value for the target position with an accuracy of 1cm. The accuracy of the radar network reaches the precision of this reference.

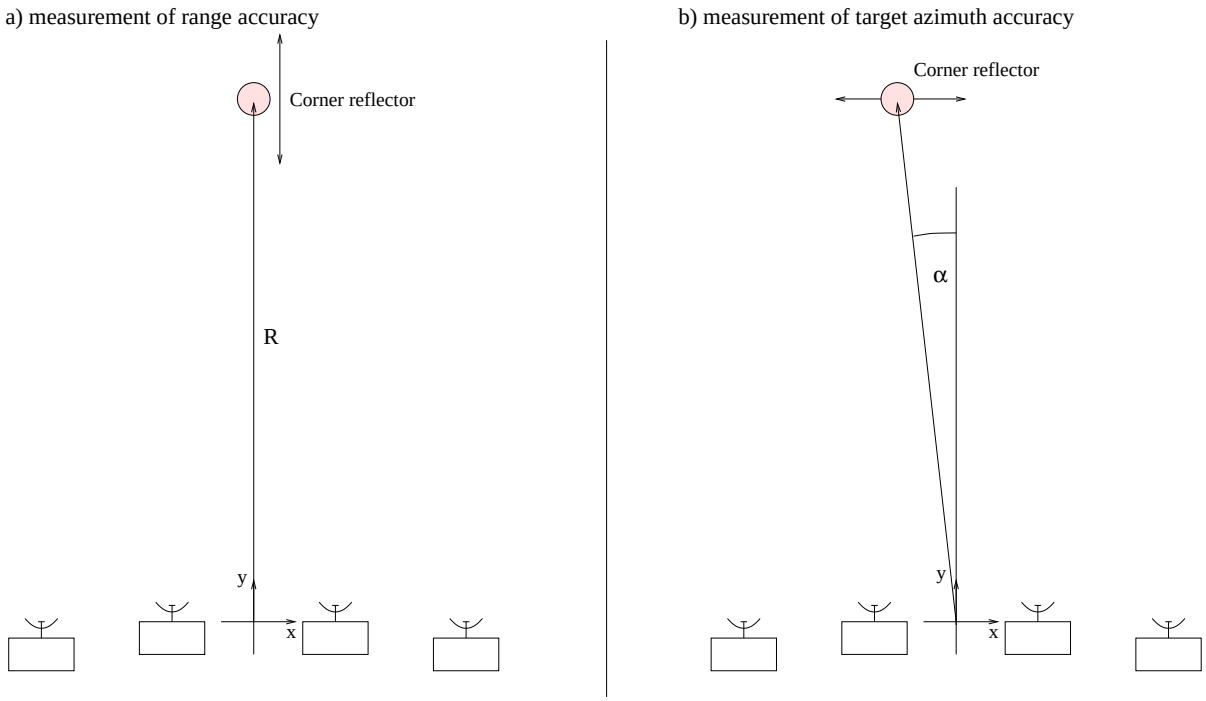

Figure 11.1: Single point target experimental setup

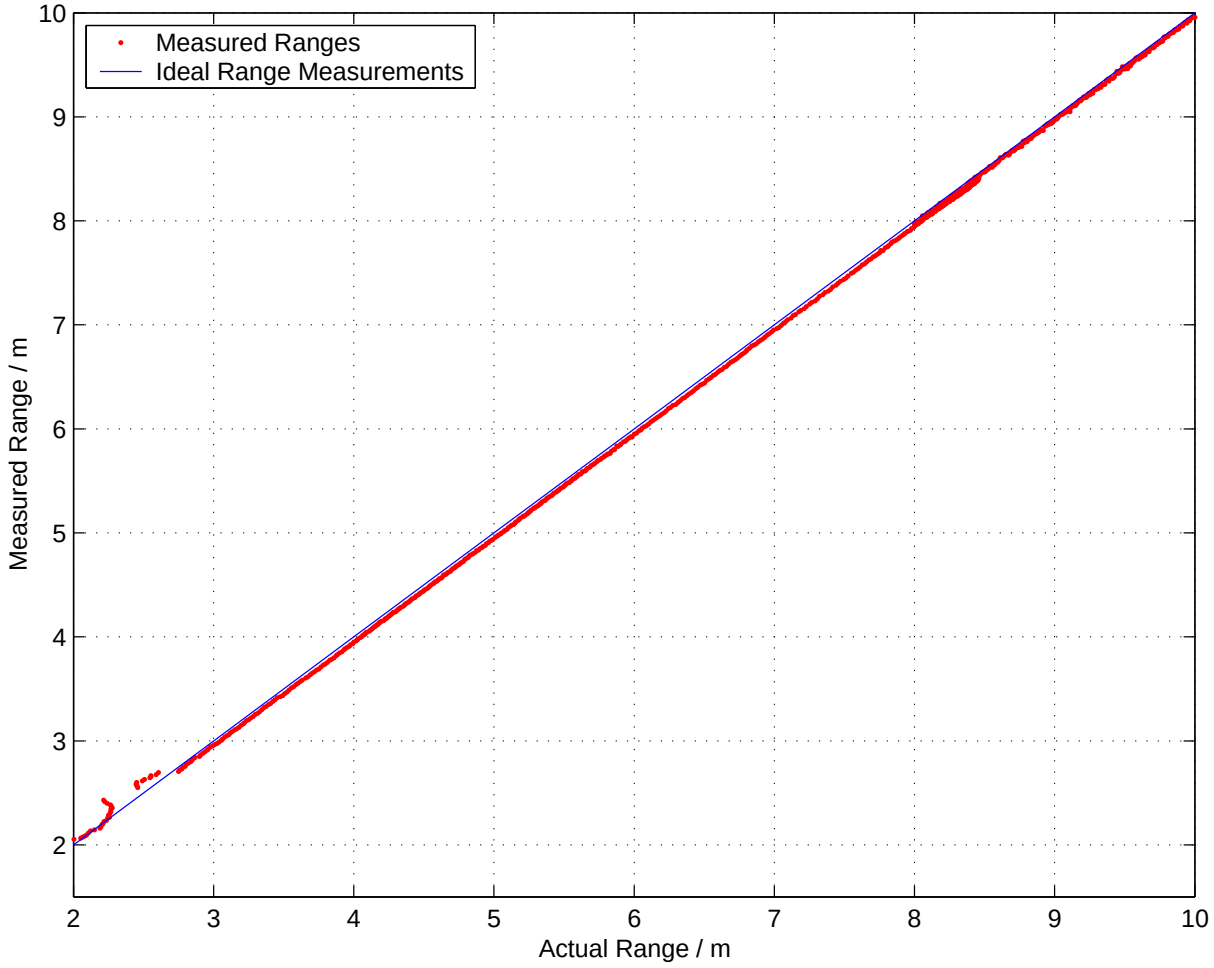

Figure 11.2: Radar network range measurements of a single point target

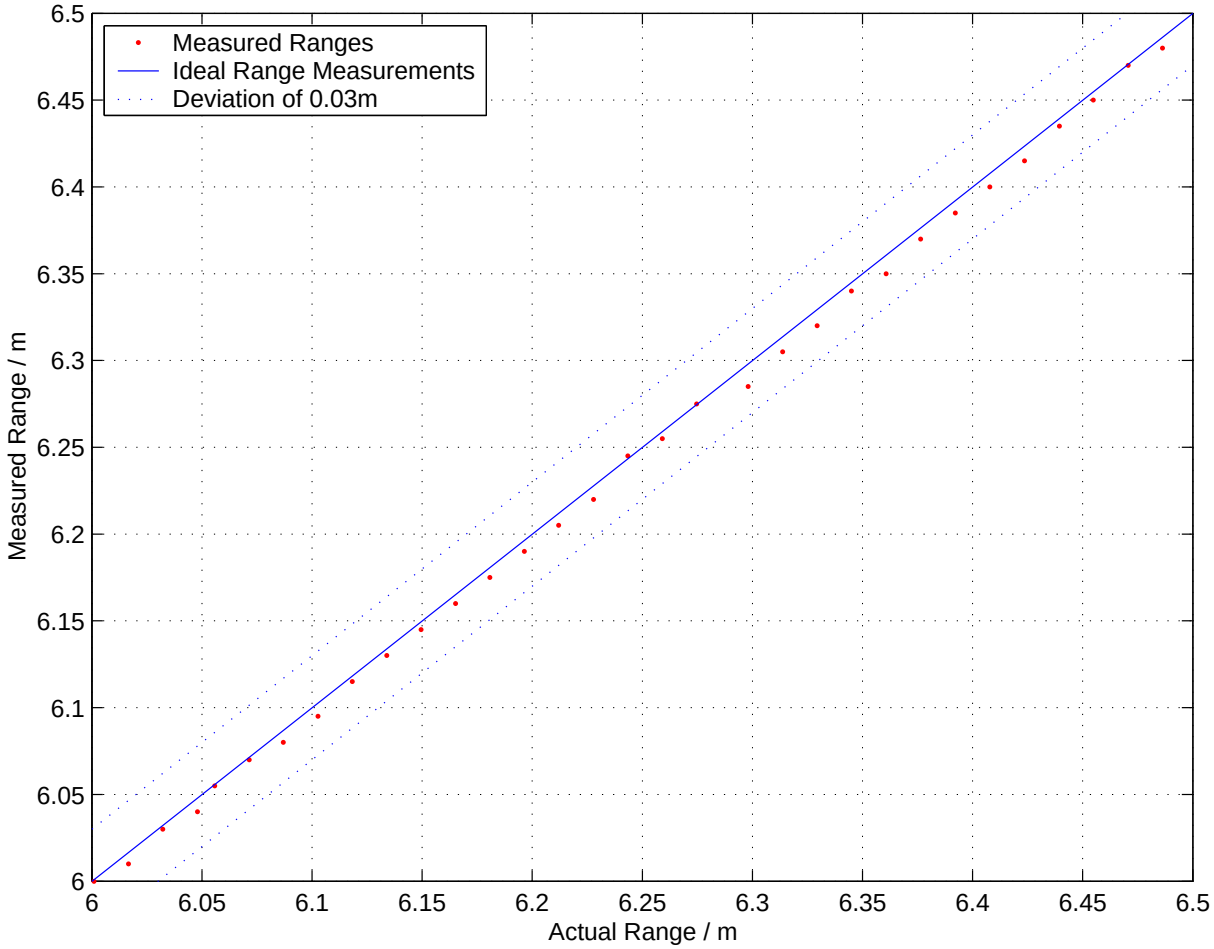

Figure 11.3: Range measurements of a single point target, closeup at 6 m

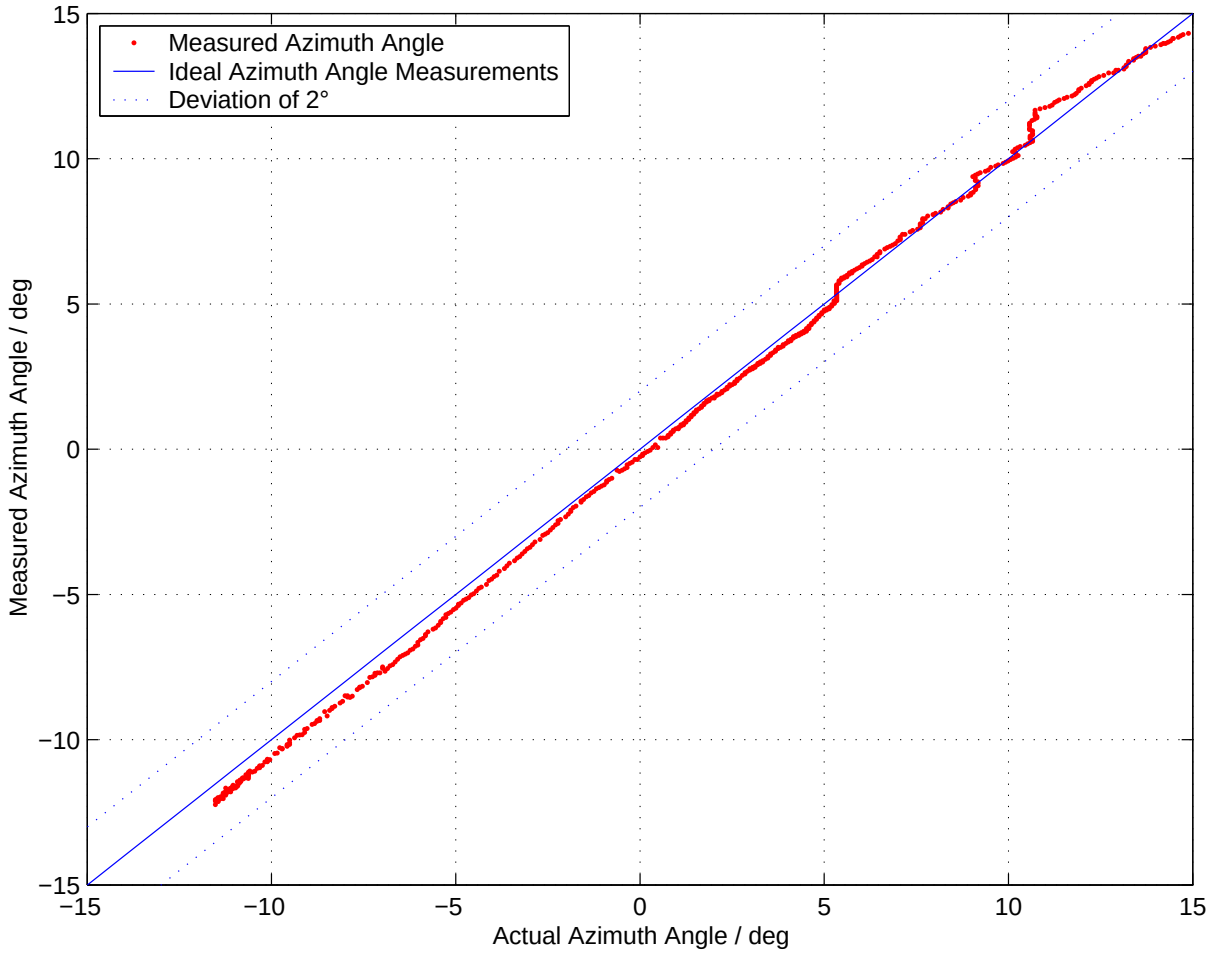

Figure 11.4: Azimuth measurements of a single point target

11.2 Measurement of an Extended Target

The results of the first experiment show that the network performance is very good under ideal circumstances. The single sensor measurements provide the basis for the target position estimation and they have the performance to obtain a useful estimation accuracy. In this section, measurement of an extended target is discussed. In this case, the differences of the three network processing strategies become relevant.

For the experiment, a passenger car was driven towards the radar network at approximately 5 m/s. The single sensor target lists were stored to have reproducible data. These data were used to test different network processing strategies and different gate sizes for the assignment procedures. The range to track assignment (described in Section 8.1) is shown in Figure 11.5 and the frequency to track assignment strategy (described in Section 8.2) is shown in Figure 11.6. For each strategy, three different gate sizes were chosen. In addition to the track trajectories, the target detections from the standard lateration procedure are shown as circles. The lateration works as described in Chapter 6.2. These target detections from the standard lateration are identical in all plots. The gate size for the lateration procedure is 0.1 m for the target range and 0.2 m/s for the target radial velocity.

As can be seen from the range to track experimental results in Figure 11.5, for small gate sizes there are disruptions in the target tracks. Using gate sizes of $\pm$0.5m for target range and $\pm$1m/s for target velocity the verified target track gets enough updates to keep the target active during the complete measurement.

Figure 11.6 shows the results for the frequency to track assignment for three different gate sizes. The most obvious difference to the range to track assignment is the enhanced accuracy of the lateral measurement. Another very important point is the more stable track maintenance while having smaller gates compared to the range and velocity gates of the range to track assignment (1 frequency bin corresponds to ~0.3 m).

In this measurement, the vehicle is oriented towards the radar network and the front face of the vehicle presents a large reflector for the radar. Reflections of vehicle parts behind the front plane are neither strong nor stable enough to produce a target detection behind the vehicle front.

The results can be interpreted in the same way as the results for the single sensor LFMCW frequency to track technique. The more the measurement to track assignment is able to choose from, the smaller the gate size can be to still get enough updates to maintain the tracks. A small gate size can reduce the false alarm rate as well as it reduces the impact of interferences between neighboring targets.

The described algorithms use the nearest neighbor / gating technique (Section 7.1). Both the range to track and the frequency to track strategy can probably be improved by means of more sophisticated assignment strategies. Measurement to track assignment techniques are a broad research topic in the field of radar technology. The assignment of range or frequency detections to (laterated) target tracks within the radar network processing still provides interesting future research topics.

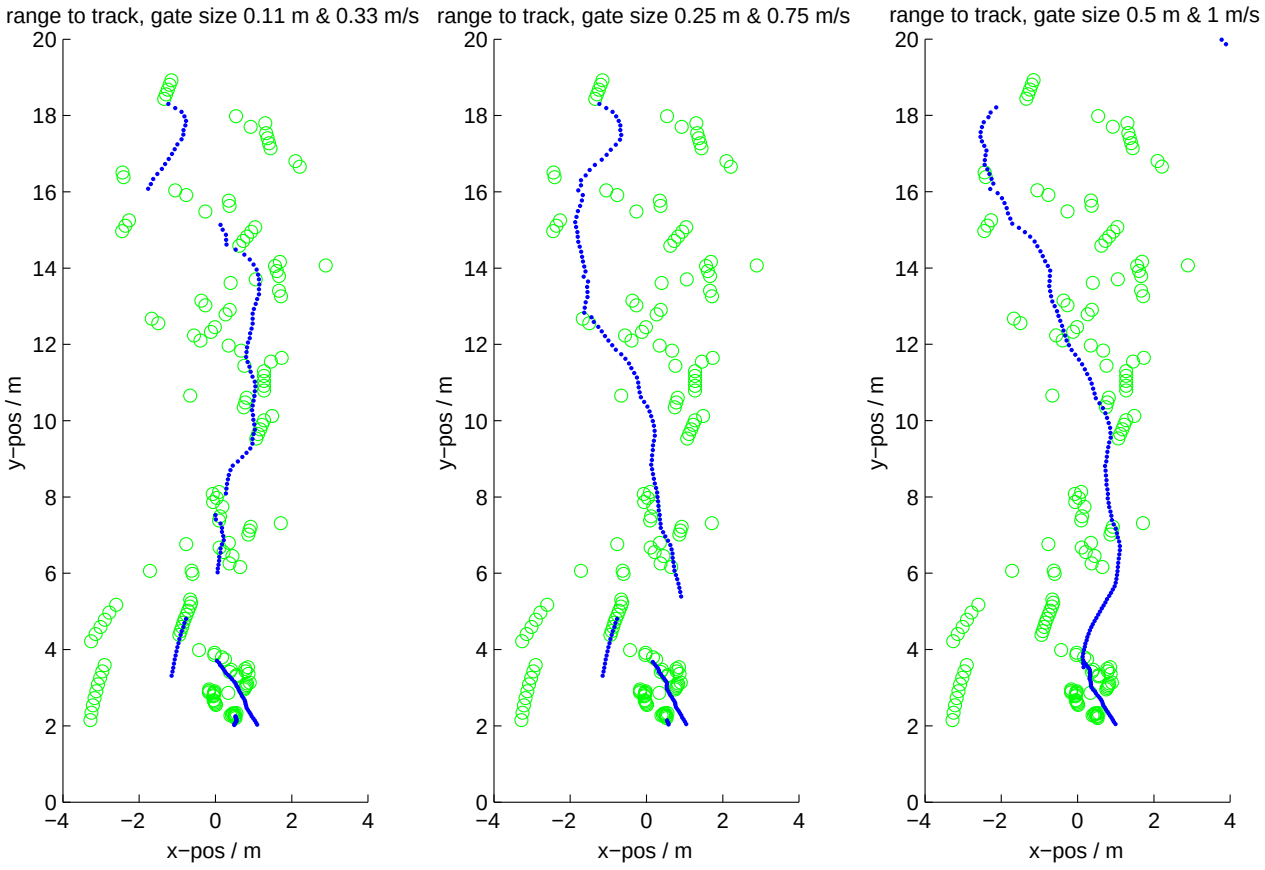

(a) Gate size R: +-0.11m, Gate size vel.: +-0.33m/s

(b) Gate size R:+-0.25m, Gate size vel.: +-0.75m/s

(c) Gate size R:+-0.5m, Gate size vel.: +-1m/s

Figure 11.5: Position estimates for an extended target using the range to track assignment. The circles show the target detections from the normal trilateration algorithm.

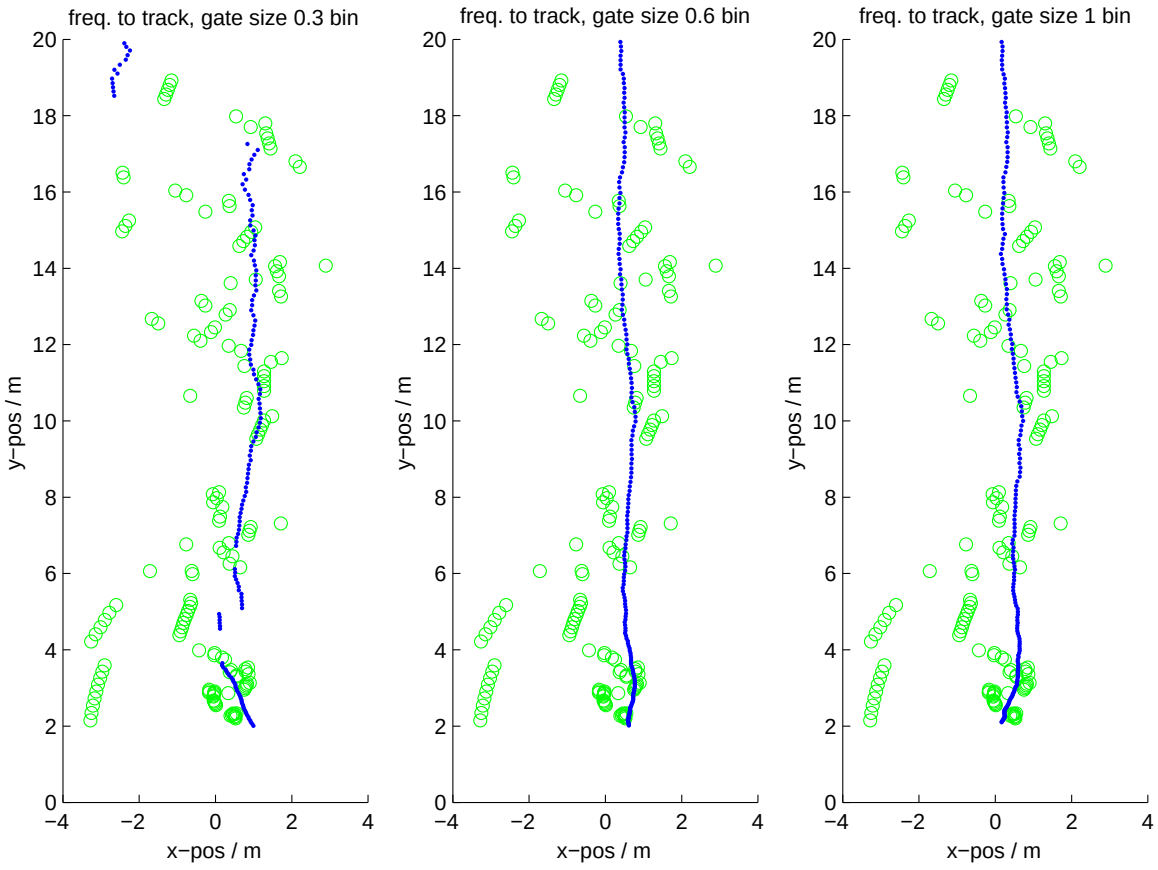

(a) Frequency gate size: +-0.3bin

(b) Frequency gate size: +-0.6bin

(c) Frequency gate size: +-1bin

Figure 11.6: Position estimates for an extended target using the frequency to track assignment. The circles show the target detections from the normal trilateration algorithm.

11.3 Arbitrarily Oriented Extended Targets

If the target vehicle is driven towards the radar network the results show a good performance in the lateral position estimation. This can be seen from the results in the previous section where the target vehicle is driven along the y-axis of the radar network. To investigate the position estimation accuracy for targets not oriented towards the network, the experiment uses the traffic scene shown in Figure 11.7. In this scene, the vehicle is driving on a trajectory that has a 25 degree deviation from the network y-axis. It intersects the network y-axis at around 17 m.

In Figure 11.8 the target measurement is shown for the instant the photograph was taken. The target position is shown from a birds eye view as a circle. A line is drawn from this circle into the direction of the estimated target velocity vector. The length of the line corresponds to the distance, the target will move within one second. This measurement reveals the precision with which the LFMCW radar network can measure not only the radial velocity but also the tangential component to deliver an accurate velocity vector.

Figure 11.9 shows the trajectories of multiple targets. The dark lines denote cars that are approaching on the opposite lane as in the example shown in Figure 11.7. The lighter lines denote cars that are moving away in the right-hand lane.

The measurements were done using the frequency to track algorithm. The classical approach and the range to track algorithm did not produce stable detections.

It can be seen that, although the single trajectory is often a stable line, the displacement between the track trajectories and the actual course of the road can be very high. The reason for this can be traced back to the single sensor range measurements. Each sensor measures a different reflection center on the car. Figure 11.10 shows a section of the Fourier spectra of all four sensors. The spectra are from the same measurement time and show a vehicle measured from the side. It can be seen that the appearance of the target is different for all four sensors. Furthermore, due to the limitation of resolution, some target reflections interfere with each other.

The results show that a precise azimuth measurement can only be guaranteed if the target is oriented towards the sensor network. For differently oriented targets the position estimates were accurate in some cases but a specific accuracy cannot be guaranteed.

As also can be seen in the spectra, interferences of reflection centers on an extended target are possible. An increase in range resolution can reduce the probability of interferences. However, this can not alter the natural effect of each sensor measuring a slightly different reflection center on the

Figure 11.7: Photograph of the traffic scenario, Hamburg Harburg, Ehestorfer Weg

target. It is believed that performance can be improved by an increase in the number of measured signal paths that are available for the lateration technique. This can be achieved by increasing the number of sensors or by using the concept of multilateration with multistatic radars.

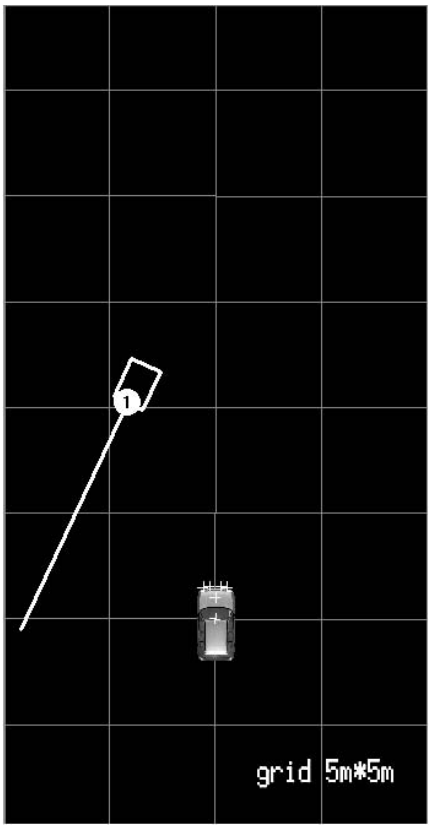

Figure 11.8: Screenshot of the traffic scenario shown in Figure 11.7

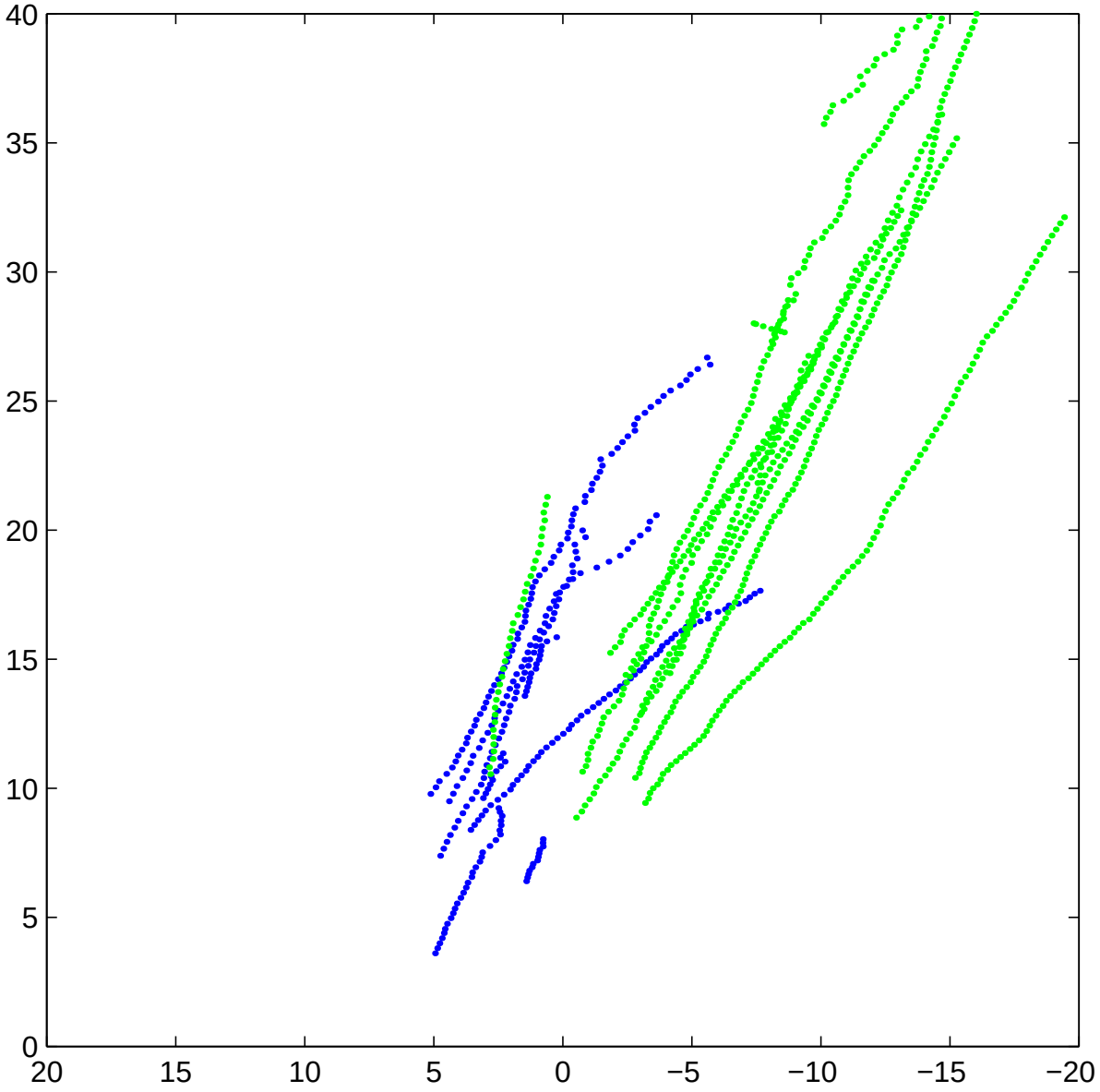

Figure 11.9: Trajectories for multiple targets

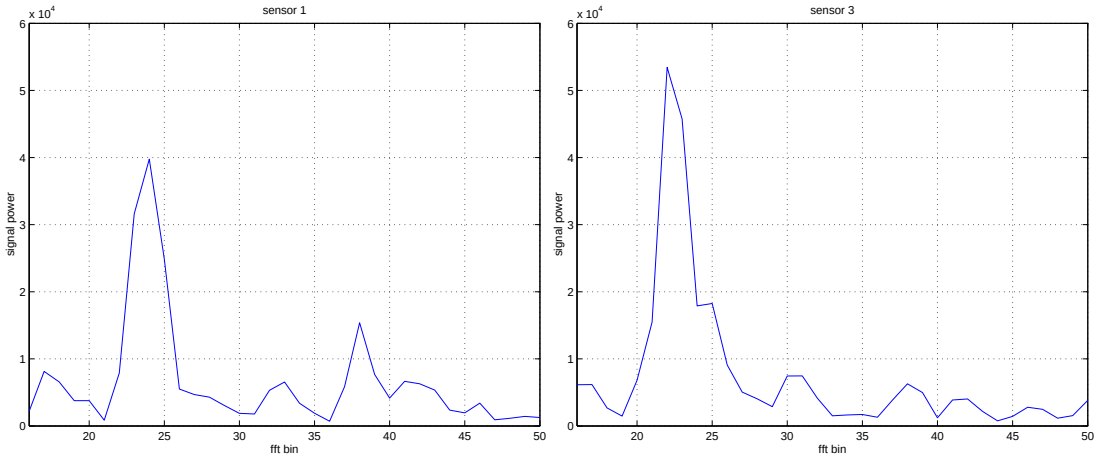

(a) left sensor

(b) middle left sensor

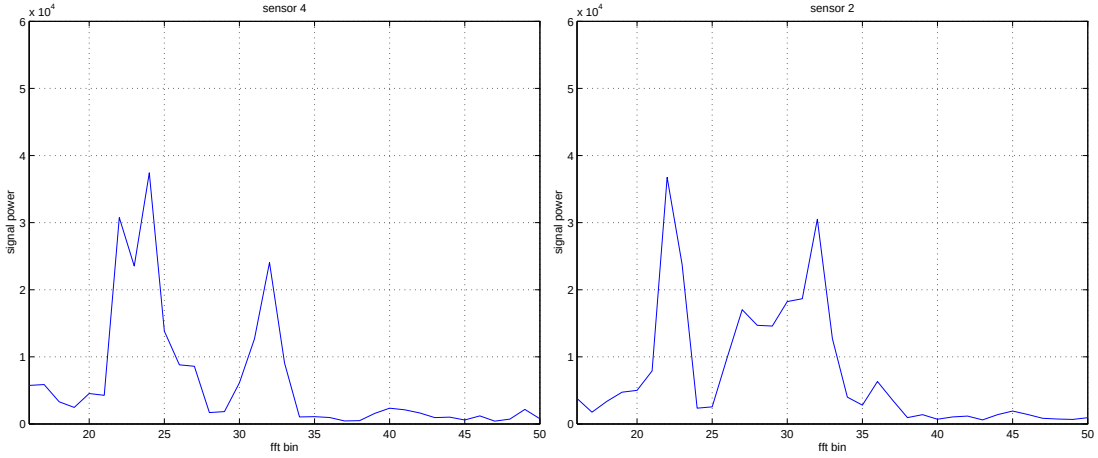

(c) middle right sensor

(d) right sensor

Figure 11.10: Comparison of sensor spectra for a passenger car in front of the radar network, oriented sideways (25deg offset).

11.4 Stop and Go Traffic Scenario

As shown in the preceeding sections, a point target and a target vehicle oriented towards the radar network can be detected well. The target position can be precisely measured for the point target while the position estimate for the target vehicle is within the bounds of the car front when using the frequency to track assignment technique.

With the experiment presented in this section, the use of the radar network is evaluated for some of the applications currently of interest. Figure 11.11 shows a standard urban traffic scene on a two lane road. The host vehicle equipped with a radar network is following another vehicle. There is one car on the opposite lane that is about to pass the host vehicle. Figure 11.12 shows the corresponding output of the radar network from a birds eye view. It shows the detected targets at their estimated positions as numbered circles. The estimated target velocity is visualized by a line starting at the target circle going into the direction of the target movement. The length of the line denotes the distance the target will travel in one second. Positions and velocities are relative to the host vehicle coordinate system. Target number 0 denotes the detection of the preceeding vehicle. Detection number 5 corresponds to the oncoming car while number 3 is a detection of a car in the right parking lane.

Figure 11.13 shows three plots on the complete 2 minute test run. The upper plot shows the target range over time. At the beginning of the test run the preceeding car enters the observation area and from then on is tracked by the network processor. The track of the preceding car is shown as a dark line while the remaining tracks are shown lighter. The middle plot shows the target relative velocities. During the test run, the preceeding car comes to a full stop and resumes driving after a short time. Also the host vehicle comes to a full stop and resumes driving.

The bottom plot shows the lateral position estimate of the target tracks. It can be seen, that the precision of the lateral position estimate is sufficiently good so that the preceeding car can constantly be assigned to the lane of the host vehicle.

Many stationary objects are detected during the test. While the range and radial velocity can be measured well, the accuracy of the lateral position estimates is not sufficient to reliably detect whether the object is in the host vehicle lane or not. The lateral position can be measured correctly and even precisely for many objects, but some objects are measured with a significant error.

Further tests demonstrated that it is possible to improve the lateral position estimates for objects at the side of the lane by decreasing the gate size of the assignment algorithm. However, decreasing the gate size decreases

Figure 11.11: Photograph of a common traffic scene, Hamburg Harburg, Eissendorfer Strasse

the detection rate to a value that is no longer useful.

The results show that the radar network has an excellent target detection rate and measures the target range and radial velocity at very high accuracy. For a safety system like the collision avoidance system, the presented radar network still needs to be improved so that lateral position accuracy is high for all targets. It is anticipated that an increase in the number of sensors and an increased single sensor range resolution can greatly improve the number of correctly estimated target positions. The use of the multilateration technique with a multistatic radar network could also improve the performance. Both these options should be investigated in practical scenarios.

It is concluded that the presented radar network performs well for ACC applications including a stop and go function.

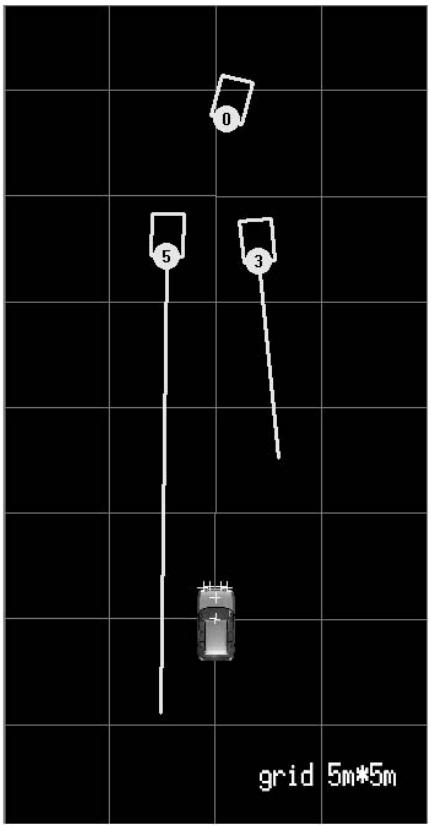

Figure 11.12: Screenshot of radar network measurement data corresponding to the photograph in Figure 11.11

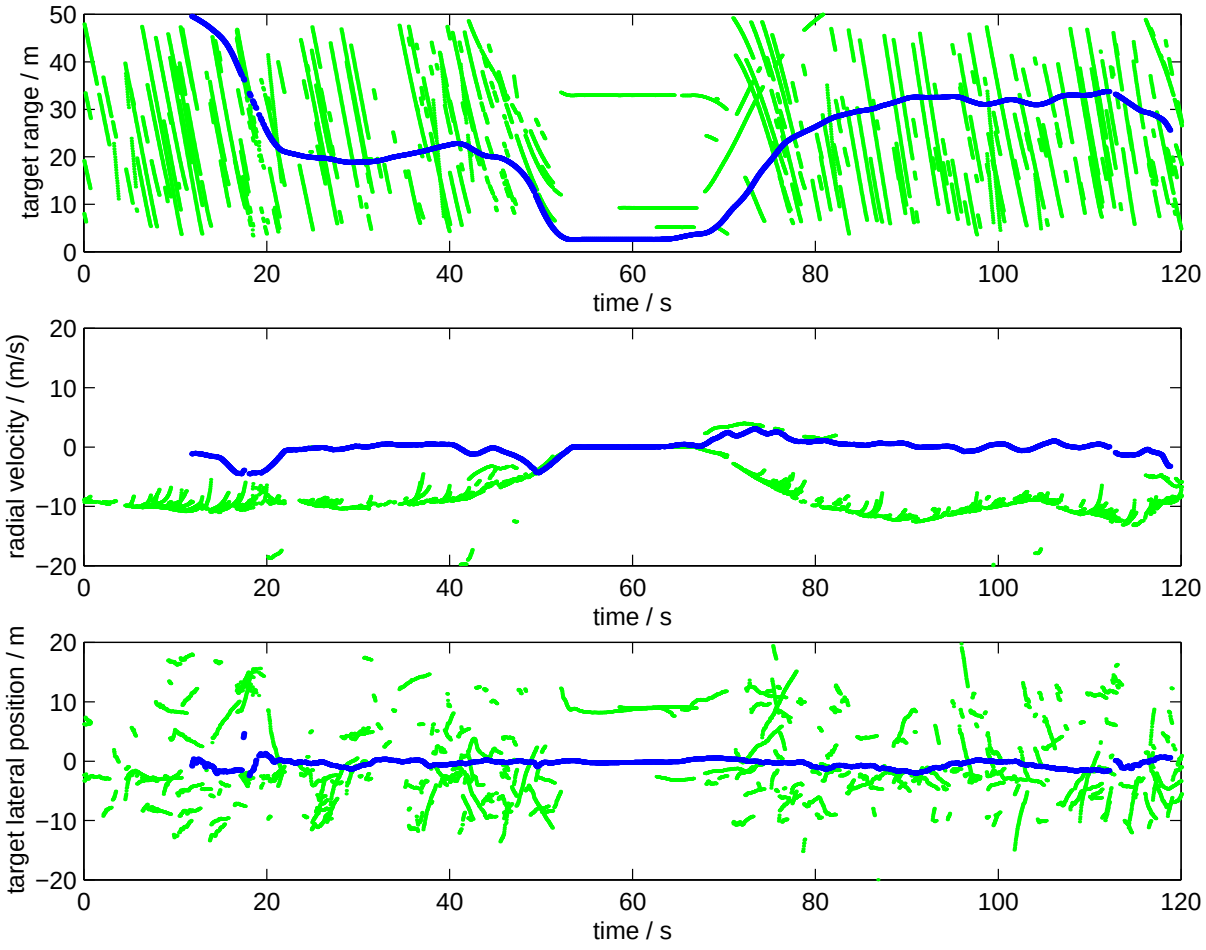

Figure 11.13: Measurement data for complete duration of stop-and-go scene

Chapter 12

Conclusions

This thesis has first described concepts of linear frequency modulated continuous wave (LFMCW) radars and the concepts of radar networks. New signal processing algorithms were investigated and developed.

For the first time, a radar network has been developed with 77 GHz LFMCW sensors that are using a bandwidth of only 450 MHz. To accomplish a good performance, improvements to the classical approaches have been explored and presented. Some improvements specifically apply to the single sensor LFMCW processing, some improvements specifically apply to the network processing algorithms. The newly proposed frequency to track strategy finally interconnects the LFMCW and the network processing through a conjoint measurement to track assignment. It was shown that the interconnection of signal processing steps makes it possible to extract information from the measurement data much more efficiently.

A recently studied network [Klotz 2002] has used pulse radars with high resolution capability. The presented network has a much lower resolution but still has a promising performance. Though the lateral position estimates have to be improved for safety applications, the usability for ACC systems with "stop and go" functionality has been demonstrated.

The accuracy of the azimuth position estimates depends on the targets spatial extension and it has been found that the sensors resolution capability and especially the number of sensors is crucial to the performance of the azimuth measurement. Also the use of the multilateration technique with a multistatic radar network should be investigated in practical scenarios.

The described signal processing algorithms were used for the European research project "A Multifunctional Automotive Radar Network" (RadarNet). RadarNet has been supported by the European Commission under the 5th Framework Programme (project no. IST-14031). At present, the

Figure 12.1: Passenger car equipped with a radar network prototype.

car manufacturers participating in the RadarNet project are gathering information with the radar network prototypes. Seven network prototypes have been constructed. As an example, the experimental car seen in Figure 12.1 is tested with pre-crash sensing applications.

This work also demonstrates that there is significant scope for further research on LFMCW radar networks, especially on multistatic networks using the multilateration technique.

Appendix A

Derivation of the LFMCW Base Band Receive Signal

The baseband signal for the LFMCW radar was derived graphically in Section 3.4. For completeness, the down-converted received signal is derived analytically for the LFMCW waveform and the stepped version. These equations can also be used for simulating radar front-end measurement data.

A.1 Continuously Rising LFM Chirp

The starting point is the linear frequency chirp that is defined by its instantaneous frequency $\omega(t)$:

$$\omega(t) = 2\pi \left(f_0 + \frac{\Delta f}{T_C} t \right)$$

The instantaneous frequency is the derivative of the instantaneous phase $\varphi(t)$:

$$\frac{d\varphi(t)}{dt} = \omega(t)$$

$$\varphi(t) = 2\pi \left(f_0 t + \frac{\Delta f}{T_C} \frac{t}{2}^2 \right) + \varphi_0$$

The transmit signal $s(t)$ can be written as a cosine function of $\varphi(t)$:

$$s(t) = \cos\left(2\pi \left(f_0 + \frac{\Delta f}{2T_C} t \right) t + \varphi_0 \right) = \cos(\varphi(t))$$

$$s(t) = \frac{1}{2}e^{j\varphi(t)} + \frac{1}{2}e^{-j\varphi(t)}$$

If the transmit signal is reflected at time t' by a target at range $R(t')$, the connection between transmit signal $s(t)$ and receive signal $r(t)$ is given by:

$$r\left(t' + \frac{R\left(t'\right)}{c}\right) = s\left(t' - \frac{R\left(t'\right)}{c}\right)$$

The electromagnetic wave only needs a very short time to travel to the target and back to the radar. Within this short time, the target movement can be neglected for the construction of the receive signal from the transmit signal:

$$r\left(t\right) = s\left(t - \frac{2R\left(t\right)}{c}\right)$$

In the equation above, a phase shift from the target reflection and the attenuation of the signal is not taken into consideration. The next step is to obtain the baseband receive signal produced by mixing the receive signal with the current transmit signal:

$$r_b^*\left(t\right) = r\left(t\right)s\left(t\right)$$

$$r_b^*\left(t\right) = \frac{1}{4}\left(e^{j\varphi\left(t-\frac{2R(t)}{c}\right)} + e^{-j\varphi\left(t-\frac{2R(t)}{c}\right)}\right)\left(e^{j\varphi(t)} + e^{-j\varphi(t)}\right)$$

A low pass filter is used to filter out the high frequency components to only keep the base band component:

$$r_b\left(t\right) = \frac{1}{4}\left(e^{j\varphi\left(t-\frac{2R(t)}{c}\right)}e^{-j\varphi(t)} + e^{-j\varphi\left(t-\frac{2R(t)}{c}\right)}e^{j\varphi(t)}\right)$$

$$r_b\left(t\right) = \frac{1}{2}cos\left(\varphi\left(t - \frac{2R\left(t\right)}{c}\right) - \varphi\left(t\right)\right) = \frac{1}{2}\cos\left(\varphi_{rb}\left(t\right)\right)$$

r_b is the signal at the output of a single channel demodulator. A quadrature demodulator produces an in-phase and a quadrature output. The two output signals can be considered as the real and imaginary part of one complex signal:

$$r_{bC}\left(t\right) = \frac{1}{2}e^{-j\varphi\left(t-\frac{2R(t)}{c}\right)+j\varphi(t)} = \frac{1}{2}e^{-j\varphi_{rb}(t)}$$

Depending on the demodulator used, the base band signal will be a real or complex function of $\varphi_{rb}(t)$. The instantaneous phase $\varphi_{rb}(t)$ can be expressed by the instantaneous target range $R(t)$:

$$\varphi_{rb}(t) = \varphi\left(t - \frac{2R(t)}{c}\right) - \varphi(t)$$

$$\varphi_{rb}(t) = 2\pi\left(f_0 + \frac{\Delta f}{2T_C}\left(t - \frac{2R(t)}{c}\right)\right)\left(t - \frac{2R(t)}{c}\right) - 2\pi\left(f_0 + \frac{\Delta f}{2T_C}t\right)t$$

$$\varphi_{rb}(t) = 2\pi\left(-f_0\frac{2R(t)}{c} + \frac{\Delta f}{2T_C}\left(-2t\frac{2R(t)}{c} + \left(\frac{2R(t)}{c}\right)^2\right)\right)$$

For the final steps of the derivation, a target with initial range R_0 and constant radial velocity v_0 is assumed:

$$R(t) = R_0 + v_0 t$$

For automotive and most other applications, an acceleration of the target can be neglected for the duration of one chirp. This holds true as long as the chirps have a duration of a few milliseconds and the target is not rocket-propelled. Insertion of the above equation of movement yields:

$$\varphi_{rb}(t) = 2\pi\left(-f_0\frac{2R_0 + 2v_0t}{c} + \frac{\Delta f}{2T_C}\left(-2t\frac{2R_0 + 2v_0t}{c} + \left(\frac{2R_0 + 2v_0t}{c}\right)^2\right)\right)$$

$$\varphi_{rb}(t) =$$
$$2\pi\left(-R_0\left(\frac{2f_0}{c} + 4t\frac{\Delta f}{2T_C c}\right) - v_0 t\left(f_0\frac{2}{c} + 4t\frac{\Delta f}{2T_C c}\right) + \frac{\Delta f}{2T_C}\left(\frac{4R_0^2 + 8R_0v_0t + 2v_0^2t^2}{c^2}\right)\right)$$

The terms quadratic in t and the last term can also be neglected. Constant phase shifts can be accumulated and are omitted. However, for simulation purposes it is a good idea to leave everything in the equation.

$$\varphi_{rb}(t) = -2\pi\left(R_0\left(\frac{2\Delta f}{T_C c}\right) + v_0\left(\frac{2f_0}{c}\right)\right)t$$

The resulting base band receive signal is approximately a harmonic oscillation with the frequency f_{rb}:

$$f_{rb} = -\frac{2R_0\Delta f}{T_C c} - \frac{2v_0 f_0}{c}$$

The first term depends on the target range, the second term depends on the target relative radial velocity and corresponds to the Doppler frequency. The result agrees with the graphical derivation. When using common system parameters for automotive radar, the impact of the simplifications made above is negligible.

A.2 Stepped LFM Chirp

In contrast to the analog LFMCW radar, the stepped LFMCW radar uses discrete frequency steps and for each of these steps it samples the received and down converted signal once. The frequency stepping and sampling of the received signal is done in a synchronized way. Each time the radar changes the frequency, it waits a given settling time after which the base band receive signal approximately remains constant. The signal is then sampled and the frequency can be changed again for the measurement at the next frequency step. The ith frequency step is given by its frequency ω_i:

$$\omega_i = 2\pi \left(f_0 + \frac{\Delta f}{T_C} T_a i \right)$$

Where T_a is the (constant) frequency stepping rate and sampling rate of the receive signal.

The transmit signal is given by:

$$s(t') = \cos\left(\omega_i t'\right) = \cos\left(\varphi\left(t'\right)\right)$$

$$s(t) = \frac{1}{2} e^{j\varphi(t)} + \frac{1}{2} e^{-j\varphi(t)}$$

As done above, the HF receive signal is derived from the transmit signal that is delayed by the signal propagation time which in turn depends on the target range $R(t)$.

$$r\left(t\right) = s\left(t - \frac{2R\left(t\right)}{c}\right)$$

Again, a phase shift and the attenuation of the signal is not taken into consideration. The baseband receive signal is produced by mixing the radars receive signal with its current transmit signal:

$$r_b^*\left(t\right) = r\left(t\right) s\left(t\right)$$

With the same steps taken as for the analog LFM sweep this yields a real or complex function of $\varphi_{rb}(t')$. The instantaneous received phase in base band $\varphi_{rb}(t')$ can be expressed by the instantaneous target range R_i:

$$\varphi_{rb}(t') = \varphi\left(t' - \frac{2R_i}{c}\right) - \varphi(t)$$

$$\varphi_{rb}(t') = 2\pi\left(f_0 + \frac{\Delta f}{T_C}T_a i\right)\left(t' - \frac{2R_i}{c}\right) - 2\pi\left(f_0 + \frac{\Delta f}{T_C}T_a i\right)t'$$

$$\varphi_{rb} = 2\pi\left(f_0 + \frac{\Delta f}{T_C}T_a i\right)\left(-\frac{2R_i}{c}\right)$$

φ_{rb} remains constant for the sampling period when target movement is negligible. In the following, we use a sampled version of the target movement from above:

$$R_i = R_0 + v_0 T_a i$$

When simulating the sampled receive signal from an LFMCW front-end, each sample can be calculated for its own. Even the most complicated target movement can easily be incorporated. Insertion of the equation of movement yields:

$$\varphi_{rb}(t) = 2\pi\left(f_0 + \frac{\Delta f}{T_C}T_a i\right)\left(-\frac{2R_0 + 2v_0 T_a i}{c}\right)$$

$$\varphi_{rb}(t) = -2\pi\left(\frac{2R_0}{c}f_0 + \frac{2R_0}{c}\frac{\Delta f}{T_C}T_a i + \frac{2v_0 T_a i}{c}f_0 + \frac{2v_0}{c}\frac{\Delta f}{T_C}T_a^2 i^2\right)$$

Again, the terms quadratic in i can be neglected, constant phase shifts can be accumulated and are omitted:

$$\varphi_{rb} = -2\pi\left(\frac{2R_0}{c}\frac{\Delta f}{T_C} + \frac{2v_0 f_0}{c}\right)T_a i$$

The resulting sampled signal is approximately a harmonic oscillation with the frequency f_{rb} sampled at rate T_a:

$$f_{rb} = -\frac{2R_0\Delta f}{T_C c} - \frac{2v_0 f_0}{c}$$

Appendix B

Detection Theory

Detection theory is used to understand the performance of a threshold detector such as the one described in Section 4.3. This understanding is the basis for the constant false alarm rate (CFAR) detector that is described afterwards in Section 4.4.

The detection task can be regarded as a binary hypothesis testing problem. With a binary hypothesis test, it is assumed, that the system of interest can have two different states. The task is to choose between two hypotheses about the current system state (H_0,H_1) from examining an observed measurement x. For the radar detection task, one hypothesis (H_0) refers to the case where only noise is received and there is no target present. The second hypothesis (H_1) refers to the case where the signal power x is coming from a target echo, additively superposed by noise.

B.1 Maximum Likelihood Detector

A detector according to the maximum likelihood criterion will choose the most "likely" hypothesis for some measurement x. To use the maximum likelihood detector, the conditional probability densities $p(x|H_0)$ and $p(x|H_1)$ must be known.

The most likely hypothesis is simply chosen by taking the hypothesis H_i with maximum $p(x|H_i)$ for a given x.

The likelihood ratio is simply defined by:

$$L(x) = \frac{p(x|H_1)}{p(x|H_0)}$$

With this, the maximum likelihood detector can be written in the following

form:

$$\phi(x) = \begin{cases} 1 & if \frac{p(x|H_1)}{p(x|H_0)} > 1 \\ \vartheta & if \frac{p(x|H_1)}{p(x|H_0)} = 1 \\ 0 & if \frac{p(x|H_1)}{p(x|H_0)} < 1 \end{cases}$$

Where $\phi(x) = 1$ means "decide for H_1", and $\phi(x) = 0$ means "decide for H_0". The case $\phi(x) = \vartheta$ is practically irrelevant, because its probability is usually 0.

The maximum likelihood is "the best" that can be done when only the conditional probability densities $p(x|H_0)$ and $p(x|H_1)$ are known.

B.2 Maximum a Posteriori Detector

In some cases, also the a priori probabilities $P(H_0)$ and $P(H_1)$ for the occurrences of the hypotheses are known. In this case, we can minimize the probability of error by finding the most probable hypotheses H_i for a given measurement x. The a posteriori probability $P(H_i|x)$ can be obtained through the Bayes rule:

$$P(H_i|x)p(x) = P(H_i)p(x|H_i)$$

$$P(H_i|x)\sum_k (p(x|H_k)P(H_k)) = P(H_i)p(x|H_i)$$

$$P(H_i|x) = \frac{P(H_i)p(x|H_i)}{\sum_k (p(x|H_k)P(H_k))}$$

With the two a posteriori probabilities, the most probable hypothesis can be determined by calculating the ratio:

$$\frac{P(H_1|x)}{P(H_0|x)} = \frac{P(H_1)p(x|H_1)}{P(H_0)p(x|H_0)} \lessgtr 1$$

If, additionally, the cost for a wrong decision can be specified, the "minimum Bayes risk criterion" can be used to minimize the cost for the decision maker. The maximum a posteriori probability criterion above is a special case of the minimum risk criterion with equal cost for each wrong decision and no cost for a right decision.

B.3 Neyman-Pearson Detector

With tasks like the radar detection, there is only some available information about the system and also the detection criteria introduced above are not suitable for the radar detection. For the radar detection task, a detector that works according to the Neyman Pearson criterion is suitable.

According to the radar detection case, we define the both hypothesis:

- H_0: "no target present"
- H_1: "target present"

The Neyman Pearson detector can be used, when

1. the conditional probability densities $p(x|H_0)$ and $p(x|H_1)$ are known.
2. the cost of wrongly detecting H_0 (missed target detection) is substantially different to the cost for wrongly detecting H_1(false alarm).

For the Neyman-Pearson criterion, the following two probabilities are considered:

- Detection probability P_d: Probability of correctly choosing H_1.
- False alarm probability P_{fa}: Probability of choosing H_1 when actually H_0 was true.

The Neyman-Pearson criterion can be stated with the above probabilities:

- maximize P_d while not exceeding P_{fa} for a given value $P_{fa} \leq \alpha$.

This criterion is very suitable for the radar detection task. It is first stated, which false alarm rate is tolerable and the detection probability is maximized for the given false alarm rate.

The following likelihood ratio test uses a threshold g to decide between to hypotheses H_0 and H_1:

$$\phi(x) = \begin{cases} 1 & if \ \frac{p(x|H_1)}{p(x|H_0)} > g \\ \vartheta & if \ \frac{p(x|H_1)}{p(x|H_0)} = g \\ 0 & if \ \frac{p(x|H_1)}{p(x|H_0)} < g \end{cases}$$

Where $\phi(x) = 1$ means H_1 is chosen and $\phi(x) = 0$ means H_0 is chosen. Similar to the maximum likelihood detector, the case $\frac{p(x|H_1)}{p(x|H_0)} = g$ is practically irrelevant because its probability is usually assumed to be infinitely small.

B.3.1 Proof of the Neyman-Pearson Lemma

The Neyman-Pearson lemma states that this test is optimal in the sense of the Neyman-Pearson criterion. The proof of this lemma is done by integrating the conditional probability densities of the measurement over the decision region R_1 (to choose H_1):

$$P_d = \int_{R1} p(x|H_1) = \int \phi(x) p(x|H_1)$$

$$P_{fa} = \int_{R1} p(x|H_0) = \int \phi(x) p(x|H_0)$$

If P_d is increased by extending the decision region R_1, also P_{fa} is increased, as long as both distribution functions are nonzero in the extension of the regions.

Let g be the threshold chosen so that $P_{fa} < \alpha$ when using the likelihood ratio decision function $\phi(x)$. For any other decision rule $\phi'(x)$ with a $P_{fa}(\phi') \leq \alpha$ the following equation must be true:

$$\int (\phi(x) - \phi'(x)) \left(p(x|H_1) - g\, p(x|H_0)\right) \geq 0$$

This is true for the following reason: If $\phi(x) = 1$ then $\phi(x) - \phi'(x) \geq 0$ and, from the definition of ϕ, also $(p(x|H_1) - g\, p(x|H_0)) \geq 0$.

The elements of the above equation are multiplied out :

$$\int (\phi(x)p(x|H_1) - g\phi(x)p(x|H_0) - \phi'(x)p(x|H_1) + g\phi'(x)p(x|H_0)) \geq 0$$

This equation can be written using the definitions of the detection and false alarm rate:

$$P_d(\phi) - gP_{fa}(\phi) - P_d(\phi') + gP_{fa}(\phi') \geq 0$$

If $P_{fa}(\phi') \leq P_{fa}(\phi)$ also the following is true:

$$P_d(\phi) - P_d(\phi') \geq 0$$

$$P_d(\phi) \geq P_d(\phi')$$

This completes the proof. The same approach can be taken to prove that the ratio test is also optimal for the maximum a posteriori criterion.

A Neyman-Pearson detector implemented directly from this definition would have to look up every measurement value in a likelihood ratio table

$l(x)$ and it chooses H_0 if $l(x) < g$ and H_1 if $l(x) > g$. This however is not necessary in most cases, since the distribution functions $p(x|H_0)$ and $p(x|H_1)$ generally have an advantageous characteristic. This advantage lies in the fact, that the likelihood ratio $l(x)$ is a monotonic function of x, which can easily be shown analytically. A detection decision can be made by comparing the measurement value directly with a threshold S. The Neyman-Pearson detector is then given by:

- choose H_0 if $x < S$
- choose H_1 if $x > S$

In this case, the detection- and false alarm- probabilities can be stated in a more usable way:

- $P_d = \int_S^\infty p(x|H_1)$
- $P_{fa} = \int_S^\infty p(x|H_0)$

When the likelihood function is monotonic, the threshold detector is optimal. It can be seen from the last equation, that in this case the distribution function $p(x|H_1)$ need not be known to adjust the threshold of the detector. The implementation of the Neyman Pearson threshold detector for use as a radar detector is discussed in Section 4.3.

Appendix C

A Radar Simulation Tool (RASI)

This chapter describes the steps in developing software for a radar system and presents a radar simulation tool. It is shown, in which way this tool supports the development. The contents of this chapter have already been published [Lübbert 2003].

The hardware of the discussed radar network was specified and developed within the European research project "A Multifunctional Automotive Radar Network" (RadarNet). The research of signal processing strategies described in this thesis has been done on the basis of the developed sensors and network hardware.

The sensor software and the software for the radar network processor have been built up from scratch. At the start of this project, initial simulations of the signal processing algorithms were made. It was soon recognized that there would be great benefits to be gained from a development environment that can host the signal processing algorithms over the complete duration of the project. Using the same system and signal processing modules from the first project stages concentrating on simulations up to the last stages of implementing and testing the algorithms on available hardware, a great reduction of cost and time needed was made.

A RAdar SImulation Tool (RASI) was developed to simulate radar target scenarios and to have a development environment to host the signal processing algorithms. The system was designed to have real time capabilities and to support hardware interfaces like CAN and Ethernet. In this way, actual measurement data can be fed into the system. The signal processing on the measurement data is done with the same modules that are used for

the simulation tests.

C.1 Simulating a Radar Scenario

The signal processing algorithms for radar systems are very complex and their development requires experience and a good understanding of the underlying systems. While experience of course is a great advantage in building up a new radar sensor, it is also very helpful to get an early insight into the planned system by the use of simulations. In most cases a huge difference is expected between real and simulated data. None the less there are some good points in using simulation as a starting point for the software development. While simulation is inevitable when the sensor hardware is not available completely, simulation also provides reproducible data to be fed into the algorithms and hardware deficiencies can be put aside. A particular measurement scenario can easily be created, and last but not least, software development is generally more convenient and efficient using workstations rather than DSP hardware.

At first, the Radar Simulation (RASI) Tool was created to provide an environment for simulation and to develop the signal processing software in a convenient and stable way. Later, RASI was extended to support many different hardware interfaces in order to be able to process actual real-world measurement data. The capability of running the algorithms in real time makes it possible to run the radar measurement with exactly the same software that was developed within the simulation.

C.2 Developing a Radar Signal Processing System

The development of a radar sensor prototype is usually separated into two work packages, one consists of the software development, the other consists of the sensor hardware development. To minimize the development time, software and hardware development is commonly carried out in parallel by two teams. The challenge for the software team is to efficiently prepare the software for the day the hardware is available.

The first step in software development is to build up the signal processing software by the help of simulations. For this purpose there are standard signal processing suites available. However, for radar signal processing software it is often decided to build up a proprietary solution. In this case, the main task is to develop algorithms for detection, checking hypotheses and

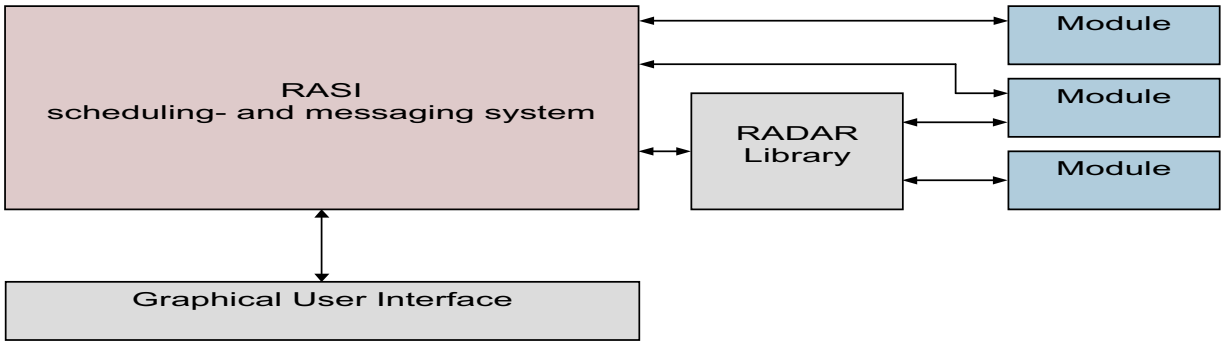

Figure C.1: Components of the radar development environment

their probabilities, and resolve ambiguities in the measurements rather than to put together readily available filters and adjusting their parameters.

The radar hardware part on the other hand can be divided into the sensor front-end and the signal processing hardware. Today, the front-end typically includes the high frequency subsystems to produce the transmit signal, the receiver amplifier, the mixer, and the antenna system. The signal processing hardware hosts the software to control the functions of the front end and to process the received data. Commonly, a digital signal processor is used for this.

There are test boards available for many signal processors. If there is one available for the chosen processor, the software may be ported to the test board before the sensor hardware is available.

If at some point in the hardware development measured data is available, it can be given to the software team to test the signal processing with real data. As soon as the hardware is available, the software can be ported to the sensor hardware.

C.3 Overview of RASI

RASI is a development environment for a PC based system. RASI consists of multiple components that run separated from each other. Figure C.1 shows these components and how they interact. The radar signal processing algorithms and sensor control software are developed as modules that are additionally loaded into the system at runtime.

The RASI scheduling and messaging system is the core of RASI. It loads the signal processing-modules at runtime, assigns processor time and manages the routing of messages between the modules. For the software development it provides a programming API and an object-framework for the modules. The modules are built up on and access RASI functions through

the framework.

The graphical user interface component provides easy access to the controlling functions of the system. The user can load and connect the necessary modules and can change all relevant parameters of the system and the modules.

For the support of the radar applications, a radar library and additional modules were built. The radar library builds up on top of the RASI base system. It provides signal processing functions and extends the object-framework by adding typical radar processing module templates.

The additional modules provide helper functions including functions for recording data to a file or graphically displaying radar target lists on the screen. During the RadarNet project, the number of support modules increased to a great pool of readily available tools. The support modules, the simulation of a radar scenario, and the signal processing modules are all implemented as modules which are loaded by the base system at runtime.

C.4 Structure of the Simulation

To properly implement and test the radar signal processing software using simulations, a radar scenario and the channel impulse responses for the available antennas are needed. Additionally, in the RadarNet case, the time synchronization of the sensors has to be modeled. The single sensor hardware is simulated by generating the front-end output signals from the channel impulse responses. These time signals can then be used to test the radar signal processing software modules that are under development. The processing modules in turn generate target lists which can finally be displayed on the screen, and be compared to the simulated scenario. The block diagram of the processing modules together with the simulation modules is shown in Figure C.2 for the classical radar network processing (Chapter 7).

The complete system was implemented in RASI. Figure C.3 shows the graphical interface of the system. The modules are loaded and interconnected at runtime and can be handled completely separately at compile time. This is useful especially in projects which are handled by several persons or even institutions.

The modularization of the example is done on a coarse functional level. The following modules are implemented:

- The "world model" simulates objects and their movements in the radar scenario. Channel impulse responses are generated for the existing antennas.

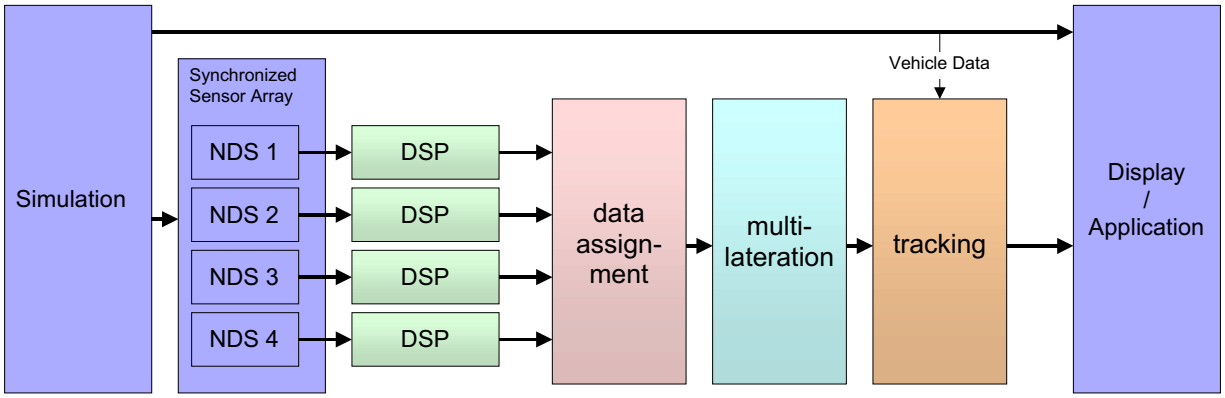

Figure C.2: Block diagram of the functional units including the simulation

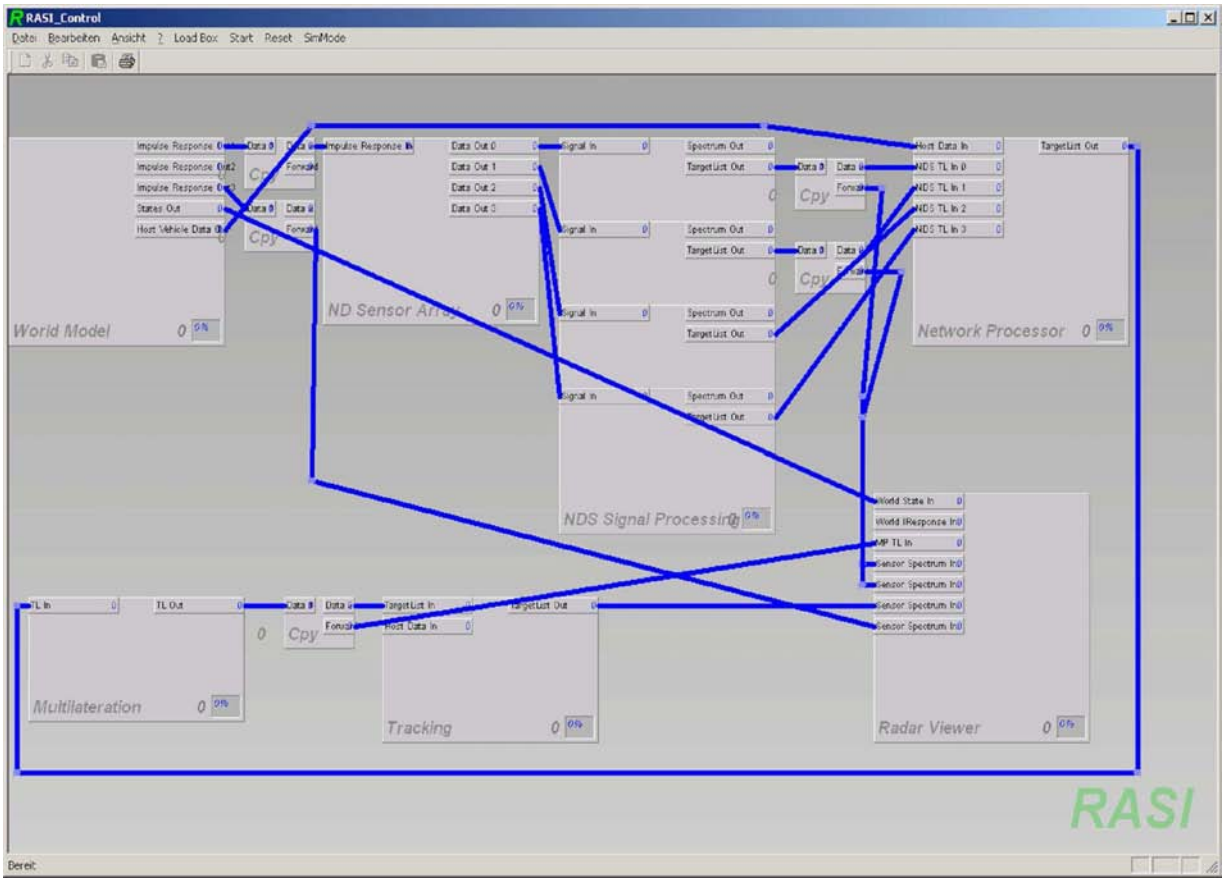

Figure C.3: Graphical interface of the run time environment

- The ND sensor array simulates the behavior of the near distance sensor array with the 4 sensor front ends that generate the measured time samples from the channel impulse responses.
- The Radar Viewer presents the simulation and the generated target lists.
- The signal processing blocks:
  - NDS Signal Processing,
  - network Processor containing the data assignment stage,
  - multilateration,
  - tracking.

The system is structured on a higher level and not into elementary signal processing blocks. In this example, the whole NDS signal processing is combined into one module while the post processing is separated into a few functional blocks.

Communication between modules is achieved by the use of a simple messaging system. It is roughly comparable to message exchange systems found in operating systems.

The flow of communication is determined at runtime by interconnecting the module pins. Additionally, the messaging system incorporates time stamps to ensure a timely synchronized message flow. RASI ensures causality of the message handling, while the modules themselves determine the time needed to process a message.

C.5 Real Time Capability and Support of Hardware

The advantages of a modular software design is well known and commonly practiced. However, with commonly known, off-the-shelve signal processing environments it is difficult to integrate hardware and run the signal processing in real time. This is the second issue that was considered during the development of RASI, and because of this, RASI not only supports the simulation of real time but also the actual execution in real time. To date, RASI supports interfaces like CAN and fast serial ports, Ethernet, and protocols like TCP/IP and UDP/IP. To support simulated and actual real time, RASI can be put into one of two modes:

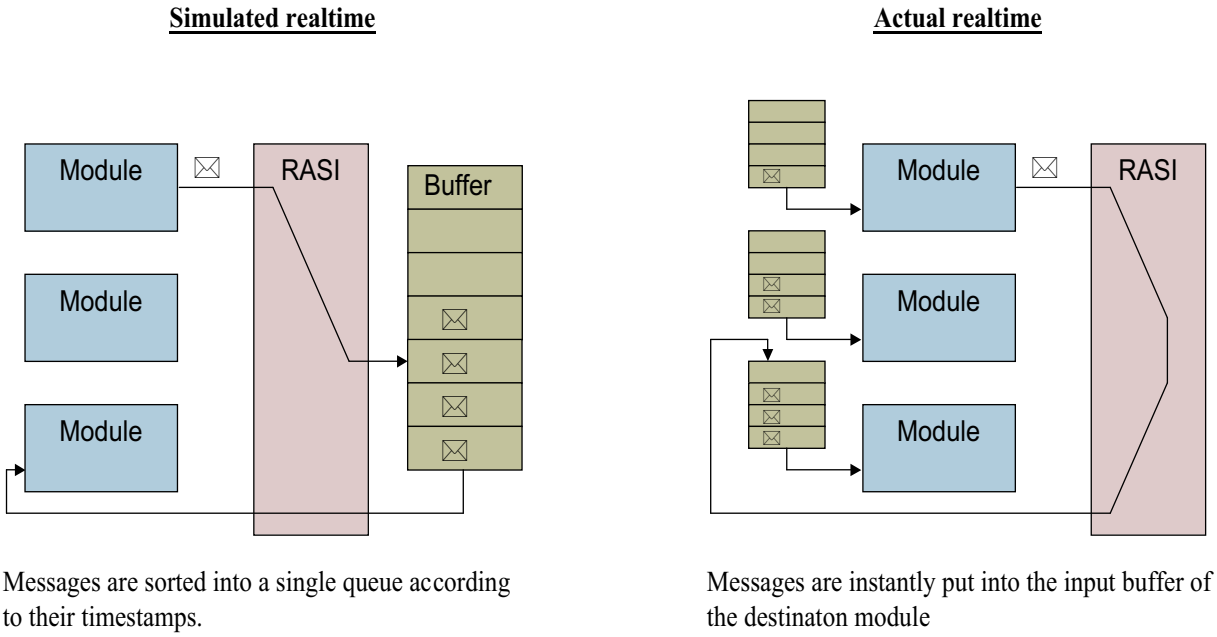

Figure C.4: Message handling in simulated real-time mode (left) and real-time mode (right)

- Using the simulated real-time mode, the messages are sorted into a queue by the value of their time stamp. The earliest message with the smallest valued time stamp is delivered to its receiving module first. In this mode, there is one queue for all modules.
- Using the actual real time mode, every module has its own message queue. The messages are instantly put into the receiving module's queue and are processed in a first in - first out manner. The latency times are in the range of 2ms.

The message handling is visualized in Figure C.4. Using the simulated real time mode, the system is configured as a cooperative multi-threading system. The actual real time mode provides preemptive multi-threading.

C.6 RASI Used as an Environment for Prototypes

In the RadarNet project, one part of the software is ported to the near distance sensor and the second part, the post processing software, remains on a PC system. Because of the properties of RASI that are described above, post processing software that is to run on a workstation can be hosted by RASI throughout the complete project. The simulation and the

final prototype runs with the same software modules. The RadarNet post processing modules have been delivered to project partners together with a minimal runtime system to run on a PC.

C.7 Results

The three main advantages of the RASI development environment are:

1. Modular design of functional signal processing units
2. Provision of a communication solution for the software modules
3. The ability to do simulations and real measurements with the same software
4. A growing pool of readily available modules

With the help of RASI, the time needed to develop a new sensor until it is operational can be strongly reduced. The system has been presented at the International Radar Symposium 2003 in Dresden, Germany [Lübbert 2003].

The sensor signal processing software was functional within the RASI signal processing environment when the sensor hardware was delivered. A small program on the sensor hardware was created to transfer the measured data to a computer running the signal processing environment. This way, the sensor was operational after 4 days. After 2 more weeks, the complete near distance sensor software was successfully ported to the sensor hardware and was ready to be presented.

List of Figures

2.1 Radar network overview 16
2.2 Concept of trilateration 16
2.3 Observation areas for some applications 17

3.1 Pulse- and linear frequency modulated waveform 22
3.2 Simple pulse radar 24
3.3 Pulse waveform, transmit and receive signal versus time . . . 25
3.4 Mono-frequency CW waveform and an example baseband signal 28
3.5 Instantaneous frequency of an LFMCW sweep 29
3.6 Frequency shift due to signal delay and Doppler 30
3.7 Single chirp waveform with positive sweep rate Δf (left) and corresponding R-v_r diagram for a single target measurement (right) 31
3.8 Two chirp waveform with sweep rates of opposite sign and corresponding R-v_r diagram for a single target 32
3.9 Two chirp waveform, corresponding R-v_r diagram for two targets. Two frequencies measured for each chirp yields 4 cross sections 33
3.10 Four chirp waveform and corresponding R-v_r diagram for two targets. Using four chirps, there are 4 lines going through the valid cross sections for the real targets. 33
3.11 Proposed waveform consisting of 4 chirps 34
3.12 Practically realized waveform 35
3.13 Difference between a) un-stepped and b) stepped waveform . 35

4.1 Overview of LFMCW sensor 38
4.2 Overview of spectral analysis 39
4.3 Single chirp, baseband signal, and its corresponding spectral power estimate 39

4.4 Probability distributions for both hypotheses; detection and false alarm rates for a threshold S can be graphically derived 42
4.5 Cell Averaging (CA) CFAR 45
4.6 Ordered Statistics (OS) CFAR 46
4.7 The center of the sampled peak is calculated by the Center of Gravity algorithm 47
4.8 Range-Doppler diagram. Due to frequency estimation errors, the lines do not intersect exactly in one point. 50

5.1 Center of gravity algorithm on different sampling rates and noise levels 57
5.2 Center of gravity algorithm weighting 3 bins ($m = 1$). The frequency estimate is plotted against the actual frequency. The results for four different window functions are shown. . 61
5.3 Center of gravity algorithm weighting 5 bins ($m = 2$). (Rectangular window behaves worst) 62
5.4 Expectation value and standard deviation of the frequency estimate when the COG algorithm is weighting 3 bins. A Hamming window and an SNR of 12 dB is used. 63
5.5 Expectation value and standard deviation of the frequency estimate when the COG algorithm is weighting 3 bins. A Hamming window and an SNR of 20 dB is used. 64
5.6 COG correction factor to achieve an unbiased frequency estimation versus SNR. 3 bins are weighted, a Hamming window is used. 65
5.7 Reference times for the compensation of target movement . . 66
5.8 Frequency validation gates for chirps 3 and 4 68
5.9 Detection rate vs. gate size, 5 simulated targets 72
5.10 False alarm rate vs. gate size, 5 simulated targets 72
5.11 Detection rate vs. false alarm rate, 5 simulated targets 73
5.12 Range accuracy vs. false alarm rate, 5 simulated targets . . . 73
5.13 Detection rate vs. gate size, 10 simulated targets 74
5.14 False alarm rate vs. gate size, 10 simulated targets 74
5.15 Detection rate vs. false alarm rate, 10 simulated targets . . . 75
5.16 Range accuracy vs. false alarm rate, 10 simulated targets . . 75
5.17 Overview of the tracking cycle 78
5.18 LFMCW processing with standard tracker 79
5.19 LFMCW processing with direct frequency track update . . . 80
5.20 LFMCW Tracking: R, v_r-measurement to track assignment (left), frequency to track assignment (right) 82

6.1 Classical definition of azimuth α and elevation ε 84

6.2 Radar antenna at Heathrow airport 85
6.3 Azimuthal scanning principle 85
6.4 Monopulse principle 86
6.5 Trilateration of one target 89
6.6 Trilateration of well separated multiple targets 90
6.7 A situation which can not be resolved by two sensors 91
6.8 Using four sensors to resolve targets with similar ranges . . . 92
6.9 System model for the Kalman filter 96
6.10 Radar network with (a) monostatic and (b) bistatic measurement 100
6.11 Example network configuration with 4 sensors 102
6.12 Accuracy of position estimation in relation to the single sensor range accuracy. 103

7.1 Straightforward network processing 106
7.2 Gate for range to target association 108
7.3 Complete cycle of the tracker, repetition of Figure 5.17. . . . 112
7.4 Assignment strategies 113
7.5 Estimation variance 114
7.6 Synchronization scheme 119

8.1 The three investigated network processing strategies 124

9.1 Radar network hardware overview 132
9.2 Experimental car equipped with the radar network 132
9.3 Radar network relative sensor positions in millimeters 134
9.4 Radar network coordinates 135

10.1 Photograph of prototype near distance sensor 138
10.2 Distribution of range error versus target distance 139
10.3 Measurement of a passing car
Upper plot: Range track of a passing car.
Lower plot: Frequency deviation over measurement cycle for the measurements of *two* 450MHz chirps
Middle plot: Histogram of the frequency deviation from tracker for complete measurement
142
10.4 Range deviation of tracked state from a 5th order polynomial fitted to data. Frequency gate: ±1bin (upper plot); ±0.2 bin (lower plot) 143
10.5 Range measurements and track states of a road traffic scenario. 146

10.6 Range measurements and track states of a road traffic scenario. 146
10.7 Range measurements and track states of a road traffic scenario. 147
10.8 Range measurements and track states of a road traffic scenario. 147
10.9 Range measurements and track states of a road traffic scenario. 148
10.10 Range measurements and track states of a traffic scenario. . . 148

11.1 Single point target experimental setup 153
11.2 Radar network range measurements of a single point target . 154
11.3 Range measurements of a single point target, closeup at 6 m 155
11.4 Azimuth measurements of a single point target 156
11.5 Position estimates for an extended target using the range to track assignment. The circles show the target detections from the normal trilateration algorithm. 159
11.6 Position estimates for an extended target using the frequency to track assignment. The circles show the target detections from the normal trilateration algorithm. 160
11.7 Photograph of the traffic scenario, Hamburg Harburg, Ehestorfer Weg 162
11.8 Screenshot of the traffic scenario shown in Figure 11.7 163
11.9 Trajectories for multiple targets 164
11.10 Comparison of sensor spectra for a passenger car in front of the radar network, oriented sideways (25deg offset). 165
11.11 Photograph of a common traffic scene, Hamburg Harburg, Eissendorfer Strasse 167
11.12 Screenshot of radar network measurement data corresponding to the photograph in Figure 11.11 168
11.13 Measurement data for complete duration of stop-and-go scene 169

12.1 Passenger car equipped with a radar network prototype. . . 172

C.1 Components of the radar development environment 187
C.2 Block diagram of the functional units including the simulation 189
C.3 Graphical interface of the run time environment 189
C.4 Message handling in simulated real-time mode (left) and real-time mode (right) 191

Bibliography

[Blackman 1999] Blackman, Samuel S.; Popoli, Robert; "Design and Analysis of Modern Tracking Systems (Artech House Radar Library)", Artech House, Boston 1999

[Chabert 2004] Chabert, M.; Mailhes, C.; Thomas, N.; Ducasse, A.; Michel, P.; Castanié, F.; "On the use of High Resolution Spectral Analysis methods in Radar Automotive," Proceedings of the 1st International Workshop on Intelligent Transportation (WIT 2004), 139-142, Hamburg 2004

[Fölster 2001] Fölster, Florian, "Multilateration in einem Radarnetzwerk für Kraftfahrzeuge," Diploma Thesis, Technical University Hamburg Harburg, Department of Telecommunications, Hamburg 2001

[Huder 1999] Huder, Bernhard, "Einführung in die Radartechnik," Teubner, Stuttgart, Leibzig, 1999

[Huelsmeyer 1904] Hülsmeyer, Christian, "Verfahren, um entfernte metallische Gegenstände mittels elektrischer Wellen einem Boabachter zu melden," Patentschrift 165546, Kaiserliches Patentamt, 1904.

[Kalman 1960] Kalman, R. E., "A New Approach to Linear Filtering and Prediction Problems," Transaction of the ASMEJournal of Basic Engineering, 82(Series D), 35-45, 1960.

[Klotz 2002] Klotz, Michael, "An Automotive Short Range High Resolution Pulse Radar Network," PhD Thesis, Technical University Hamburg Harburg, Shaker Verlag, Aachen, 2002

[Levanon 1988] Levanon, Nadav, "Radar Principles," Wiley & Sons, New York, 1988

[Ludloff 2002] Ludloff, Albrecht, "Praxiswissen Radar und Radarsignalverarbeitung," 3rd edition, Vieweg Verlag, Braunschweig, 2002

[Lübbert 2002] Rohling, Hermann; Höß, Alfred; Lübbert, Urs; Schiementz, Mark; "Multistatic Radar Principles for Automotive RadarNet Applications," Proceedings of the German Radar Symposium, 181-185, Bonn 2002

[Lübbert 2003] Lübbert, Urs; Rohling, Hermann; "RASI - A Flexible RAdar SImulation Tool," Proceedings of the International Radar Symposium 2003, 753-758, Dresden, October 2003

[Lüke 1999] Lüke, Hans Dieter, "Signalübertragung," Springer Verlag, Berlin Heidelberg, 1999

[Meinecke 1998] Meinecke, Marc-Michael; Rohling, Hermann; Klotz, Michael; Mende, Ralph; "Experiences with an Experimental Car controlled by a 77 GHz Radar Sensor," Proceedings of the International Radar Symposium, Vol. 1, 345-354, IRS 98, München, 1998

[Meinecke 2001] Meinecke, Marc-Michael, "Zum optimierten Sendesignalentwurf für Automobilradare," PhD Thesis, Technical University Hamburg Harburg, Shaker Verlag, Aachen, 2001

[Mende 1999] Mende, Ralph, "Radarsysteme zur automatischen Abstandsregelung in Automobilen," PhD Thesis, Technical University Braunschweig, 1999.

[Oprisan 2002] Oprisan, Dan; Rohling, Hermann; "Tracking Systems for Automotive Radar Networks," Proceedings of IEE Radar 2002, 339-343, Edinburgh, 2002.

[Rohling 1983] Rohling, Hermann, "Radar CFAR Thresholding in Clutter and Multiple Target Situations," IEEE Transactions on Aeorospace and Electronics Systems, Vol. AES-19, No.4, July 1983

[Rohling 1995] Rohling, Hermann; Lissel, Ernst; "77 GHz Radar Sensor for Car Application," Proceedings of the IEEE International Radar Conference, 373-379, Alexandria, VA, 1995

[Rohling 1998] Rohling, Hermann; Meinecke, Marc-Michael; Mende, Ralph; "A 77 GHz Automotive Radar System for AICC Applications," Proceedings of the International Conference on Microwaves and Radar MIKON 98, Kraków, 1998

[Sorenson 1970] Sorenson, H. W. "Least-Squares estimation: from Gauss to Kalman," IEEE Spectrum, 7, 63-68, July 1970

[Swerling 1954] Swerling, Peter, "Probability of detection for fluctuating targets," Rand Research Memorandum, RM-1217, Mar. 17, 1954.

[Wagner 1997] Wagner, Klaus Peter, "Winkelauflösende Radarverfahren für Kraftfahrzeuganwendungen," PhD Thesis, Technischen Universität München, Lehrstuhl für Hochfrequenztechnik, 1997

[Willis 1991] Willis, Nicholas J., "Bistatic Radar," Artec House, Norwood, MA, 1991.

Lebenslauf

Urs Lübbert
geboren am 25. Juli 1973 in Hannover

Beruf

2005	-		Entwicklungsingenieur im Bereich Automotive Radar bei der Valeo Schalter und Sensoren GmbH, Bietigheim-Bissingen
1999	-	2004	Wissenschaftlicher Mitarbeiter an der Technischen Universität Hamburg Harburg im Arbeitsbereich Nachrichtentechnik

Studium

1994	-	1999	Studium der Elektrotechnik mit Studienschwerpunkt Nachrichtentechnik an der Technischen Universität Braunschweig Abschluss: Diplom im Juni 1999

Wehrdienst

1993	-	1994	Grundwehrdienst

Schulbildung

	-	1993	Helene-Lange-Schule, Hannover Abschluss: Abitur